Hydrodynamic Studies of Dipolar Quantum Gases

im Fachbereich Physik der
Freien Universität Berlin
eingereichte
Dissertation
von

Aristeu Rosendo Pontes Lima

Die in vorliegender Dissertation dargestellte Arbeit wurde in der Zeit zwischen April 2006 und Dezember 2010 im Fachbereich Physik an der Freien Universität Berlin unter Betreuung von Priv.-Doz. Dr. Axel Pelster durchgeführt.

Erstgutachter: Priv.-Doz. Dr. Axel Pelster

Zweitgutachter: Prof. Dr. Jürgen Bosse

Tag der Disputation: 31. Januar 2011

Abstract

In recent years, dilute quantum degenerate gases interacting through the long-range and anisotropic dipole-dipole interaction have attracted much attention. At first, magnetic dipolar effects have been unambiguously demonstrated in atomic Bose-Einstein condensates of ^{52}Cr, ^{87}Rb, and ^{7}Li. In addition, further fascinating possibilities have been recently opened, as fermionic ^{40}K^{87}Rb molecules with an electric dipole moment of about 0.5 Debye were brought close to quantum degeneracy by using stimulated Raman adiabatic passage to efficiently convert these heteronuclear molecules into their rovibrational ground state. Due to a large electric dipole moment, the dipole-dipole interaction between such molecules might be up to $10,000$ times larger than in magnetic atomic systems. In this thesis we theoretically investigate the static and the dynamic properties of polarized dipolar quantum gases at zero temperature. The first part deals with dipolar Bose-Einstein condensates, while the second part is dedicated to dipolar Fermi gases in the non-superfluid phase.

Concerning dipolar condensates, we calculate beyond-mean-field corrections to the physical quantities of interest for both homogeneous and harmonically trapped systems by working out the Bogoliubov-de Gennes theory. In the homogeneous case, we determine the Bogoliubov amplitudes and use them to evaluate the condensate ground-state energy beyond the mean-field approximation, the condensate depletion due to interactions, and the corresponding Lee-Huang-Yang correction to the equation of state. The corrected chemical potential is, then, used to obtain the Beliaev term for the sound velocity. In the trapped condensate, we derive the Bogoliubov excitation spectrum analytically within the local density approximation. By calculating the beyond-mean-field correction to the ground-state energy, we determine the corresponding equations of motion for the Thomas-Fermi radii of the condensate. In equilibrium, we obtain from these equations the quantum correction to the mean-field Thomas-Fermi radii. In addition, we also discuss the influence of quantum fluctuations on the mean-field stability diagram. Since dynamic properties constitute a key diagnostic tool for ultracold gases, we also consider the quantum corrections to the low-lying oscillation frequencies as well as to the time-of-flight expansion of the condensate. Due to the interplay between the dipolar interaction and the condensate geometry, we find that the influence of quantum fluctuations is strongly affected by the trap aspect ratio so that future experiments should be able to detect them.

In order to investigate the physical properties of dipolar Fermi gases in a harmonic trap, we derive a variational time-dependent Hartree-Fock theory within the Wigner representation. We focus on the hydrodynamic regime, where collisions assure the equilibrium locally. This is appropriate for strong interactions. After deriving the equations of motion for the Thomas-Fermi radii in phase space, we first explore their static solutions and discuss the aspect ratios in both real and momentum space as well as the stability diagram. In the case where the polarization direction coincides with one of the trap axis, we find that the momentum distribution remains cylindrical, even for a triaxial trap. Afterwards, we study the hydrodynamic excitations. Thereby, we show that the corresponding oscillations in momentum space are anisotropic due to the presence of the dipole-dipole interaction. Finally, we study the time-of-flight dynamics and find that the real-space aspect ratios are inverted during the expansion, while the one in momentum space becomes asymptotically unity. All these results could be particularly useful for future experiments with strong dipolar fermionic molecules deep in the quantum degenerate regime.

Kurzzusammenfassung

In den letzten Jahren erregten verdünnte Quantengase mit der anisotropen und langreichweitigen Dipol-Dipol Wechselwirkung viel Aufmerksamkeit. Zunächst wurden dipolare Effekte bei atomaren Bose-Einstein Kondensaten aus ^{52}Cr, ^{87}Rb und ^{7}Li nachgewiesen. Ein weiterer Fortschritt wurde vor kurzem dadurch erzielt, dass fermionische ^{40}K^{87}Rb Moleküle mit einem Dipolmoment von etwa 0.5 Debye in die Nähe der Quantenentartung gebracht wurden. Dies gelang durch Einsatz von der sogenannten STIRAP-Methode (Stimulated Raman Adiabatic Passage), um solche Molekülen in den Rotations- und Vibrationsgrundzustand zu bringen. Wegen des hohen Dipolmomentes kann die Dipol-Dipol-Wechselwirkung zwischen heteronuklearen Molekülen bis zu 10.000 Mal stärker als in magnetischen Systemen sein. In dieser Arbeit werden die statischen und dynamischen Eigenschaften polarisierter dipolarer Quantengase am absoluten Temperaturnullpunkt theoretisch untersucht. Der erste Teil behandelt dipolare Bose-Einstein-Kondensate, während der zweite Teil dipolaren Fermi-Gasen in der nichtsuperfluiden Phase gewidmet ist.

Bei dipolaren Kondensaten untersuchen wir sowohl das homogene als auch das in einer harmonischen Falle gefangene Bose-Gas im Rahmen der Bogoliubov-de Gennes Theorie. Dabei berechnen wir die Quantenkorrekturen der physikalisch interessierenden Größen, die über die Molekularfeldtheorie hinausgehen. Im homogenen Fall bestimmen wir die Bogoliubov-Amplituden und gewinnen aus diesen die Grundzustandsenergie des Kondensates jenseits der Molekularfeldtheorie, die durch die Wechselwirkung entstehende Entleerung des Kondensates, und die entsprechende Lee-Huang-Yang-Korrektur zur Zustandsgleichung. Danach erhalten wir aus dem korrigiertem chemischem Potenzial den Beliaev-Term der Schallgeschwindigkeit. Für das harmonisch gefangene Kondensat leiten wir das Bogoliubov-Anregungsspektrum im Rahmen der lokalen Dichte-Näherung analytisch her. Durch die Berechnung der Quantenkorrekturen zur Grundzustandsenergie bestimmen wir die Bewegungsgleichungen für die Thomas-Fermi-Radien des Kondensates. Aus den entsprechenden Gleichgewichtslösungen bestimmen wir dann die Thomas-Fermi-Radien jenseits der Molekularfeldtheorie. Außerdem diskutieren wir den Einfluß der Quantenfluktuationen auf das Stabilitätsdiagramm. Weil dynamische Eigenschaften ein wichtiges experimentelles Hilfsmittel darstellen, Quantensysteme zu charakterisieren, untersuchen wir auch die niederenergetischen Anregungen sowie die Flugzeit-Expansion. Dabei ergibt sich, dass die von der dipolaren Wechselwirkung erzeugten Quantenfluktuationen so stark vom Verhältnis der Fallenfrequenzen abhängen, dass sie in künftigen Experimenten beobachtbar sein müßten.

Als nächstes behandeln wir die polarisierten dipolaren Fermi Gase in einer allgemeinen tri-axialen harmonischen Falle. Um die physikalischen Eigenschaften solcher Systemen zu untersuchen, leiten wir als erstes ein zeitabhängiges Hartree-Fock-Variationsverfahren her. Dabei beschränken wir uns auf das hydrodynamische Regime, bei dem häufige Stöße zu einem lokalen Gleichgewicht führen. Nachdem wir die Bewegungsgleichungen für die Thomas-Fermi-Radien im Phasenraum hergeleitet haben, betrachten wir zuerst deren statische Lösungen und diskutieren dabei das Längenverhältnis sowohl im Orts- als auch im Impulsraum sowie das Stabilitätsdiagramm. Für den Fall, dass die Dipolmomente parallel zu einer der drei Achsen der Falle orientiert sind, ergibt sich, dass die Impulsverteilung auch dann zylindersymmetrisch ist, wenn die harmonische Falle keine Symmetrie aufweist. Danach untersuchen wir die hydrodynamischen Anregungen des Gases und finden dabei, dass die entsprechenden Oszillationen im Impulsraum wegen der Dipol-Dipol-Wechselwirkung anisotrop sind. Zum Schluß studieren

wir die Flugzeit-Dynamik. Es stellt sich heraus, dass die Längenverhältnisse im Ortsraum im Laufe der Expansion invertiert werden, während das im Impulsraum asymptotisch gegen eins strebt. All diese Resultate könnten für künftige Experimente mit stark dipolaren fermionischen Molekülen tief im quantenentarteten Regime nützlich sein.

Contents

1 Introduction

This chapter provides a broad overview on the physics of ultracold quantum gases. Here, we will discuss in an approximate chronological order the main experimental and theoretical advances which laid the ground for the emergence of the research field of cold atoms and molecules. Starting from the experimental discoveries, which triggered some of the major developments in physics in the last 100 years, we present a historical account containing the concepts and advances introduced in the context in which they were involved. Special attention is given to the achievements in the scientific research of bosonic and fermionic gases featuring the long-range and anisotropic dipole-dipole interaction.

1.1 Low-Temperature Physics

Low-temperature phenomena have enchanted many generations of physicists and its history involves some of the greatest minds of the last century. As its very beginning, one could possibly refer to the discovery of superconductivity in solid mercury by Heike Kammerlingh Onnes in 1911 [1], only three years after he had started to perform experiments with cooled helium. For this discovery, Onnes was awarded the 1913-Nobel Prize in physics, one of the many that the low-temperature physics community would receive in the following decades.

The next marking event would be the prediction by A. Einstein in 1924 of the phenomenon that is now known as Bose-Einstein condensation [2]. Satyendra Nath Bose was a talented Indian physicist who discovered that identical quantum particles are actually indistinguishable, as opposed to classical objects, which have distinguishable trajectories. This was the missing part of the puzzle which provided a clean derivation of Planck's formula of black body radiation. Bose wrote a paper containing this derivation and sent it to Einstein [3]. Recognizing its importance, Einstein translated Bose's paper into German and had it published in the prestigious *Zeitschrift für Physik* [4]. Shortly after that, by generalizing Bose's reasoning to the case of a gas of non-interacting *massive* particles, Einstein realized that there should be a critical temperature T_c, under which the number of particles in the one-particle ground state should become of the order of the total number of particles N [2]. At first, not many people took this idea seriously and this phenomenon was regarded as a pathology exhibited by the non-interacting Bose gas.

The physics community remained skeptical with respect to Bose-Einstein condensation as a phenomenon which could ever be realized in the real world of interacting particles. This initially well-spread viewpoint started to faint in 1937 with the discovery of the lambda transition for superfluidity in ^{4}He at $T = 2.17$ K by P. Kapitza [5], J. F. Allen, and D. Misener [6]. Immediately after that, F. London put forward the hypothesis that superfluidity in liquid helium should "be regarded as the condensation phenomenon of Bose-Einstein statistics, distorted, of course, by the presence of molecular forces..." [7]. London's hypothesis had support, for example, from the fact that the critical temperature

for Bose-Einstein condensation for a non-interacting gas of helium atoms is $T_C = 3.13$ K, remarkably close to the actual lambda-transition temperature. In addition, the fermionic isotope, ^{3}He, did not seem to show the same phenomenon. Nonetheless, it should be remarked that the highly successful Landau theory of helium did not mention the word condensation and that Laszlo Tisza's phenomenological two-fluid model, equally well tested and confirmed by experiments on transport properties of helium, did not seem to need such an assumption, although it is mentioned as a possible microscopic model [8].

Even though other theoreticians pushed further the consequences of London's hypothesis, such as R. P. Feynman [9] and T. Matsubara [10], it was not until 1956 that a common criterion for Bose-Einstein condensation was formulated [11]. In that work, O. Penrose and L. Onsager showed that the previous theoretical approaches to Bose-Einstein condensation, including the famous paper by N. N. Bogoliubov [12], are all closely related and possess the same underlying criterion for that phenomenon, formulated in terms of the emergence of long-range order. In particular the paper by Bogoliubov became well known and the ideas and methods contained there became the standard procedure in order to treat beyond mean-field effects in Bose-Einstein condensates.

The next important contribution to the theoretical description of low-temperature phenomena is the construction of the pseudo-potential for the Van der Waals forces in 1957 in two seminal papers by K. Huang, and C. N. Yang [13] and T. D. Lee, Huang and Yang [14]. The pseudo-potential approach had a significant simplification as the effective potential at low-temperatures is governed by a single parameter: the s-wave scattering length a_s. Those authors calculated the interaction corrections to the ground-state energy of homogeneous dilute Bose and Fermi gases. The impact of their work is still large nowadays, where the theory has been applied, for example, to inhomogeneous Bose gases [15].

In the 1950's a theory was devised which could explain superconductivity microscopically. The first step in that direction was given by L. N. Cooper, who showed in 1956 that two electrons in the presence of a filled Fermi sea will form a pair if the interaction between them is attractive, no matter how weak the interaction might actually be [16]. Building on that observation, which is known as the Cooper instability, J. Bardeen, Cooper himself, and J. R. Schrieffer derived the theory of superconductivity [17]. In the BCS theory, the superfluidity of the electrons has its origin in the Bose-Einstein condensation of Cooper pairs. For that contribution, the three authors were awarded the Nobel prize in physics in 1972.

In 1961 L. Pitaevskii and E. P. Gross derived the most important equation for Bose-Einstein condensation, which was named after them. While it was initially used to investigate vortices in weakly interacting Bose gases, the Gross-Pitaevskii equation has since then been applied to a quite broad range of phenomena, specially after the experimental realization of Bose-Einstein condensation in dilute trapped gases, where the Gross-Pitaevskii theory is most successfully employed.

Following the course of history in this brief overview on low-temperature physics, it now becomes time to turn our attention to a great experimental discovery dealing with fermionic particles: superfluidity in the fermionic isotope of helium, i.e. ^{3}He. In 1972, D. Osheroff and colleagues were performing experiments on the melting curve of the fermionic helium and found that, at the temperature 2.7 mK, the derivative of the pressure with respect to the temperature revealed a sudden change [18]. Further evidence for the new phase was found shortly after by nuclear magnetic resonance measurements [19].

In the very same year, A. J. Leggett disclosed the BCS nature of the transition in superfluid ^{3}He [20]. For this discovery D. Lee, Osheroff, and R. C. Richardson were awarded the Nobel Prize for physics in 1996 and Leggett received part of the Nobel Prize of 2003 for the corresponding theoretical explanation.

Although low-temperature phenomena appeared to be abundant and rich in new physics, as we have just seen, much was still to come which depended on the development of techniques capable of allowing to reach even lower temperatures. One of these techniques is the laser cooling method, which was developed in the 1980's by the combined efforts of many physicists. Particularly remarkable are the contributions of C. Cohen-Tannoudji, S. Chu, and W. D. Phillips, which were honored by the Nobel Prize of the year 1997. The impact of this technique is hard to overestimate, since it allowed for the first time to achieve temperatures in the μK range. In the same decade, a theoretical paper appeared which was written by experimentalists of the Massaschusetts Institute of Technology (MIT). They studied quantities such as the critical temperature for condensation and the condensate fraction in the case of trapped ideal gases [21]. Besides the fact that these results were strikingly confirmed by the experiments to come, the importance of that study lies on the guidance that it provided to the following experimental investigations which were soon to be realized.

The race for Bose-Einstein condensation became more and more intense, pushed by many developments in related fields. An interesting detail to be considered here is that the internal degrees of freedom play a decisive role in the cooling schemes, making the success of the cooling methods species dependent. The race was finally won in 1995 by rubidium, condensed by C. Wieman and E. Cornell at the University of Colorado at Boulder, and sodium, condensed by W. Ketterle at the MIT. The experimental realization of the phenomenon of condensation, predicted 71 years before by Einstein, is considered to be one of the greatest breakthroughs in physics of the last century. For their achievement, Wieman, Cornell, and Ketterle were awarded the Nobel Prize for Physics of the year 2001.

In the last 15 years since the first achievement of Bose-Einstein condensation the field of atomic and molecular physics (AMOP) has become a robust and fast growing branch of low-temperature physics. Meanwhile, in addition to sodium [22] and rubidium [23], other elements in the first column of the periodic table, i.e., hydrogen [24], lithium [25], potassium [26], and cesium [27], have been Bose-condensed. The first two-electron atom to be Bose condensed was the rare-earth element ytterbium in 2003 [28], but recent developments have also made possible the condensation of alkaline earth metals such as calcium [29] and strontium [30,31]. In addition, other elements of special interest due to their large magnetic interactions have either been condensed, such as chromium [32], or are promisingly close to it, as dysprosium [33]. We will consider these two elements in some detail, when we come to introduce the reader to the dipolar subbranch of AMOP which is of direct interest to this thesis. In this context, it is also important to remark that Bose-Einstein condensation has also been achieved in metastable helium [34,35] and quasi-equilibrium magnon systems at room temperature [36].

1.2 Bose-Einstein Condensation in Trapped Gases

As predicted by Einstein, condensation corresponds to the accumulation of a macroscopic number of particles in the one-particle ground state. This phenomenon is brought about by a peculiar charac-

teristic of bosonic particles: they tend to occupy states which are already occupied instead of empty ones. It, therefore, reflects the quantum nature of the gas particles and is expected to play a crucial role at low temperatures. By lowering the temperature, one eventually achieves T_C, the critical temperature for condensation, and a transition from a gas of bosonic particles to a new state of matter occurs. This transition links, on the higher temperature side $T > T_C$, a state in which the particles have random velocities and positions according to their thermal distribution to another state, for lower temperatures $T < T_C$, in which also an aggregate of coherent particles is present. This aggregate is called the condensate. The quantum coherence of the condensate implies, for example, that the particles constituting it can by no means be individually distinguished. It is important to remark that the condensate, being a macroscopically occupied *single-particle* state, offers a unique visual demonstration of quantum mechanics. In particular the concept of wave functions acquires a "new level of reality", to quote a popular paper by the Ketterle group [37]. In the meantime, many experiments have probed this character of Bose-Einstein condensates. Emblematic examples of such investigations are double-well interferometry experiments [38] as well as the presence of vortices [39] and vortex lattices in a rotating condensate [40].

The critical temperature for condensation in a gas of non-interacting particles can be estimated based on the following reasoning. Condensation should appear when the quantum nature of the particles becomes non-negligible. Consider a homogeneous system of volume V containing N bosons with mass M. We are interested in the thermodynamic limit, i.e., in the regime for very large N and V such that the ratio $n = N/V$, which represents the density of the particles, remains constant. Therefore, we estimate the average distance between the particles to be $n^{-1/3}$. In addition, for particles in an ensemble at temperature T, we can assign to them a wave length measuring their quantum properties: the thermal de-Broglie wave length $\lambda_{\mathrm{dB}}(T) = \sqrt{2\pi\hbar^2/Mk_{\mathrm{B}}T}$, where $\hbar$ represents Planck's constant divided by 2π and k_{B} the Boltzmann constant. We, then, expect quantum effects to be important when these two lengths become comparable, i.e., the critical temperature should satisfy

$$n\lambda_{\mathrm{dB}}^3(T_{\mathrm{C}}) \approx 1. \tag{1.1}$$

Indeed, more sophisticated calculations lead to a critical temperature for condensation which is given by the relation [3]

$$n\lambda_{\mathrm{dB}}^3(T_{\mathrm{C}}) = \zeta(3/2) \approx 2.612, \tag{1.2}$$

where the Riemann zeta function $\zeta(x)$ is defined according to

$$\zeta(x) = \sum_{k=1}^{\infty} k^{-x}. \tag{1.3}$$

Equation (1.2) implies that, in order to reach condensation, one has either to reach low temperatures or high densities. However, a high density gas would suffer from many drawbacks which make condensation under such circumstances unachievable. Three-body recombinations, for example, are a major obstacle because it leads to chemical reactions and atom losses. In addition, at high densities the ground states of most chemical elements is a solid rather than a gas. It could also be a liquid, as in the case of helium, but no element is known to have a gaseous ground state at high densities. For

these reasons, preference was given for dilute, low-temperature samples in order to reach Bose-Einstein condensation.

The typical route followed by the atoms on their way to condensation starts at an atom beam oven, from which they are emitted at temperatures of several hundred Kelvins. Then they go through a Zeeman slower, where laser cooling combined with applied inhomogeneous magnetic fields allow for reducing the temperature down to the few-Kelvin range. In the Zeeman slower, a counterpropagating radio-frequency laser beam imparts momentum to the atoms slowing them down in the propagation direction. Since the absorbed photons are reemitted spontaneously in a random direction, the net effect is that of cooling the atoms. As the velocities are lowered, the laser frequency no longer corresponds to that of the atomic transition due to the Doppler effect. Therefore, an inhomogeneous magnetic field is applied along the slower and uses the Zeeman effect to compensate the Doppler shift. At this point, the atoms come into a magnetic trap where further cooling by other optical methods bring the sample to temperatures of about 100 mK.

Magnetic trapping of neutral atoms relies on the Zeeman effect and can be roughly explained as follows. In an inhomogeneous magnetic field, the atoms "feel" a spatially varying potential, which can be used to confine them. Depending on whether the magnetic moment of the atom in a given Zeeman substate is positive or negative, atoms in that state are forced to occupy regions of high or low magnetic field, respectively. These states are, therefore, called high- and low-field seeking states. According to a general theorem [41], which is a partial analogon to the Earnshaw's theorem for electric fields [42], no configuration can lead to a local maximum in a magnetic field in a current-free region. Thus, the trap must be implemented by configurations which lead to a local minimum, and only low-field seeking states can be trapped.

It is also possible to trap neutral atoms purely by optical means. This has the advantage of allowing for studies of the Zeeman substates, as these traps cannot distinguish them [43]. Indeed, since the seminal experimental studies of the Ketterle group realizing an optical confinement for the first time [44] and the paper by T.-L. Ho deriving the low-energy Hamiltonian of cold atomic systems in an optical trap [45], spinor quantum gases have become an important subbranch in cold-atoms physics (see, e.g., the Nature News and Views by N. Bigelow [46]). To name just two major achievements made possible by optical traps, we mention the realization of a multi-component condensate of sodium atoms with the total spin $F = 2$ [47] and the observation of itinerant magnetism in fermionic ^{6}Li-atoms [48]. In this thesis, we will work on bosonic and fermionic quantum systems with their spin degree of freedom completely frozen out, i.e., with a single Zeeman substate present. Therefore, we restrict the discussion to magnetic traps. Furthermore, we will consider harmonic trapping potentials of the form

$$U_{\text{trap}}(\mathbf{x}) = \frac{M}{2}\left(\omega_x^2 x^2 + \omega_y^2 y^2 + \omega_z^2 z^2\right), \tag{1.4}$$

where ω_i are trapping frequencies in the i-direction. At this point, it is convenient to introduce the trap aspect ratios

$$\lambda_x = \frac{\omega_z}{\omega_x}, \qquad \lambda_y = \frac{\omega_z}{\omega_y}. \tag{1.5}$$

In case of cylinder symmetric traps, i.e., for $\omega_x = \omega_y$, one has $\lambda_x = \lambda_y = \lambda$. Moreover, let us also

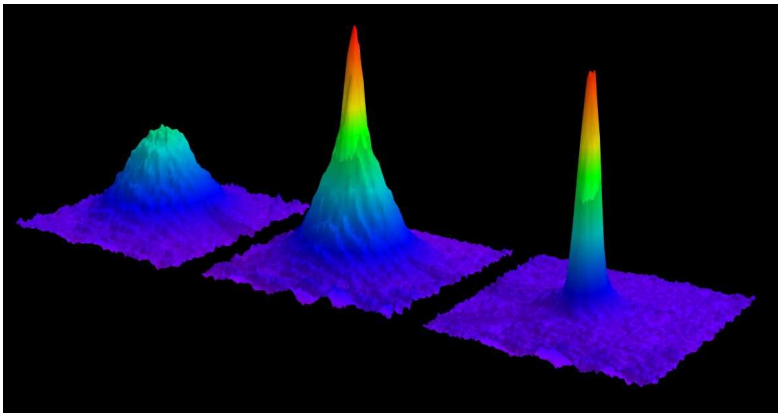

Figure 1.1: Observation of Bose-Einstein condensation through absorption imaging from the MIT-group [37]. After a few milliseconds of time-of-flight expansion, the cloud is illuminated by resonant light and its shadow is recorded in a CCD-camera. The absorption is shown as a function of two spatial directions (1mm × 1mm). The left-hand side picture shows a sample cooled just above the critical temperature for condensation and one sees the broad Gaussian distribution. The middle picture was taken at temperatures just below the critical temperature. It is possible to identify clearly the presence of a peak in the distribution in addition to the Gaussian cloud. The peak representing the condensate appears essentially alone in the picture of the right-hand side.

define for future reference the geometric average of the trap frequencies

$$\overline{\omega} = (\omega_x \omega_y \omega_z)^{1/3}. \tag{1.6}$$

For the densities which can be obtained in usual experimental setups without significant losses from the trap due to three-body encounters, the temperature range reached through laser cooling is still prohibitively large for Bose-Einstein condensation. The decisive step is the so called evaporative cooling, which addresses the most energetic atoms in the sample and throws them out of the trap, thereby lowering considerably the temperature of the remaining atoms [49]. The evaporative cooling process meant here has little to do with the liquid helium experiments performed at the beginning of the experimental studies in low-temperature physics, where a mechanical pump was used to evaporatively cool the helium samples. This is not what happens here, because such a pump would completely evacuate the condensate away. For cold atomic systems, evaporative cooling is performed by applying a radio-frequency pulse at the frequency of the Zeeman shift for flipping the spins of the atoms. This transfers the atoms from low- to high-field seeking states and, thus, removes them from the trap. This step leads to the appearance of the condensate, as demonstrated in Fig. 1.1: after evaporative cooling, the system becomes a bimodal distribution where a Gaussian cloud contains the thermal atoms and a peak distribution suddenly shows up representing the condensate. Further evaporative cooling with lower frequencies eventually removes the thermal component leaving the condensate alone.

The onset of Bose-Einstein condensation has also consequences for the expanded cloud after release from the trap. The non-condensate, thermal component of the system has an isotropic momentum distribution. As a result of this spherical symmetry, the cloud becomes spherical after a large expansion time. For the condensate, on the other hand, the aspect ratio at large times approaches the inverse

aspect ratio of the trap, due to the fact that the condensate momentum distribution is broader in the direction of tighter trapping and vice-versa, due to the Heisenberg uncertainty relation. Therefore, after release from the trap, the acceleration is larger in the direction in which the cloud was more strongly squeezed.

We have restricted the discussion until now on non-interacting Bose-Einstein condensates, because they essentially represent the first realized condensates. It is now time to introduce the effects of interactions and we will focus on the topics of interest for what we shall describe later as our own work. Interactions change considerably both the density profile and the dynamical properties of Bose-Einstein condensates. We consider at first condensates interacting through the isotropic and short-range contact interaction. In the course of this thesis, we shall have more to say about the mathematical description of the contact interaction. For the moment, it suffices to know that, at the low temperatures of interest, the interaction can be characterized by a single parameter, the s-wave scattering length a_s, which we assume to be positive. Then, the s-wave scattering length a_s can be interpreted as the radius of the particles. For a large number of particles the interaction energy becomes the dominating energy contribution and the zero-point energy can be neglected. This is the Thomas-Fermi approximation, which turns out to be fullfilled for the majority of current experiments. The first consequence of the interaction mean-field energy is that, since the interaction is repulsive, it tends to spread the condensate over larger regions and this effectively weakens the trap confinement. In the Thomas-Fermi regime, the condensate acquires well-defined borders in the three directions of space, known as Thomas-Fermi radii, and the condensate aspect ratios turn out to be the inverse of the trap aspect ratio (1.5).

An important tool to characterize interacting condensates is displayed by the collective oscillations. Indeed, already for helium, where the low-lying excitations possess a phonon-nature, they played a crucial role in determining its superfluid properties [50]. For trapped quantum gases, the excitations are characterized according to their energy and angular momentum, rather than according to linear momentum (see Section 2.4.). The analysis of the collective modes also offers a possibility to study interactions, since the frequencies are affected by them [51]. Consider the case of a spherically symmetric trap, i.e., $\omega_x = \omega_y = \omega_z = \omega$. In the absence of interactions the oscillations behave according to the harmonic oscillator model and their dispersion is given by

$$\Omega_{\mathrm{HO}}(n,l) = \omega(2n+l), \tag{1.7}$$

where n and l are the principal and the angular momentum quantum numbers, respectively. In the Thomas-Fermi limit of strong interactions and large number of particles, on the other hand, instead of the harmonic oscillator behaviour discussed previously, the excitations for an interacting condensate acquire a hydrodynamic nature and the dispersion relation reads [51]

$$\Omega_{\mathrm{HD}}(n,l) = \omega\left(2n^2 + 2nl + 3n + l\right)^{1/2}, \tag{1.8}$$

It is illustrative to compare in both regimes the so called surface modes, for which $n = 0$. While the frequency of these modes is given by $\Omega_{\mathrm{HO}}(0,l) = \omega l$ in the harmonic oscillator regime, the hydrodynamic model predicts $\Omega_{\mathrm{HD}}(0,l) = \omega\sqrt{l}$, which is smaller for $l \neq 1$. The case of $l = 1$ corresponds to the dipole mode and is of special interest. As is known from Kohn's theorem [52], the frequency

of the dipole mode is not affected by any two-particle interaction, since it corresponds to the motion of the center of mass. In addition, it coincides with the trapping frequency, providing a mechanism for calibrating the trap. In the hydrodynamic regime, the interaction is large and dominates over the kinetic energy and this is the opposite of what happens in the harmonic oscillator model, where interactions are negligible. For completeness, let us mention that, in order to study regimes between these two limits for given modes, one can use the sum rules approach [51].

The differences from the harmonic oscillator regime to the hydrodynamic one also show up in the time-of-flight analysis. Here the asymptotic aspect ratio is larger than unity, if the aspect ratio of the condensate in the trap is smaller than one and vice-versa, but these two quantities turn out not to be the inverse of each other anymore, as in the absence of interactions.

1.3 Degenerate Fermi Gases

After the realization of Bose-Einstein condensation in dilute quantum gases, the attention of the scientific community turned to fermionic gases since they exhibit obvious analogies with ordinary condensed matter systems. Unlike their bosonic counterpartners, fermionic atoms are not allowed to scatter into occupied states due to the Pauli exclusion principle. As the temperature is lowered and the states inside the Fermi sea are gradually occupied, the efficiency of the previously mentioned cooling processes is dramatically reduced. This constitutes a major challenge in obtaining quantum degenerate Fermi gases.

In order to increase the thermalization of fermionic gases, one can include more than one Zeeman substate in the trap. In addition, the evaporative cooling has to be performed in such a way as to maintain the balance between the populations of both substates. This was achieved by B. deMarco and D. Jin at JILA in 1999 [53]. They applied an evaporative cooling strategy which selectively removes atoms from both states called *forced evaporative cooling* to bring $N = 7 \times 10^5$ ^{40}K atoms to about half the corresponding Fermi temperature. The quantum nature of the sample became evident through clear deviations from classical values of quantities such as the internal energy and the particle density as functions of temperature, which were in agreement with the predictions for a degenerate Fermi gas.

The next major step in the investigation of Fermi gases was the implementation of Feshbach resonances as a mean to control interactions in these systems. We will discuss Feshbach resonances in some detail in the context of the BCS-BEC crossover. For the moment, it suffices to know that they are a unique knob for controlling the interactions in ultracold quantum gases, which was initially implemented in a ^{40}K-gas in JILA [54] and subsequently in a ^{6}Li gas at the MIT [55]. As an immediate consequence the first unambiguous observation of a strongly interacting Fermi gas followed in which collisional hydrodynamics through the time-of-flight technique could be detected [56]. Collisional hydrodynamics had been predicted to be present even at zero-temperature Fermi gases as a consequence of the effect of the stretching of the Fermi sphere [57]. The importance of that prediction lies at the heart of the quest for fermionic superfluidity. Indeed, in a Bose-Einstein condensate, hydrodynamic behaviour had been used as a criterion for condensation itself, as the normal gas is collisionless. Therefore, it was an important point to define the role played by collisions in the Fermi case.

All these developments pointed to a single goal: to achieve superfluidity in fermionic quantum

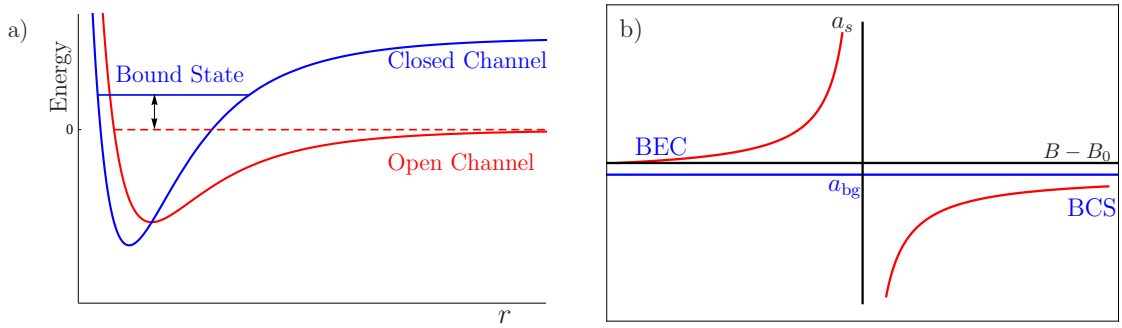

Figure 1.2: a) Schematic interaction potentials versus the interparticle distance r for the open (red) and closed (blue) channel. b) Schematic representation of the s-wave scattering length a_s as a function of the applied magnetic field $B - B_0$ near a Feshbach resonance described by Eq. (1.9).

gases. This milestone of atomic physics still had to wait a while but a further step was given with the achievement of Bose-Einstein condensation in molecules composed of two fermionic atoms. The experimental groups from JILA [58], Innsbruck [59], and MIT [60] managed to produce molecules out of potassium (JILA) and lithium (Innsbruck and MIT). The JILA experiment was particularly impressive because, unlike the other two experiments, in which the molecules were produced during the forced evaporative cooling process, it started from a highly degenerate quantum gas with two Zeeman substates present at the trap and tuned the interactions in such a way to form weakly bound *condensed molecules*. This was completely different from Bose-Einstein condensation of bosonic atoms. Indeed, these also possess fermionic constituents but they are so tightly linked that the fermionic nature is lost and they can be considered as point-like bosonic particles in contrast to weakly bound molecules.

At this point of the narrative it is just impossible not to think about Cooper pairs in the BCS theory of superconductivity. In the famous and quite successful microscopic BCS theory, superconductivity arises as a consequence of the condensation of Cooper pairs, which are loosely bound pairs of electrons. Indeed, superfluidity of loose Cooper pairs, on the one hand, and Bose-Einstein condensation of tightly bound molecules, on the other hand, are the two extremes of one and the same physical phenomenon called BEC-BCS crossover [61–65], which can be experimentally accessed in cold atomic systems by means of a so called Feshbach resonance. Let us briefly discuss how this can be done. Consider the inter-particle potential as a function of the relative distance r, as depicted in Fig. 1.2a). If the potential is independent of the atomic internal degrees of freedom, an incoming low-energetic particle will approach the well in the potential with enough energy to be scattered back by the barrier at $r = 0$ and nothing interesting happens. This is usually referred to as the open scattering channel. If, on the other hand, the inter-particle potential *does* depend on the internal degrees of freedom and provides a coupling between different sub-states due to the hyperfine interaction, for example, atoms colliding in the open channel might be scattered into a bound state of the closed channel, from which they do not have enough energy to escape. A Feshbach resonance occurs when the asymptotic energy of the open channel is equal to the energy of a bound state of the closed channel. In the case of the hyperfine interaction, one can tune the energy difference between these states with the help of an external magnetic field, thereby varying the s-wave scattering length.

Detailed scattering theory calculations [66–68] show that for a Feshbach resonance taking place at

the value B_0 of the magnetic field B, the scattering length is given by

$$a_s = a_{\mathrm{bg}} \left(1 - \frac{\Delta B}{B - B_0}\right), \tag{1.9}$$

where a_{bg} denotes the background value of the s-wave scattering length and ΔB represents the width of the resonance.

Consider the s-wave scattering length a_s as a function of the applied magnetic field $B - B_0$, as measured from the resonant value B_0, for a negative background value, as shown in Fig. 1.2b). For large magnetic fields the scattering length is negative and its absolute value is small. Therefore, this regime of weakly interacting attractive fermions is called the BCS regime. Despite the absence of a bound-state, superfluidity occurs due to the formation of Cooper pairs. As the magnetic field is reduced towards the resonance, the attraction between the particles becomes larger and the pairs become smaller. Passing through the resonance, the interaction becomes repulsive and, at the same time, loose molecules are formed in the bound state of the closed channel. These molecules, known as Feshbach molecules, can form a Bose-Einstein condensate and are responsible for superfluidity at that side of the resonance. Reducing the magnetic field further, the size of the molecules decreases and eventually reaches the BEC-regime of repulsively interacting Bose-condensed point-particles.

The characterization of the BCS-BEC crossover was a far-reaching achievement but the question of superfluidity remained unanswered until 2005 when it was unmistakably observed in a gas fermionic lithium atoms by the MIT group [69]. The characterization of superfluidity in that system was striking: by using a laser beam to rotate the sample around its own axis with varying angular velocity the formation of the Abrikosov lattice of vortices was observed on both the BEC- and the BCS-side of the Feshbach resonance.

1.4 Quantum Fluctuations in Trapped Gases

The role of quantum fluctuations in ultracold systems has been experimentally investigated in different contexts [70,71], but we will restrict ourselves to discussing the case of *trapped* Bose-Einstein condensates and degenerate Fermi gases.

The stage was first set for studying of quantum fluctuations in dilute quantum gases, or, put in another way, the very *concept* of quantum fluctuations in the modern form was introduced in the seminal paper by Bogoliubov presenting a quantum field theoretical approach in terms of a canonical transformation of the Bose fields to describe weakly interaction Bose gases [12]. In that work, the quantum fields were split into a mean-field contribution plus a quantum fluctuation around the mean field, the latter being considered as small. Shortly afterwards, S. T. Beliaev introduced a Greens function approach [72] and extended Bogolioubovs theory to include the quadratic fluctuations as corrections, thereby deriving the quantum corrected sound velocity [73].

In trapped quantum gases the investigations of quantum fluctuations were triggered by the obtention of Bose-Einstein condensation and focused on the spatial dependence of the condensate depletion [74] and on the shift of the low-lying excitation frequencies [15,75]. In particular, the work of Pitaevskii and Stringari [15] argued that the low-lying excitation frequencies would have much better perspectives

in typical experimental setups to provide signatures of quantum fluctuations than measurements of the condensate depletion. They found that the frequency correction would amount to as much as 1%, being, therefore, possible to resolve from usual experimental errors in frequency measurements, which in some experiments were not larger than 0.4% [76].

The measurement of the quantum corrected oscillation frequencies as suggested in Ref. [15] seemed to be quite realistic, as interaction tunability by means of a Feshbach resonance was implemented in ^{85}Rb-samples [77]. Indeed, in that system, the shift of the collective excitations were expected to be about 10%. However, these measurements in atomic alkali never took place, mainly due to the fact that these condensates are short lived at large values of the s-wave scattering length a_s. Nonetheless, the results of Refs. [15,75] were supported by Monte-Carlo simulations [78] and the corresponding measurements of the breathing mode in the BEC side of a Feshbach resonance [79].

1.5 Dipolar Quantum Gases

The experimental realization of Bose-Einstein condensation in dilute quantum gases triggered further developments in cold-atoms physics besides those related to the realization of quantum degeneracy in Fermi gases. Attracted by the possibility of studying the long-range and anisotropic dipole-dipole interaction in a controlled way, many theorists dedicated themselves to develop the appropriate framework for investigating dipolar systems and set the stage for the experimental studies which would follow. In this section, we will give a broad overview on the properties and techniques involved in the study of dipolar quantum gases focusing on the experimental realizations. For detailed information, we refer to recent review articles [80–82].

Let us start the description of dipolar quantum gases by commenting on the construction of the corresponding pseudo-potential by L. You and coworkers [83–86]. Assuming that the van der Waals forces between the atoms can be approximated at low energies by and effective contact interaction, the interaction potential in the presence of a dc-field takes the form

$$V(\mathbf{x}) = g\delta(\mathbf{x}) + V_{\mathrm{dd}}(\mathbf{x}), \tag{1.10}$$

where the strength of the contact interaction reads

$$g = \frac{4\pi\hbar^2 a_s}{M} \tag{1.11}$$

and the second term in Eq. (1.10) is given by

$$V_{\mathrm{dd}}(\mathbf{x}) = \frac{C_{\mathrm{dd}}}{4\pi|\mathbf{x}|^3}\left(1 - 3\cos^2\theta\right). \tag{1.12}$$

Here the constant C_{dd} is related to the atomic electric polarizability and θ is the angle between the direction of polarization and the relative position of the dipoles. Due to the anisotropy in the dipolar interaction potential (1.12), dipolar quantum gases tend to be stretched along the polarization direction, since this leads to a lower interaction energy. This effect is depicted in Fig. 1.3 which was produced by the group of T. Pfau in order to illustrate their results on a ^{52}Cr condensate [87]. Nonetheless, the

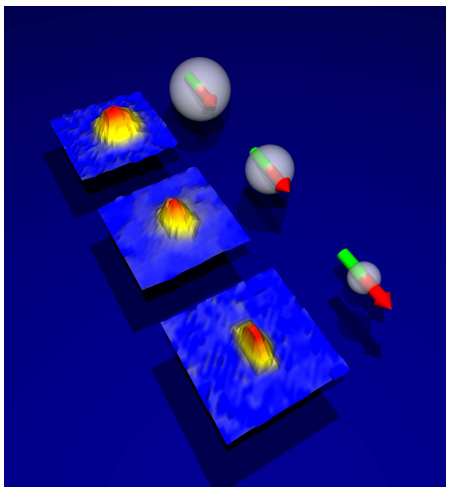

Figure 1.3: Schematic representation of the effect observed on Bose-Einstein condensates due to the anisotropy of the dipole-dipole interaction. From top to bottom the relative importance of the long-range and anisotropic dipole-dipole interaction is increased with respect to the isotropic and short-range contact interaction. The resulting condensate elongation along the polarization direction of the dipoles, represented by the sizes of the spheres relative to the arrows, is shown in the corresponding experimental images. The picture was obtained from the homepage of research group of T. Pfau [87], which contains a brief explanation of their experimental results obtained with ^{52}Cr-atoms [89].

same reasoning remains valid for fermionic dipoles. Soon after that, the first study involving magnetic dipoles appeared [88].

For definiteness, we will not stick to the notations and particular considerations of the many authors involved but will, instead, adopt a notation which became later on more or less standard. Therefore, troughout this thesis, the dipole-dipole interaction of magnetic origin, i.e., for particles with magnetic dipoles m, is characterized by $C_{\mathrm{dd}} = \mu_0 m^2$, with μ_0 being the magnetic permeability in vacuum. Magnetic moments are expressed in units of the Bohr magneton μ_{B}. In the case of electric dipole moments, the interaction strength is $C_{\mathrm{dd}} = 4\pi d^2$, with the electric dipole moment d being expressed in the unit of Debye.

As a result of a sophisticate multi-channel scattering theory, the s-wave scattering length becomes a function of the dipolar interaction strength and the interaction potential (1.10) can be written as

$$V_{\mathrm{int}}(\mathbf{x}) = \frac{4\pi\hbar^2 a_s(C_{\mathrm{dd}})}{M}\delta(\mathbf{x}) + V_{\mathrm{dd}}(\mathbf{x}). \tag{1.13}$$

Thus, in general, the dependence of the s-wave scattering length on the dipole moment has to be taken into account. This is particularly important if an external electric field is used to modify the dipole moment close to a shape resonance [86]. Away from these resonances the s-wave scattering length can be approximately considered as independent of the dipolar interaction strength C_{dd}. Since it is not possible to single out the contribution of the Van der Waals forces from that of the dipole-dipole interaction in experiments, we will leave in this thesis the separation implicit and refer to the s-wave scattering length a_s as the length occurring in the coefficient of the delta distribution function in the interaction potential.

It is useful to define the relative interaction strength for single-component quantum gases according to

$$\epsilon_{\mathrm{dd}}^{\mathrm{b}} = \frac{C_{\mathrm{dd}}}{3g}, \tag{1.14}$$

in the case of bosonic dipoles and, correspondingly

$$\epsilon_{\mathrm{dd}}^{\mathrm{f}} = \frac{C_{\mathrm{dd}}}{4\pi} \left(\frac{M^3 \overline{\omega}}{\hbar^5} \right)^{\frac{1}{2}} N^{\frac{1}{6}}, \tag{1.15}$$

for fermionic dipoles, where the geometric averaged trap frequency $\overline{\omega}$ is defined in Eq. (1.6).

The main difference between the two definitions lies in the Pauli exclusion principle. While Bose gases are allowed to collide in the s-wave scattering channel, this is forbidden for fermions. Furthermore, while bosons can accumulate in the one-particle ground-state, fermions can only occupy empty energy levels. As a result, in the case of particles with frozen spin at low temperatures, bosonic gases are stabilized by a repulsive contact interaction and fermionic ones by the Fermi pressure. This explains why $\epsilon_{\mathrm{dd}}^{\mathrm{f}}$ in Eq. (1.15) depends on both the mean trapping frequency $\overline{\omega}$ and the particle number N.

In the next subsections we will outline the experimental and the theoretical situation concerning both bosonic and fermionic systems where the dipole-dipole interaction is important.

1.5.1 Dipolar Bose-Einstein Condensates

Let us start the discussion about dipolar condensates by stating what this expression means. In this thesis, we will call a dipolar condensate all Bose-Einstein condensates in which the dipole-dipole interaction plays a measurable role. To date, the condensate where the dipole-dipole interaction is most important is the one of Chromium ^{52}Cr, which possesses a magnetic dipole moment of six Bohr magnetons μ_{B} and was first realized by the Pfau group in Stuttgart back in 2005 [32]. In the meantime, condensation of chromium has also been achieved by the group of O. Gorceix in Paris [90]. The Paris group also investigates the fermionic isotope ^{53}Cr which they were able to trap simultaneously with the bosonic one [91].

Following the construction of the pseudo-potential for the dipolar quantum gases, other studies were performed that considered Bose-Einstein condensation in dipolar systems. Either by solving the Gross-Pitaevskii equation numerically [88] or by considering a Gaussian trial wave function [85,92,93], static and dynamic properties of dipolar condensates were investigated. Among these investigations, the exhibition of a roton in the excitation spectrum of a dipolar condensate is a remarkable property because of the link to the physics of helium [94,95].

A major development in the theoretical description of dipolar condensates was achieved by C. Eberlein and coworkers in 2003, who proved that the exact density profile of a dipolar condensate in the Thomas-Fermi regime remains parabolic, as in the contact case, but is stretched by the presence of the dipole-dipole interaction along the polarization direction. These authors used the exact static Thomas-Fermi solution of the Gross-Pitaevskii equation [96] to investigate the hydrodynamic excitations in these systems [97].

The first observable signature of the dipole-dipole interaction was obtained in ^{52}Cr using the time-of-flight technique in a well suited trap configuration [98]. Indeed, due to the anisotropy of the interaction

the condensate aspect ratio as a function of time after release from the trap behaves differently depending on whether the dipoles are aligned along or perpendicular to the trap symmetry axis. By exploring this feature, the Stuttgart group was able to characterize the presence of the dipole-dipole interaction unambiguously in chromium samples away from Feshbach resonances, where the relative interaction strength (1.14) takes the value $\epsilon_{\mathrm{dd}}^{\mathrm{b}} = 0.16$. The measurement of this small effect was just the first of a series of far-reaching experiments in ^{52}Cr.

The relative importance of the dipole-dipole interaction can be enhanced by using a Feshbach resonance to tune the s-wave scattering length to smaller values, thereby enhancing $\epsilon_{\mathrm{dd}}^{\mathrm{b}}$ according to Eq. (1.14) [99]. This was the crucial step which made many important studies of dipolar interactions in chromium possible. For example, this technique allowed for exploring the stability diagram in the $\lambda - \epsilon_{\mathrm{dd}}^{\mathrm{b}}$-plane [100], where a purely dipolar condensate was stabilized, as well as the observation of a strongly dipolar condensate [89], in which the characteristic inversion of the aspect ratio in the course of time was suppressed.

The most astonishing experiment on the dipolar nature of chromium was the observation of the d-wave Bose-nova [101,102]. By using a Feshbach resonance to tune the contact interaction, which is the source of stabilization against the attractive part of the dipole-dipole interaction, below a critical limit, the famous Bose-nova experiment in ^{7}Li by C. A. Sackett et al. [103] could be reedited, this time featuring an explosion with d-wave character. The experiment also exhibited remarkable agreement with simulations of the Gross-Pitaevskii equation once an additional term was included, which takes into account three-body losses.

As a matter of fact, the control of interactions in atomic system has achieved such a high level of precision that the dipolar effects were shown to exist even in gases of alkali atoms, which possess $m = 1\mu_{\mathrm{B}}$. Indeed, a helical spin structure in a ^{87}Rb condensate with total spin $F = 1$ has been shown to decay in favor of spontaneous spin textures due to the presence of the dipole-dipole interaction [104]. Furthermore, tuning the s-wave scattering length in ^{7}Li also provides evidence for the anisotropy of the dipole-dipole interaction as it affects the geometry of the sample [105].

1.5.2 Dipolar Degenerate Fermi Gases

The experimental developments in dipolar Bose-Einstein condensates triggered much theoretical effort in understanding and exploring the properties of dipolar Fermi gases. The first theoretical study of dipolar Fermi gases dates back to 2001 and considered a semiclassical theory of normal fermionic dipoles [106]. This was shortly afterwards applied to the investigation of hydrodynamic excitations in that system [107]. To this end a Gaussian ansatz for the particle density was considered under the assumption that the momentum distribution is isotropic. The next step was the consideration of anisotropic pairing in polarized dipolar gases in both homogeneous [108] and harmonically trapped samples [109]. In addition, a few other remarkable predictions have been made for trapped dipolar gases such as fractional quantum Hall states [110] and Wigner crystallization in rotating two-dimensional systems [111].

The initial investigations of dipolar Fermi gases had overseen an important point: the fact that the momentum distribution of a Fermi gas is deformed by the presence of the dipole-dipole interaction. This was only recently clarified by H. Pu and coworkers [112]. Since then, many theoretical investigations

have followed, which took this effect into account. Concerning homogeneous gases, the Kosterlitz-Thouless phase transition [113] and the existence of nematic phases [114,115] have been considered. Moreover, Fermi liquid theoretical studies have been carried out [116,117] and the existence of density wave ordering has been investigated in two-dimensional systems [118].

From the experimental point of view there are different possibilities of realizing dipolar Fermi gases. One of them is to use atoms which have large permanent magnetic dipole moments m, such as the isotope ^{53}Cr of chromium, which has already been magneto-optically trapped [91]. In addition, recent developments in laser cooling of the isotope ^{66}Dy of dysprosium, which has a magnetic dipole moment of the order $m \sim 10\ \mu_{\mathrm{B}}$, promises to increase the variety of highly magnetic atomic gases in the quantum degenerate regime [33]. A few other elements could be used to investigate magnetic dipolar interactions such as ytterbium and erbium. The former has been brought to quantum degeneracy and possesses a metastable state with a magnetic moment of $m = 3\ \mu_{\mathrm{B}}$ while the latter element has a dipole moment of $m = 7\ \mu_{\mathrm{B}}$ and has been recently magneto-optically trapped [119].

A further exciting possibility is displayed by samples of heteronuclear polar molecules because they possess large electric dipole moments. For them, prospects for collisional control through applied electric fields [120] indicate that dipolar gases could be explored all the way from the weak- (collisionless) to the strong-interaction (hydrodynamic) regime, since this may lead to interaction strengths changing by orders of magnitude depending on the applied electric field [121]. This is in close analogy to the use of Feshbach resonances to tune the contact interaction to unitarity as has been carried out with success to observe hydrodynamic behavior in the normal phase of atomic Fermi gases [122]. Experimentally this is very promising and, recently, 4×10^4 fermionic ^{40}K^{87}Rb molecules with an electric dipole moment of about 0.5 Debye have been brought close to quantum degeneracy by using stimulated Raman adiabatic passage (STIRAP) to efficiently convert the molecules into the rovibrational ground state [123]. After that, further progress towards probing quantum degeneracy has been made by bringing this system into the hyperfine ground state as well [124]. Later on, ^{40}K^{87}Rb-samples at the temperature $T = 1.4\ T_{\mathrm{F}}$, where T_{F} is the Fermi temperature, have become available, where thermodynamic measurements led to the observation of the anisotropy which is the characteristic feature of the dipole-dipole interaction [125]. Further studies of this molecular system close to quantum degeneracy have made it possible to measure the momentum and spatial distribution by direct absorption imaging combined with the time-of-flight technique [126].

As we have seen, quantum degenerate heteronuclear polar molecules possess strong dipolar interactions which might lead to a collisional regime combined with an anisotropic momentum distribution. For this reason, we have recently developed a complete theory for normal dipolar Fermi gases in the hydrodynamic regime in the presence of a cylinder-symmetric harmonic trap [127]. A subsequent extension of our theory to the general case of a triaxial trap was carried out in Ref. [128], which allowed to study important aspects of the physics of dipolar Fermi gases such as the radial quadrupole excitation as well as to sort out the different anisotropic effects of the dipole-dipole interaction.

1.6 This Thesis

The present thesis deals with the physical properties of quantum degenerate gases - both bosonic and fermionic - interacting through the anisotropic and long-range dipole-dipole potential. In order to increase clarity in the exposition of the topics, this thesis is divided into two parts. Part I is dedicated to dipolar Bose-Einstein condensates while Part II is devoted to dipolar Fermi gases.

In **Chapter 2** we present the basic techniques involving the study of Bose-Einstein condensed gases in a general and concise form. Starting from the definition of Bose-Einstein condensation and following the Bogoliubov prescription, we investigate both the Gross-Pitaevskii mean-field theory and the first corrections due to quantum fluctuations. We show that the mean-field description of a condensate is carried out through the analysis of the Gross-Pitaevskii equation, from which we develop the corresponding hydrodynamic equations. To investigate the quantum fluctuations, we generalize the Bogoliubov-de Gennes approach to include non-local interactions and devise explicit expressions for the physical quantities of interest such as the ground-state energy and the spectrum of excitations. In the following three chapters we explicitly apply this theory to investigate Bose-Einstein condensates including the effects of the dipole-dipole interaction.

The physical properties of homogeneous dipolar Bose-Einstein condensates are considered in detail in **Chapter 3**. Despite the fact that homogeneous quantum gases are not available experimentally, analyzing them is quite often of great help for understanding the properties of their trapped counterpart. In the present case, the Bogoliubov theory of homogeneous condensates with pure contact interaction is extended to dipolar condensates. With the help of a Bogoliubov transformation, we derive analytical expressions for the physical quantities of interest such as the condensate depletion as well as the ground-state energy. In addition, having calculated the equation of state beyond the mean-field approximation, we apply the hydrodynamic theory in order to obtain the Beliaev correction to the speed of sound.

The properties of *harmonically trapped* dipolar Bose-Einstein condensates is the main object of investigation of the first part of this thesis. For this reason, their discussion is presented in two chapters so that Chapter 4 contains the mean-field description of trapped dipolar condensates, where we revisit the problem once solved through the effort of many authors by using our own original approach. Chapter 5, on the other hand, contains original results concerning beyond mean-field corrections to the properties of dipolar Bose-Einstein condensates, which are being prepared for publication [129].

In the beginning of **Chapter 4**, an original proof is provided for the exact result that the Thomas-Fermi density profile of a dipolar condensate remains an inverted parabola as in the case of pure contact interaction. We then use this result as an input of a time-dependent variational approach which is able to deal adequately with the mean-field physics of the system, thereby using the Thomas-Fermi radii as variational parameters. This procedure is the starting point for investigating the static as well as the dynamic properties of the system by means of the corresponding equations of motion for the Thomas-Fermi radii. Then, we are able to study in detail quantities such as the equilibrium values of the Thomas-Fermi radii and the stability diagram. In addition, we also consider the low-lying oscillations and the time-of-flight dynamics of the system.

In **Chapter 5**, we specialize the Bogoliubov-de Gennes formalism to the case of a harmonically trapped dipolar condensate. As the Bogoliubov-de Gennes equations are very hard to solve due to

the non-locality of the dipole-dipole interaction, we resort to the local density approximation for the exchange interaction between the condensate and the excited particles. In this way we are able to derive analytical expressions for the condensate depletion and for the ground-state energy. The latter expression, in turn, allows us to derive the quantum corrected equations of motion with which the effects of quantum fluctuations in trapped dipolar Bose-Einstein condensates are investigated. Thereby, we identify the anisotropy of the dipole-dipole interaction as a key feature, which allows to switch from regimes where quantum fluctuations play no role into other regimes where quantum corrections cannot be neglected, by changing the trap aspect ratio. This offers a unique way to tune the effects of quantum fluctuations in cold atomic systems.

We present, in **Chapter 6**, the Hartree-Fock theory of strongly interacting normal Fermi gases. Starting from the quantum field theoretical approach to fermionic gases in the Hartree-Fock approximation, we derive the equations of motion for the creation and annihilation fields. Subsequently, we combine them to obtain the equation governing the time-evolution of the one-body density matrix, from which we derive the hydrodynamic equations for a Fermi gas by means of the center-of-mass expansion. By switching to the Wigner representation, we show that the classical limit of the Hartree-Fock equation is the Boltzmann-Vlasov equation without collision term and discuss general scaling solutions of that equation. In order to derive a variational approach for the dipolar Fermi gas in the collisional regime, we show that the hydrodynamic equations can be derived from an action principle in terms of one-particle orbitals together with the assumption that the phases of all these orbitals coincide. We then adapt this variational approach to the Wigner representation, where it can be implemented most directly.

In **Chapter 7**, we treat one-component fermionic dipolar quantum gases semi-analytically by assuming that the gas is in the hydrodynamic regime. By applying the variational time-dependent Hartree-Fock method, we obtain a complete description of strongly interacting normal dipolar Fermi gases which encompasses their static as well as dynamic properties. At first, we write down the action governing the dynamics of the system in the case of three different trapping frequencies and extremize it with respect to the widths in spatial and momentum distributions, obtaining, thus, the corresponding equations of motion. Having the Thomas-Fermi radii and momenta for the non-interacting degenerate Fermi gas as the units measuring theses quantities in the dipolar gas, we obtain dimensionless variables which make the physical interpretation of the results more enlightening. Then, we derive the equilibrium properties such as the momentum and real-space aspect ratios as functions of the dipolar strength and the trap anisotropies. We also investigate the low-lying oscillations around the equilibrium, where we show that the dipole-dipole interaction gives rise to anisotropic momentum oscillations. Following that, we address the time-of-flight dynamics and discuss the large-time asymptotic values of the momentum and the spatial aspect ratios.

The thesis is concluded in **Chapter 8**, where an overview on the discussed topics is presented which includes a detailed account of the achieved results in both dipolar Bose-Einstein condensates and dipolar degenerate Fermi gases.

Part I

Dipolar Bose Gases

2 Theoretical Description of Bose-Einstein Condensation

In this chapter, we will present the fundamental concepts and theoretical methods involved in the physical description of Bose-Einstein condensates. Starting from the very definition of Bose-Einstein condensation, we will present the field-theoretical formulation of the problem. At first, we will investigate the mean-field approximation through the Gross-Pitaevskii theory. Subsequently, will describe how to take into account the contribution of quantum fluctuations within the Bogoliubov-de Gennes theory, which includes the inhomogeneity due to trapping potential. This chapter settles down the basic formalism to be applied in the first part of this thesis, which is dedicated to bosonic dipoles. For this reason, the theoretical considerations presented here will have a general character in the sense that they apply to different types of interaction and trapping potentials. In the following chapters, we will, therefore, continuously refer to the results derived here.

2.1 Definition of Bose-Einstein Condensation: Long-range Order

We start the discussion of Bose-Einstein condensation by considering a system with N bosonic particles. The particles are supposed to be distributed statistically over the one-particle states of an arbitrary Hamiltonian. We denote these states with an index ν and order them according to the values of their energies ε_ν so that the ground-state energy is $\hbar\omega_0$. At temperature T, the average occupation number for each single-particle state in the grand-canonical ensemble is, according to statistical mechanics, given by the Bose-Einstein distribution

$$\overline{n}_\nu = \frac{1}{e^{(\varepsilon_\nu - \mu)/(k_\mathrm{B}T)} - 1}, \tag{2.1}$$

where μ represents the chemical potential, which is used to fix the number of particles, and k_B represents the Boltzmann constant.

From the physical point of view, only a positive average number $\overline{n}_\nu$ makes sense, thus, imposing the constraint $\varepsilon_\nu - \mu \geq 0$. It is then clearly seen that, if μ is allowed to equal the energy ε_ν of a given single-particle state, the average population of that state diverges and becomes comparable to the total particle number. This can only happen in the ground-state, otherwise some states would acquire a negative occupation number. This macroscopic occupation of the ground-state is precisely the definition of Bose-Einstein condensation.

We would like to remark that, depending on factors such as the existence of internal degrees of freedom like spin or natural labels for the types of bosons such as the two wells of a double well potential, more than one condensate might occur [130]. This phenomenon receives the name of fragmentation of

condensates and will not be treated in this thesis.

In fact, for the one-component systems we are interested in, the chemical potential is obtained by summing the number of particles over all states and requiring the sum to give the total particle number N. In this way, one gets the chemical potential μ as a function of temperature. At high temperatures, the particles are expected to be spread in many high energetic states. From Eq. (2.1), one obtains that a chemical potential μ consistent with this picture for every energy ε_ν should be large and negative. But as the temperature is lowered, the particles will be distributed over the states in such a way that, below a certain critical temperature T_C, μ becomes equal to $\hbar\omega_0$ and Bose-condensation starts to occur.

The implications of the condensation over the whole system are astonishing. For example, the sample becomes quantum coherent even in the long-range limit. To appreciate that, consider the one-body density matrix, defined through

$$n^{(1)}\left(\mathbf{x},\mathbf{x}'\right) = \langle\hat{\Psi}^\dagger(\mathbf{x})\hat{\Psi}(\mathbf{x}')\rangle, \tag{2.2}$$

where the symbol $\langle\bullet\rangle$ denotes the grand-canonical average of the operator $\bullet$ constructed over many-particle states. In addition, the quantum field operators $\hat{\Psi}^\dagger(\mathbf{x})$ and $\hat{\Psi}(\mathbf{x})$ create and annihilate one particle at position $\mathbf{x}$, respectively, and obey the bosonic commutation relations

$$\left[\hat{\Psi}(\mathbf{x}),\hat{\Psi}^\dagger(\mathbf{x}')\right] = \delta(\mathbf{x}-\mathbf{x}'), \quad \left[\hat{\Psi}^\dagger(\mathbf{x}),\hat{\Psi}^\dagger(\mathbf{x}')\right] = 0, \quad \left[\hat{\Psi}(\mathbf{x}),\hat{\Psi}(\mathbf{x}')\right] = 0. \tag{2.3}$$

In second quantized language, one can write the bosonic fields as

$$\hat{\Psi}(\mathbf{x}) = \sum_\nu \hat{a}_\nu\phi_\nu(\mathbf{x}), \quad \hat{\Psi}^\dagger(\mathbf{x}) = \sum_\nu \hat{a}_\nu^\dagger\phi_\nu^*(\mathbf{x}), \tag{2.4}$$

where $\{\phi_\nu(\mathbf{x})\}$ denotes a set of orthonormal one-body wave functions. For the one-body states labeled by ν, the creation and annihilation operators $\hat{a}_\nu$ and $\hat{a}_\nu^\dagger$ satisfy

$$\left[\hat{a}_\nu,\hat{a}_{\nu'}^\dagger\right] = \delta_{\nu,\nu'}, \quad \left[\hat{a}_\nu^\dagger,\hat{a}_{\nu'}^\dagger\right] = 0, \quad [\hat{a}_\nu,\hat{a}_{\nu'}] = 0. \tag{2.5}$$

Due to the special role played by the ground state, it is illustrative to separate it in Eq. (2.5). By doing so, one has

$$\hat{\Psi}(\mathbf{x}) = \hat{a}_0\phi_0(\mathbf{x}) + {\sum_\nu}'\hat{a}_\nu\phi_\nu(\mathbf{x}), \tag{2.6}$$

where the prime after the summation sign indicates that the ground state should be excluded.

Now, the one-body density matrix (2.2) with Eq. (2.6) becomes

$$n^{(1)}\left(\mathbf{x},\mathbf{x}'\right) = \langle n_0\rangle\phi_0^*(\mathbf{x})\phi_0(\mathbf{x}') + {\sum_\nu}'\langle n_\nu\rangle\phi_\nu^*(\mathbf{x})\phi_\nu(\mathbf{x}'), \tag{2.7}$$

where the average of the crossed terms vanishes. For the excited states $\nu \neq 0$, the occupation numbers $\langle n_\nu\rangle$ are of the order one. As a consequence, in the thermodynamic limit, the sum involved in the second term becomes an integral which vanishes for a large value of $|\mathbf{x}-\mathbf{x}'|$ due to the completeness of the one-body orbitals. The first term, on the contrary, might stay finite provided the system is Bose

condensed. In a homogeneous system with volume V, for example, one has

$$\lim_{|\mathbf{x}-\mathbf{x}'|\to\infty} n^{(1)}\left(\mathbf{x},\mathbf{x}'\right) = \frac{N_0}{V}, \tag{2.8}$$

where the condensate density

$$\langle n_0 \rangle = N_0 \tag{2.9}$$

does not vanish in the thermodynamic limit because it is of the order of the particle number N. In the absence of the condensation, however, N_0 is negligible. Thus, the one-body density matrix vanishes at large distances

$$\lim_{|\mathbf{x}-\mathbf{x}'|\to\infty} n^{(1)}\left(\mathbf{x},\mathbf{x}'\right) = 0 \tag{2.10}$$

and no long-range order is present.

In case of an inhomogeneous systems, the correlations do not extend all over to infinity but the one-body density matrix remains finite in the presence of the condensate over a range which is determined by the orbitals $\phi_0(\mathbf{x})$.

2.2 Order Parameter and Bogoliubov Prescription

In the previous section we have seen that the one-body ground state plays a special role and, at very low temperatures, carries most of the physical information about a Bose-condensed gas. This led Bogoliubov to suggest that one could describe a weakly interacting Bose gas at low temperatures through the following substitution

$$\hat{\Psi}(\mathbf{x}) = \Psi(\mathbf{x}) + \delta\hat{\psi}(\mathbf{x}), \tag{2.11}$$

where $\Psi(\mathbf{x})$ is a classical field and $\delta\hat{\psi}(\mathbf{x})$ represents the contribution to the bosonic field coming from quantum or thermal fluctuations.

The field $\Psi(\mathbf{x})$ does not possess any operator character and behaves like a wave function for the condensate. Above the critical temperature T_C, it vanishes while it becomes nonzero if the temperature is lower than T_C. For this reason, $\Psi(\mathbf{x})$ is called the order parameter of the phase transition from an ordinary Bose gas to a condensate.

Referring to the expansion in Eq. (2.4) and the one-body density matrix (2.7), one can identify the order parameter as

$$\Psi(\mathbf{x}) = \sqrt{N_0}\phi_0(\mathbf{x}), \tag{2.12}$$

which is normalized to contain N_0 particles. In general, the interaction has the effect that the spacial distribution of the order parameter has little to do with the one-particle ground-state wave function of the non-interacting Hamiltonian and, therefore, we will work preferentially with the function $\Psi(\mathbf{x})$. Nonetheless, the picture of a wave function for the whole condensate remains valid.

We would like to remark that the Bogoliubov prescription Eq. (2.11) can also be expressed as the substitution of the operators by numbers $\hat{a}_0 \to \sqrt{N_0}$ and $\hat{a}_0^\dagger \to \sqrt{N_0}$. The error committed in doing so is of the order of the commutator $[\hat{a}_0, \hat{a}_0^\dagger] = 1$. This is much smaller than the size of the average values of these operators in the many-particle ground-state, that is of the order N, and can, therefore,

be neglected.

The additional term in Eq. (2.11), given by

$$\delta\hat{\psi}(\mathbf{x}) = \sum_{\nu}{}' \hat{a}_\nu \phi_\nu(\mathbf{x}), \tag{2.13}$$

is assumed to be small and takes fluctuations in the system into account. Of course, for higher temperatures and stronger interactions the role of the fluctuations cannot be neglected and a significant fraction of the system could be excited away from the condensate. Indeed, for strongly interacting systems, such as liquid ^{4}He, the condensate fraction amounts only to about 8% of the particles [11]. But, in contrast to that, Bose-Einstein condensates realized to date have been mostly very well described by the mean-field theory, which amounts to setting $\delta\hat{\psi}(\mathbf{x}) = 0$. Indeed, for current condensates, the demonstration of quantum fluctuation effects is an interesting task both from a theoretical and an experimental point of view [15,77,131].

2.3 Gross-Pitaevskii Theory

In this section, we describe the mean-field theory of Bose-Einstein condensates. At zero temperature and when the interaction is not too strong, one can consider the Bose gas to be governed by a single wave function, which plays the role of an order parameter, as discussed above. These conditions seem, at first, to be quite restrictive, but they apply to the condensates commonly produced in the labs worldwide.

Let us remark that, since we are also interested in the dynamical aspects of the problem, we have to take into account the Heisenberg picture with an explicitly time-dependent field operator $\hat{\Psi}(\mathbf{x}, t)$ and start the analysis by considering the second quantized Hamiltonian which can be divided into two parts

$$\hat{H} = \hat{H}_0 + \hat{H}_{\text{int}}. \tag{2.14}$$

The first part is the one-particle Hamiltonian, which reads

$$\hat{H}_0 = \int \mathrm{d}^3x\, \hat{\Psi}^\dagger(\mathbf{x}, t) \left[-\frac{\hbar^2\nabla^2}{2M} + U_{\text{trap}}(\mathbf{x}) \right] \hat{\Psi}(\mathbf{x}, t). \tag{2.15}$$

The subscript 0 stands for the fact the this Hamiltonian is free of interactions. In addition to the kinetic energy operator $-\hbar^2\nabla^2/2M$, the Hamiltonian $\hat{H}_0$ includes also the effects of an external trapping potential $U_{\text{trap}}(\mathbf{x})$. The interaction Hamiltonian, in turn, is given by

$$\hat{H}_{\text{int}} = \frac{1}{2} \int \mathrm{d}^3x \int \mathrm{d}^3x'\, \hat{\Psi}^\dagger(\mathbf{x}, t)\hat{\Psi}^\dagger(\mathbf{x}', t) V_{\text{int}}\left(\mathbf{x} - \mathbf{x}'\right) \hat{\Psi}(\mathbf{x}', t)\hat{\Psi}(\mathbf{x}, t) \tag{2.16}$$

with a general interaction $V_{\text{int}}(\mathbf{x})$ between two bosons with relative coordinate $\mathbf{x}$. Due to the diluteness of the ultracold quantum gases, three- and higher-particle interactions can be safely neglected.

The most significant interactions realized experimentally until now in Bose-Einstein condensates are the short-range and isotropic contact interaction and the long-range and anisotropic dipole-dipole interaction. For the former, a pseudo-potential has been constructed for low energies which reads

[13,14]

$$V_\delta(\mathbf{x}) = g\delta(\mathbf{x}), \tag{2.17}$$

with $g = 4\pi\hbar^2 a_s/M$. Indeed, the contact interaction works as an effective model for the more realistic van der Waals potential. If the van der Waals potential is approximated by a hard sphere with diameter a_s, Eq. (2.17) is the pseudo-potential which reproduces the true s-wave scattering length a_s at low temperatures [13,14]. As for the dipolar interaction, a pseudo potential was constructed by Li You and coworkers [83,85,86]. For magnetic dipole moments $\mathbf{m}$, for example, the long-range part of the dipolar pseudo-potential reads

$$V_{\rm dd}(\mathbf{x}) = \sum_{i,j} \frac{\mu_0 m_i m_j}{4\pi|\mathbf{x}|^3}\left[\delta_{ij} - \frac{3x_i x_j}{|\mathbf{x}|^2}\right]. \tag{2.18}$$

In this thesis, we will treat the dipolar interaction irrespective whether it is of magnetic or electric nature. In addition, we will consider dipoles polarized along one of the trap symmetry axes, which we assume to be along the z-direction, for definiteness. This corresponds, at present, to the most common experimental situation. Thus, the dipolar interaction potential reads

$$V_{\rm dd}(\mathbf{x}) = \frac{C_{\rm dd}}{4\pi|\mathbf{x}|^3}\left(1 - 3\frac{z^2}{|\mathbf{x}|^2}\right). \tag{2.19}$$

For magnetic dipole moments m the dipole-dipole interaction is characterized by $C_{\rm dd} = \mu_0 m^2$, with μ_0 being the magnetic permeability in vacuum, whereas for electric dipole moments the interaction strength is $C_{\rm dd} = 4\pi d^2$, with the electric dipole moment d expressed in units of Debye.

Here, we shall be interested in systems where both the contact and the dipolar interaction are relevant. Therefore, the total interaction potential is given by

$$V_{\rm int}(\mathbf{x}) = V_\delta(\mathbf{x}) + V_{\rm dd}(\mathbf{x}). \tag{2.20}$$

Having in mind the type of two-body interaction we will work with, let us consider the equations of motion for the field operators, but still keep the interaction unspecified to make the notation succinct, on the one hand, and to highlight the generality of the results, on the other hand. The motion of the field operator $\hat{\Psi}(\mathbf{x},t)$ is governed by the Heisenberg equation

$$i\hbar\frac{\partial}{\partial t}\hat{\Psi}(\mathbf{x},t) = \left[\hat{\Psi}(\mathbf{x},t), \hat{H}\right], \tag{2.21}$$

which leads together with Eqs. (2.14)–(2.16) to

$$i\hbar\frac{\partial}{\partial t}\hat{\Psi}(\mathbf{x},t) = \left[-\frac{\hbar^2\nabla^2}{2M} + U_{\rm trap}(\mathbf{x}) + \int {\rm d}^3x'\, \hat{\Psi}^\dagger(\mathbf{x}',t) V_{\rm int}\left(\mathbf{x}-\mathbf{x}'\right)\hat{\Psi}(\mathbf{x}',t)\right]\hat{\Psi}(\mathbf{x},t). \tag{2.22}$$

At this point we return to the Bogoliubov prescription (2.11) and retain only the leading term in that expression

$$\hat{\Psi}(\mathbf{x},t) \to \Psi(\mathbf{x},t), \quad \hat{\Psi}^\dagger(\mathbf{x},t) \to \Psi^*(\mathbf{x},t). \tag{2.23}$$

Proceeding in this way, we obtain the equation of motion for the order parameter

$$i\hbar\frac{\partial}{\partial t}\Psi(\mathbf{x},t) = \left[-\frac{\hbar^2\nabla^2}{2M} + U_{\text{trap}}(\mathbf{x}) + \int \mathrm{d}^3x'\, \Psi^*(\mathbf{x}',t)V_{\text{int}}\left(\mathbf{x}-\mathbf{x}'\right)\Psi(\mathbf{x}',t)\right]\Psi(\mathbf{x},t). \tag{2.24}$$

This is the time-dependent Gross-Pitaevskii equation, which has become the main tool for theoretical studies of Bose-Einstein condensates. It was derived independently by E. P. Gross [132] and L. P. Pitaevskii [133] in 1961 and was first used to investigate the presence of vortices in weakly interacting Bose gases.

2.3.1 Gross-Pitaevskii Equation from an Action Principle

The Gross-Pitaevskii theory is a classical field theory for the order parameter $\Psi(\mathbf{x},t)$. As such, it can be derived from an action principle and it will turn out to be very instructive to do so. Indeed, as will be shown in Chapter 4, it is sometimes easier to investigate the properties of the condensates at the action level with the help of a suitable variational ansatz than to solve the Gross-Pitaevskii equation itself.

To derive the equation of motion for the condensate wave function $\Psi(\mathbf{x},t)$, consider the action principle

$$\delta\mathcal{A}[\Psi,\Psi^*] = 0, \tag{2.25}$$

where the action $\mathcal{A}[\Psi,\Psi^*]$ takes the form

$$\mathcal{A}[\Psi,\Psi^*] = \int \mathrm{d}^3x \int_{t_1}^{t_2} \mathrm{d}t\, \Psi^*(\mathbf{x},t)\left[i\hbar\frac{\partial}{\partial t} - H(\mathbf{x},t)\right]\Psi(\mathbf{x},t). \tag{2.26}$$

For practical purposes, it is useful to maintain the decomposition of the Hamiltonian $H(\mathbf{x},t)$ according to

$$H(\mathbf{x},t) = H_0(\mathbf{x},t) + H_{\text{int}}(\mathbf{x},t). \tag{2.27}$$

The first component in Eq. (2.27) includes the one-particle energies corresponding to the kinetic and trapping energies and reads

$$H_0(\mathbf{x},t) = -\frac{\hbar^2\nabla^2}{2M} + U_{\text{trap}}(\mathbf{x}), \tag{2.28}$$

while the two-particle interaction is given in the Hamiltonian

$$H_{\text{int}}(\mathbf{x},t) = \frac{1}{2}\int \mathrm{d}^3x'\, V_{\text{int}}(\mathbf{x}-\mathbf{x}')|\Psi(\mathbf{x}',t)|^2. \tag{2.29}$$

The Gross-Pitaevskii equation (2.24) can now be derived by extremizing the classical action (2.26) with respect to the complex conjugate of the order parameter $\Psi^*(\mathbf{x},t)$ by considering the Hamilton functions expressed through equations (2.27)–(2.29):

$$\frac{\delta\mathcal{A}\left[\Psi,\Psi^*\right]}{\delta\Psi^*(\mathbf{x},t)} = 0. \tag{2.30}$$

This equation is a very powerful tool for describing the statics and dynamics of weakly interacting

Bose-Einstein condensates at zero temperature. In the following we will use it to derive general conservation laws which apply for interacting trapped Bose-Einstein condensates and correspond to superfluid hydrodynamics.

2.3.2 Time-independent Gross-Pitaevskii Theory

In order to study static properties of Bose-Einstein condensation such as the equilibrium density, for example, one uses the time independent version of the Gross-Pitaevskii Eq. (2.24). To obtain this equation, we insert into Eq. (2.24) the factorization ansatz

$$\Psi(\mathbf{x},t) = \Psi(\mathbf{x})e^{-i\mu t/\hbar}, \tag{2.31}$$

where μ denotes the chemical potential. The justification for this comes from the spontaneous symmetry-breaking formalism of Bose-Einstein condensation. There, the order parameter is given by

$$\Psi(\mathbf{x},t) = \langle N|\hat{\Psi}(\mathbf{x},t)|N+1\rangle, \tag{2.32}$$

with $\hat{\Psi}(\mathbf{x},t)$ being the annihilation operator in the Heisenberg picture. If one considers the states involved in the average to evolve in time like $e^{iE(N)t/\hbar}$, where $E(N)$ denotes the energy of a state with N particles, Eq. (2.31) follows from the relation $\mu = E(N) - E(N-1)$. This equation shows that the chemical potential μ, i.e., the amount of energy needed to add a particle to the condensate, governs the time evolution of the condensate wave function. For future reference, let us remark that in the thermodynamic limit $N \to \infty$, this leads to the common thermodynamic relation [134]

$$\mu = \frac{\partial E}{\partial N} \tag{2.33}$$

Then, Eq. (2.24) takes the form

$$\Psi(\mathbf{x})\,\mu = \left[-\frac{\hbar^2\nabla^2}{2M} + U_{\rm trap}(\mathbf{x}) + \int \mathrm{d}^3x'\, V_{\rm int}(\mathbf{x}-\mathbf{x}')|\Psi(\mathbf{x}')|^2\right]\Psi(\mathbf{x}), \tag{2.34}$$

which is a non-linear partial differential equation and can also be non-local, depending on the type of interaction.

The first term on the right-hand side of Eq. (2.34) is responsible for the quantum mechanical pressure, which is reflected as a curvature of the particle density. This term is usually negligible under typical laboratory conditions and can be safely neglected in both static and dynamical problems if the interaction is strong enough [135,136]. This neglection of the kinetic energy is defined as the *Thomas-Fermi approximation*, which is opposite to the case of non-interacting condensates, where this term represents an important contribution.

Since the Thomas-Fermi limit is characterized by a negligible kinetic energy, if compared to the interaction energy, the parameter governing the transition from one regime to the other is the ratio between these two energies. In the case of a pure contact interaction, one can estimate the parameter region where the Thomas-Fermi approximation holds. Consider a Gaussian density characterized by a width of the order $\sim a_{\rm ho}$, with the oscillator length $a_{\rm ho} = \sqrt{\hbar/M\overline{\omega}}$ and the geometric mean of

the trap frequencies (1.6). Then, the kinetic energy goes with $N\hbar^2/\left(2Ma_{\rm ho}^2\right)$, while the interaction energy goes with $N^2\hbar^2 a_s/\left(Ma_{\rm ho}^3\right)$, so that the dimensionless parameter governing the transition to the Thomas-Fermi regime is $Na_s/a_{\rm ho}$, which is typically of the order of a few hundred. Concerning the case of a dominantly or even pure dipolar condensate, the picture just described does not apply anymore. This is due to the fact that the dipole-dipole interaction is partially attractive, which renders the condensate unstable. Indeed, experimental studies, in which the s-wave scattering length of ^{52}Cr was reduced, have shown that such a condensate explodes, so to speak, featuring thereby a d-wave pattern, which is characteristic for the dipole-dipole interaction [101,102].

In the Thomas-Fermi regime, the time-independent Gross-Pitaevskii Eq. (2.34) becomes an integral equation from which the condensate density

$$n(\mathbf{x}) = \Psi^*(\mathbf{x})\Psi(\mathbf{x}) \tag{2.35}$$

can be obtained from the integral equation

$$\int \mathrm{d}^3x'\, V_{\rm int}(\mathbf{x}-\mathbf{x}')n(\mathbf{x}') = \mu - U_{\rm trap}(\mathbf{x}). \tag{2.36}$$

If the interaction is given by the contact potential (2.17), Eq. (2.36) is easily solved and the density reads

$$n(\mathbf{x}) = \begin{cases} \frac{\mu - U_{\rm trap}(\mathbf{x})}{g}; & \mu - U_{\rm trap}(\mathbf{x}) \geq 0 \\ 0; & \text{otherwise} \end{cases}. \tag{2.37}$$

The value of the chemical potential is obtained by normalizing the density (2.37) to N particles. We emphasize that the Thomas-Fermi solution of the harmonically trapped condensate with contact interaction alone, given in Eq. (2.37), differs in many aspects from the non-interacting case. Particularly worth mentioning is the fact that the gas acquires well defined borders given by the Thomas-Fermi radii

$$R_i^{\rm TF} = \sqrt{\frac{2\mu}{M\omega_i^2}}. \tag{2.38}$$

One can also write the mean Thomas-Fermi radius in terms of the s-wave scattering length a_s and the oscillator length $a_{\rm ho}$ and finds

$$R^{\rm TF} = a_{\rm ho}\left(\frac{15Na_s}{a_{\rm ho}}\right)^{1/5}. \tag{2.39}$$

Indeed, investigations of the condensate shape have been carried out theoretically and confirmed (2.39) experimentally [137]. Also the measurement of the energy of the condensate after release from the trap, the so called release energy, is consistent with this picture [138].

In the case of a non-local interaction, like the dipole-dipole (2.18), the solution of Eq. (2.36) is much more involved. In Section 4.1 we will solve Eq. (2.36) exactly for a Bose-Einstein condensate featuring the dipole-dipole interaction by showing that the condensate density retains the parabolic character as in solution (2.37) but the anisotropy of the dipolar interaction has to be carefully taken into account.

2.4 Hydrodynamics of Bose-Einstein Condensates

Solving the time-dependent Gross-Pitaevskii Eq. (2.24) is not always the most adequate way to study the properties of Bose-Einstein condensates. When it comes to the low-lying excitations, for example, it is often useful to switch to an equivalent treatment which is provided by the hydrodynamic equations [51].

In a homogeneous system, the hydrodynamic excitations are sound waves, i.e., density fluctuations in the sample. For trapped gases the excitations are not plane waves anymore and have to be classified according to the symmetries present in the trap geometry. Besides the low-lying excitations, which are studied by shaking the gas out of the ground state into the lowest excited states, it is also important to consider time-of-flight experiments, in which the sample is released from the trap, and expands freely in space. Both type of phenomena can be investigated within the hydrodynamic formalism, which we derive now starting from the time-dependent Gross-Pitaevskii Eq. (2.24).

Suitable manipulations of Eq. (2.24) and of its complex conjugate lead to the continuity equation

$$\frac{\partial n(\mathbf{x},t)}{\partial t} + \nabla \cdot \mathbf{j}(\mathbf{x},t) = 0, \tag{2.40}$$

with the current density defined as

$$\mathbf{j}(\mathbf{x},t) = \frac{\hbar}{2Mi}\left[\Psi^*(\mathbf{x},t)\nabla\Psi(\mathbf{x},t) - \Psi(\mathbf{x},t)\nabla\Psi^*(\mathbf{x},t)\right], \tag{2.41}$$

and the particle density

$$n(\mathbf{x},t) = \Psi^*(\mathbf{x},t)\Psi(\mathbf{x},t). \tag{2.42}$$

Building on the fact that the order parameter $\Psi^*(\mathbf{x},t)$ is a complex field, we factorize the condensate wave function according to the Madelung transformation [139]

$$\Psi(\mathbf{x},t) = \sqrt{n(\mathbf{x},t)}e^{iS(\mathbf{x},t)}, \tag{2.43}$$

where the phase $S(\mathbf{x},t)$ is a real quantity. Moreover, we consider that the phase $S(\mathbf{x},t)$ does not contain any singularity. Inserting (2.43) into (2.24) one gets two independent equations corresponding to its real and imaginary part. The latter delivers again the continuity equation Eq. (2.40), provided one uses the definition $\mathbf{j}(\mathbf{x},t) = n(\mathbf{x},t)\mathbf{v}(\mathbf{x},t)$ and identifies the velocity field as

$$\mathbf{v}(\mathbf{x},t) = \frac{\hbar}{M}\nabla S(\mathbf{x},t). \tag{2.44}$$

Correspondingly, the real part yields the Euler equation

$$M\frac{\partial \mathbf{v}(\mathbf{x},t)}{\partial t} = -\nabla\left[-\frac{\hbar^2}{2M}\frac{\nabla^2\sqrt{n(\mathbf{x},t)}}{\sqrt{n(\mathbf{x},t)}} + \frac{M}{2}\mathbf{v}(\mathbf{x},t)^2 + U_{\mathrm{trap}}(\mathbf{x}) + \int \mathrm{d}^3x'\, V_{\mathrm{int}}(\mathbf{x}-\mathbf{x}')n(\mathbf{x}',t)\right], \tag{2.45}$$

which together with Eq. (2.40) forms a closed system of equations for n and $\mathbf{v}$ which is completely equivalent to the Gross-Pitaevskii Eq. (2.24).

It is also enlightening to write down the Euler equation (2.45) in the Thomas-Fermi regime

$$M\frac{\partial \mathbf{v}(\mathbf{x},t)}{\partial t} = -\nabla\left[\frac{M}{2}\mathbf{v}(\mathbf{x},t)^2 + U_{\mathrm{trap}}(\mathbf{x}) + \int \mathrm{d}^3x'\, V_{\mathrm{int}}(\mathbf{x}-\mathbf{x}')n(\mathbf{x}',t)\right], \tag{2.46}$$

since this is the form in which this equation is mostly employed.

Indeed, the static properties of the condensate studied in the previous section can be investigated by setting $\partial n/\partial t = 0$ and $\mathbf{v} = \mathbf{0}$ in Eqs. (2.40) and (2.45). Notice that, in this thesis, we restrict ourselves to condensates which have $\mathbf{v} = \mathbf{0}$ in the ground state.

Despite the fact that they can be used to study static properties, the best application of the hydrodynamic equations is the investigation of the low-lying excitations. Since these are low energetic excitations, their study can be carried out by considering small density fluctuation around the equilibrium $\delta n(\mathbf{x},t)$ so that the total density is $n(\mathbf{x},t) = n(\mathbf{x}) + \delta n(\mathbf{x},t)$. In addition, the velocity field is also small in this range of the excitations. Therefore, one can linearize equations (2.40) and (2.46) around the equilibrium values of the density $n(\mathbf{x})$ and the velocity $\mathbf{v} = \mathbf{0}$. Combining the equations one gets

$$-M\frac{\partial^2 \delta n(\mathbf{x},t)}{\partial t^2} = \nabla\cdot\left\{n(\mathbf{x})\nabla\left[\int \mathrm{d}^3x'\, V_{\mathrm{int}}(\mathbf{x}-\mathbf{x}')\delta n(\mathbf{x}',t)\right]\right\}. \tag{2.47}$$

The wave equation (2.47) is well suited to investigate the hydrodynamic oscillations in the case of pure contact interaction, where it reduces to

$$-M\frac{\partial^2 \delta n(\mathbf{x},t)}{\partial t^2} = \nabla\cdot\left\{\left[\mu - U_{\mathrm{trap}}(\mathbf{x})\right]\nabla\delta n(\mathbf{x},t)\right\}. \tag{2.48}$$

For an uniform system with volume V and density $n = N/V$, the plane wave character of the excitations allows to determine the sound velocity $c = \sqrt{gn/M}$ from Eq. (2.48). For a non-homogeneous gas, though, momentum is not a good quantum number anymore, due to lack of translation invariance. The symmetries of the trapping potential determine the type of excitations which are present. In spherical traps, i.e., for $\omega_x = \omega_y = \omega_z$, for example, angular momentum is a good quantum number and the excitations are characterized by the indexes n, m, and l, characterizing a density deformation of the form [51]

$$\delta n(\mathbf{x},t) = P_l^{2n}(\mathbf{x}/R_{\mathrm{TF}})|\mathbf{x}|^l Y_{l,m}(\theta,\phi)e^{i\Omega t}, \tag{2.49}$$

where R_{TF} is the Thomas-Fermi radius Eq. (2.38). By inserting the density fluctuation Eq. (2.49) into Eq. (2.48), one can obtain the dispersion relation (1.8).

For condensates in cylinder-symmetric traps, i.e., for $\omega_x = \omega_y \neq \omega_z$, only the the z-component of the orbital angular momentum remains a good quantum number and excitations can be classified accordingly. In this case, excitations possessing the same eigenvalue m of the angular momentum in the z-direction become coupled. The two modes corresponding to lowest frequencies are coupled for $m = 0$. They are called the monopole$(+)$ and the quadrupole $(-)$ correspond to in- and out-of-phase oscillations in the z-direction and the $z = 0$-plane, respectively. Their frequencies are given by

$$\Omega_{\pm}^{(0)} = \omega_x\sqrt{\frac{1}{2}\left[4 + 3\lambda^2 \pm \sqrt{9\lambda^4 - 16\lambda^2 + 16}\right]}, \tag{2.50}$$

a result which was first derived by Sandro Stringari [51] and has been verified experimentally by the Ketterle group in MIT [76].

It is interesting to remark that, even in the case of a triaxial trap, where no two frequencies coincide, non-trivial symmetries are present. These symmetries are responsible for the fact that the linearized hydrodynamic equations also admit exact solutions, which separate in elliptic coordinates [140].

It remains to mention the scaling approach to the hydrodynamic equations derived above. It is commonly used to study dynamical properties of cold atomic systems and consists of applying a scaling ansatz of the form

$$n_{\mathrm{sc}}(\mathbf{x},t) = \frac{n(\mathbf{X})}{\mathcal{V}(t)}, \tag{2.51}$$

where the scaling variables read $X_i = x_i/b_i(t)$ and the volume $\mathcal{V}(t)$ is given by $\mathcal{V}(t) = b_x(t)b_y(t)b_z(t)$. In particular, the scaling ansatz satisfies the initial condition $n_{\mathrm{sc}}(\mathbf{x},0) = n(\mathbf{x})$, i.e., $b_i(0) = 1$. Inserting Eq. (2.51) into the continuity equation (2.40), one obtains for the velocity

$$v_i = \frac{\dot{b}_i x_i}{b_i}. \tag{2.52}$$

Combining the scaled versions of the corresponding contributions to the Euler Eq. (2.46), one can derive an equation of motion for the scaling parameters b_i, such that, in equilibrium, one obtains $b_i = 1$ as a solution, as required. The low-lying collective excitations can then be investigated by linearizing this equation around its equilibrium value, as performed in Ref. [141]. In addition, it can also be employed to study the time evolution of Bose-Einstein condensates after release from the harmonic trap. To that end, one should solve these equations in the absence of the term which accounts for the harmonic trap, under the initial conditions $b_i(0) = 1$ and $\dot{b}_i(0) = 1$ [136].

This scaling approach has been widely used to investigate Bose-Einstein condensates with both short-range and long-range interactions [97]. In the following, we shall concern ourselves with long-range interactions, where we find it to be more appropriate to apply a variational method instead.

2.5 Quantum Fluctuations

In this section, we discuss beyond mean-field effects on Bose-Einstein condensates by applying the Bogoliubov formalism, which was initially devised to study homogeneous systems, to non-uniform condensates [12]. In this case, it is called Bogoliubov-de Gennes theory and we refer to the book by P.-G. de Gennes, where it was developed for non-uniform superconductors [142]. Here we will be concerned with the corresponding formalism for a condensate with a general two-particle interaction.

In the framework of the Bogoliubov-de Gennes theory, the time dependence of the fields is not taken explicit account. Nonetheless, we will still be able to study the excitations of the system. This is done by diagonalizing the Hamilton operator by means of a canonical transformation and, thereby, deriving the spectrum of the excitations. The starting point is the grand-canonical Hamilton operator, which takes the form

$$\hat{H}' = \hat{H} - \mu\hat{N}, \tag{2.53}$$

where the Hamiltonian $\hat{H}$ is given in Eqs. (2.14)–(2.16) with the time arguments dropped. In addition,

μ is the Lagrange parameter responsible for the conservation of the total number of particles, which is described by the operator

$$\hat{N} = \int \mathrm{d}^3x\, \hat{\Psi}^\dagger(\mathbf{x})\hat{\Psi}(\mathbf{x}). \tag{2.54}$$

Once more, we make use of the Bogoliubov prescription Eq. (2.11), but this time we consider both the mean value of the quantum fields $\Psi(\mathbf{x})$ and $\Psi^*(\mathbf{x})$ as well as their fluctuations $\delta\hat{\psi}(\mathbf{x})$ and $\delta\hat{\psi}^\dagger(\mathbf{x})$ up to second order in the fluctuations. Replacing the field operators $\hat{\Psi}(\mathbf{x})$ and $\hat{\Psi}^\dagger(\mathbf{x})$ by $\Psi(\mathbf{x})+\delta\hat{\psi}(\mathbf{x})$ and $\Psi^*(\mathbf{x})+\delta\hat{\psi}^\dagger(\mathbf{x})$, respectively, the grand-canonical Hamilton operator $\hat{H}'$ can be written as

$$\begin{aligned}\hat{H}' &= E_{\mathrm{G}}^{(0)\prime} + \int \mathrm{d}^3x\, \delta\hat{\psi}^\dagger(\mathbf{x})H_{\mathrm{Fl}}(\mathbf{x})\delta\hat{\psi}(\mathbf{x}) + \frac{1}{2}\int \mathrm{d}^3x \int \mathrm{d}^3x'\, V_{\mathrm{int}}\left(\mathbf{x}-\mathbf{x}'\right)\Big[\delta\hat{\psi}^\dagger(\mathbf{x})\delta\hat{\psi}^\dagger(\mathbf{x}')\Psi(\mathbf{x}')\Psi(\mathbf{x}) \\ &\quad +2\delta\hat{\psi}^\dagger(\mathbf{x})\delta\hat{\psi}(\mathbf{x}')\Psi^*(\mathbf{x}')\Psi(\mathbf{x}) + \delta\hat{\psi}(\mathbf{x})\delta\hat{\psi}(\mathbf{x}')\Psi^*(\mathbf{x}')\Psi^*(\mathbf{x})\Big] + \cdots,\end{aligned} \tag{2.55}$$

where we have assumed that the interaction possesses the symmetry $V_{\mathrm{int}}\left(\mathbf{x}-\mathbf{x}'\right) = V_{\mathrm{int}}\left(\mathbf{x}'-\mathbf{x}\right)$. The first term in Eq. (2.55), which is of zeroth order in the fluctuations, is related to the ground-state energy of the Gross-Pitaevskii theory

$$E_{\mathrm{G}}^{(0)} = \int \mathrm{d}^3x\, \Psi^*(\mathbf{x})H(\mathbf{x})\Psi(\mathbf{x}). \tag{2.56}$$

according to

$$E_{\mathrm{G}}^{(0)\prime} = E_{\mathrm{G}}^{(0)} - \mu N_0. \tag{2.57}$$

The terms in Hamiltonian (2.55) which are of first order in the fluctuations vanish due to the fact that the order parameter obeys the Gross-Pitaevskii theory. In addition, we have introduced the short-hand

$$H_{\mathrm{Fl}}(\mathbf{x}) = H_0 - \mu + \int \mathrm{d}^3x'\, \Psi^*(\mathbf{x}')V_{\mathrm{int}}\left(\mathbf{x}-\mathbf{x}'\right)\Psi(\mathbf{x}') \tag{2.58}$$

for the part of the Hamiltonian which is diagonal in the fluctuations $\delta\hat{\psi}^\dagger$ and $\delta\hat{\psi}$. It is interesting to remark that the fluctuation Hamiltonian (2.58) contains a Hartree interaction potential, which is represented by the third term in the right-hand side of Eq. (2.58).

In order to diagonalize the Hamiltonian above, we follow de Gennes [142] and introduce the expansion of the quantum fluctuations

$$\delta\hat{\psi}(\mathbf{x}) = \sum_\nu{}' \left[\mathcal{U}_\nu(\mathbf{x})\hat{\alpha}_\nu + \mathcal{V}_\nu^*(\mathbf{x})\hat{\alpha}_\nu^\dagger\right], \quad \delta\hat{\psi}^\dagger(\mathbf{x}) = \sum_\nu{}' \left[\mathcal{U}_\nu^*(\mathbf{x})\hat{\alpha}_\nu^\dagger + \mathcal{V}_\nu(\mathbf{x})\hat{\alpha}_\nu\right], \tag{2.59}$$

where the creation and annihilation operators $\hat{\alpha}_\nu^\dagger$ and $\hat{\alpha}_\nu$ also satisfy bosonic commutation relations.

The Bogoliubov-de Gennes transformation in Eq. (2.59) is a canonical transformation if the functions $\mathcal{U}_\nu(\mathbf{x})$ and $\mathcal{V}_\nu(\mathbf{x})$ satisfy the condition

$$\int \mathrm{d}^3x\, \left[\mathcal{U}_\nu^*(\mathbf{x})\mathcal{U}_{\nu'}(\mathbf{x}) - \mathcal{V}_\nu^*(\mathbf{x})\mathcal{V}_{\nu'}(\mathbf{x})\right] = \delta_{\nu,\nu'}. \tag{2.60}$$

To determine the amplitudes $\mathcal{U}_\nu(\mathbf{x})$ and $\mathcal{V}_\nu(\mathbf{x})$, we first calculate the commutators of the Hamiltonian

(2.55) with the fluctuations $\delta\hat{\psi}(\mathbf{x})$ and $\delta\hat{\psi}^\dagger(\mathbf{x})$

$$\begin{aligned}\left[\hat{H}', \delta\hat{\psi}(\mathbf{x})\right] &= -H_{\rm Fl}(\mathbf{x})\delta\hat{\psi}(\mathbf{x}) - \int \mathrm{d}^3x'\, V_{\rm int}\left(\mathbf{x}-\mathbf{x}'\right)\left[\Psi(\mathbf{x})\Psi(\mathbf{x}')\delta\hat{\psi}^\dagger(\mathbf{x}') + \Psi^*(\mathbf{x}')\Psi(\mathbf{x})\delta\hat{\psi}(\mathbf{x}')\right], \\ \left[\hat{H}', \delta\hat{\psi}^\dagger(\mathbf{x})\right] &= H_{\rm Fl}(\mathbf{x})\delta\hat{\psi}^\dagger(\mathbf{x}) + \int \mathrm{d}^3x'\, V_{\rm int}\left(\mathbf{x}-\mathbf{x}'\right)\left[\Psi^*(\mathbf{x})\Psi(\mathbf{x}')\delta\hat{\psi}^\dagger(\mathbf{x}') + \Psi^*(\mathbf{x}')\Psi^*(\mathbf{x})\delta\hat{\psi}(\mathbf{x}')\right].\end{aligned} \tag{2.61}$$

Since we will diagonalize the Hamiltonian (2.55) through the transformation Eq. (2.59), it will have the final form

$$\hat{H}' = E'_{\rm G} + {\sum_\nu}' \varepsilon_\nu \hat{\alpha}^\dagger_\nu \hat{\alpha}_\nu, \tag{2.62}$$

where $E'_{\rm G}$ represents the corrected ground-state energy. As a consequence of Eq. (2.62), the creation and annihilation operators $\hat{\alpha}^\dagger_\nu$ and $\hat{\alpha}_\nu$ satisfy the following commutation relations

$$\begin{aligned}\left[\hat{H}', \hat{\alpha}_\nu\right] &= -\varepsilon_\nu \hat{\alpha}_\nu, \\ \left[\hat{H}', \hat{\alpha}^\dagger_\nu\right] &= \varepsilon_\nu \hat{\alpha}^\dagger_\nu.\end{aligned} \tag{2.63}$$

Inserting (2.59) into (2.61) and comparing the coefficients of the corresponding operators with the ones in Eq. (2.63), one arrives at the Bogoliubov-de Gennes equations for a Bose-Einstein condensate:

$$\begin{aligned}\varepsilon_\nu \mathcal{U}_\nu(\mathbf{x}) &= H_{\rm Fl}(\mathbf{x})\mathcal{U}_\nu(\mathbf{x}) + \int \mathrm{d}^3x'\, V_{\rm int}\left(\mathbf{x}-\mathbf{x}'\right)\left[\Psi(\mathbf{x}')\Psi(\mathbf{x})\mathcal{V}_\nu(\mathbf{x}') + \Psi^*(\mathbf{x}')\Psi(\mathbf{x})\mathcal{U}_\nu(\mathbf{x}')\right], \\ -\varepsilon_\nu \mathcal{V}_\nu(\mathbf{x}) &= H_{\rm Fl}(\mathbf{x})\mathcal{V}_\nu(\mathbf{x}) + \int \mathrm{d}^3x'\, V_{\rm int}\left(\mathbf{x}-\mathbf{x}'\right)\left[\Psi^*(\mathbf{x}')\Psi^*(\mathbf{x})\mathcal{U}_\nu(\mathbf{x}') + \Psi(\mathbf{x}')\Psi^*(\mathbf{x})\mathcal{V}_\nu(\mathbf{x}')\right].\end{aligned} \tag{2.64}$$

Notice that besides the direct interaction between the condensate and the excited particles, which is contained in the fluctuation Hamiltonian (2.58), the Bogoliubov-de Gennes equations (2.64) also contain exchange terms. In case of a contact interaction, the integrals become trivial and the exchange terms do not represent a major difficulty. In the presence of a long-range interaction, however, evaluating the corresponding convolutions requires knowledge of both the condensate wave function $\Psi(\mathbf{x})$ as well as of the Bogoliubov amplitudes $\mathcal{U}_\nu(\mathbf{x})$ and $\mathcal{V}_\nu(\mathbf{x})$.

Let us examine the energy ε_ν, which emerges as a solution of the Bogoliubov-de Gennes Eqs. (2.64). We are interested in solutions for which the energy ε_ν is real and this is guaranteed by the normalization condition Eq. (2.60). To see it better, let us consider the following equation

$$(\varepsilon_\nu - \varepsilon^*_\nu)\int \mathrm{d}^3x\, \left[\mathcal{U}^*_\nu(\mathbf{x})\mathcal{U}_\nu(\mathbf{x}) - \mathcal{V}^*_\nu(\mathbf{x})\mathcal{V}_\nu(\mathbf{x})\right] = 0, \tag{2.65}$$

which is obtained from suitable manipulations of the Bogoliubov-de Gennes Eqs. (2.64). By using the normalization condition (2.60), it follows from Eq. (2.65) that the energy ε_ν must be real. Moreover,

by proceeding along the same lines, one finds that the energy ε_ν is given by

$$\begin{aligned}\varepsilon_\nu &= \int \mathrm{d}^3x \left\{ H_{\mathrm{Fl}}(\mathbf{x}) \left[\mathcal{U}_\nu^*(\mathbf{x})\mathcal{U}_\nu(\mathbf{x}) + \mathcal{V}_\nu^*(\mathbf{x})\mathcal{V}_\nu(\mathbf{x})\right] + \int \mathrm{d}^3x' \, V_{\mathrm{int}}\left(\mathbf{x}-\mathbf{x}'\right) \left[\Psi(\mathbf{x}')\Psi(\mathbf{x})\mathcal{U}_\nu^*(\mathbf{x})\mathcal{V}_\nu(\mathbf{x}')\right.\right. \\ &\left.\left. + \Psi^*(\mathbf{x}')\Psi(\mathbf{x})\mathcal{U}_\nu^*(\mathbf{x})\mathcal{U}_\nu(\mathbf{x}') + \Psi^*(\mathbf{x}')\Psi^*(\mathbf{x})\mathcal{V}_\nu^*(\mathbf{x})\mathcal{U}_\nu(\mathbf{x}') + \Psi(\mathbf{x}')\Psi^*(\mathbf{x})\mathcal{V}_\nu^*(\mathbf{x})\mathcal{V}_\nu(\mathbf{x}')\right] \right\}, \quad (2.66)\end{aligned}$$

which is explicitly real.

It is also important to consider some properties of the Bogoliubov-de Gennes equations Eq. (2.64). For example, if $\begin{pmatrix} \mathcal{U}_\nu \\ \mathcal{V}_\nu \end{pmatrix}$ is a solution with energy ε_ν, then $\begin{pmatrix} \mathcal{V}_\nu^* \\ \mathcal{U}_\nu^* \end{pmatrix}$ corresponds to a solution with energy $-\varepsilon_\nu$. Since these two solutions must be orthogonal to each other, one obtains the important identities

$$\int \mathrm{d}^3x \, \left[\mathcal{U}_\nu(\mathbf{x})\mathcal{V}_{\nu'}(\mathbf{x}) - \mathcal{U}_{\nu'}(\mathbf{x})\mathcal{V}_\nu(\mathbf{x})\right] = \int \mathrm{d}^3x \, \left[\mathcal{U}_\nu^*(\mathbf{x})\mathcal{V}_{\nu'}^*(\mathbf{x}) - \mathcal{U}_{\nu'}^*(\mathbf{x})\mathcal{V}_\nu^*(\mathbf{x})\right] = 0, \quad (2.67)$$

where ν and ν' might be equal or not. In fact, these identities are responsible for the Hamiltonian (2.53) actually assuming the diagonal form given by Eq. (2.62).

Let us now return to the Hamiltonian (2.53) and explore the physical content of the diagonalized form (2.62). By definition, the ground state $|0\rangle$ of the diagonalized Hamiltonian Eq. (2.62) is a state which does not contain any excitation and, therefore, can be found from the equation

$$\hat{\alpha}_\nu|0\rangle = 0. \quad (2.68)$$

Since the operators $\hat{\alpha}_\nu$ and $\hat{\alpha}_\nu^\dagger$ are superpositions of the creation and annihilation operators for the real particles $\hat{a}^\dagger$ and $\hat{a}$, this state is called a quasiparticle vacuum. In addition, the excitations are described in terms of quasiparticles, which exist in a space generated by the $\hat{\alpha}$-operators.

It is interesting to consider the number of particles in the many-body ground state $|0\rangle$, which can be obtained by letting the number operator (2.54) act on it by taking into account the Bogoliubov prescription (2.11) and the transformation (2.59). The final result is

$$\langle 0|\hat{N}|0\rangle = N_0 + \sum_\nu{}' \int \mathrm{d}^3x \, \mathcal{V}_\nu^*(\mathbf{x})\mathcal{V}_\nu(\mathbf{x}). \quad (2.69)$$

We conclude that the total number of particles is a sum of the condensed particles, which occupy the one-particle ground state, and excited particles, which are moved due to the interaction from the one-particle ground-state to one-particle excited states. This phenomenon is called *depletion* of the condensate. For future reference, we shall like to have the condensate depletion $\Delta N = N - N_0$ defined through the expression

$$\Delta N = \sum_\nu{}' \int \mathrm{d}^3x \, \mathcal{V}_\nu^*(\mathbf{x})\mathcal{V}_\nu(\mathbf{x}) \quad (2.70)$$

as well as the corresponding depletion density

$$\Delta n(\mathbf{x}) = \sum_\nu{}' \mathcal{V}_\nu^*(\mathbf{x})\mathcal{V}_\nu(\mathbf{x}). \quad (2.71)$$

In order to obtain the ground-state energy, one must evaluate the expectation value of Hamiltonian (2.53) with respect to the ground state $|0\rangle$, provided one writes the fluctuation operators according to the canonical transformation (2.59). This leads to

$$\begin{aligned}\langle 0|\hat{H}'|0\rangle &= E_{\mathrm{G}}^{(0)\prime} + \frac{1}{2}{\sum_{\nu}}' \Big\{ \varepsilon_\nu - \int \mathrm{d}^3x \, \left[\mathcal{U}_\nu^*(\mathbf{x}) H_{\mathrm{Fl}}(\mathbf{x}) \mathcal{U}_\nu(\mathbf{x}) - \mathcal{V}_\nu^*(\mathbf{x}) H_{\mathrm{Fl}}(\mathbf{x}) \mathcal{V}_\nu(\mathbf{x})\right] \\ &\quad - \int \mathrm{d}^3x' \int \mathrm{d}^3x \, V_{\mathrm{int}}\left(\mathbf{x}-\mathbf{x}'\right) \Psi^*(\mathbf{x}')\Psi(\mathbf{x}) \left[\mathcal{U}_\nu^*(\mathbf{x})\mathcal{U}_\nu(\mathbf{x}') - \mathcal{V}_\nu^*(\mathbf{x})\mathcal{V}_\nu(\mathbf{x}')\right] \Big\}. \quad (2.72)\end{aligned}$$

In this way, we see that the ground state obtained under consideration of the quantum fluctuations differs from that of the Gross-Pitaevskii theory. More precisely, we see that the ground-state energy is shifted by

$$\begin{aligned}\Delta E &= \frac{1}{2}{\sum_{\nu}}' \Big\{ \varepsilon_\nu - \int \mathrm{d}^3x \, \left[\mathcal{U}_\nu^*(\mathbf{x}) H_{\mathrm{Fl}}(\mathbf{x}) \mathcal{U}_\nu(\mathbf{x}) - \mathcal{V}_\nu^*(\mathbf{x}) H_{\mathrm{Fl}}(\mathbf{x}) \mathcal{V}_\nu(\mathbf{x})\right] \\ &\quad - \int \mathrm{d}^3x' \int \mathrm{d}^3x \, V_{\mathrm{int}}\left(\mathbf{x}-\mathbf{x}'\right) \Psi^*(\mathbf{x}')\Psi(\mathbf{x}) \left[\mathcal{U}_\nu^*(\mathbf{x})\mathcal{U}_\nu(\mathbf{x}') - \mathcal{V}_\nu^*(\mathbf{x})\mathcal{V}_\nu(\mathbf{x}')\right] \Big\}. \quad (2.73)\end{aligned}$$

The corrected ground-state energy (2.72) is an important result in what concerns the effects of quantum fluctuations upon Bose-Einstein condensates. Indeed, differentiating the total energy with respect to the number of particles according to Eq. (2.33) allows one to obtain the corrected chemical potential and, therefore, the corresponding equation of state $\mu(n)$ with the chemical potential as a function of the density. Using this new equation of state in the hydrodynamic formalism discussed in Section 2.4 leads to measurable effects in the frequencies of the low-lying modes [15].

The Bogoliubov-de Gennes equations (2.64) are a very powerful tool for describing the excitations of a Bose-Einstein condensate over the whole range from the one-particle regime, where the spectrum is that of a harmonic oscillator (1.7), until deep in the collective, or hydrodynamic regime, where the spectrum has the form (1.8) [143]. Of special interest is the Thomas-Fermi approximation, where the kinetic energy can be neglected and the condensate density is given by Eq. (2.36). In this approximation, the Bogoliubov-de Gennes equations reduce to

$$\begin{aligned}\varepsilon_\nu \mathcal{U}_\nu(\mathbf{x}) &= -\frac{\hbar^2\nabla^2}{2M}\mathcal{U}_\nu(\mathbf{x}) + \int \mathrm{d}^3x' \, V_{\mathrm{int}}\left(\mathbf{x}-\mathbf{x}'\right) \left[\Psi(\mathbf{x}')\Psi(\mathbf{x})\mathcal{V}_\nu(\mathbf{x}') + \Psi^*(\mathbf{x}')\Psi(\mathbf{x})\mathcal{U}_\nu(\mathbf{x}')\right], \\ -\varepsilon_\nu \mathcal{V}_\nu(\mathbf{x}) &= -\frac{\hbar^2\nabla^2}{2M}\mathcal{V}_\nu(\mathbf{x}) + \int \mathrm{d}^3x' \, V_{\mathrm{int}}\left(\mathbf{x}-\mathbf{x}'\right) \left[\Psi^*(\mathbf{x}')\Psi^*(\mathbf{x})\mathcal{U}_\nu(\mathbf{x}') + \Psi(\mathbf{x}')\Psi^*(\mathbf{x})\mathcal{V}_\nu(\mathbf{x}')\right]. \quad (2.74)\end{aligned}$$

Notice that the Thomas-Fermi approximation implies neglecting the kinetic energy of the ground state, not the one of the excited states. On the one hand, equations (2.74) represent a restriction since they do not contain the one-particle character anymore. On the other hand, they are now much simpler to solve in most cases of interest and allow one to access the low-lying excitations even analytically.

3 Homogeneous Dipolar Bose-Einstein Condensates

Homogeneous cold atomic systems cannot be realized experimentally. Nonetheless, it is important to study them carefully because such studies quite often provide a reasonable starting point for the description of the corresponding trapped system, which, in turn, is of experimental interest. In this chapter, we consider a homogeneous gas of bosonic particles interacting both through the contact and the dipole-dipole interaction beyond the mean-field approximation [129]. To this end, we apply the the Bogoliubov theory of weakly interacting condensates to evaluate the quantities of physical interest. Of particular importance are the depletion of the condensate and the correction to the ground-state energy due to the quantum fluctuations. The latter provides the correction to the equation of state of the condensate and is, therefore, employed to evaluate the sound velocity beyond the mean-field approximation.

3.1 Bogoliubov Theory

Let us consider N interacting bosonic particles which occupy a volume V. We are interested in the thermodynamic limit, where both N and V are very large but the ratio $n = N/V$, which defines the particle density, remains finite. Due to the homogeneity of the system, the condensate order parameter does not depend on the position and the grand-canonical energy can be written as

$$H' = \int \mathrm{d}^3x\, \Psi^* \left[-\frac{\hbar^2\nabla^2}{2M} - \mu + \frac{1}{2}\int \mathrm{d}^3x'\, \Psi^*\Psi V_{\mathrm{int}}\left(\mathbf{x}-\mathbf{x}'\right)\right]\Psi, \tag{3.1}$$

where the interaction potential contains both the short-range isotropic contact term and the dipole-dipole term:

$$V_{\mathrm{int}}\left(\mathbf{x}\right) = g\delta\left(\mathbf{x}\right) + V_{\mathrm{dd}}\left(\mathbf{x}\right), \tag{3.2}$$

with the parameter g being related to the s-wave scattering length a_s through

$$g = \frac{4\pi\hbar^2 a_s}{M} \tag{3.3}$$

and the dipolar potential having the form (1.12), given by

$$V_{\mathrm{dd}}(\mathbf{x}) = \frac{C_{\mathrm{dd}}}{4\pi|\mathbf{x}|^3}\left(1-3\cos^2\theta\right). \tag{3.4}$$

The s-wave scattering length a_s is assumed to be repulsive, otherwise the system becomes unstable. In addition, the contact term is also considered to be the dominant interaction. This is necessary due to

the fact that the dipole-dipole interaction is partially attractive, which renders a purely, or dominantly dipolar homogeneous condensate unstable.

In a homogeneous system the one-particle wave functions are plane waves. Therefore, the one-particle quantum number is provided by the wave vector $\mathbf{k}$ and the fluctuation Hamiltonian (2.58) of the last chapter can be identified as

$$H_{\mathrm{Fl}} = \frac{\hbar^2 \mathbf{k}^2}{2M}. \tag{3.5}$$

In this way, the grand-canonical Hamiltonian (3.1) becomes a function of the density of particles in the ground state $n_0 = \Psi^* \Psi$. Recalling that the condensate carries zero momentum and extremizing the Hamiltonian with respect to the density, one obtains the mean-field equation of state

$$\mu = n_0 \lim_{|\mathbf{k}| \to 0} \tilde{V}_{\mathrm{int}} (\mathbf{k}) . \tag{3.6}$$

This equation corresponds to the time-independent Gross-Pitaevskii Eq. (2.36) and relates the chemical potential to the density and the value of the interaction potential in momentum space at the origin. We remark that this limit is not unique in the presence of dipolar interactions. In the following, we denote it through

$$\lim_{|\mathbf{k}| \to 0} \tilde{V}_{\mathrm{int}} (\mathbf{k}) = \tilde{V}_{\mathrm{int}} (|\mathbf{k}| = 0) . \tag{3.7}$$

Due to the convenience of working in Fourier space when dealing with a homogeneous gas, let us consider the corresponding representation of the interaction potential. For a contact term in Eq. (3.2), the Fourier transformed is quite simple and reads

$$\tilde{V}_{\delta}(\mathbf{k}) = g. \tag{3.8}$$

As for the Fourier transformed of the dipolar potential, given by

$$\tilde{V}_{\mathrm{dd}}(\mathbf{k}) = \int \mathrm{d}^3 x \, V_{\mathrm{dd}}(\mathbf{x}) e^{i \mathbf{k} \cdot \mathbf{x}} = \sum_{i,j} \frac{\mu_0 m_i m_j}{3} \left(\frac{3 k_i k_j}{k^2} - \delta_{ij} \right) , \tag{3.9}$$

it was first evaluated in Ref. [88] by introducing a cutoff in the lower limit of the radial integral. In addition, a detailed derivation is given in Appendix B of Ref. [144]. For the case of interest for this thesis, where the polarization is along the z-direction, $\tilde{V}_{\mathrm{dd}}(\mathbf{k})$ can be written as

$$\tilde{V}_{\mathrm{dd}}(\mathbf{k}) = \frac{C_{\mathrm{dd}}}{3} \left(3 \cos^2 \theta - 1 \right) , \tag{3.10}$$

with θ being the angle between the vector $\mathbf{k}$ and the polarization direction.

With the explanations given before, we can now pass to the Bogoliubov equations of a homogeneous condensate with general two-particle interactions, which are the homogeneous versions of Eqs. (2.64) and read

$$\begin{aligned} \varepsilon_{\mathbf{k}} \mathcal{U}_{\mathbf{k}} &= \frac{\hbar^2 \mathbf{k}^2}{2M} \mathcal{U}_{\mathbf{k}} + n_0 \tilde{V}_{\mathrm{int}} (\mathbf{k}) \left[\mathcal{U}_{\mathbf{k}} + \mathcal{V}_{\mathbf{k}} \right] , \\ -\varepsilon_{\mathbf{k}} \mathcal{V}_{\mathbf{k}} &= \frac{\hbar^2 \mathbf{k}^2}{2M} \mathcal{V}_{\mathbf{k}} + n_0 \tilde{V}_{\mathrm{int}} (\mathbf{k}) \left[\mathcal{U}_{\mathbf{k}} + \mathcal{V}_{\mathbf{k}} \right] . \end{aligned} \tag{3.11}$$

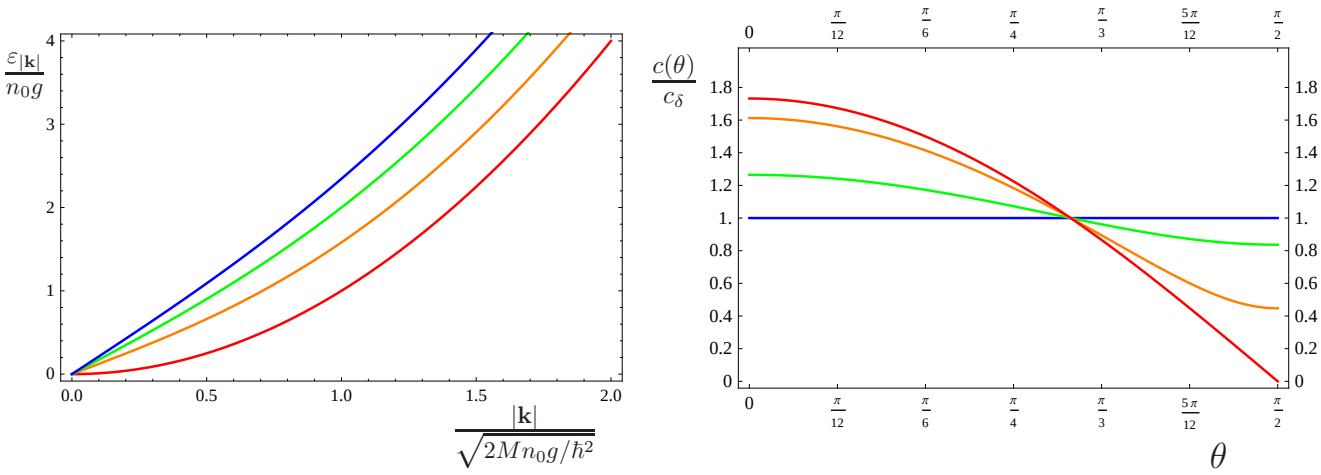

Figure 3.1: Left: Bogoliubov spectrum as given by Eq. (3.15) for $\epsilon_{\mathrm{dd}}^{\mathrm{b}} = 1$ and different values of the angle: $\theta = 0$ (blue), $\theta = \pi/6$ (green), $\theta = \pi/4$ (orange), and $\theta = \pi/2$ (red). Right: Sound velocity in units of the contact value c_δ as a function of the angle θ for $\epsilon_{\mathrm{dd}}^{\mathrm{b}} = 0$ (blue), $\epsilon_{\mathrm{dd}}^{\mathrm{b}} = 0.3$ (green), $\epsilon_{\mathrm{dd}}^{\mathrm{b}} = 0.8$ (orange), and $\epsilon_{\mathrm{dd}}^{\mathrm{b}} = 1$ (red).

Without loss of generality, we restrict the solutions of this equation to be real and remark that they satisfy the normalization condition

$$\mathcal{U}_{\mathbf{k}}^2 - \mathcal{V}_{\mathbf{k}}^2 = 1, \tag{3.12}$$

which stems from Eq. (2.60). An algebraic manipulation of the Bogoliubov Eqs. (3.11) together with the normalization condition (3.12), then leads to the values of the $\mathcal{V}_{\mathbf{k}}$ and $\mathcal{U}_{\mathbf{k}}$ functions

$$\mathcal{U}_{\mathbf{k}}^2 - 1 = \mathcal{V}_{\mathbf{k}}^2 = \frac{1}{2\varepsilon_{\mathbf{k}}}\left[\frac{\hbar^2\mathbf{k}^2}{2M} + n_0\tilde{V}_{\mathrm{int}}(\mathbf{k}) - \varepsilon_{\mathbf{k}}\right] \tag{3.13}$$

as well as to the energy spectrum

$$\varepsilon_{\mathbf{k}}^2 = \left[\frac{\hbar^2\mathbf{k}^2}{2M} + n_0\tilde{V}_{\mathrm{int}}(\mathbf{k})\right]^2 - n_0^2\tilde{V}_{\mathrm{int}}^2(\mathbf{k}), \tag{3.14}$$

which can be brought to the explicit form

$$\varepsilon_{\mathbf{k}} = \sqrt{\frac{\hbar^2\mathbf{k}^2}{2M}\left\{\frac{\hbar^2\mathbf{k}^2}{2M} + 2gn_0\left[1 + \epsilon_{\mathrm{dd}}^{\mathrm{b}}\left(3\cos^2\theta - 1\right)\right]\right\}}. \tag{3.15}$$

The parameter $\epsilon_{\mathrm{dd}}^{\mathrm{b}}$ in the equation above denotes the relative interaction strength of the dipole-dipole interaction with respect to the contact interaction and was introduced in Eq. (1.14) according to

$$\epsilon_{\mathrm{dd}}^{\mathrm{b}} = \frac{C_{\mathrm{dd}}}{3g}. \tag{3.16}$$

To the best of our knowledge, the Bogoliubov spectrum given in Eq. (3.15) has been first calculated by Santos et al. [92] and is plotted in the left-hand side of Fig. 3.1 as a function of the momentum for different values of the angle θ. The energy is given in units of $n_0 g$ and the absolute value of the wave vector $|\mathbf{k}|$ is given in units of $\sqrt{2Mn_0g/\hbar^2}$. One sees that it possesses interesting properties in the

presence of the dipole-dipole interaction. The sound velocity c, for example, is obtained by considering the limit of the spectrum at small wave vector $|\mathbf{k}|$ and is defined by

$$c = \lim_{|\mathbf{k}|\to 0} \frac{\varepsilon_{\mathbf{k}}}{\hbar|\mathbf{k}|}. \tag{3.17}$$

For the dipolar interaction, the limit above is not unique and we obtain the sound velocity as a function of the angle θ according to

$$c(\theta) = c_\delta \sqrt{1 + \epsilon_{\rm dd}^{\rm b}\,(3\cos^2\theta - 1)}, \tag{3.18}$$

with the sound velocity in the case of pure contact interaction c_δ defined according to

$$c_\delta = \sqrt{\frac{g n_0}{M}}, \tag{3.19}$$

Notice that the sound velocity $c(\theta)$ becomes imaginary for $\epsilon_{\rm dd}^{\rm b} \geq 1$ and $\cos^2\theta < 1/3$. This is a sign of the general instability present in homogeneous gases with attractive interactions.

The right-hand side of Fig. 3.1 shows the speed of sound in units of c_δ, given in Eq. (3.19), as a function of the angle θ (in radians) for different values of the relative interaction strength $\epsilon_{\rm dd}^{\rm b}$. One sees that the speed of sound decreases with increasing $\epsilon_{\rm dd}^{\rm b}$ and θ and vanishes for $\epsilon_{\rm dd}^{\rm b} = 1$ and $\theta = \pi/2$.

3.2 Sound Velocity from Hydrodynamic Equations

It is instructive to observe that the sound velocity as given by Eq. (3.18) can also be derived from the mean-field equation of state Eq. (3.6). This can be done by considering the hydrodynamic equations obeyed by the condensate, which have been discussed in Section 2.4. Indeed, these equations are even more general and are still valid in the presence of a non-condensed component [15]. In this case, one should replace the condensate density $n_0(\mathbf{x}, t)$ by the total density $n(\mathbf{x}, t)$. Consider first the equation for the velocity field (2.46), as written in the form

$$M\frac{\partial \mathbf{v}(\mathbf{x},t)}{\partial t} = -\nabla\left[\frac{M}{2}\mathbf{v}(\mathbf{x},t)^2 + \mu\left(n(\mathbf{x},t)\right)\right], \tag{3.20}$$

ant then the continuity equation (2.40), written as

$$\frac{\partial n(\mathbf{x},t)}{\partial t} + \nabla\cdot\left[n(\mathbf{x},t)\mathbf{v}(\mathbf{x},t)\right] = 0. \tag{3.21}$$

The speed of sound can be calculated by linearizing these two equations around the equilibrium values for the density and the velocity according to

$$n(\mathbf{x},t) = n(\mathbf{x}) + \delta n(\mathbf{x},t), \tag{3.22}$$

$$\mathbf{v}(\mathbf{x},t) = \mathbf{0} + \delta\mathbf{v}(\mathbf{x},t). \tag{3.23}$$

Combining the linearized equations, one obtains

$$M\frac{\partial^2\delta n(\mathbf{x},t)}{\partial t^2} = \nabla\cdot\left\{n(\mathbf{x})\nabla\left[\frac{\partial\mu}{\partial n}\delta n(\mathbf{x},t)\right]\right\}. \tag{3.24}$$

In a homogeneous gas, the density does not depend on position and that the low-energy excitations have the form of plane waves

$$\delta n(\mathbf{x},t) \propto e^{i(\mathbf{k}\cdot\mathbf{x}-\Omega t)}. \tag{3.25}$$

Inserting the density fluctuation (3.25) into the wave equation (3.24) leads to

$$M\Omega^2 = n\frac{\partial\mu}{\partial n}\mathbf{k}^2, \tag{3.26}$$

which together with the definition for the sound velocity (3.17) yields

$$c = \sqrt{\frac{n}{M}\frac{\partial\mu}{\partial n}}. \tag{3.27}$$

Along these lines, using the mean-field equation of state (3.6) in the definition for the sound velocity (3.27) leads to the same expression (3.18) as we found by means of the Bogoliubov spectrum Eq. (3.15).

Notice that there is no contradiction in identifying the total density n of the hydrodynamic equations with the condensate density n_0 at the mean-field level because they are identical in this approximation. This distinction becomes necessary only when one considers corrections to the mean-field expressions. Indeed, as we have remarked before, the Euler Eq. (3.20) and the continuity Eq. (3.21) are valid in general and that the equation of state $\mu(n)$ has to be given as an additional source of information. In particular, this means that the sound velocity can be obtained beyond the mean-field approximation if one has determined the corresponding equation of state. In the rest of this chapter, we shall implement this possibility for a homogeneous dipolar Bose-Einstein condensate.

3.3 Condensate Depletion

As we have seen in the previous chapter, the presence of the interaction expels particles from the one-particle ground state into excited states and, thus, causes a depletion of the condensate even at zero temperature. The number of excited particles can be found according to the Bogoliubov theory in Eq. (2.70). For a homogeneous gas, the Bogoliubov amplitudes have been evaluated in Eq. (3.13) and, therefore, the condensate depletion is given by

$$\Delta n = \sum_{\mathbf{k}}{}' \mathcal{V}_{\mathbf{k}}^2 = \sum_{\mathbf{k}}{}' \frac{1}{2\varepsilon_{\mathbf{k}}}\left[\frac{\hbar^2\mathbf{k}^2}{2M} + n_0\tilde{V}_{\text{int}}(\mathbf{k}) - \varepsilon_{\mathbf{k}}\right], \tag{3.28}$$

where the prime once more means exclusion of the lowest energy level, i.e., the $\mathbf{k}=\mathbf{0}$-state in the present case. As emphasized at the beginning of this chapter, we are concerned with the thermodynamic limit in which the quantum numbers become continuous variables and the summations can be replaced by

integrals according to

$$\sum_{\mathbf{k}}{}' \to V \int \frac{\mathrm{d}^3 k}{(2\pi)^3}. \tag{3.29}$$

The resulting integrals appearing in the general expression for the depletion are separately ultraviolet divergent. Combined together, however, they do converge but only slowly. One possible method to deal with these integrals is a dimensional regularization [145]. Another procedure relies on introducing a large $|\mathbf{k}|$-cutoff, which may be let to infinity after the integrals have been calculated. Indeed, we have performed the calculation through both methods obtaining the following result for the condensate depletion

$$\Delta n = \frac{8}{3\sqrt{\pi}} \left(n a_s\right)^{3/2} \mathcal{D}(\epsilon_{\mathrm{dd}}^{\mathrm{b}}). \tag{3.30}$$

Thereby, the prefactor

$$\Delta n_\delta = \frac{8}{3\sqrt{\pi}} \left(n a_s\right)^{3/2} \tag{3.31}$$

corresponds to the standard expression for the depletion of a condensate with short-ranged interactions (see, for example, Ref. [146]), while the influence of the dipole-dipole interaction on the condensate depletion is expressed through the function $\mathcal{D}(\epsilon_{\mathrm{dd}}^{\mathrm{b}})$. The depletion function $\mathcal{D}(\epsilon_{\mathrm{dd}}^{\mathrm{b}})$ stems from the dependence of $\tilde{V}_{\mathrm{int}}(\mathbf{k})$ on the direction in $\mathbf{k}$-space and is defined according to

$$\mathcal{D}(x) \;=\; \int_0^1 \mathrm{d}u \, \left(1 - x + 3\,x\,u^2\right)^{3/2}. \tag{3.32}$$

Performing the elementary integration, an analytical result for $\mathcal{D}(x)$ is obtained according to

$$\mathcal{D}(x) \;=\; -\frac{\sqrt{3}(x-1)^2 \log\left[3x(x-1)\right]}{16\sqrt{x}} + \frac{(5+x)\sqrt{1+2x}}{8} + \frac{\sqrt{3}(x-1)^2}{8\sqrt{x}} \log\left[3x + \sqrt{3x}\sqrt{1+2x}\right]. \tag{3.33}$$

For a fixed value of the contact interaction strength g the condensate depletion is found to be a monotone increasing function of the relative strength $\epsilon_{\mathrm{dd}}^{\mathrm{b}}$, which varies from $\mathcal{D}(0) = 1$ to $\mathcal{D}(1) = 3\sqrt{3}/4 \approx 1.30$ (see Fig. 3.2). It should be emphasized that, for $\epsilon_{\mathrm{dd}}^{\mathrm{b}} = 0$, the usual result (3.31) is recovered, while for $\epsilon_{\mathrm{dd}}^{\mathrm{b}}$ larger than 1, the dipolar depletion (3.30) becomes imaginary, as a sign of the instability already mentioned in the discussion of the excitation spectrum.

To our knowledge, the condensate depletion due to contact interaction (3.31) has never been measured due to difficulties in measuring the condensate density with sufficient accuracy. Little hope can be brought by the inclusion of the dipole-dipole interaction, as the condensate depletion as given by formula (3.30) does not strongly depend on the relative interaction strength $\epsilon_{\mathrm{dd}}^{\mathrm{b}}$. For $\epsilon_{\mathrm{dd}}^{\mathrm{b}} \approx 1$ it can be about 30% larger than in the case pure of contact interaction but the most important quantity remains the s-wave scattering length a_s. Nonetheless, the establishment of Eq. (3.30) is an important result from the theoretical point of view since it establishes the dependence of the depletion on the relative interaction strength $\epsilon_{\mathrm{dd}}^{\mathrm{b}}$ [129].

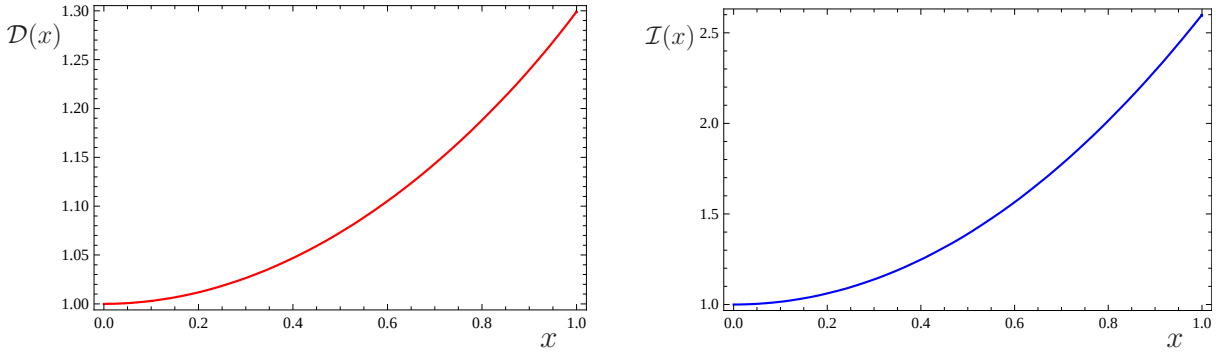

Figure 3.2: Left: Function $\mathcal{D}(x)$ from Eq. (3.33), which governs the dependence of the condensate depletion on the relative dipolar interaction strength $x = \epsilon_{\mathrm{dd}}^{\mathrm{b}}$ given in Eq. (3.30). Right: Function $\mathcal{I}(x)$ from Eq. (3.38), which characterizes the ground-state energy correction Eq. (3.36).

3.4 Ground-state Energy

The ground-state energy of the condensate is also corrected, when one considers the effects of quantum fluctuations. In the framework of the Bogoliubov theory, this correction is, in general, given by Eq. (2.73). In the case of a homogeneous gas, the Bogoliubov amplitudes satisfy the normalization condition (3.12) and are given in Eq. (3.13). Accordingly, the ground-state energy shift reads

$$\Delta E = \frac{1}{2}{\sum_{\mathbf{k}}}' \left\{ \varepsilon_{\mathbf{k}} - \left[\frac{\hbar^2 \mathbf{k}^2}{2M} + n_0 \tilde{V}_{\mathrm{int}}\left(\mathbf{k}\right) \right] \right\}. \tag{3.34}$$

Performing the passage to the thermodynamic limit leads again to slowly converging integrals which can be evaluated in the same way as the depletion integrals in Eq. (3.28). In the case of a Bose gas with contact interaction only, the energy correction reads

$$\Delta E_{\delta} = V \frac{2\pi\hbar^2 a_s n^2}{M} \frac{128}{15} \sqrt{\frac{a_s^3 n}{\pi}}, \tag{3.35}$$

which is a textbook expression [146]. In the presence of the dipole-dipole interaction, the correction to the ground-state energy is given by

$$\Delta E = V \frac{2\pi\hbar^2 a_s n^2}{M} \frac{128}{15} \sqrt{\frac{a_s^3 n}{\pi}} \mathcal{I}(\epsilon_{\mathrm{dd}}^{\mathrm{b}}), \tag{3.36}$$

where the function $\mathcal{I}(\epsilon_{\mathrm{dd}}^{\mathrm{b}})$ is defined according to

$$\mathcal{I}(x) \quad = \quad \int_0^1 \mathrm{d}u \, \left(1 - x + 3\,x\,u^2\right)^{5/2}. \tag{3.37}$$

We remark that the function $\mathcal{I}(x)$ can be brought to the following analytical form

$$\begin{aligned}\mathcal{I}(x) &= \frac{1}{96\sqrt{x}}\left\{-5\sqrt{3}(x-1)^3\log\left[3x(x-1)\right]+2\left[3\sqrt{x}\sqrt{1+2x}\left(11+4x+9x^2\right)\right.\right.\\ &\left.\left.+5\sqrt{3}(x-1)^3\log\left[3x+\sqrt{3x}\sqrt{1+2x}\right]\right]\right\}. \end{aligned} \tag{3.38}$$

The function $\mathcal{I}(\epsilon_{\rm dd}^{\rm b})$ is also a monotonic increasing function, which becomes imaginary for $\epsilon_{\rm dd}^{\rm b} > 1$. It assumes the value $\mathcal{I}(0) = 1$ for a non-dipolar gas and increases until $\mathcal{I}(1) = 3\sqrt{3}/2 \approx 2.60$ (See Fig. 3.2). Since it increases more rapidly than $\mathcal{D}(\epsilon_{\rm dd}^{\rm b})$, we see that the ground-state energy with dipolar interaction departs from the pure contact-interaction case much more strongly, as $\epsilon_{\rm dd}^{\rm b}$ becomes nonzero, if compared to the condensate depletion [129].

3.5 Beyond Mean-field Sound Velocity

Now that we have calculated the correction to the ground-state energy of a homogeneous dipolar condensate due to quantum fluctuations, we can also obtain the corrected equation of state. Indeed, by using the thermodynamic relation (2.33) we obtain

$$\mu = n\tilde{V}_{\rm int}\left(|\mathbf{k}|=0\right) + \frac{32gn}{3}\sqrt{\frac{a_s^3 n}{\pi}}\mathcal{I}(\epsilon_{\rm dd}^{\rm b}), \tag{3.39}$$

which represents the generalization to a dipolar condensate of the famous Lee-Huang-Yang relation [14]. Interestingly, the correction represented by the second term in Eq. (3.39) is uniquely defined and does not depend on the direction in momentum space.

We can now apply the general formula stemming from the hydrodynamical derivation for the sound velocity (3.27) together with the equation of state (3.39) to obtain the quantum corrected sound velocity. A direct calculation yields

$$c(\theta) = c_\delta\sqrt{1+\epsilon_{\rm dd}^{\rm b}\left(3\cos^2\theta-1\right)+\frac{16\sqrt{a_s^3 n}\mathcal{I}(\epsilon_{\rm dd}^{\rm b})}{\sqrt{\pi}}}. \tag{3.40}$$

Since the last term in the square root contains the gas parameter $a_s^3 n$, it can be consider small. For this reason, one has

$$c(\theta) \approx c_\delta\sqrt{1+\epsilon_{\rm dd}^{\rm b}\left(3\cos^2\theta-1\right)}\left\{1+\frac{8\sqrt{a_s^3 n}\mathcal{I}(\epsilon_{\rm dd}^{\rm b})}{\sqrt{\pi}\left[1+\epsilon_{\rm dd}^{\rm b}\left(3\cos^2\theta-1\right)\right]}\right\}, \tag{3.41}$$

which represents the dipolar version of Beliaev's result for the speed of sound in a Bose-Einstein condensate with contact interaction [73].

In Fig. 3.3, we plot the corrected sound velocity (3.40), represented by the solid curves, for $\epsilon_{\rm dd}^{\rm b} = 0.8$ and $\epsilon_{\rm dd}^{\rm b} = 1$, and compare it with the corresponding curves for the mean-field value given by Eq. (3.18), represented by the dashed curves. For these plots, we took the value of the gas parameter for a chromium condensate at the center of the trap in typical experiments [89]. This quantity assumes small values, such as $n(\mathbf{0})a_s^3 \approx 4\times10^{-7}$, but the correction involved in Eq. (3.40) for $\epsilon_{\rm dd}^{\rm b} = 1$ amounts

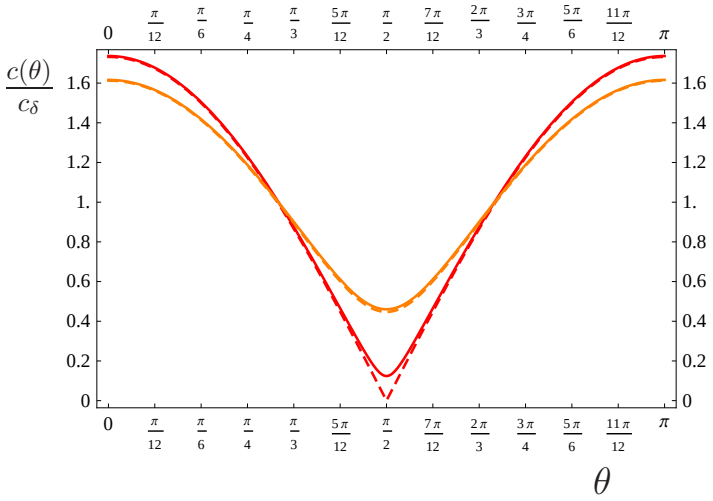

Figure 3.3: Comparison between the sound velocities in the mean-field approximation (3.18), plotted in dashed curves, and its quantum corrected version (3.40), represented here in solid curves. The orange and the red curves are for $\epsilon_{\rm dd}^{\rm b} = 0.8$ and $\epsilon_{\rm dd}^{\rm b} = 1$, respectively. The difference between the corresponding ones for the same value of $\epsilon_{\rm dd}^{\rm b}$ is very small. It is most appreciable for $\epsilon_{\rm dd}^{\rm b} = 1$. Notice, for example, that the slope of the sound velocity vanishes at $\theta = \pi/2$ for the quantum corrected expression but not for the mean-field one.

to

$$\frac{16\sqrt{a_s^3 n}\mathcal{I}(\epsilon_{\rm dd}^{\rm b}=1)}{\sqrt{\pi}} = \frac{16\sqrt{4\times 10^{-7}}}{\sqrt{\pi}}\frac{3\sqrt{3}}{2} \approx 0.015, \tag{3.42}$$

which makes a considerable difference, when the first term inside the square root in Eq. (3.40) vanishes. Notice that the derivative of the quantum corrected sound velocity with respect to the angle is zero at $\theta = \pi/2$ for $\epsilon_{\rm dd}^{\rm b} = 1$. In addition, also for $\theta = \pi/2$ and $\epsilon_{\rm dd}^{\rm b} = 1$, the speed of sound itself does not vanish. Nonetheless the threshold for a stable dipolar condensate is still $\epsilon_{\rm dd}^{\rm b} = 1$. For values of the relative interaction strength $\epsilon_{\rm dd}^{\rm b}$ slightly larger than unity, the function $\mathcal{I}(\epsilon_{\rm dd}^{\rm b})$ becomes imaginary and so does the whole expression (3.40). This result is a consequence of the fact that quantum fluctuations only have physical consequences when the mean-field ground state around which they are considered is itself a stable ground state.

4 Harmonically Trapped Dipolar Bose-Einstein Condensates

The physics of Bose-Einstein condensation is directly affected by the presence of external trapping potentials. In particular, the interplay between the trap and the interaction shapes the condensate into different forms. This effect is further enhanced by the anisotropy of the dipole-dipole interaction. In this chapter, we explore the Gross-Pitaevskii mean-field theory of trapped dipolar condensates. At first, we provide an original proof that a parabolic density is an exact solution of the Gross-Pitaevskii equation in the Thomas-Fermi regime. Then, we use such a parabolic density profile as a variational ansatz to investigate the static as well as the dynamic properties of such a dipolar condensate. The results presented here have been derived before in the literature and the corresponding authors are listed throughout the chapter.

4.1 Exact Thomas-Fermi Solution of the Gross-Pitaevskii Equation

In this section, we will obtain an exact class of solutions for the time-independent Gross-Pitaevskii equation (2.34) within the Thomas-Fermi approximation, i.e., neglecting the kinetic energy in comparison with the interaction and trapping energies. The conditions for the validity of this assumption represent the current experimental situation and have been widely verified experimentally (see Ref. [81] for a review from experimental point of view).

The parabolic solution we shall present here for the static and dynamic properties of a dipolar condensate was first found by Eberlein et al. [96] and was used to study the hydrodynamics of a cylinder-symmetric dipolar condensate [97]. Those studies proved the exactness of the parabolic solution by reducing the problem of finding the self-consistent dipolar mean field of a condensate to an electrostatic analogon, where the corresponding electrostatic potential is calculated starting from a parabolic "charge" density. In fact, that calculation has the advantage of coping also with the dipolar potential outside the condensate, which allows, for instance, to study Saturn-ring instabilities. Nevertheless, this approach is unnecessarily complicated from a mathematical point of view. Recently, an alternative calculation has appeared in the literature which relies on calculations of the gravitational potential in astrophysics [148]. In this thesis, however, we do not follow any of these methods but present our own analytic calculation of the dipolar mean-field potential of a dipolar condensate. It will be based on the assumption of a parabolic density distribution, in resemblance to the other two calculations found in the literature, but is considerably simpler.

In the Thomas-Fermi regime, the time-independent Gross-Pitaevskii Eq. (2.34) takes the form

$$\Psi(\mathbf{x})\,\mu = \left[U_{\mathrm{trap}}(\mathbf{x}) + \int \mathrm{d}^3x'\, V_{\mathrm{int}}(\mathbf{x}-\mathbf{x}')|\Psi(\mathbf{x}')|^2\right]\Psi(\mathbf{x}), \tag{4.1}$$

which is that of a non-linear integral equation, due to the dipolar contribution.

Solving Eq. (4.1) in general is very difficult. Nonetheless, as we mentioned before, a parabolic density profile has been found to be an exact solution of this integral equation. Initially, the problem was solved for a cylinder-symmetric trap [96] and then, the solution was extended to the case of a triaxial trap [149]. In this section, we restrict ourselves to a cylinder-symmetric trap ($\omega_x = \omega_y = \omega_\rho$) and, therefore, adopt an ansatz for the condensate wave function with explicit cylinder symmetry

$$\Psi(\mathbf{x}) = \begin{cases} \sqrt{n_0}\left[1 - \frac{\rho^2}{R_\rho^2} - \frac{z^2}{R_z^2}\right]^{\frac{1}{2}}; & 1 - \frac{\rho^2}{R_\rho^2} - \frac{z^2}{R_z^2} \geq 0 \\ 0; & \text{otherwise} \end{cases}, \tag{4.2}$$

where the constant

$$n_0 = \frac{15N}{8\pi R_\rho^2 R_z} \tag{4.3}$$

assures the normalization and $\rho^2 = x^2 + y^2$. Here, the parameters R_ρ and R_z, which will be determined self-consistently in the following, denote the spatial extension of the dipolar condensate in the radial and axial directions, respectively. The dipolar term in Eq. (4.1) can be calculated with the help of the Fourier transform of the dipole-dipole interaction, which was discussed in Section 3.1, and of the condensate density $n_0(\mathbf{x}) = |\Psi(\mathbf{x})|^2$, which reads

$$\tilde{n}_0(\mathbf{k}) = \int \mathrm{d}^3x\, n_0(\mathbf{x}) e^{i\mathbf{k}\cdot\mathbf{x}} = \frac{n_0 R_\rho^2 R_z (2\sqrt{\pi})^3}{\sqrt{2}} \frac{J_{\frac{5}{2}}\left(\left(R_\rho^2 k_\rho^2 + R_z^2 k_z^2\right)^{\frac{1}{2}}\right)}{\left(R_\rho^2 k_\rho^2 + R_z^2 k_z^2\right)^{\frac{5}{4}}}. \tag{4.4}$$

Here $J_\nu(x)$ denotes a Bessel function of the first kind [176]. Now, we must calculate the dipolar potential, which is given by the convolution

$$\Phi_{\mathrm{dd}}(\mathbf{x}) = \int \mathrm{d}^3x\, V_{\mathrm{dd}}(\mathbf{x} - \mathbf{x}') n_0(\mathbf{x}'). \tag{4.5}$$

Due to the depence of the interaction potential $V_{\mathrm{dd}}(\mathbf{x} - \mathbf{x}')$ on the relative position $\mathbf{x} - \mathbf{x}'$, it turns out to be more convenient to perform the calculation of the potential (4.5) in Fourier space, where it reads

$$\Phi_{\mathrm{dd}}(\mathbf{x}) = \int \frac{\mathrm{d}^3k}{(2\pi)^3} \tilde{V}_{\mathrm{dd}}(\mathbf{k}) \tilde{n}_0(\mathbf{k}) e^{-i\mathbf{k}\cdot\mathbf{x}}. \tag{4.6}$$

Using Eq. (3.10) and Eq. (4.4) yields

$$\Phi_{\mathrm{dd}}(\mathbf{x}) = \frac{n_0 C_{\mathrm{dd}}}{3}\left[\frac{\rho^2}{R_\rho^2} - \frac{2z^2}{R_z^2} - f_s\left(\frac{R_\rho}{R_z}\right)\left(1 - \frac{3}{2}\frac{\rho^2 - 2z^2}{R_\rho^2 - R_z^2}\right)\right]. \tag{4.7}$$

In this equation we have introduced the definition of the cylinder-symmetric anisotropy function

$$f_s(x) = -\frac{1}{2}\int_0^\pi \mathrm{d}\theta \sin\theta \left(\frac{3x^2\cos^2\theta}{\sin^2\theta + x^2\cos^2\theta} - 1\right), \tag{4.8}$$

which is valid for all x (see Fig. 4.1). For actual calculations, it is useful to put the anisotropy function

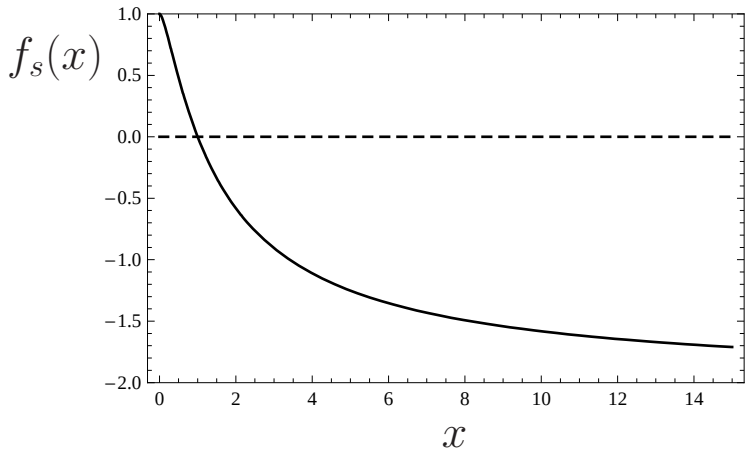

Figure 4.1: $f_s(x)$ as a function of x. Notice that $f_s(x)$ changes its sign at $x = 1$.

(4.8) in the form [86,150,97]

$$f_s(x) = \frac{1 + 2x^2 - 3x^2\,\Xi(x)}{1 - x^2}, \tag{4.9}$$

together with the abbreviation

$$\Xi(x) \equiv \begin{cases} \frac{1}{\sqrt{1-x^2}} \tanh^{-1}\sqrt{1-x^2}; & 0 \le x < 1 \\ \frac{1}{\sqrt{x^2-1}} \tan^{-1}\sqrt{x^2-1}; & x \ge 1 \end{cases}. \tag{4.10}$$

Inserting the result for the dipolar potential (4.7) and the harmonic trap (1.4) with $\omega_x = \omega_y = \omega_\rho$ into Eq. (4.1), and comparing the respective coefficients of 1, ρ^2, and z^2, we obtain three coupled equations involving the parameters μ, R_ρ and R_z. The constant term, for instance, leads to an expression for the chemical potential

$$\mu = g n_0 \left[1 - \epsilon_{\rm dd}^{\rm b} f_s\left(\frac{R_\rho}{R_z}\right)\right], \tag{4.11}$$

where the dipolar interaction strength is the same as in the case of homogeneous condensates (1.14) and reads

$$\epsilon_{\rm dd}^{\rm b} = \frac{C_{\rm dd}}{3g}. \tag{4.12}$$

It is interesting to notice that the dipolar contribution to the chemical potential μ is governed by the anisotropy function $f_s(\kappa)$ and depends only on the condensate aspect ratio

$$\kappa = \frac{R_\rho}{R_z}. \tag{4.13}$$

The Thomas-Fermi radii R_ρ and R_z have to be obtained as a function of the interaction strength $\epsilon_{\rm dd}^{\rm b}$ from the coupled equations involving the coefficients of ρ^2 and z^2. First, one finds the equation

$$R_\rho = \left\{\frac{15 N g \kappa}{4\pi M \omega_\rho^2}\left[1 - \epsilon_{\rm dd}^{\rm b}\left(1 + \frac{3}{2}\frac{\kappa^2 f_s(\kappa)}{\kappa^2 - 1}\right)\right]\right\}^{\frac{1}{5}}, \tag{4.14}$$

which gives the Thomas-Fermi radius in the radial direction R_ρ for given aspect ratio κ and interaction

strength $\epsilon_{\mathrm{dd}}^{\mathrm{b}}$. Secondly, the following transcendental equation is obtained

$$3\kappa^2\epsilon_{\mathrm{dd}}^{\mathrm{b}}\left[\left(\frac{\lambda^2}{2}+1\right)\frac{f_s(\kappa)}{1-\kappa^2}-1\right]+\left(\epsilon_{\mathrm{dd}}^{\mathrm{b}}-1\right)\left(\kappa^2-\lambda^2\right)=0, \tag{4.15}$$

which relates the condensate aspect ratio κ to the trap aspect ratio $\lambda = \omega_z/\omega_\rho$ and the dipolar interaction strength $\epsilon_{\mathrm{dd}}^{\mathrm{b}}$.

Equations (4.14) and (4.15) allow to calculate the Thomas-Fermi radii as functions of the interaction strength and the trap aspect ratio λ. They are precisely the ones originally found by Eberlein et al. in a more involved way [96].

Although we have proved that the ansatz Eq. (4.2), which represents an inverted parabola for the particle density, is an exact solution of the Gross-Pitaevskii equation in the Thomas-Fermi regime, we will not explore the physical properties of these solutions yet but postpone this discussion for a while. Instead, in the next section, the same equations are derived variationally. The main advantages of the variational approach are the mathematical simplicity and the straightforward inclusion of dynamical effects.

4.2 Variational Approach to Dipolar Bose-Einstein Condensates

In this section, we consider dipolar condensates in the Thomas-Fermi approximation through a variational approach. By adopting the parabolic density as an ansatz and specifying the phase of the condensate wave function, we are able to derive the equations of motion for the Thomas-Fermi radii of dipolar condensate.

The starting point of the present study is the least action principle (2.25) with the action (2.26)–(2.29). Instead of deriving an equation of motion for the condensate wave function $\Psi(\mathbf{x},t)$, we adopt the factorization ansatz

$$\Psi(\mathbf{x},t) = e^{iM\chi(\mathbf{x},t)/\hbar}\Psi_0(\mathbf{x},t), \tag{4.16}$$

which can be done for a general complex function with real functions $\chi(\mathbf{x},t)$ and $\Psi_0(\mathbf{x},t)$. Inserting the ansatz (4.16) into (2.26)–(2.29) and requiring that the number of particles is conserved, a partial integration leads to

$$\mathcal{A}[n_0,\chi] = -M\int_{t_1}^{t_2}\mathrm{d}t\int\mathrm{d}^3x\,\sqrt{n_0(\mathbf{x},t)}\left[\dot{\chi}(\mathbf{x},t)+\frac{1}{2}\nabla\chi(\mathbf{x},t)\cdot\nabla\chi(\mathbf{x},t)+H_0(\mathbf{x},t)\right]\sqrt{n_0(\mathbf{x},t)} \tag{4.17}$$

with the condensate density $n_0(\mathbf{x},t) = \Psi_0^*(\mathbf{x},t)\Psi_0(\mathbf{x},t)$ and the Hamiltonian

$$H_0(\mathbf{x},t) = -\frac{\hbar^2\nabla^2}{2M}+U_{\mathrm{trap}}(\mathbf{x})+\frac{1}{2}gn_0(\mathbf{x},t)+\frac{1}{2}\int\mathrm{d}^3x'\,V_{\mathrm{dd}}(\mathbf{x}-\mathbf{x}')n_0(\mathbf{x}',t). \tag{4.18}$$

The identification

$$\mathbf{v}(\mathbf{x},t) = \nabla\chi(\mathbf{x},t) \tag{4.19}$$

together with extremization of the action (4.17) with respect to the phase $\chi(\mathbf{x},t)$ and the condensate

density $n_0(\mathbf{x},t)$ would give the continuity Eq. (2.40) as well as the Euler Eq. (2.45), respectively. But we shall follow an even simpler approach to study dipolar condensates by assuming that the particle density is given by

$$n_0(\mathbf{x},t) = n_0(t)\left[1 - \frac{x^2}{R_x^2(t)} - \frac{y^2}{R_y^2(t)} - \frac{z^2}{R_z^2(t)}\right] \tag{4.20}$$

whenever the right-hand side is positive and vanishes otherwise. Due to normalization, the Thomas-Fermi radii are related to the quantity $n_0(t)$ through

$$n_0(t) = \frac{15N}{8\pi R_x(t)R_y(t)R_z(t)}. \tag{4.21}$$

The lengths $R_i(t)$, which correspond to the Thomas-Fermi radii, are, in general, time dependent and are treated as variational parameters. In addition, an explicit ansatz for the condensate phase is made

$$\chi(\mathbf{x},t) = \frac{1}{2}\alpha_x(t)x^2 + \frac{1}{2}\alpha_y(t)y^2 + \frac{1}{2}\alpha_z(t)z^2, \tag{4.22}$$

where $\alpha_i(t)$ are the variational parameters responsible for the dynamics of the system. Notice that, contrary to the procedure in Section 4.1, we do not presume that the trap possesses any kind of symmetry.

Let us proceed and evaluate the components of action (4.17) as functions of the variation parameters. The first term can be immediately calculated and gives

$$-M\int \mathrm{d}^3x\dot{\chi}(\mathbf{x},t)n_0(\mathbf{x},t) = -\frac{MN}{14}\left[\dot{\alpha_x}(t)R_x^2(t) + \dot{\alpha}_y(t)R_y^2(t) + \dot{\alpha}(t)R_z^2(t)\right]. \tag{4.23}$$

Consider now the kinetic energy. Under the Thomas-Fermi approximation, we neglect the term $\nabla\Psi_0(\mathbf{x},t)\cdot\nabla\Psi_0(\mathbf{x},t)$. Despite that, the contribution for the kinetic energy coming from the phase survives. Indeed, identifying the velocity field (4.19), the corresponding flow energy is defined as [3]

$$E_{\text{flow}}(t) = \frac{M}{2}\int \mathrm{d}^3x\, n_0(\mathbf{x},t)\nabla\chi(\mathbf{x},t)\cdot\nabla\chi(\mathbf{x},t). \tag{4.24}$$

Then, with the help of ansatz (4.22), the flow energy becomes

$$E_{\text{flow}}(t) = \frac{MN}{14}\left[\alpha_x^2(t)R_x^2(t) + \alpha_y^2(t)R_y^2(t) + \alpha_z^2(t)R_z^2(t)\right]. \tag{4.25}$$

Before we evaluate action (4.17), let us discuss each of the energy contributions separately. To this end, it is convenient to define the mean-field energy density according to

$$E_{\text{MF}}(\mathbf{x},t) = \sqrt{n_0(\mathbf{x},t)}\left[U_{\text{trap}}(\mathbf{x}) + \frac{1}{2}gn_0(\mathbf{x},t) + \int \mathrm{d}^3x'\, V_{\text{dd}}(\mathbf{x}-\mathbf{x}')n_0(\mathbf{x}',t)\right]\sqrt{n_0(\mathbf{x},t)} \tag{4.26}$$

and the corresponding mean-field energy

$$E_{\text{MF}}(t) = \int \mathrm{d}^3x\, E_{\text{MF}}(\mathbf{x},t). \tag{4.27}$$

Notice that this definition neglects the kinetic energy. This is justified since we will be interested in

the Thomas-Fermi regime. In this way, the mean-field energy E_{MF} can be decomposed according to

$$E_{\mathrm{MF}}(t) = E_{\mathrm{trap}}(t) + E_{\delta}(t) + E_{\mathrm{dd}}(t). \tag{4.28}$$

The trapping energy $E_{\mathrm{trap}}(t)$, for example, is proportional to the particle number N and reads

$$E_{\mathrm{trap}}(t) = \int \mathrm{d}^3x\, n_0(\mathbf{x},t) U_{\mathrm{trap}}(\mathbf{x}) = \frac{MN}{14}\left[\omega_x^2 R_x^2(t) + \omega_y^2 R_y^2(t) + \omega_z^2 R_z^2(t)\right]. \tag{4.29}$$

The contact interaction energy $E_\delta(t)$, in turn, carries a factor N^2 and is given by

$$\begin{aligned} E_\delta(t) &= \frac{1}{2}\int \mathrm{d}^3x \int \mathrm{d}^3x'\, n_0(\mathbf{x},t) g\delta(\mathbf{x}-\mathbf{x}') n_0(\mathbf{x}',t) \\ &= \frac{15gN^2}{28\pi R_x(t) R_y(t) R_z(t)}. \end{aligned} \tag{4.30}$$

Let us turn to the term which is responsible for the dipole-dipole interaction. Indeed, to obtain the energy as a function of the variational parameters, one does not need the dipolar potential $\Psi_{\mathrm{dd}}(\mathbf{x})$, calculated in Eq. (4.7), which is the hardest part of that computation. In fact, we find

$$\begin{aligned} E_{\mathrm{dd}}(t) &= \frac{1}{2}\int \mathrm{d}^3x \int \mathrm{d}^3x'\, n_0(\mathbf{x},t) V_{\mathrm{dd}}(\mathbf{x}-\mathbf{x}') n_0(\mathbf{x}',t) \\ &= \frac{1}{2}\int \frac{\mathrm{d}^3k}{(2\pi)^3} \tilde{n}_0(\mathbf{k},t) \tilde{V}_{\mathrm{dd}}(\mathbf{k}) \tilde{n}_0(-\mathbf{k},t). \end{aligned} \tag{4.31}$$

The Fourier transform of the density (4.4), which reflects the cylinder symmetry assumed in the last section, can be immediately extended to the case of three different Thomas-Fermi radii. This leads to

$$\tilde{n}_0(\mathbf{k},t) = \frac{n_0 R_x(t) R_y(t) R_z(t) (2\sqrt{\pi})^3}{\sqrt{2}} \frac{J_{\frac{5}{2}}\left(\left(R_x^2(t)k_x^2 + R_y^2(t)k_y^2 + R_z^2(t)k_z^2\right)^{\frac{1}{2}}\right)}{\left(R_x^2(t)k_x^2 + R_y^2(t)k_y^2 + R_z^2(t)k_z^2\right)^{\frac{5}{4}}}. \tag{4.32}$$

Together with the Fourier transform of the dipolar potential (3.10), we readily obtain

$$E_{\mathrm{dd}}(t) = -\frac{15g\epsilon_{\mathrm{dd}}^{\mathrm{b}} N^2}{28\pi R_x(t) R_y(t) R_z(t)} f\left(\frac{R_x(t)}{R_z(t)}, \frac{R_y(t)}{R_z(t)}\right). \tag{4.33}$$

The anisotropy function $f(x,y)$, which reflects the geometrical properties of the dipole-dipole interaction, is defined according to (see Fig. 4.2)

$$f(x,y) = 1 + 3xy \frac{E(\varphi,k) - F(\varphi,k)}{(1-y^2)\sqrt{1-x^2}}, \tag{4.34}$$

where $F(\varphi,k)$ and $E(\varphi,k)$ are the elliptic integrals of the first and second kind, respectively, with $\varphi = \arcsin\sqrt{1-x^2}$ and $k^2 = (1-y^2)/(1-x^2)$. This function has appeared often in the literature of dipolar Bose-Einstein condensates and its properties are discussed in detail in Appendix A. Notice that $f(x,y)$ is bounded between 1 and -2 passing through 0 at $x = y = 1$. This reflects the fact that the dipole-dipole interaction is both partially attractive and partially repulsive, depending on whether

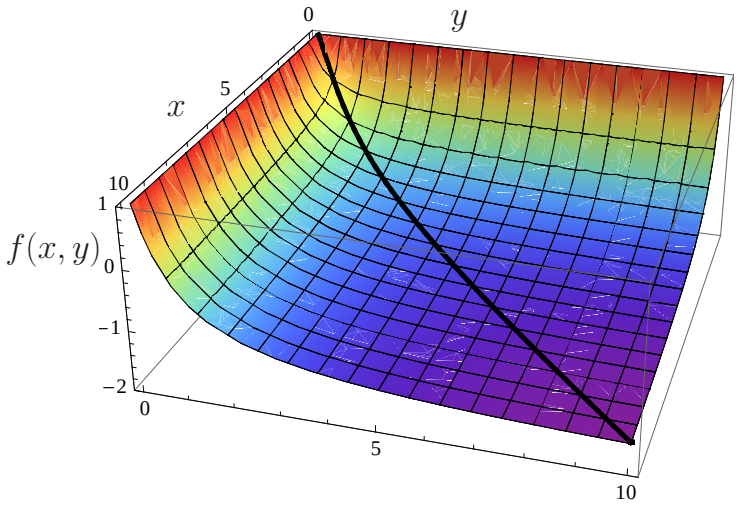

Figure 4.2: Anisotropy function $f(x, y)$ from (4.34), which is bounded between 1 for small values of either x or y and -2 for large values of both arguments. Notice the symmetry $f(x, y) = f(y, x)$ and that $f(x, y)$ reduces to $f_s(x)$ (black curve) in the case of cylindrical symmetry [151,149].

the dipoles are head-to-tail or side-by-side to one another, respectively. In a cylinder symmetric system and for polarization along the symmetry axis, the interaction is, therefore, dominantly attractive in cigar- (prolate) and repulsive in pancake-shaped (oblate) systems. We remark that the anisotropy function $f(x, y)$ obeys the identity

$$f(x, x) = f_s(x), \tag{4.35}$$

with $f_s(x)$ being defined in equation (4.9).

Let us go back to the complete action, which can now be written as a function of the variational parameters

$$\mathcal{A}\left(\mathbf{R}, \boldsymbol{\alpha}, \dot{\boldsymbol{\alpha}}, t\right) = \int_{t_1}^{t_2} \mathrm{d}t\, \mathcal{L}\left(\mathbf{R}, \boldsymbol{\alpha}, \dot{\boldsymbol{\alpha}}, t\right), \tag{4.36}$$

where the Lagrangian function is given by

$$\mathcal{L}\left(\mathbf{R}, \boldsymbol{\alpha}, \dot{\boldsymbol{\alpha}}, t\right) = -\frac{MN}{7}\left\{\sum_i \frac{R_i^2(t)}{2}\left[\dot{\alpha}_i(t) + \alpha_i^2(t) + \omega_i^2\right] + \frac{15Ng/(4\pi M)}{R_x(t)R_y(t)R_z(t)}\left[1 - \epsilon_{\mathrm{dd}}^{\mathrm{b}} f\left(\frac{R_x(t)}{R_z(t)}, \frac{R_y(t)}{R_z(t)}\right)\right]\right\}. \tag{4.37}$$

The corresponding equations of motion are then obtained from the Euler-Lagrange equations

$$\frac{d}{dt}\left(\frac{\partial \mathcal{L}}{\partial \dot{q}}\right) - \frac{\partial \mathcal{L}}{\partial q} = 0, \tag{4.38}$$

with q being one of the variational parameters.

Concerning the variational parameters for the condensate phase, their equations of motion read

$$\alpha_i(t) = \frac{\dot{R}_i(t)}{R_i(t)} \tag{4.39}$$

and serve as auxiliary relations in order to eliminate the variational parameters $\alpha_i(t)$ from the equations of motion for the Thomas-Fermi radii. The final equations of motion for the Thomas-Fermi radii are

$$\frac{NM}{7}\ddot{R}_i(t) = -\frac{\partial}{\partial R_i} E_{\rm MF}\left(R_x, R_y, R_z\right). \tag{4.40}$$

For future reference, let us write Eqs. (4.40) explicitly

$$\begin{aligned}
\ddot{R}_x &= -\omega_x^2 R_x + \frac{15gN}{4\pi M R_x^2 R_y R_z}\left\{1 - \epsilon_{\rm dd}^{\rm b}\left[1 - R_x\partial_{R_x}\right] f\left(\frac{R_x}{R_z}, \frac{R_y}{R_z}\right)\right\}, \\
\ddot{R}_y &= -\omega_y^2 R_y + \frac{15gN}{4\pi M R_x R_y^2 R_z}\left\{1 - \epsilon_{\rm dd}^{\rm b}\left[1 - R_y\partial_{R_y}\right] f\left(\frac{R_x}{R_z}, \frac{R_y}{R_z}\right)\right\}, \\
\ddot{R}_z &= -\omega_z^2 R_z + \frac{15gN}{4\pi M R_x R_y R_z^2}\left\{1 - \epsilon_{\rm dd}^{\rm b}\left[1 - R_z\partial_{R_z}\right] f\left(\frac{R_x}{R_z}, \frac{R_y}{R_z}\right)\right\}.
\end{aligned} \tag{4.41}$$

Equations (4.41) describe the physics of dipolar Bose-Einstein condensates in triaxial traps and were first derived by Giovanazzi et al., who used them to investigate the time-of-flight dynamics in those systems. Indeed, a triaxial time-of-flight analysis provided the first experimental proof of the presence of the dipole-dipole interaction in chromium [98]. It is convenient to observe that the dynamics of the Thomas-Fermi radii can be studied as the Newtonian problem of a fictitious particle moving in a potential which is given by the mean-field energy $E_{\rm MF}\left(R_x, R_y, R_z\right)$.

It should be emphasized that in the particularly interesting case of cylinder-symmetric traps, where dipolar condensates were initially investigated, Eqs. (4.41) reduce to

$$\ddot{R}_\rho(t) = -\omega_\rho^2 R_\rho(t) + \frac{15gN}{4\pi M R_\rho(t)^3 R_z(t)}\left\{1 - \epsilon_{\rm dd}^{\rm b}\left[1 + \frac{3}{2}\frac{R_\rho^2(t) f_s(R_\rho(t)/R_z(t))}{R_\rho^2(t) - R_z^2(t)}\right]\right\}, \tag{4.42}$$

$$\ddot{R}_z(t) = -\omega_z^2 R_z(t) + \frac{15gN}{4\pi M R_\rho^2(t) R_z^2(t)}\left\{1 + 2\epsilon_{\rm dd}^{\rm b}\left[1 + \frac{3}{2}\frac{R_z^2(t) f_s(R_\rho(t)/R_z(t))}{R_\rho^2(t) - R_z^2(t)}\right]\right\}. \tag{4.43}$$

In deriving Eqs. (4.42) and (4.43), we have employed the mathematical identities

$$\lim_{y\to x} x\frac{\partial f(x,y)}{\partial x} = \lim_{y\to x} y\frac{\partial f(x,y)}{\partial y} = \frac{1}{2}x f_s'(x) = -1 + \frac{2+x^2}{2(1-x^2)} f_s(x) \tag{4.44}$$

for the anisotropy function $f(x,y)$, where the prime denotes derivative with respect to the argument.

Equations (4.42) and (4.43) give the exact properties of cylinder-symmetric dipolar condensates in the Thomas-Fermi regime. They were first obtained by O'Dell et al., who used the hydrodynamic formalism to study the oscillations of a chromium condensate around the parabolic equilibrium solution [97,96]. Here, we will employ these equations to study the static properties like the condensate aspect ratio as well as dynamic properties like the low-lying oscillations and the time-of-flight expansion.

4.3 Static Properties

In this section, we discuss the static solutions of the equations of motion for a dipolar condensate obtained by setting $\ddot{R}_i = 0$ in Eq. (4.41). We will initially present a brief discussion of the non-dipolar

condensate, in order to establish the background for the specific effects of the dipole-dipole interaction. In addition, this discussion will also provide appropriate unities for expressing the main quantities of interest throughout this chapter. When we come to the static properties themselves, we will first concentrate on the case of a cylinder-symmetric trap, thereby revisiting the most important known results. Then we will analyze a few aspects of the triaxial case with focus on the changes in the stability diagram that were not yet discussed in the literature.

Combining Eqs. (4.42) and (4.43), we could reproduce precisely the equations for the Thomas-Fermi radius in the radial direction, Eq. (4.14), and the equation for the condensate aspect ratio, Eq. (4.15), from the exact solution in Section 4.1. These equations allow for calculating the static properties of the dipolar condensate, but it should be remarked that they represent extrema, not necessarily minima. Therefore, the behavior of the mean-field energy, supplemented by physical intuition, will help us to identify the different types of equilibrium solutions.

Let us start the discussion of the static properties with the case of a non-dipolar condensate. To that end, we set $\epsilon_{\mathrm{dd}}^{\mathrm{b}} = 0$ and denote non-dipolar quantities with the superscript (0). In this case, the Thomas-Fermi radii are given by

$$R_i^{(0)} = \left(\frac{2\mu^{(0)}}{M\omega_i^2}\right)^{1/2}, \qquad \mu^{(0)} = gn_0, \tag{4.45}$$

and define clear borders for the condensate. This is in contrast with Bose-Einstein condensation in trapped ideal gases, for which the wave function is Gaussian and, therefore, the condensate density falls fast but not abruptly.

The Thomas-Fermi radii of condensates with pure contact interactions will provide us with the physical unities for describing the dipolar condensate. The dimensionless radii are denoted by

$$\tilde{R}_i = \frac{R_i}{R_i^{(0)}}. \tag{4.46}$$

Before we discuss the stationary solutions of Eqs. (4.42) and (4.43), let us consider the mean-field energy in equilibrium. In units of the non-interacting energy

$$E^{(0)} = \frac{5}{14} N M \omega_\rho^2 {R_\rho^{(0)}}^2, \tag{4.47}$$

the mean-field energy is given by the following expression

$$\frac{E_{\mathrm{MF}}\left(\tilde{R}_x, \tilde{R}_y, \tilde{R}_z\right)}{E^{(0)}} = \frac{2}{5}\left\{\frac{1}{2}\sum_i \tilde{R}_i^2 + \frac{1}{\tilde{R}_x\tilde{R}_y\tilde{R}_z}\left[1 - \epsilon_{\mathrm{dd}}^{\mathrm{b}} f\left(\frac{\tilde{R}_x\lambda_x}{\tilde{R}_z}, \frac{\tilde{R}_y\lambda_y}{\tilde{R}_z}\right)\right]\right\}, \tag{4.48}$$

which outlines the role of the trap frequency ratios λ_x and λ_y, defined in Eq. (1.5) according to

$$\lambda_x = \frac{\omega_z}{\omega_x}, \qquad \lambda_y = \frac{\omega_z}{\omega_y}.$$

Let us first discuss the cylinder-symmetric situation, in which $\lambda_x = \lambda_y = \lambda$. In this case, the

symmetry of the mean-field energy (4.48) implies $\tilde{R}_x = \tilde{R}_y$, the function $f\left(\frac{\tilde{R}_x\lambda_x}{\tilde{R}_z}, \frac{\tilde{R}_y\lambda_y}{\tilde{R}_z}\right)$ reduces to $f_s\left(\frac{\tilde{R}_\rho\lambda}{\tilde{R}_z}\right)$, and we recover the energy of Ref. [96], where this problem was first solved exactly.

Since the maximum value of $f_s(x)$ is 1, taken at $x = 0$ (see Fig. 4.1.), the mean-field energy is bounded from below whenever $\epsilon_{\rm dd}^{\rm b} < 1$. Therefore, for these values of the dipolar interaction strength, the energy $E_{\rm MF}\left(\tilde{R}_\rho, \tilde{R}_z\right)$ possesses a global minimum and equilibrium is always stable. Another interesting feature of $f_s(x)$ is that it is positive for $x < 1$, passes through zero at $x = 1$, and is negative for $x > 1$. This is responsible for stretching the condensate along the polarization axis, which leads to a lower total energy. In the following we discuss how these dipolar effects show up in the static properties of Bose-Einstein condensates by considering the aspect ratio and the stability diagram as concrete examples.

In Fig. 4.3a), we have plotted the condensate aspect ratio as a function of the dipolar interaction strength $\epsilon_{\rm dd}^{\rm b}$ for different trap aspect ratios λ. The corresponding values of λ for each curve can be read off by noticing that, in the non-dipolar case, condensate and trap aspect ratios coincide, i.e., $\kappa(\epsilon_{\rm dd}^{\rm b} = 0) = \lambda$. For an interaction strength $\epsilon_{\rm dd}^{\rm b} < 1$, a single aspect ratio emerges, which corresponds to an absolute minimum of the mean-field energy (4.48). This configuration is, therefore, stable. As $\epsilon_{\rm dd}^{\rm b}$ eventually becomes larger than one, the upper branch ceases to be a global and becomes only a local minimum. It is, therefore, called metastable. In addition, for $\epsilon_{\rm dd}^{\rm b} > 1$, another branch appears, which is unstable, since it does not correspond to a minimum. Stable or metastable branches of the aspect ratio are depicted with continuous curves while the unstable branches are represented by broken ones. The mathematical criterion to distinguish a metastable from an unstable configuration is the analysis of the Hessian matrix corresponding to the total energy Eq. (4.48). Nonetheless, a simple physical criterion is also available. Polarized dipoles can either attract or repel each other, depending if they are aligned head-to-tail or side-by-side, respectively. Thus, a head-to-tail configuration along the Oz-axis lowers the total energy and this lowering is stronger the stronger the interaction strength is. Based on these grounds, one expects a physically acceptable solution to have a negative derivative of the aspect ratio κ with respect to the interaction strength $\epsilon_{\rm dd}^{\rm b}$, explaining the behavior found in Fig. 4.3a).

Considering the stability diagram, shown in Fig. 4.3b), interesting features of Bose-Einstein condensates can be explored. The region in gray is given by $\epsilon_{\rm dd}^{\rm b} < 1$ and represents a stable region, where only one solution is available. The green area, in which two solutions coexist, is called metastable. This area is bounded by $1 < \epsilon_{\rm dd}^{\rm b} < \epsilon_{\rm dd}^{\rm b,crit}$ but, for values $\lambda \gtrapprox 5.17$ on, $\epsilon_{\rm dd}^{\rm b,crit}$ becomes infinite, explaining why the stable and unstable aspect ratios for $\lambda = 6$ in Fig. 4.3a) do not meet each other. This has the important experimental implication that a dipolar condensate can always be stabilized by a sufficiently flat trap, no matter how strong the interaction is. This important observation was first made in Ref. [96].

Now we consider the case in which the cylinder symmetry is not present. Let us first study the aspect ratios in the x and y directions, denoted by

$$\kappa_x = \frac{R_x}{R_z}, \qquad \kappa_y = \frac{R_y}{R_z}, \tag{4.49}$$

respectively. To this end, it is convenient to investigate the case of a varying λ_y, while λ_x is kept

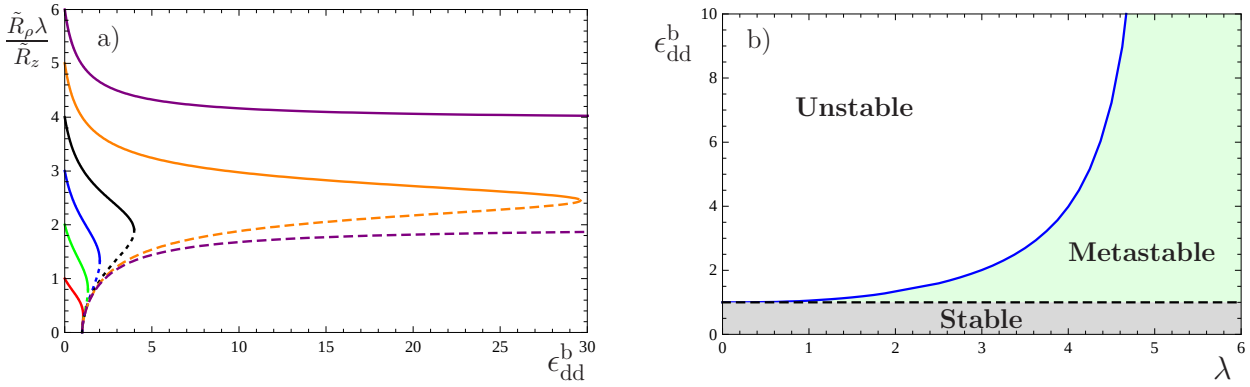

Figure 4.3: a) Aspect ratio $\kappa = \tilde{R}_\rho \lambda / \tilde{R}_z$ as a function of the dipolar interaction strength ϵ_{dd}^b for different values of $\lambda = \kappa(\epsilon_{dd}^b = 0)$. For $\epsilon_{dd}^b < 1$, the transcendental equation (4.15) gives a single condensate aspect ratio κ, which corresponds to a stable configuration and is depicted in solid curves. For $\epsilon_{dd}^b > 1$, a second, unstable branch, depicted in broken curves, shows up for the aspect ratio, which meets the stable one at $\epsilon_{dd}^b = \epsilon_{dd}^{b,crit}$. For $\epsilon_{dd}^b > \epsilon_{dd}^{b,crit}$, no solution is available. b) Stability diagram of a cylinder-symmetric Bose-Einstein condensate. The blue line depicts the critical value of the interaction strength $\epsilon_{dd}^{b,crit}$, above which no solution is available for Eqs. (4.42) and (4.43). The colored area represents stable configurations, in which an additional unstable solution is present (light green) or not (gray).

constant. Indeed, the symmetry of the problem allows to understand by analogy the properties of the system in the inverse case, i.e., when λ_y is hold fixed and λ_x changes. We show in Fig. 4.4a) the aspect ratio κ_x as a function of the dipolar interaction strength ϵ_{dd}^b for $\lambda_x = 4$ and $\lambda_y = 2, 3, 4, 5, 6$. The solid lines represent the stable solutions of the stationary versions of Eqs. (4.41) while the broken ones mark the unstable solutions. The orange curve depicts the cylinder-symmetric case for $\lambda_x = \lambda_y = 4$. As λ_y increases to $\lambda_y = 5$ (purple) and $\lambda_y = 6$ (gray), the maximum value of the interaction strength supporting a stable solution increases, the contrary being true for decreasing λ_y. This can be understood as a consequence of the fact that a larger trap aspect ratio implies a more pancake-shaped cloud, which favors the repulsive part of the dipolar interaction.

The absence of the cylinder symmetry can be displayed in a more dramatic way by considering the stability diagram of a dipolar condensate. Fig. 4.4b) shows the value of the critical interaction strength as a function of the trap aspect ratio λ_x. In addition to the cylinder-symmetric curve $\lambda_y = \lambda_x$ (black), the stability diagram is also calculated and shown for $\lambda_y = 2\lambda_x$ (red) and $\lambda_y = \lambda_x/2$ (blue). We omit the classification of the corresponding regions in order to highlight the importance of the asymmetry for the stability diagram.

4.4 Low-Lying Excitations

The study of the low-lying excitations is a very important diagnostic tool for the physics of cold atoms. In this section, we will discuss these excitations in a dipolar condensate by giving a general description of the eigenvectors as well as semi-analytic expressions for the frequencies of oscillation in the cylinder-symmetric dipolar condensate.

Let us start by considering the equations of motion for the Thomas-Fermi radii (4.41). For the

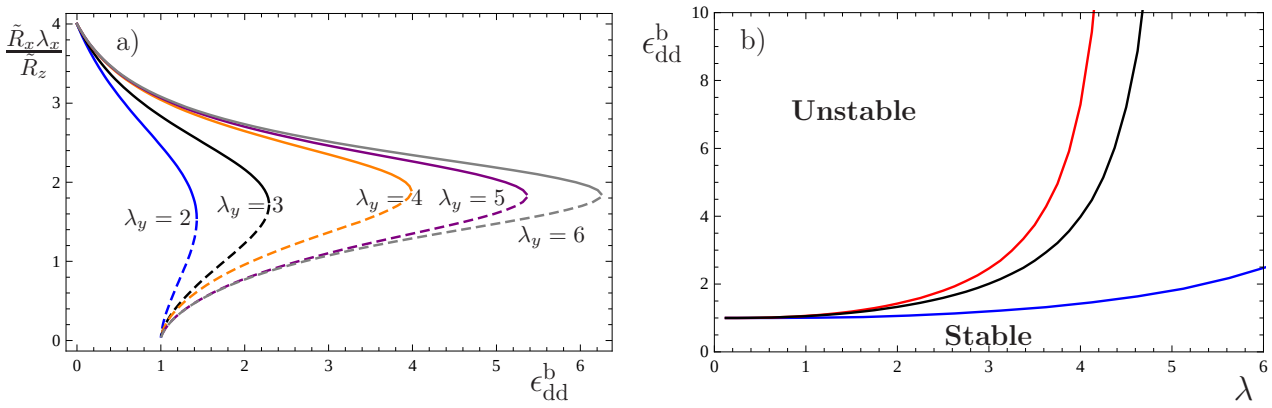

Figure 4.4: a) Aspect ratio $\kappa_x = \tilde{R}_x\lambda_x/\tilde{R}_z$ as a function of the dipolar interaction strength ϵ_{dd}^b for fixed $\lambda_x = 4$ and $\lambda_y = 2, 3, 4, 5, 6$. The solid curves depict stable solutions while the broken ones correspond to unstable configurations. b) Stability diagram of a triaxially trapped Bose-Einstein condensate. The black curve reproduces the results in Fig. 4.3b) of a cylinder-symmetric trap ($\lambda_y = \lambda_x$), while the red and the blue curves stand for the cases $\lambda_y = 2\lambda_x$ and $\lambda_y = \lambda_x/2$, respectively.

lowest excitations, it is useful to look for solutions which represent small deviations from equilibrium. Therefore, we assume the Thomas-Fermi radii to oscillate with frequency Ω in the form

$$R_i(t) = R_i(0) + \eta_i \sin(\Omega t + \varphi), \tag{4.50}$$

where $R_i(0)$ is the equilibrium value of the radius, η_i represents a small oscillation amplitude, and φ is a phase determined by the initial conditions. We then insert Eq. (4.50) into the equations of motion (4.41) and expand them around the equilibrium values, keeping terms which are of first order in the amplitudes. The frequencies of the oscillations are then given by the solutions of the eigenvalue problem

$$O_{ij}\eta_j = \Omega^2\eta_j, \tag{4.51}$$

where the matrix elements in Eq. (4.51) are given by

$$O_{ij} = \frac{7}{NM}\frac{\partial^2}{\partial R_i \partial R_j} E_{\mathrm{MF}}(R_x, R_y, R_z)\Big|_{R_k = R_k(0)} \tag{4.52}$$

and the index k is summed over the directions x, y, and z.

For a cylinder-symmetric trap, the eigenvectors of oscillation have a well defined behavior and their frequencies can be expressed in semi-analytic form. Therefore, we will restrict ourselves to present the results for this case. A broad discussion of the lowest excitation modes of a dipolar Bose-Einstein condensate in a triaxial trap can be found in Ref. [152].

At first, we recover the expressions for the three-dimensional monopole and quadrupole oscillation frequencies, denoted by the sub-indexes $+$ and $-$, respectively. The indexes stand for the fact that monopole (quadrupole) oscillations are characterized by the radial and axial variables R_ρ and R_z varying in (out of) phase. The monopole mode is, therefore, also known as the breathing mode. The

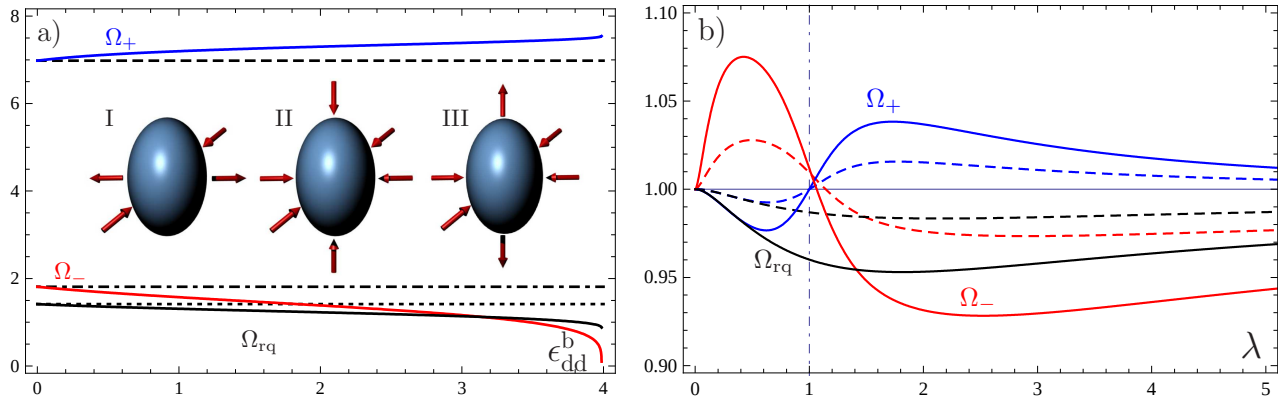

Figure 4.5: a) Frequencies of the low-lying modes in units of ω_x as functions of the dipolar interaction strength $\epsilon_{\rm dd}^{\rm b}$ for $\lambda = 4$. The blue (red) curve corresponds to the monopole (quadrupole) mode, while the broken lines represent the non-dipolar values of the frequencies $\Omega_+^{(0)} = 6.98\ \omega_x$ and $\Omega_-^{(0)} = 1.81\ \omega_x$. The inset schematically shows the shape of the length oscillations. The amplitudes are identical. b) Excitation frequencies in units of the corresponding non-dipolar values as functions of the trap aspect ratio λ for $\epsilon_{\rm dd}^{\rm b} = 0.15$ (dashed) and $\epsilon_{\rm dd}^{\rm b} = 0.42$ (continuous).

frequencies are given by the general expression,

$$\Omega_\pm = \sqrt{\frac{1}{2}\left[O_{xx} + O_{xy} + O_{zz} \pm \sqrt{(O_{xx} + O_{xy} - O_{zz})^2 + 8O_{xz}^2}\right]}, \tag{4.53}$$

where the cylinder-symmetric limits of the corresponding matrix elements (4.52) can be evaluated with the help of the identities, which are derived in Section A.5, and read

$$\begin{aligned}
\lim_{y\to x}(O_{xx}+O_{xy}) &= \omega_\rho^2 + 3\omega_\rho^2 \frac{1+\epsilon_{\rm dd}^{\rm b}\left[\frac{2R_\rho^2-R_z^2}{R_z^2-R_\rho^2} - \frac{R_\rho^2\left(R_z^2+4R_\rho^2\right)f_s(R_\rho/R_z)}{2\left(R_z^2-R_\rho^2\right)^2}\right]}{1+\epsilon_{\rm dd}^{\rm b}\left[\frac{3}{2}\frac{R_\rho^2 f_s(R_\rho/R_z)}{R_z^2-R_\rho^2} - 1\right]}, \\
\lim_{y\to x} O_{zz} &= \lambda^2\omega_\rho^2 + 2\omega_\rho^2 \frac{R_\rho^2}{R_z^2} \frac{1+\epsilon_{\rm dd}^{\rm b}\left[\frac{5R_z^2-2R_\rho^2}{R_z^2-R_\rho^2} - \frac{3R_z^2\left(4R_z^2+R_\rho^2\right)f_s(R_\rho/R_z)}{2\left(R_z^2-R_\rho^2\right)^2}\right]}{1+\epsilon_{\rm dd}^{\rm b}\left[\frac{3}{2}\frac{R_\rho^2 f_s(R_\rho/R_z)}{R_z^2-R_\rho^2} - 1\right]}, \\
\lim_{y\to x} O_{xz} &= \omega_\rho^2 \frac{R_\rho}{R_z} \frac{1+\epsilon_{\rm dd}^{\rm b}\left[-\frac{R_z^2+2R_\rho^2}{R_z^2-R_\rho^2} + \frac{15R_\rho^2R_z^2 f_s(R_\rho/R_z)}{2\left(R_z^2-R_\rho^2\right)^2}\right]}{1+\epsilon_{\rm dd}^{\rm b}\left[\frac{3}{2}\frac{R_\rho^2 f_s(R_\rho/R_z)}{R_z^2-R_\rho^2} - 1\right]}.
\end{aligned} \tag{4.54}$$

It is worth remarking that, in the case of vanishing dipolar interaction $\epsilon_{\rm dd}^{\rm b} = 0$, Eq. (4.53) yields the frequencies found for a condensate with contact interaction in the Thomas-Fermi regime, already discussed in Eq. (2.50).

Assuming a priori that the harmonic trap is a triaxial one and applying later on the cylinder symmetry makes it also possible to derive an expression for the radial quadrupole frequency. It is given

according to

$$\Omega_{\mathrm{rq}} = \sqrt{\lim_{y\to x}\left(O_{xx}-O_{xy}\right)} = \omega_\rho \sqrt{1+\frac{1-\epsilon_{\mathrm{dd}}^{\mathrm{b}}\left[\frac{\left(2R_z^2-5R_\rho^2\right)}{2\left(R_z^2-R_\rho^2\right)}+\frac{\left(6R_\rho^2R_z^2+9R_\rho^4\right)f_s(R_\rho/R_z)}{4\left(R_z^2-R_\rho^2\right)^2}\right]}{1+\epsilon_{\mathrm{dd}}^{\mathrm{b}}\left[\frac{3}{2}\frac{R_\rho^2 f_s(R_\rho/R_z)}{R_z^2-R_\rho^2}-1\right]}} \tag{4.55}$$

and reproduces the corresponding non-dipolar value $\Omega_{\mathrm{rq}} = \sqrt{2}\omega_\rho$ for $\epsilon_{\mathrm{dd}}^{\mathrm{b}} = 0$ [51].

Let us discuss the physical aspects brought about by the dipole-dipole interaction on Bose-Einstein condensates. In Fig. 4.5a), we show the dependence of the frequencies on the interaction strength $\epsilon_{\mathrm{dd}}^{\mathrm{b}}$ for $\lambda = 4$ in units of ω_ρ. The upper curves represent the monopole frequencies Ω_+: The blue curve shows the dependence on the dipolar interaction strength $\epsilon_{\mathrm{dd}}^{\mathrm{b}}$, while the dashed line stands for the non-dipolar frequency $\Omega_+^{(0)} = 6.98\ \omega_\rho$. The presence of the interaction leads to a monotonic increase of the monopole frequency. As $\epsilon_{\mathrm{dd}}^{\mathrm{b}}$ approaches the critical value, above which no solution exists, the derivative with respect to the interaction strength becomes very large. The inverse behavior is observed for the quadrupole frequency, which is a monotonically decreasing function of $\epsilon_{\mathrm{dd}}^{\mathrm{b}}$. This mode clearly characterizes the mechanical instability of the system, since its frequency approaches zero as the interaction strength gets closer to the critical value.

In what concerns the eigenvectors of the oscillation, we will not present a detailed discussion and focus on the relative phases of the amplitudes because they determine the physical character of the mode. In the inset of Fig. 4.5a), the vibration modes are displayed. Part I corresponds to two-dimensional quadrupole mode ($\eta_x = -\eta_y, \eta_z = 0$) while II depicts the monopole mode ($\eta_x \sim \eta_y \sim \eta_z$) and part III the three-dimensional quadrupole mode ($\eta_x = \eta_y \sim -\eta_z$).

Concerning the dependence on the trap aspect ratio λ, typical anisotropic effects can be observed. Fig. 4.5b) shows the oscillation frequencies in units of their non-dipolar values as functions of λ for $\epsilon_{\mathrm{dd}}^{\mathrm{b}} = 0.15$ (broken) and $\epsilon_{\mathrm{dd}}^{\mathrm{b}} = 0.42$ (continuous). For example, the monopole frequency is smaller in the presence than in the absence of the dipole-dipole interaction for $\lambda \lessapprox 1$, but the situation changes when the relation $\lambda \gtrapprox 1$ holds. For the quadrupole frequency, precisely the opposite is true. The black curves mark the two-dimensional quadrupole frequency, which is lowered by the interaction for $0 < \lambda < \infty$. The broken curves, for which the interaction strength is $\epsilon_{\mathrm{dd}}^{\mathrm{b}} = 0.15$, already show effects of about 2% to 3% and correspond to a typical sample of chromium without using a Feshbach resonance [149]. If, instead, bosonic dysprosium atoms are considered with the same particle number and assuming the same s-wave scattering length, one obtains the value $\epsilon_{\mathrm{dd}}^{\mathrm{b}} = 0.42$, due to the larger magnetic dipole moment $m = 10\ \mu_B$ [33]. In that case, a difference of about 7% appears for $\lambda \approx 0.5$ and $\lambda \approx 2.4$.

4.5 Time-of-flight Expansion

The importance of time-of-flight experiments in the area of ultracold atoms can hardly be overemphasized. For example, this technique was responsible for the first demonstration of Bose-Einstein condensation back in 1995, where the atoms were allowed to expand after turning off the trap and were imaged by absorption methods showing the characteristic central peak in the momentum distribution [22,23,153]. Since then, it has become standard to use time-of-flight measurements of the aspect ratio to observe the difference between the superfluid hydrodynamic expansion of a condensate from

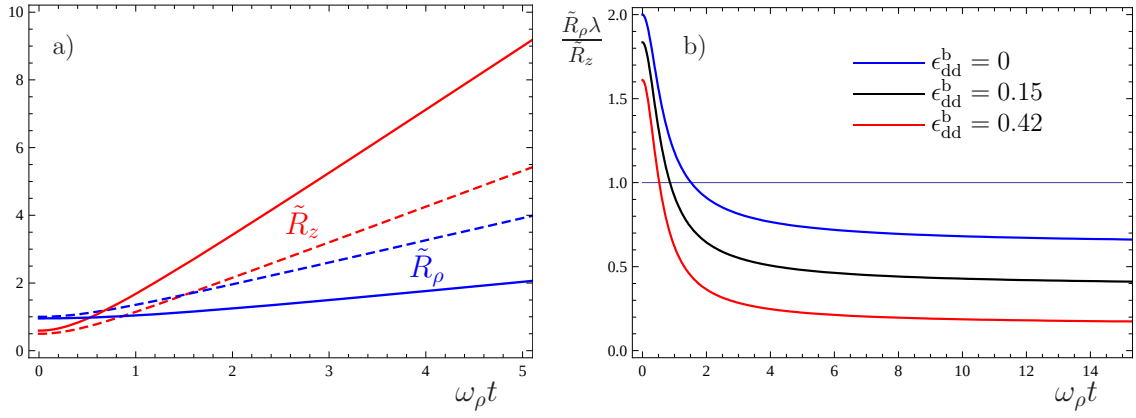

Figure 4.6: a) Thomas-Fermi radii as functions of time (ω_ρ^{-1}) in units of $R_\rho^{(0)}$ for $\epsilon_{dd}^b = 0$ (broken), $\epsilon_{dd}^b = 0.42$ (continuous), and trap aspect ratio $\lambda = 2$. The blue (red) curve represents the radius in the radial (axial) direction. Notice that the presence of the dipolar interaction (continuous curves) enhances the faster expansion of the axial radius. b) Aspect ratio $\kappa = \tilde{R}_\rho \lambda / \tilde{R}_z$ as function of time (ω_ρ^{-1}) for $\epsilon_{dd}^b = 0$ (blue), $\epsilon_{dd}^b = 0.15$ (black), and $\epsilon_{dd}^b = 0.42$ (red) with $\lambda = 2$.

the collisionless one of a normal weakly interacting Bose gas. Indeed, this technique also provided the first observation of the dipole-dipole interaction in chromium condensates. Initially, a small deviation was measured in the expansion dynamics of a condensate, which was due to the weak magnetic dipole-dipole interaction [98]. Then, strong dipolar interactions were obtained by using a Feshbach resonance to decrease the s-wave scattering length exposing for the first time the nature of a quantum ferrofluid [89].

In this section we will study this important topic of the physics of dipolar bosons by solving the equations of motion (4.42) and (4.43) without the first term, which represents the trap. Indeed, in units of the non-dipolar condensate, given by Eq. (4.45), these equations read

$$\begin{aligned}
\frac{d^2\tilde{R}_\rho(t)}{dt^2} &= \frac{\omega_\rho^2}{\tilde{R}_\rho(t)^3\tilde{R}_z(t)}\left\{1-\epsilon_{dd}^b\left[1+\frac{3}{2}\frac{\tilde{R}_\rho^2(t)\lambda^2 f_s\left(\tilde{R}_\rho(t)\lambda/\tilde{R}_z(t)\right)}{\tilde{R}_\rho^2(t)\lambda^2-\tilde{R}_z^2(t)}\right]\right\}, \\
\frac{d^2\tilde{R}_z(t)}{dt^2} &= \frac{\omega_z^2}{\tilde{R}_\rho^2(t)\tilde{R}_z^2(t)}\left\{1+2\epsilon_{dd}^b\left[1+\frac{3}{2}\frac{\tilde{R}_z^2(t) f_s\left(\tilde{R}_\rho(t)\lambda/\tilde{R}_z(t)\right)}{\tilde{R}_\rho^2(t)\lambda^2-\tilde{R}_z^2(t)}\right]\right\}.
\end{aligned} \tag{4.56}$$

The initial conditions needed for solving Eqs. (4.56) are obtained from the equilibrium values of the Thomas-Fermi radii and their derivatives at $t = 0$, i.e.,

$$\frac{d\tilde{R}_\rho(t=0)}{dt} = 0, \frac{d\tilde{R}_z(t=0)}{dt} = 0. \tag{4.57}$$

Without the dipolar interaction, one expects from Eqs. (4.56), that both radii will expand with the time scale given by their respective inverse trap frequency. For weak enough dipolar interaction, the general picture remains the same, but the expansion rate of the different radii will be slightly affected, since the dipole-dipole interaction retains the tendency to stretch the condensate along the z-direction.

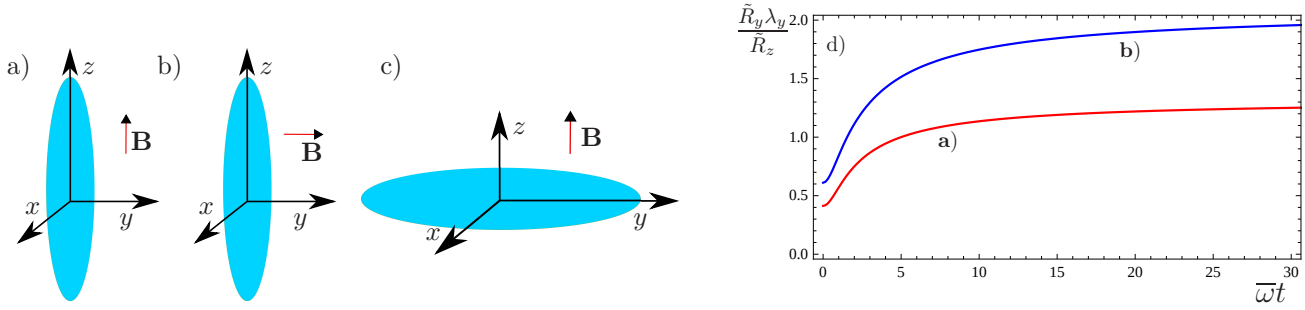

Figure 4.7: a-c) Configurations of the external aligning field with respect to the symmetry axis of cylinder-symmetric condensates. Part a) has $\lambda_x = \lambda_y = 0.5$ with $\mathbf{B} = B\hat{z}$. For part b) the trap is the same, $\lambda_x = \lambda_y = 0.5$, but with $\mathbf{B} = B\hat{y}$, which is equivalent to configuration c), which has $\lambda_x = 1$, $\lambda_y = 2$, with $\mathbf{B} = B\hat{z}$. d) Radial aspect ratio $\tilde{R}_y\lambda_y/\tilde{R}_z$ as functions of time (in units of $\overline{\omega}$) for $\epsilon_{\rm dd}^{\rm b} = 0.42$ in configurations a) and b).

We show the time-of-flight dynamics of a dipolar condensate including the dipole-dipole interaction in Fig. 4.6 for trap aspect ratio $\lambda = 2$. In part a), we plot the Thomas-Fermi radii in units of the non-interacting radius $R_\rho^{(0)}$ as a function of $\omega_\rho t$. While the broken curves are for $\epsilon_{\rm dd}^{\rm b} = 0$, the solid ones were obtained for $\epsilon_{\rm dd}^{\rm b} = 0.42$. It becomes clear that, in this case, the hydrodynamic characteristic of the expansion, where the radius with the tighter trap expands faster, is enhanced by a polarization along that direction.

With respect to the condensate aspect ratio, the usual inversion, which is a hydrodynamic characteristic, is also influenced by the dipole-dipole interaction, as can be seen from Fig. 4.6b), where the aspect ratio as a function of time is plotted for $\epsilon_{\rm dd}^{\rm b} = 0$ in blue, for $\epsilon_{\rm dd}^{\rm b} = 0.15$ in black, and for $\epsilon_{\rm dd}^{\rm b} = 0.42$ in red. Indeed, the larger the dipolar interaction strength the smaller the asymptotic value of the condensate aspect ratio, as already anticipated by the plots in Fig. 4.6a).

In addition to the effects of the dipole-dipole interaction over the time-of-flight dynamics of cylinder-symmetric Bose-Einstein condensates, that we have explored so far, we would like to point out a way to evidence the anisotropic character of the expansion. Suppose, we have a cylinder-symmetric trap with the dipoles pointed out along the symmetry axis, as in Fig. 4.7a), where we have $\lambda_x = \lambda_y = 0.5$. It is an interesting question, to investigate the influence of the polarization direction upon the aspect ratio R_y/R_z as a function of time. More precisely, we would like to know how this aspect ratio changes if we would have, instead, the external field perpendicular to the symmetry axis, according to Fig. 4.7b). Changing the orientation of the external field might not be an easy task. Nevertheless, this configuration can be studied by noticing that the aspect ratio R_y/R_z in the latter situation is equivalent to R_z/R_y, if the trap is characterized by $\lambda_x = 1$ and $\lambda_y = 2$ with the external field kept along the z-direction, as in Fig. 4.7c). Indeed, both situations are cylinder symmetric but they require nonetheless the triaxial formalism. Therefore, we have solved Eqs. (4.41) and present the results in Fig. 4.7d). The red curve, on the one hand, was produced for $\lambda_x = \lambda_y = 0.5$ and represents the aspect ratio $\frac{R_y}{R_z}$ in configuration a). On the other hand, the blue curve represents the aspect ratio $\frac{R_y}{R_z}$ plotted for $\lambda_x = 1$ and $\lambda_y = 2$, which corresponds to configuration c). The anisotropic character of the dipolar interaction in Bose-Einstein condensates is immediately made evident by such a study and can be recognized in both static (reproduced at $t = 0$ s) and dynamic values of the aspect ratio [98].

5 Beyond Mean-field Effects in Trapped Dipolar Condensates

In this chapter, we will explore the Bogoliubov-de Gennes theory of Section 2.5 to study the effects of quantum fluctuations in a harmonically trapped condensate of dipolar particles [129]. Starting from the equations for the fluctuation amplitudes, we will introduce a semiclassical approximation, which allows to perform the summation over the quantum numbers of the Bogoliubov modes in the limit of large particle numbers. In agreement with the semiclassical approach, we also make use of the so called local density approximation in order to derive an analytical expression for the exchange interaction between the condensate and the excited particles. Then we specify our general results to obtain beyond mean-field corrections to the condensate fraction, to the ground-state energy, and to the equation of state. The corrected ground-state energy allows for deriving equations of motion for the condensate widths, which include the effects of quantum fluctuations. With these equations at hand, the influence of the fluctuations can be studied in both static and dynamic properties of the system. The condensate aspect ratio, for example, is investigated and an anisotropic correction is found, which is not present in condensates with pure contact interaction. As the best prospects to measure these beyond mean-field effects in condensates are displayed by the low-lying excitations, we will give special emphasis to their investigation and show that the anisotropic aspect ratio correction plays an important role for the excitation frequencies. To conclude, we also investigate the time-of-flight dynamics and show how it is affected by quantum fluctuations for adequately chosen trap configurations.

5.1 Bogoliubov-de Gennes Equations

Let us start our analysis by specializing the Bogoliubov-de Gennes equations (2.74), where the Thomas-Fermi approximation for a trapped dipolar condensate has already been taken into account. That is, we remind that in the following equations the interaction potential of the condensate takes the form

$$V_{\mathrm{int}}\left(\mathbf{x}\right) = g\delta\left(\mathbf{x}\right) + V_{\mathrm{dd}}\left(\mathbf{x}\right), \tag{5.1}$$

with the contact interaction strength (1.11) and the long-range dipolar potential (1.12). Apart from the interaction potential, we first consider Eqs. (2.74), in their general form

$$\begin{aligned}
\varepsilon_\nu \mathcal{U}_\nu(\mathbf{x}) &= -\frac{\hbar^2\nabla^2}{2M}\mathcal{U}_\nu(\mathbf{x}) + \sqrt{n_0(\mathbf{x})}\int \mathrm{d}^3x'\, V_{\mathrm{int}}\left(\mathbf{x}-\mathbf{x}'\right)\sqrt{n_0(\mathbf{x}')}\left[\mathcal{V}_\nu(\mathbf{x}')+\mathcal{U}_\nu(\mathbf{x}')\right], \\
-\varepsilon_\nu \mathcal{V}_\nu(\mathbf{x}) &= -\frac{\hbar^2\nabla^2}{2M}\mathcal{V}_\nu(\mathbf{x}) + \sqrt{n_0(\mathbf{x})}\int \mathrm{d}^3x'\, V_{\mathrm{int}}\left(\mathbf{x}-\mathbf{x}'\right)\sqrt{n_0(\mathbf{x}')}\left[\mathcal{V}_\nu(\mathbf{x}')+\mathcal{U}_\nu(\mathbf{x}')\right],
\end{aligned} \tag{5.2}$$

with the Bogoliubov energy ε_ν and the Bogoliubov amplitudes $\mathcal{U}_\nu(\mathbf{x})$, $\mathcal{V}_\nu(\mathbf{x})$ for each mode ν. Notice that we have made use of the broken $U(1)$-symmetry by introducing the condensate density via $\Psi_0(\mathbf{x}) = \Psi_0^*(\mathbf{x}) = \sqrt{n_0(\mathbf{x})}$.

As we have remarked before, the Bogoliubov-de Gennes equations can be used to investigate the excitation spectrum of condensates over the whole range from single-particle like all the way to hydrodynamic, i.e., collective excitations [143]. Indeed, such an analysis for $N \approx 10^3$ dipoles in a cylinder-symmetric harmonic trap has been conducted before, where the Bogoliubov modes were studied numerically [154]. Here, however, we are interested in the Thomas-Fermi regime where the number of particles is large and the kinetic energy is negligible with respect to the interaction energy. This regime corresponds to the actual situation in most experiments.

Solving these equations in general is a hard task, even numerically [154]. Nonetheless, we can find analytical solutions by applying a semiclassical approximation for the energy ε_ν of the modes as well as for the Bogoliubov amplitudes $\mathcal{U}_\nu$ and $\mathcal{V}_\nu$ according to [74,155]

$$\begin{aligned} \varepsilon_\nu &\rightarrow \varepsilon(\mathbf{x},\mathbf{k}), \\ \mathcal{U}_\nu &\rightarrow \mathcal{U}(\mathbf{x},\mathbf{k})\, e^{i\mathbf{k}\cdot\mathbf{x}}, \\ \mathcal{V}_\nu &\rightarrow \mathcal{V}(\mathbf{x},\mathbf{k})\, e^{i\mathbf{k}\cdot\mathbf{x}}. \end{aligned}$$

We remark that the functions $\mathcal{U}(\mathbf{x},\mathbf{k})$ and $\mathcal{V}(\mathbf{x},\mathbf{k})$ are *slowly varying* functions of position. Therefore, their spatial derivatives can be neglected. In addition, the semiclassical approximation also has crucial implications for the normalization condition of Bogoliubov amplitudes, given, in general, in Eq. (2.60). In the continuum limit, the right-hand side of the normalization condition (2.60) contains a Dirac delta of the type $\delta(\mathbf{k}-\mathbf{k}')$. Therefore, the Bogoliubov amplitudes should obey [74]

$$\mathcal{U}(\mathbf{x},\mathbf{k})\,\mathcal{U}^*(\mathbf{x},\mathbf{k}) - \mathcal{V}(\mathbf{x},\mathbf{k})\,\mathcal{V}^*(\mathbf{x},\mathbf{k}) = 1. \tag{5.3}$$

Within this semiclassical approximation, the Bogoliubov-de Gennes become

$$\begin{aligned} \varepsilon(\mathbf{x},\mathbf{k})\,\mathcal{U}(\mathbf{x},\mathbf{k}) &= \frac{\hbar^2\mathbf{k}^2}{2M}\mathcal{U}(\mathbf{x},\mathbf{k}) + \sqrt{n_0(\mathbf{x})}\int \mathrm{d}^3x'\, V_{\mathrm{int}}(\mathbf{x}-\mathbf{x}')\,\sqrt{n_0(\mathbf{x}')}\left[\mathcal{V}(\mathbf{x}',\mathbf{k}) + \mathcal{U}(\mathbf{x}',\mathbf{k})\right] e^{i\mathbf{k}\cdot(\mathbf{x}'-\mathbf{x})}, \\ -\varepsilon(\mathbf{x},\mathbf{k})\,\mathcal{V}(\mathbf{x},\mathbf{k}) &= \frac{\hbar^2\mathbf{k}^2}{2M}\mathcal{V}(\mathbf{x},\mathbf{k}) + \sqrt{n_0(\mathbf{x})}\int \mathrm{d}^3x'\, V_{\mathrm{int}}(\mathbf{x}-\mathbf{x}')\,\sqrt{n_0(\mathbf{x}')}\left[\mathcal{V}(\mathbf{x}',\mathbf{k}) + \mathcal{U}(\mathbf{x}',\mathbf{k})\right] e^{i\mathbf{k}\cdot(\mathbf{x}'-\mathbf{x})}. \end{aligned} \tag{5.4}$$

Though we have achieved a considerable simplification of the Bogoliubov-de Gennes equations (5.2), we are still not able to solve them because of the non-local term on the right-hand side. To treat this problem, we take the next step in the semiclassical procedure and invoke the local density approximation [154]. Denoting either $\mathcal{U}(\mathbf{x},\mathbf{k})$ or $\mathcal{V}(\mathbf{x},\mathbf{k})$ by $q(\mathbf{x},\mathbf{k})$, a general term involving a convolution of the interaction potential and $q(\mathbf{x},\mathbf{k})$ is approximated, according to the local density approximation, by

$$\begin{aligned} (\xi q)(\mathbf{x},\mathbf{k}) &\equiv \sqrt{n_0(\mathbf{x})}\int \mathrm{d}^3x'\, \left[g\delta(\mathbf{x}-\mathbf{x}') + V_{\mathrm{dd}}(\mathbf{x}-\mathbf{x}')\right]\sqrt{n_0(\mathbf{x}')}\, q(\mathbf{x}',\mathbf{k})\, e^{i\mathbf{k}\cdot(\mathbf{x}'-\mathbf{x})}, \\ &\approx \xi(\mathbf{x},\mathbf{k})\, q(\mathbf{x},\mathbf{k}), \end{aligned} \tag{5.5}$$

together with the abbreviation

$$\xi(\mathbf{x},\mathbf{k}) = gn_0(\mathbf{x})\left[1+\epsilon_{\rm dd}^{\rm b}\left(3\cos^2\theta-1\right)\right], \tag{5.6}$$

where the angle θ is defined according to $\cos\theta = k_z/|\mathbf{k}|$.

Basically, the local density approximation amounts to considering that a *slowly varying* quantity in an inhomogeneous system can be evaluated by calculating it first in a homogeneous counterpart, where neither the condensate density nor the Bogoliubov amplitudes depend on the position and, after the calculation, restoring the position dependence of the corresponding quantities. In the thermodynamical limit of infinite particle number and energy levels, which are arbitrarily close to each other, this is plausible. However, it is important to point out that, besides the plausibility of the physical arguments, the semiclassical procedure of the transformations (5.3) can be justified within the realm of a systematic gradient expansion in the Wigner representation, where the local density approximation is shown to be the leading contribution [74]. This has the important consequence that systematic quantum corrections to the leading semiclassical term can be implemented, as in the case of the Thomas-Fermi model for heavy atoms [156].

In this approximation, all the quantities involved in Eq. (5.4) become local and the spectrum can be obtained algebraically by taking into account the normalization condition (5.3), yielding

$$\varepsilon^2(\mathbf{x},\mathbf{k}) = \varepsilon_{\rm LDA}^2(\mathbf{x},\mathbf{k}) - \xi^2(\mathbf{x},\mathbf{k}), \tag{5.7}$$

with the abbreviation

$$\varepsilon_{\rm LDA}(\mathbf{x},\mathbf{k}) = \frac{\hbar^2\mathbf{k}^2}{2M} + \xi(\mathbf{x},\mathbf{k}). \tag{5.8}$$

Moreover, the semiclassical Bogoliubov amplitudes are given by

$$\mathcal{U}(\mathbf{x},\mathbf{k})^2 - 1 = \mathcal{V}(\mathbf{x},\mathbf{k})^2 = \frac{1}{2}\left[\frac{\varepsilon_{\rm LDA}(\mathbf{x},\mathbf{k})}{\varepsilon(\mathbf{x},\mathbf{k})} - 1\right]. \tag{5.9}$$

We can now explore the effects of quantum fluctuations on interesting physical quantities such as the Bogoliubov depletion, the corrections to the ground-state energy, and the chemical potential.

5.2 Condensate Depletion

In this section we will consider the number of particles which are expelled from the condensate by the contact and the dipolar interactions, i.e., the condensate depletion, in the case of a dipolar Bose-Einstein condensate trapped in a harmonic potential, which corresponds to the real experimental situation. The condensate depletion, in general, can be calculated according to the Bogoliubov-de Gennes theory, which was worked out in Section 2.5 and is given by Eq. (2.70). For a homogeneous dipolar system, it has already been discussed in Section Eq. (3.3). In a trapped gas, the depletion becomes a function of position due to the inhomogeneity brought about by the trap.

Let us first consider the depletion density. In the semiclassical approximation, we replace the sum-

mation over the states by the momentum integral (3.29) and obtain

$$\Delta n(\mathbf{x}) = \int \frac{\mathrm{d}^3k}{(2\pi)^3} \mathcal{V}\left(\mathbf{x},\mathbf{k}\right) \mathcal{V}^*\left(\mathbf{x},\mathbf{k}\right) = \int \frac{\mathrm{d}^3k}{(2\pi)^3} \frac{1}{2} \left[\frac{\varepsilon_{\mathrm{LDA}}\left(\mathbf{x},\mathbf{k}\right)}{\varepsilon\left(\mathbf{x},\mathbf{k}\right)} - 1 \right], \tag{5.10}$$

where, in order to derive the second equality, we have made use of Eq. (5.9). After performing the momentum integrals, which proceeds in close analogy with the homogeneous case of Eq. (3.30), we obtain

$$\Delta n(\mathbf{x}) = \frac{8}{3} \mathcal{D}(\epsilon_{\mathrm{dd}}^{\mathrm{b}}) \sqrt{\frac{n(\mathbf{x})^3 a_s^3}{\pi}}, \tag{5.11}$$

with the depletion function $\mathcal{D}(\epsilon_{\mathrm{dd}}^{\mathrm{b}})$ which has been already introduced in Eq. (3.33) of Chapter 3. For a gas with pure contact interaction, where $\mathcal{D}(0) = 1$, Eq. (5.11) reduces to the expression derived by Timmermans, Tommasini, and Huang [74]. It is useful to remark that the particle density in Eq. (5.11) is given by its value in mean-field approximation, i.e., by the parabolic profile given by Eq. (4.20).

For the excited fraction, obtained by integrating over the Thomas-Fermi parabolic profile (4.20), one gets

$$\frac{\Delta N}{N} = \frac{5\sqrt{\pi}}{8} \mathcal{D}(\epsilon_{\mathrm{dd}}^{\mathrm{b}}) \sqrt{n(\mathbf{0}) a_s^3}, \tag{5.12}$$

showing that the depletion in a trapped system depends on the gas parameter evaluated at the center of the trap. Also Eq. (5.12) is in agreement with the well established expression for the condensate with contact interaction [74,157].

Due to the local density approximation, the depletion in a harmonically trapped Bose-Einstein condensation turns out to be governed by the same function $\mathcal{D}(\epsilon_{\mathrm{dd}}^{\mathrm{b}})$ as in the homogeneous case. The presence of the dipole-dipole interaction affects the depletion of the condensate in two ways. On the one hand, it controls the prefactor of Eq. (5.12) through the depletion function $\mathcal{D}(\epsilon_{\mathrm{dd}}^{\mathrm{b}})$ and, on the other hand, it also affects the gas parameter at the trap center, since it alters the values of the Thomas-Fermi radii. For typical ^{52}Cr experiments [100], the gas parameter is approximately $n(\mathbf{0})a_s^3 \approx 2\times10^{-4}$ in a spherical configuration and does not vary appreciably as $\epsilon_{\mathrm{dd}}^{\mathrm{b}}$ is varied from 0 to 1. The function $\mathcal{D}(\epsilon_{\mathrm{dd}}^{\mathrm{b}})$, on the contrary, grows monotonically from 1 to approximately 1.30. Nonetheless, the quantum depletion, which amounts to $\frac{\Delta N}{N} \approx 1.7\%$, is still too small to be experimentally resolved from measurement errors.

5.3 Ground-state Energy and Equation of State

The presence of quantum fluctuations also yields corrections to the ground-state energy of a dipolar condensate. The general expression providing this correction can be inferred from Eq. (2.72), which corresponds to the ground-state energy of a condensate as given by the Bogoliubov-de Gennes theory of Section 2.5. In the semiclassical approximation, the spatial density of the energy correction is given by

$$\Delta E(\mathbf{x}) = \int \frac{\mathrm{d}^3k}{(2\pi)^3} \frac{1}{2} \left[\varepsilon\left(\mathbf{x},\mathbf{k}\right) - \varepsilon_{\mathrm{LDA}}\left(\mathbf{x},\mathbf{k}\right) \right]. \tag{5.13}$$

Performing the momentum integration in an analogous manner as in the calculation of the depletion (5.11) yields the local correction to the ground-state energy

$$\Delta E(\mathbf{x}) = \frac{64}{15} g n(\mathbf{x})^2 \mathcal{I}(\epsilon_{\mathrm{dd}}^{\mathrm{b}}) \sqrt{\frac{n(\mathbf{x}) a_s^3}{\pi}}, \tag{5.14}$$

where $\mathcal{I}(\epsilon_{\mathrm{dd}}^{\mathrm{b}})$ from Eq. (3.38) is the function which appears in the correction to the ground-state energy of a homogeneous dipolar condensate. Performing the elementary spatial integration over the extension of the parabolic profile Eq. (4.20), the correction to the ground-state energy finally becomes

$$\Delta E = \frac{5\sqrt{\pi}}{8} g n(\mathbf{0}) \mathcal{I}(\epsilon_{\mathrm{dd}}^{\mathrm{b}}) \sqrt{n(\mathbf{0}) a_s^3}. \tag{5.15}$$

This integrated energy correction is of much practical interest because it can be used to implement corrections due to quantum fluctuations in the mean-field equations of motion Eq. (4.41). This can be done variationally by noticing that the density at the center of the trap at mean-field level is given through the constant n_0, defined in Eq. (4.21). Alternatively, one can implement the corrections to the mean-field theory by means of the equation of state. To this end we determine the corrected equation of state by varying the quantum corrected total energy

$$E_{\mathrm{Q}} = E_{\mathrm{MF}} + \Delta E \tag{5.16}$$

with respect to the density. The resulting beyond mean-field equation of state follows from Eq. (2.33) and reads

$$\mu(\mathbf{x}) = \frac{\delta}{\delta n(\mathbf{x})} \int \mathrm{d}^3 y \, [E_{\mathrm{MF}}(\mathbf{y}) + \Delta E(\mathbf{y})] = U_{\mathrm{trap}}(\mathbf{x}) + g n(\mathbf{x}) + \Phi_{\mathrm{dd}}(\mathbf{x}) + \frac{32}{3} g n(\mathbf{x}) \mathcal{I}(\epsilon_{\mathrm{dd}}^{\mathrm{b}}) \sqrt{\frac{n(\mathbf{x}) a_s^3}{\pi}}, \tag{5.17}$$

where $E_{\mathrm{MF}}(\mathbf{y})$ in Eq. (5.17) corresponds to the density (4.20).

The importance of Eq. (5.17) lies in the fact that it provides the local chemical potential as a function of the particle density. In this form it can be immediately used in the hydrodynamic formalism to study beyond mean-field properties of dipolar condensates. Indeed, S. Stringari and L. Pitaevskii have performed a corresponding study in the case of a condensate with pure contact interaction [15]. We will discuss their results in more detail in the following. Even though we rather treat the corrections due to the quantum fluctuations through a variational instead of a hydrodynamic approach, we recover the results of Pitaevskii and Stringari in a quite natural way. Despite the fact that both methods are equivalent, the variational approach seems to be more adequate to include dipolar interactions.

5.4 Equations of Motion

We have calculated the correction to the ground-state energy by assuming that the condensate retains its inverse parabolic profile from Eq. (4.20). These calculations are only justified if the gas properties are dominated by the repulsive contact interaction and if the quantum fluctuations are not too strong. Therefore, it is not only legitimate to calculate the quantum corrections for a mean-field like density profile but also to treat this correction as being a small one. With these assumptions in mind, we

derive the corresponding equations of motion for a dipolar condensate

$$\frac{MN}{7}\ddot{R}_i = -\frac{\partial E_{\mathrm{Q}}\left(R_x, R_y, R_z,\right)}{\partial R_i}, \tag{5.18}$$

where the quantum corrected energy density (5.16) is composed by the mean-field energy Eq. (4.28) and the correction (5.14).

The beyond mean-field energy is explicitly given by

$$\frac{7}{MN}E_{\mathrm{Q}}\left(R_x, R_y, R_z\right) = \frac{1}{2}\sum_i \omega_i^2 R_i^2 + \frac{15gN}{4\pi M\overline{R}^3}\left[1 - \epsilon_{\mathrm{dd}}^{\mathrm{b}} f\left(\frac{R_x}{R_z}, \frac{R_y}{R_z}\right) + \frac{2}{3}\frac{\gamma\mathcal{I}(\epsilon_{\mathrm{dd}}^{\mathrm{b}})a_s^{3/2}N^{1/2}}{\overline{R}^{3/2}}\right]. \tag{5.19}$$

The quantum fluctuations are accounted for by the last term and the constant γ appearing in the prefactor reads

$$\gamma = \sqrt{\frac{3^3 \cdot 5^3 \cdot 7^2}{2^{13}}} \approx 4.49. \tag{5.20}$$

It will be useful to introduce as an abbreviation the function

$$\beta(\epsilon_{\mathrm{dd}}^{\mathrm{b}}) = \gamma\mathcal{I}(\epsilon_{\mathrm{dd}}^{\mathrm{b}})a_s^{3/2}N^{1/2}, \tag{5.21}$$

which characterizes the influence of the quantum fluctuations. With this definition, the equations of motion (5.18) can be written as

$$\begin{aligned}
\ddot{R}_x &= -\omega_x^2 R_x + \frac{15gN}{4\pi M R_x^2 R_y R_z}\left\{1 - \epsilon_{\mathrm{dd}}^{\mathrm{b}}\left[1 - R_x\partial_{R_x}\right] f\left(\frac{R_x}{R_z}, \frac{R_y}{R_z}\right) + \frac{\beta}{(R_x R_y R_z)^{1/2}}\right\}, \\
\ddot{R}_y &= -\omega_y^2 R_y + \frac{15gN}{4\pi M R_x R_y^2 R_z}\left\{1 - \epsilon_{\mathrm{dd}}^{\mathrm{b}}\left[1 - R_y\partial_{R_y}\right] f\left(\frac{R_x}{R_z}, \frac{R_y}{R_z}\right) + \frac{\beta}{(R_x R_y R_z)^{1/2}}\right\}, \\
\ddot{R}_z &= -\omega_z^2 R_z + \frac{15gN}{4\pi M R_x R_y R_z^2}\left\{1 - \epsilon_{\mathrm{dd}}^{\mathrm{b}}\left[1 - R_z\partial_{R_z}\right] f\left(\frac{R_x}{R_z}, \frac{R_y}{R_z}\right) + \frac{\beta}{(R_x R_y R_z)^{1/2}}\right\}.
\end{aligned} \tag{5.22}$$

These equations represent the generalization of Eqs. (4.41) in order to include beyond mean-field effects. Notice that we choose to omit the argument of the function β. The beyond mean-field equations of motion (5.22) represent the main result of this chapter. They allow us to investigate the effects of quantum fluctuations in a dipolar condensate in a triaxial harmonic trap. Indeed, solving these equations in general is both difficult and physically useless, due to the fact that the quantum corrections only have the particular form presented here, if they are small. For this reason, we will treat all the β terms as small and calculate the physical quantities always only up to first order in β.

As a matter of fact, most experiments are carried out in cylinder-symmetric traps. For this reason it is important to study this case carefully. To this end, we specialize Eqs. (5.22) to the case of a cylinder-symmetric trap with the dipoles oriented along the Oz-axis. By doing so, we have to take into account the properties of the anisotropy function $f_{\mathrm{s}}(x)$, which are summarized in Appendix A. The

corresponding equations of motion, in this case, reduce to

$$\begin{aligned}\ddot{R}_\rho &= -\omega_\rho^2 R_\rho + \frac{15gN}{4\pi M R_\rho^3 R_z}\left[1 - \epsilon_{\rm dd}^{\rm b} A + \frac{\beta}{R_\rho R_z^{1/2}}\right], \\ \ddot{R}_z &= -\omega_z^2 R_z + \frac{15gN}{4\pi M R_\rho^2 R_z^2}\left[1 + 2\epsilon_{\rm dd}^{\rm b} B + \frac{\beta}{R_\rho R_z^{1/2}}\right],\end{aligned} \tag{5.23}$$

together with the definitions

$$\begin{aligned}A\left(\frac{R_\rho}{R_z}\right) &= 1 + \frac{3}{2}\frac{R_\rho^2}{R_\rho^2 - R_z^2} f_s\left(\frac{R_\rho}{R_z}\right), \\ B\left(\frac{R_\rho}{R_z}\right) &= 1 + \frac{3}{2}\frac{R_z^2}{R_\rho^2 - R_z^2} f_s\left(\frac{R_\rho}{R_z}\right),\end{aligned} \tag{5.24}$$

In the absence of quantum fluctuations, the mean-field equations of motion (4.43) are reproduced by Eqs. (5.23). In addition, we find it appropriate for the following calculations to introduce the abbreviations

$$\begin{aligned}A_i\left(\frac{R_\rho}{R_z}\right) &= \partial_{R_i} A\left(\frac{R_\rho}{R_z}\right), \\ B_i\left(\frac{R_\rho}{R_z}\right) &= \partial_{R_i} B\left(\frac{R_\rho}{R_z}\right).\end{aligned} \tag{5.25}$$

Notice that, in order to make the notation more compact, we will sometimes omit the argument of the functions as long as no confusion can possibly arise.

5.5 Static Properties

In this section, we will investigate the static properties of a dipolar condensate beyond the mean-field approximation. After discussing the influence of the quantum fluctuations on the stability diagram, we will proceed to calculate the correction to the condensate aspect ratio and study the dependence of this quantity on both the relative interaction strength $\epsilon_{\rm dd}^{\rm b}$ and the trap aspect ratio λ. The starting point of the discussion of the statics of dipolar Bose-Einstein condensates beyond the mean-field approximation is the static version of the system of equations (5.23), which read

$$\begin{aligned}\omega_\rho^2 R_\rho &= \frac{15gN}{4\pi M R_\rho^3 R_z}\left[1 - \epsilon_{\rm dd}^{\rm b} A + \frac{\beta}{R_\rho R_z^{1/2}}\right], \\ \omega_z^2 R_z &= \frac{15gN}{4\pi M R_\rho^2 R_z^2}\left[1 + 2\epsilon_{\rm dd}^{\rm b} B + \frac{\beta}{R_\rho R_z^{1/2}}\right].\end{aligned} \tag{5.26}$$

Let us first consider the effects of the beyond mean-field corrections on the stability diagram presented in the right-hand side of Fig. 4.3. There, we have shown that a stable ground-state only exists for values of the dipolar interaction strength within the range $0 \leq \epsilon_{\rm dd}^{\rm b} \leq 1$. For values of $\epsilon_{\rm dd}^{\rm b}$ larger than 1, the ground state is, at best, metastable. Quantum fluctuations cannot alter this. When evaluating

corrections due to quantum fluctuations within the Bogoliubov theory, an expansion is performed up to second order in the fluctuations of the field operators around their mean-field value. Such an expansion can only be carried out if the corresponding ground-state is stable. Therefore, the effects of quantum fluctuations on the properties of a dipolar condensate are only physically meaningful as long as $0 \leq \epsilon_{\mathrm{dd}}^{\mathrm{b}} \leq 1$.

The Thomas-Fermi radii, in opposition to the stability diagram, are affected by the presence of quantum fluctuations. In order to study this effect quantitatively, we expand the Thomas-Fermi radii in the form

$$R_\rho = R_\rho^0 + \delta R_\rho, \quad R_z = R_z^0 + \delta R_z, \tag{5.27}$$

where δR_i is a correction of the order β. Inserting the ansatz (5.27) into the equations (5.26) and keeping only terms up to first order in β, a straightforward calculation yields

$$\begin{pmatrix} \delta R_\rho \\ \delta R_z \end{pmatrix} = \frac{\beta}{5R_\rho^0 R_z^{0\,1/2}} \begin{pmatrix} \frac{R_\rho^0\left[2+2\epsilon_{\mathrm{dd}}^{\mathrm{b}}\left(3B^0-R_z^0B_z^0\right)+\epsilon_{\mathrm{dd}}^{\mathrm{b}}\left(A^0-R_z^0A_z^0\right)\right]}{2+\epsilon_{\mathrm{dd}}^{\mathrm{b}}[2(2B^0-R_z^0B_z^0)-(2A^0+R_z^0A_z^0)]-2\left(\epsilon_{\mathrm{dd}}^{\mathrm{b}}\right)^2[A^0(B^0-R_z^0B_z^0)+B^0(A^0+R_z^0A_z^0)]} \\ \frac{R_z^0\left[2-2\epsilon_{\mathrm{dd}}^{\mathrm{b}}\left(2B^0+R_z^0B_z^0\right)-\epsilon_{\mathrm{dd}}^{\mathrm{b}}\left(4A^0+R_z^0A_z^0\right)\right]}{2+\epsilon_{\mathrm{dd}}^{\mathrm{b}}[2(2B^0-R_z^0B_z^0)-(2A^0+R_z^0A_z^0)]-2\left(\epsilon_{\mathrm{dd}}^{\mathrm{b}}\right)^2[A^0(B^0-R_z^0B_z^0)+B^0(A^0+R_z^0A_z^0)]} \end{pmatrix}. \tag{5.28}$$

To arrive at Eq. (5.28) we have used the identities $R_zA_z = -R_\rho A_\rho$ and $R_zB_z = -R_\rho B_\rho$, which follow directly from the definitions (5.24). Furthermore, the superscript ^{0} is used to denote the mean-field values of the corresponding quantities.

According to Eq. (5.28), in the absence of the dipole-dipole interaction, i.e., for $\epsilon_{\mathrm{dd}}^{\mathrm{b}} = 0$, the corrections to the radius in ith direction is proportional to the corresponding radius and the proportionality constants are the same for different directions. This has the consequence that, for a gas with pure contact interaction, the Thomas-Fermi radii in the different directions are changed by different amounts but their ratio remains constant. This is due to the isotropy of the contact interaction. In general, however, the aspect ratio of the dipolar condensate will change due to the presence of the quantum fluctuations. Let us consider the beyond mean-field aspect ratio, defined as

$$\kappa \equiv \frac{R_\rho}{R_z} = \kappa^0 + \Delta\kappa, \tag{5.29}$$

where $\Delta\kappa$ is of order β and we denote by κ^0 the mean-field aspect ratio

$$\kappa^0 = \frac{R_\rho^0}{R_z^0}. \tag{5.30}$$

Is is useful to define the relative correction according to

$$\delta\kappa = \frac{\Delta\kappa}{\kappa^0}. \tag{5.31}$$

Using the corrections of the Thomas-Fermi radii (5.28), the relative correction of the aspect ratio,

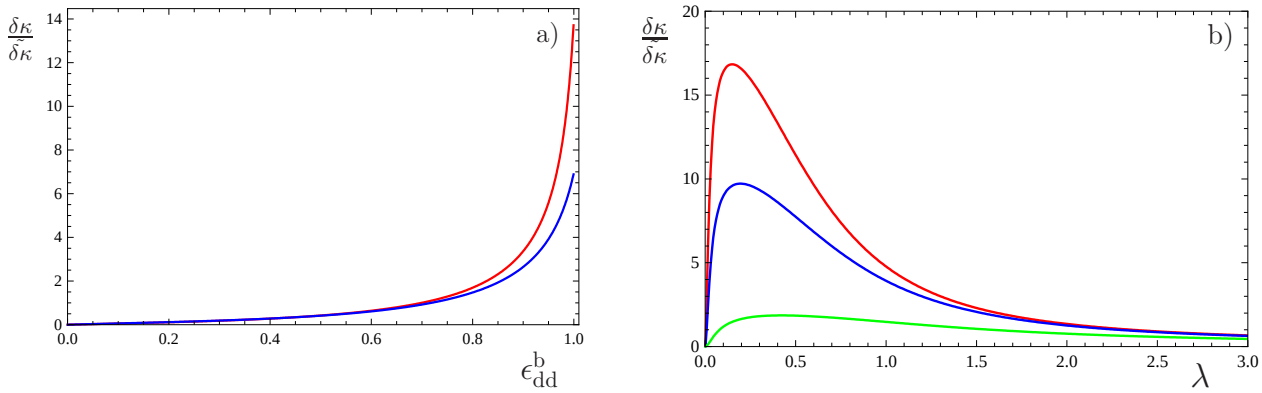

Figure 5.1: a) Relative correction to the aspect ratio $\delta\kappa = \frac{\Delta\kappa}{\kappa^0}$ as a function of $\epsilon_{\rm dd}^{\rm b}$ for $\lambda = 0.75$ (red) and $\lambda = 1.00$ (blue) in units of $\tilde{\delta\kappa}$, as defined in Eq. (5.33). b) Same quantity $\delta\kappa$ as a function of λ for $\epsilon_{\rm dd}^{\rm b} = 0.8$ (green), $\epsilon_{\rm dd}^{\rm b} = 0.95$ (blue), and $\epsilon_{\rm dd}^{\rm b} = 0.97$ (red).

becomes, to first order in β, equal to

$$\delta\kappa = \frac{\tilde{\delta\kappa}\left(\lambda^2-\kappa^2\right)\left(1-\epsilon_{\rm dd}^{\rm b}A^0\right)}{\left\{2+\epsilon_{\rm dd}^{\rm b}\left[2\left(2B^0-R_z^0B_z^0\right)-\left(2A^0+R_z^0A_z^0\right)\right]-2\left(\epsilon_{\rm dd}^{\rm b}\right)^2\left[A^0\left(B^0-R_z^0B_z^0\right)+B^0\left(A^0+R_z^0A_z^0\right)\right]\right\}}, \tag{5.32}$$

where we have introduced the abbreviation

$$\tilde{\delta\kappa} = \frac{105\sqrt{\pi}}{32}\sqrt{a_s^3 n(\mathbf{0})}. \tag{5.33}$$

In addition, we have made use of the relation between the auxiliary functions

$$\epsilon_{\rm dd}^{\rm b}\left(A^0+2B^0\right) = \frac{R_\rho^{0\,2}R_z^0}{15gN}\left(\omega_\rho^2 R_\rho^{0\,2}-\omega_z^2 R_z^{0\,2}\right), \tag{5.34}$$

which is valid at equilibrium to zeroth order in β due to Eqs. (5.24)–(5.26).

An important feature of the aspect ratio correction Eq. (5.32) is the role played by the trap anisotropy due to the presence of the dipole-dipole interaction. In Fig. 5.1a), we plot the correction $\delta\kappa/\tilde{\delta\kappa}$ as a function on the relative interaction strength $\epsilon_{\rm dd}^{\rm b}$ at a fixed trap aspect ratio λ. The red curve is for $\lambda = 0.75$ and the blue one for $\lambda = 1.00$. For a vanishing dipolar interaction, the condensate aspect ratio is not affected by the quantum fluctuations. As $\epsilon_{\rm dd}^{\rm b}$ increases, a nonvanishing correction shows up. When approaching the critical value $\epsilon_{\rm dd}^{\rm b} = 1$, above which the correction to the ground-state energy due to quantum fluctuations becomes imaginary, the role of quantum fluctuations in the condensate aspect ratio cannot be neglected anymore. In order to estimate the importance of this correction, let us adopt the experimental values of the average trap frequencies and number of condensed particles from the ^{52}Cr-experiment reported in Ref. [89]. In that case, the gas parameter at the center of the trap is such that the unit of the variation of the aspect ratio is $\tilde{\delta\kappa} \approx 0.06$, which renders the observation very difficult, since it would only become appreciable at large values of $\epsilon_{\rm dd}^{\rm b}$.

5.6 Hydrodynamic Excitations

In this section, we address the question of how large the impact of quantum fluctuations is for the low-lying excitations in a dipolar condensate. Indeed, the excitation frequencies have been proposed as an adequate diagnostic tool for this kind of investigation in a condensate with contact interaction as early as 1998 [15], only three years after the condensation in quasi ideal Bose gases was achieved. In that work, Pitaevskii and Stringari showed that quantum fluctuations are the leading factor in shifting the frequencies of the collective oscillations in stable Bose-condensed gases. We will extend their work to include the dipole-dipole interaction and explore the novel features due to its presence.

We proceed to calculate the shift in the excitation frequencies due to quantum fluctuations by separating the Thomas-Fermi radii as a function of time in two contributions

$$R_i(t) = R_i(0) + \eta_i \sin(\Omega t + \varphi), \tag{5.35}$$

where $R_i(0)$ is the equilibrium value of the radius and η_i represents a small amplitude of oscillation with frequency Ω. In addition, φ denotes a phase which is determined by the initial conditions. The calculation follows in close analogy with the mean-field analysis performed in Section 4.4. The main difference is twofold: on the one hand, the equilibrium values of the Thomas-Fermi radii are themselves corrected by a term of order β due to the presence of quantum fluctuations according to Eq. (5.27) with $\delta R_i \propto \beta$, calculated in Eq. (5.28), and R_i^0 being the mean-field Thomas-Fermi radius; on the other hand, the matrix defining the eigenvalue problem, i.e.,

$$\begin{pmatrix} h_{\rho\rho} & h_{\rho z} \\ 2h_{\rho z} & h_{zz} \end{pmatrix} \begin{pmatrix} \eta_\rho \\ \eta_z \end{pmatrix} = \Omega^2 \begin{pmatrix} \eta_\rho \\ \eta_z \end{pmatrix}, \tag{5.36}$$

is also corrected by matrix elements of the order β. Therefore, we write the matrix elements occurring in the left-hand side of Eq. (5.36) as

$$h_{ij} = h_{ij}^0 + \delta h_{ij}, \tag{5.37}$$

with $\delta h_{ij} \propto \beta$ and identify the mean-field matrix elements with the ones of the cylinder-symmetric limit of the corresponding triaxial problem

$$\begin{aligned} h_{\rho\rho}^0 &= \lim_{y\to x} (O_{xx} + O_{xy}), \\ h_{\rho z}^0 &= \lim_{y\to x} O_{xz}, \\ h_{zz}^0 &= \lim_{y\to x} O_{zz}, \end{aligned} \tag{5.38}$$

which have been given explicitly in Eq. (4.54). We now take advantage of the fact that the mean-field matrix elements (5.38) are functions of the aspect ratio $\kappa = R_\rho/R_z$ alone and not of the radii individually. This allows us to calculate the contribution to the corrected eigenvalue problem due to the change in the aspect ratio. In addition, there is a further contribution coming from the fact that the equations of motion Eqs. (5.23) have also been corrected. Together, both contributions are given

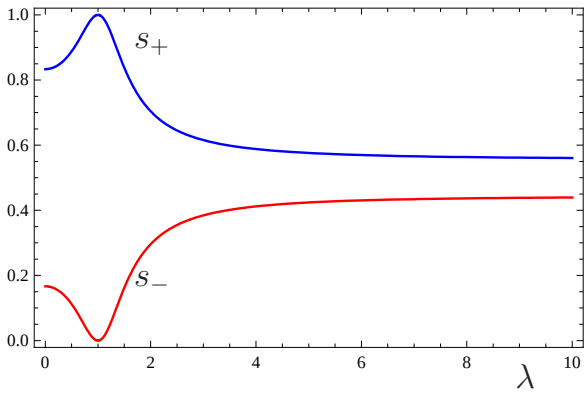

Figure 5.2: Functions s_+ (blue) and s_- (red) providing the dependence on the trap aspect ratio λ of the corrections to the monopole and quadrupole frequencies, respectively, of a condensate with contact interaction alone [15]. Notice that the extremal values of these functions appear at $\lambda = 1$, where $s_+(\lambda = 1) = 1$ and $s_-(\lambda = 1)$ vanishes.

by

$$\begin{aligned}
\delta h_{\rho\rho} &= \left.\frac{\partial h_{\rho\rho}}{\partial \kappa}\right|_{\kappa=\frac{R_\rho^0}{R_z^0}} \Delta\kappa + \frac{\beta\omega_\rho^2}{R_\rho^0 R_z^{0\,1/2}} \frac{\left[1-\epsilon_{\rm dd}^{\rm b}\left(A^0 - R_z^0 A_z^0\right)\right]}{\left(1-\epsilon_{\rm dd}^{\rm b} A^0\right)^2}, \\
\delta h_{\rho z} &= \left.\frac{\partial h_{\rho z}}{\partial \kappa}\right|_{\kappa=\frac{R_\rho^0}{R_z^0}} \Delta\kappa + \frac{\beta\omega_\rho^2}{2R_\rho^0 R_z^{0\,1/2}} \frac{\left[1-\epsilon_{\rm dd}^{\rm b}\left(A^0 + 2R_z^0 A_z^0\right)\right]}{\left(1-\epsilon_{\rm dd}^{\rm b} A^0\right)^2}, \\
\delta h_{zz} &= \left.\frac{\partial h_{zz}}{\partial \kappa}\right|_{\kappa=\frac{R_\rho^0}{R_z^0}} \Delta\kappa + \frac{\beta\omega_\rho^2}{2R_\rho^0 R_z^{0\,1/2}} \left(\frac{R_\rho^0}{R_z^0}\right)^2 \frac{\left[1-\epsilon_{\rm dd}^{\rm b}\left(5A^0 + 8B^0 - R_z^0 B_z^0\right)\right]}{\left(1-\epsilon_{\rm dd}^{\rm b} A^0\right)^2}.
\end{aligned} \tag{5.39}$$

To obtain the corrected oscillation frequencies we proceed as we did in the mean-field analysis but we treat the terms of the order β as a perturbation and expand the corresponding frequencies up to first order in that term. By doing this, we recover the mean-field frequencies already discussed in Eqs. (4.53) and (4.54). For the relative correction to the frequencies we obtain

$$\frac{\Delta\Omega_\pm}{\Omega_\pm} = \frac{1}{4{\Omega_\pm^0}^2}\left[\delta h_{\rho\rho} + \delta h_{zz} \pm \frac{2\left(h_{\rho z}^0 \delta h_{z\rho} + h_{z\rho}^0 \delta h_{\rho z}\right) + \left(h_{\rho\rho}^0 - h_{zz}^0\right)\left(\delta h_{\rho\rho} - \delta h_{zz}\right)}{\sqrt{4h_{\rho z}^0 h_{z\rho}^0 + \left(h_{\rho\rho}^0 - h_{zz}^0\right)^2}}\right]. \tag{5.40}$$

In order to estimate how large the corrections to the oscillation frequencies can be, it is convenient to introduce the quantity

$$\delta\tilde{\Omega} = \frac{63\sqrt{\pi}}{128}\sqrt{a_s^3\, n(\mathbf{0})}, \tag{5.41}$$

which relates the size of the shift in the frequencies to the gas parameter at the center of the trap $a_s^3\, n(\mathbf{0})$. In the case of pure contact interaction, i.e., $\epsilon_{\rm dd}^{\rm b} = 0$, the correction to the excitation frequencies becomes [15]

$$\frac{\Delta\Omega_{\delta,\pm}}{\Omega_{\delta,\pm}} = \frac{3\beta\left(\epsilon_{\rm dd}^{\rm b}\right)}{20R_\rho^0 R_z^{0\,1/2}} s_\pm(\lambda) = \delta\tilde{\Omega}\, s_\pm(\lambda), \tag{5.42}$$

where the functions s_+ and s_- correspond to the monopole and quadrupole corrections, respectively.

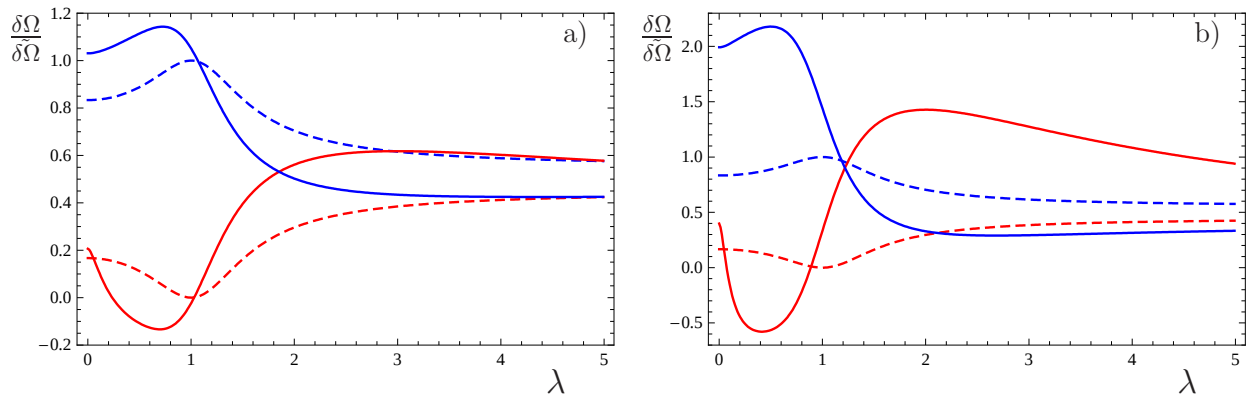

Figure 5.3: Dependence on the trap anisotropy λ of the relative correction to the collective oscillation frequencies of dipolar Bose-Einstein condensates $\frac{\Delta\Omega_\pm}{\Omega_\pm}$ in units of $\tilde{\Delta\Omega}$. The dashed lines are for non-dipolar gases. a) Frequency correction for ^{52}Cr for the parameters of the experiment in Ref. [89] by assuming a relative interaction strength of $\epsilon_{\rm dd}^{\rm b} \approx 0.16$. This yields $\tilde{\Delta\Omega} \approx 0.01$. b) Same curve for Dy. Since the s-wave scattering length for dysprosium has not yet been measured, we assume that at least one of its isotopes could have a scattering length as large as three times that of chromium, i.e., $a_s \approx 300\ a_0$, where a_0 denotes the Bohr radius. This yields an approximate relative interaction strength for dysprosium of about $\epsilon_{\rm dd}^{\rm b} \approx 0.45$. In addition, we also assume that a dysprosium condensate could be produced in the same setup used for chromium in Ref. [89]. Besides the fact that the λ-dependence is much stronger in b) than in a), the larger s-wave scattering length leads to $\tilde{\Delta\Omega} \approx 0.03$. This nourishes hope for observing quantum fluctuations in trapped dysprosium systems.

These functions characterize the dependence of the correction on the trap anisotropy parameter λ are given by

$$s_\pm(\lambda) = \frac{1}{2} \pm \frac{8+\lambda^2}{6\sqrt{16-16\lambda^4+9\lambda^4}} \tag{5.43}$$

and are plotted in Fig. 5.2. From the figure we see that the largest value of the functions $s_\pm(\lambda)$ is $s_+(\lambda = 1) = 1$, which corresponds to a spherical trap. In that case, for a chromium condensate the monopole frequency is corrected by $\Delta\Omega_{\delta,+}/\Omega_{\delta,+}$, i.e., by less than 1%, which is far too small to be measurable. For strongly interacting Fermi gases along the BEC-BCS crossover, on the other hand, these corrections have been confirmed on the BEC, due to the larger value of the s-wave scattering length [79].

Let us now consider the effects of the dipole-dipole interaction, by assuming that the gas parameter $a_s^3\ n(\mathbf{0})$ is not altered considerably. Varying $\epsilon_{\rm dd}^{\rm b}$ from 0 to a larger value close to $\epsilon_{\rm dd}^{\rm b} = 1$ has two effects on the frequency correction. The prefactor of the correction can become up to 2.6 times larger, due to the function $\mathcal{I}(\epsilon_{\rm dd}^{\rm b})$, which was defined in Eq. (3.38). The other, and more important, effect is the anisotropy of the condensate which is influenced by $\epsilon_{\rm dd}^{\rm b}$ and also by the trap aspect ratio λ. In Fig. 5.3, we plot the relative frequency corrections as functions of λ for chromium, with $\epsilon_{\rm dd}^{\rm b} = 0.16$, and for dysprosium, with $\epsilon_{\rm dd}^{\rm b} = 0.45$, and compare them with the case for which $\epsilon_{\rm dd}^{\rm b} = 0$ (dashed curves). The experimental parameters for ^{52}Cr in Fig. 5.3a) are taken from Ref. [89], where the background value of the s-wave aspect ratio is $a_s = 100\ a_0$. Under these circumstances, the unit of the frequency shift in Fig. 5.3a) amounts to $\tilde{\Delta\Omega} \approx 0.01$. In this case, one sees that the λ-dependence of the shift departs clearly from the non-dipolar case. Nonetheless, since the actual value of the total shift is too small, the

total correction cannot be measured and, consequently, the same is true for the dipolar contribution. The frequency shifts for dysprosium, which are shown in Fig. 5.3b), on the contrary, might become reachable to experiments. Since the s-wave scattering length for dysprosium is not yet known, we can hope that at least one of its bosonic isotopes has a s-wave scattering length as large as, say, $a_s \approx 300\ a_0$, which is three times larger than that of chromium. In this case, one arrives at the value $\epsilon_{\rm dd}^{\rm b} = 0.45$ for the relative interaction strength, which is adopted in the plots, and the characteristic λ-dependence of the corrections becomes more pronounced. Moreover, such a large scattering length leads to $\Delta\tilde{\Omega} \approx 0.03$ for the same trap frequencies and particle numbers as for chromium. As a whole, the frequency shift might be as large as $\Delta\Omega_+/\Omega_+ \approx 7\%$ for the monopole frequency and $\Delta\Omega_-/\Omega_- \approx -2\%$ for the quadrupole frequency. This in clear contrast with the λ-dependence of the corresponding corrections in a condensate with pure contact interaction, shown in Fig. 5.2, where the corrections for both frequencies retain appreciable values and become equal for infinitely large trap aspect ratio λ. At least for the monopole mode, one can hope that future measurements can clearly identify the effects of quantum fluctuations in Bose-Einstein condensates as well as distinguish the contributions from the short-range and isotropic contact interaction from that of the long-range and anisotropic dipole-dipole interaction.

5.7 Beyond Mean-field Time-of-flight Dynamics

In this Section we present the study of the time-of-flight dynamics of dipolar Bose-Einstein condensates including the effects of quantum fluctuations. As we have explained in the mean-field calculations of section 4.5, turning the trap off amounts to setting the restoring oscillator forces in Eq. (5.23) to zero. In this case, the equations of motion become

$$\begin{aligned} \ddot{R}_\rho(t) &= \frac{15gN}{4\pi M R_\rho(t)^3 R_z(t)} \left[1 - \epsilon_{\rm dd}^{\rm b} A\left(\frac{R_\rho(t)}{R_z(t)}\right) + \frac{\beta}{R_\rho(t) R_z(t)^{1/2}}\right], \\ \ddot{R}_z(t) &= \frac{15gN}{4\pi M R_\rho(t)^2 R_z(t)^2} \left[1 + 2\epsilon_{\rm dd}^{\rm b} B\left(\frac{R_\rho(t)}{R_z(t)}\right) + \frac{\beta}{R_\rho(t) R_z(t)^{1/2}}\right], \end{aligned} \tag{5.44}$$

where the last term in the right-hand side accounts for the quantum fluctuations and, therefore, can be treated as small. After the release from the trap, the gas expands and the Thomas-Fermi radii become larger and larger. As a result, the influence of quantum fluctuations vanishes asymptotically in time, since the term responsible for them goes as $\frac{\beta}{R_\rho(t) R_z(t)^{1/2}}$ and decreases faster than the other terms in brackets in Eqs. (5.44). Nonetheless, provided that the the s-wave scattering length a_s and the relative dipolar strength $\epsilon_{\rm dd}^{\rm b}$ have appreciable values, quantum fluctuations have a measurable impact on the time-of-flight dynamics of dipolar Bose-Einstein condensates. On the one hand, they alter the initial conditions which should be obeyed by the gas, since, at $t = 0$, one has

$$R_\rho(0) = R_\rho^0(0) + \delta R_\rho(0), \quad R_z(0) = R_z^0(0) + \delta R_z(0). \tag{5.45}$$

On the other hand, the equations of motion for the Thomas-Fermi radii are themselves modified by the presence of the term $\frac{\beta}{R_\rho(t) R_z(t)^{1/2}}$ inside the brackets in Eqs. (5.44). For this reason, it seems to be natural to solve these equations by separating the mean-field from the quantum contributions

according to

$$R_\rho(t) = R_\rho^0(t) + \delta R_\rho(t), \quad R_z(t) = R_z^0(t) + \delta R_z(t). \tag{5.46}$$

Our goal is to determine the four quantities and study the behaviour of the beyond mean-field aspect ratio

$$\kappa(t) = \frac{R_\rho^0(t) + \delta R_\rho(t)}{R_z^0(t) + \delta R_z(t)} \tag{5.47}$$

as a function of time. To that end, let us first insert Eq. (5.46) into Eq. (5.44) and retain only the mean-field terms. One, then, obtains the equations

$$\begin{aligned}
\ddot{R}_\rho^0(t) &= \frac{15gN}{4\pi M R_\rho^0(t)^3 R_z^0(t)} \left[1 - \epsilon_{\mathrm{dd}}^{\mathrm{b}} A\left(\frac{R_\rho^0(t)}{R_z^0(t)}\right)\right], \\
\ddot{R}_z^0(t) &= \frac{15gN}{4\pi M R_\rho^0(t)^2 R_z^0(t)^2} \left[1 + 2\epsilon_{\mathrm{dd}}^{\mathrm{b}} B\left(\frac{R_\rho^0(t)}{R_z^0(t)}\right)\right].
\end{aligned} \tag{5.48}$$

Together with the initial condition for the mean-field Thomas-Fermi radii, Eqs. (5.48) can be solved to yield $R_\rho^0(t)$ and $R_z^0(t)$. By considering the first order terms, one obtains the equations obeyed by the fluctuations of the radii according to

$$\begin{aligned}
\delta\ddot{R}_\rho(t) &= F_{\rho,\rho}\left(R_\rho^0(t), R_z^0(t)\right)\delta R_\rho(t) + F_{\rho,z}\left(R_\rho^0(t), R_z^0(t)\right)\delta R_z(t) + \frac{15gN}{4\pi M R_\rho^0(t)^3 R_z^0(t)} \frac{\beta}{R_\rho^0(t) R_z^0(t)^{1/2}}, \\
\delta\ddot{R}_z(t) &= F_{z,\rho}\left(R_\rho^0(t), R_z^0(t)\right)\delta R_\rho(t) + F_{z,z}\left(R_\rho^0(t), R_z^0(t)\right)\delta R_z(t) + \frac{15gN}{4\pi M R_\rho^0(t)^2 R_z^0(t)^2} \frac{\beta}{R_\rho^0(t) R_z^0(t)^{1/2}},
\end{aligned} \tag{5.49}$$

where we have introduced the auxiliary functions

$$\begin{aligned}
F_{\rho,\rho}\left(R_\rho^0(t), R_z^0(t)\right) &= \frac{15gN}{4\pi M R_\rho^0(t)^3 R_z^0(t)} \frac{1}{R_\rho^0(t)} \left\{-3 + \epsilon_{\mathrm{dd}}^{\mathrm{b}} \left[3A\left(\frac{R_\rho^0(t)}{R_z^0(t)}\right) + R_z^0(t) A_z\left(\frac{R_\rho^0(t)}{R_z^0(t)}\right)\right]\right\}, \\
F_{\rho,z}\left(R_\rho^0(t), R_z^0(t)\right) &= \frac{15gN}{4\pi M R_\rho^0(t)^3 R_z^0(t)} \frac{1}{R_z^0(t)} \left\{-1 + \epsilon_{\mathrm{dd}}^{\mathrm{b}} \left[A\left(\frac{R_\rho^0(t)}{R_z^0(t)}\right) - R_z^0(t) A_z\left(\frac{R_\rho^0(t)}{R_z^0(t)}\right)\right]\right\}, \\
F_{z,\rho}\left(R_\rho^0(t), R_z^0(t)\right) &= \frac{15gN}{4\pi M R_\rho^0(t)^2 R_z^0(t)^2} \frac{1}{R_\rho^0(t)} \left\{-2 - 2\epsilon_{\mathrm{dd}}^{\mathrm{b}} \left[2B\left(\frac{R_\rho^0(t)}{R_z^0(t)}\right) + R_z^0(t) B_z\left(\frac{R_\rho^0(t)}{R_z^0(t)}\right)\right]\right\}, \\
F_{z,z}\left(R_\rho^0(t), R_z^0(t)\right) &= \frac{15gN}{4\pi M R_\rho^0(t)^2 R_z^0(t)^2} \frac{1}{R_z^0(t)} \left\{-2 - 2\epsilon_{\mathrm{dd}}^{\mathrm{b}} \left[2B\left(\frac{R_\rho^0(t)}{R_z^0(t)}\right) - R_z^0(t) B_z\left(\frac{R_\rho^0(t)}{R_z^0(t)}\right)\right]\right\}.
\end{aligned} \tag{5.50}$$

It now becomes clear that one can only solve Eqs. (5.49) for the quantum corrections if one has solved Eq. (5.48) which determines the mean-field dynamics and the functions $F_{i,j}\left(R_\rho^0(t), R_z^0(t)\right)$ become external driving forces for the motion of the radii fluctuations $\delta R_\rho(t)$ and $\delta R_z(t)$.

Having explained how we solve the coupled equations for the mean-field Thomas-Fermi radii and their fluctuations, let us now present and discuss numerical examples in which the effect of quantum fluctuations on the time-of-flight dynamics can be identified. Fig. 5.4 presents a comparison of the

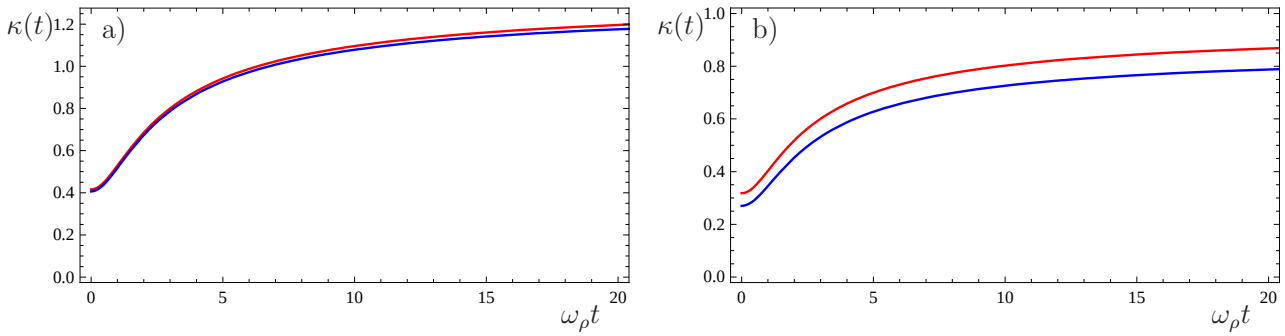

Figure 5.4: Time-of-flight dynamics for different values of the s-wave scattering length and the relative interaction strength $\epsilon_{\rm dd}^{\rm b}$. The vertical axis shows the corrected aspect ratio (5.46) as a function of time (in units of ω_ρ^{-1}) a) $a_s = 300\ a_0$ and $\epsilon_{\rm dd}^{\rm b} = 0.45$. b) $a_s = 150\ a_0$ and $\epsilon_{\rm dd}^{\rm b} = 0.9$.

mean-field aspect ratio (blue) as a function of time (in units of ω_ρ^{-1}) with the aspect ratio (5.47) which includes quantum fluctuations (red). In Fig. 5.4a) the parameters adopted are $a_s = 300\ a_0$ and $\epsilon_{\rm dd}^{\rm b} = 0.45$, while in Fig. 5.4b), we have adopted the s-wave scattering length of $a_s = 150\ a_0$ and a relative dipolar strength of $\epsilon_{\rm dd}^{\rm b} = 0.9$. As we can see, the influence of the quantum fluctuations is more clearly seen for a larger value of the dipolar strength relative to the contact interaction $\epsilon_{\rm dd}^{\rm b}$ than for a larger value of the s-wave scattering length. Nonetheless, it should be remarked that for systems in which the contact interaction is as small as $a_s = 150\ a_0$, no effect of quantum fluctuations can be seen in the time-of-flight dynamics.

Part II

Dipolar Fermi Gases

6 Theoretical Methods for Interacting Normal Fermi Gases

In this chapter we introduce the general theoretical methods that will be used later on for describing dipolar Fermi gases. We are interested in the case of quantum degenerate nonsuperfluid Fermi samples. Starting from the time-dependent Hartree-Fock theory of Fermi gases, formulated in terms of one-particle orbitals, we derive the hydrodynamic equations as they are commonly used in studies of the hydrodynamic properties of Fermi gases. Subsequently, we switch to the Wigner representation of quantum mechanics and derive the collisionless Boltzmann-Vlasov equation by assuming a spatially smooth Wigner function. Exploring the interpretion of the collisionless Boltzmann-Vlasov equation as the total derivative of the phase space distribution, we introduce the collision term as the balance of what is scattered in- and outwards a differential volume in phase space. We then briefly discuss the full Boltzmann-Vlasov equation within the relaxation-time approximation and, thereby, introduce the physical aspects of the collisionless and of the hydrodynamic regimes. In addition, we also discuss how the relaxation time can be obtained. As we aim for a variational approach in the hydrodynamic theory of Fermi gases, we derive the hydrodynamic equations from an action principle and show how the corresponding action can be written in terms of an appropriate Wigner function by assuming that all the one-particle wave functions have the same phase. This variational procedure is then considered in detail, where we focus on the effects of the Fock exchange contribution to the interaction energy.

6.1 Time-dependent Hartree-Fock Theory

Let us start by making two remarks about the problem we are interested in. The first remark concerns fact that we restrict ourselves to the nonsuperfluid phase and, therefore, do not consider the possibility of pairing in a one-component fermionic system even at zero temperature. This can be safely done because the critical temperatures for superfluidity in these systems is usually much smaller than the Fermi temperature. Therefore, superfluidity shows up at much lower temperatures than the effects of quantum degeneracy.

To illustrate this point, consider the critical temperature of superfluidity as obtained from the BCS-theory of one-component, homogeneous, dipolar fermions. Denoting the Fermi energy and the dipole moment by E_{F} and d, respectively, the critical temperature for superfluidity is given by [108]

$$k_B T_{\mathrm{C}} \approx 1.44\, E_{\mathrm{F}}\, e^{-\frac{\pi E_{\mathrm{F}}}{12 n d^2}}, \tag{6.1}$$

where n represents the particle density. Since the BCS-theory is only valid when the interaction energy nd^2 is much smaller than the Fermi energy E_{F}, it becomes clear that superfluidity becomes important

at much lower temperatures than quantum degeneracy and can, therefore, be safely neglected. Indeed, even for Fermi gases with contact interaction, which is usually much stronger than the dipolar one, superfluidity can only be observed in the presence of a Feshbach resonance (see Section 1.3). It should be remarked that, at the present moment, there is no theory available which can deal with superfluidity of dipolar fermions in the strong interaction regime [82].

A further remark is in order to explain the internal degrees of freedom, such as spin. As in the case of bosonic particles, we deal with single-component fermionic gases so that the internal degrees of freedom are frozen. At the very low temperatures under consideration here, collisions in the s-wave channel are not allowed. Therefore, short-range interactions are not included in the formalism below. This is of no importance for us because our main purpose is to study Fermi gases with long-range interactions, where an infinite number of *odd* partial waves are included. In particular, we will apply the theory derived here to Fermi gases interacting through the dipole-dipole potential (1.12).

We now turn our attention to the system in question. Consider a gas containing N trapped interacting fermionic particles of mass M. The Hamilton operator of such a quantum many-particle system is given in first quantization by

$$\hat{H} = \sum_{i=1}^{N} \left[-\frac{\hbar^2 \nabla_{\mathbf{x}_i}^2}{2M} + U_{\mathrm{tr}}(\mathbf{x}_i) \right] + \frac{1}{2} \sum_{i \neq j}^{N} V_{\mathrm{int}}(\mathbf{x}_i - \mathbf{x}_j), \tag{6.2}$$

where $V_{\mathrm{int}}(\mathbf{x}_i - \mathbf{x}_j)$ is the general two-body interaction potential between particles with relative position $\mathbf{x}_i - \mathbf{x}_j$. The same diluteness condition as in the bosonic case (see Section 2.3) is assumed to be valid for fermionic gases, so that three-body interactions can be neglected.

In the absence of interactions, Hamiltonian (6.2) is reduced to its one-particle component, given by

$$\hat{H}^{(1)} = \sum_{i=1}^{N} \left[-\frac{\hbar^2 \nabla_{\mathbf{x}_i}^2}{2M} + U_{\mathrm{tr}}(\mathbf{x}_i) \right] \equiv \sum_{i=1}^{N} \hat{h}_i^{(1)}, \tag{6.3}$$

which can be exactly diagonalized. In this situation, the many-body Hilbert space is the direct product of the N one-particle Hilbert spaces involved. Consider a complete set of one-particle orbitals $\{\phi_n(\mathbf{x}_i)\}$ obeying the eigenvalue equation

$$\hat{h}_i^{(1)} \phi_n(\mathbf{x}) = \varepsilon_n \phi_n(\mathbf{x}) \tag{6.4}$$

with the energy eigenvalues ε_n corresponding to the one-particle wave functions $\phi_n(\mathbf{x})$. Due to the Pauli exclusion principle, each orbital can only be occupied by a single fermion. In addition, the statistics of fermionic particles implies that the many-body wave function, i.e., the coordinate space representation of a state in the many-body Hilbert space discussed above, is antisymmetric with respect to the permutation of any two particles. Therefore, the many-body ground-state wave function is totally antisymmetric and is constructed out of N one-particle states with energy inferior than a given level, called the Fermi energy. Such a wave function $\langle \mathbf{x}_1, \mathbf{x}_2, \cdots, \mathbf{x}_N | \Phi \rangle$ is called a Slater determinant. This denomination comes from the fact that the function $\langle \mathbf{x}_1, \mathbf{x}_2, \cdots, \mathbf{x}_N | \Phi \rangle$ is most conveniently written

as

$$\langle \mathbf{x}_1, \mathbf{x}_2, \cdots, \mathbf{x}_N | \Phi \rangle = \frac{1}{\sqrt{N!}} \begin{vmatrix} \phi_1(\mathbf{x}_1) & \cdots & \phi_1(\mathbf{x}_N) \\ \vdots & \ddots & \vdots \\ \phi_N(\mathbf{x}_1) & \cdots & \phi_N(\mathbf{x}_N) \end{vmatrix}. \tag{6.5}$$

The presence of interactions changes this picture considerably, due to the two-particle correlations. In order to account for the effect of interactions approximatively, we will apply the Hartree-Fock theory, in which the two-particle interaction potential is replaced by a self-consistent mean-field.

6.2 Action Principle for the Hartree-Fock Theory

As we have done in the case of bosons, we will derive a variational approach to describe the physics of interacting Fermi gases. In opposition to the Gross-Pitaevskii theory, where a single one-particle orbital is important, the mean-field Hartree-Fock theory of Fermi gases is constructed with N such functions, in analogy to the noninteracting case discussed above. Let us assume that the ground state of the interacting system is also given by a time-dependent state $|\Phi(t)\rangle$, which is antisymmetric under the interchange of any two fermions. Working with these states in the Schrödinger representation, the Hartree-Fock equations can be derived by extremizing the action

$$\mathcal{A} = \int_{t_1}^{t_2} \mathrm{d}t \langle \Phi(t) | i\hbar \frac{\partial}{\partial t} - \hat{H} | \Phi(t) \rangle \tag{6.6}$$

in coordinate space with respect to the one-particle orbitals. In order to see how this can be done, let us consider the corresponding many-body wave function, which is given by

$$\Phi(\mathbf{x}_1, \cdots, \mathbf{x}_N; t) = \langle \mathbf{x}_1, \mathbf{x}_2, \cdots, \mathbf{x}_N | \Phi(t) \rangle, \tag{6.7}$$

where the right-hand side denotes a Slater determinant constructed in terms of the one-particle orbitals $\phi_i(\mathbf{x}, t)$ as in Eq. (6.5). The difference with respect to the noninteracting case is the fact that, instead of being determined by Eq. (6.4), the one-particle orbitals have yet to be determined self-consistently, i.e., from equations which presume their knowledge. In order to obtain these equations, let us initially consider the first term in the action (6.6). Inserting the many-body wave function (6.7) into that term, one obtains

$$\langle \Phi(t) | i\hbar \frac{\partial}{\partial t} | \Phi(t) \rangle = \sum_{i=1}^{N} \int \mathrm{d}^3 x \phi_i^*(\mathbf{x}, t) i\hbar \frac{\partial}{\partial t} \phi_i(\mathbf{x}, t), \tag{6.8}$$

where we have used the antisymmetry property of the Slater determinant (6.7). The properties of the Slater determinant also allow to obtain the second term in action (6.6), given by the expected value

$\langle\Phi(t)|\hat{H}|\Phi(t)\rangle$. Indeed, a direct calculation yields

$$\begin{aligned}\langle\Phi(t)|\hat{H}|\Phi(t)\rangle &= \sum_{i=1}^{N}\int \mathrm{d}^3x\phi_i^*(\mathbf{x},t)\left[-\frac{\hbar^2\nabla_{\mathbf{x}}^2}{2M}+U_{\mathrm{tr}}(\mathbf{x})+\frac{\Gamma^{\mathrm{Dir}}(\mathbf{x},t)}{2}\right]\phi_i(\mathbf{x},t)\\ &\quad+\frac{1}{2}\sum_{i=1}^{N}\int \mathrm{d}^3x\int \mathrm{d}^3x'\phi_i^*(\mathbf{x},t)\Gamma^{\mathrm{Ex}}(\mathbf{x},\mathbf{x}';t)\phi_i(\mathbf{x}',t). \qquad (6.9)\end{aligned}$$

Thus, the expected value of the interaction potential $V_{\mathrm{int}}(\mathbf{x}_i-\mathbf{x}_j)$ in Hamiltonian (6.2) with respect to a Slater determinant is decomposed into two main contributions called the direct, or Hartree, and the exchange, or Fock terms. These contributions are given in terms of one-particle potentials which read

$$\Gamma^{\mathrm{Dir}}(\mathbf{x},t) = \int \mathrm{d}^3y V_{\mathrm{int}}(\mathbf{y},\mathbf{x})\sum_{i=1}^{N}\phi_i^*(\mathbf{y},t)\phi_i(\mathbf{y},t), \qquad (6.10)$$

$$\Gamma^{\mathrm{Ex}}(\mathbf{x},\mathbf{x}';t) = -V_{\mathrm{int}}(\mathbf{x},\mathbf{x}')\sum_{i=1}^{N}\phi_i^*(\mathbf{x}',t)\phi_i(\mathbf{x},t), \qquad (6.11)$$

for the Hartree and the Fock terms, respectively. By inserting equations (6.8) and (6.9) into the action (6.6) and extremizing it with respect to $\phi_i(\mathbf{x},t)$ and $\phi_i^*(\mathbf{x},t)$, one obtains the Hartree-Fock equations for the one-particle orbitals $\phi_i^*(\mathbf{x},t)$ and $\phi_i(\mathbf{x},t)$, which read

$$i\hbar\frac{\partial}{\partial t}\phi_i(\mathbf{x},t) = \left[-\frac{\hbar^2\nabla_{\mathbf{x}}^2}{2M}+U_{\mathrm{tr}}(\mathbf{x})+\frac{\Gamma^{\mathrm{Dir}}(\mathbf{x},t)}{2}\right]\phi_i(\mathbf{x},t)+\int \mathrm{d}^3x'\Gamma^{\mathrm{Ex}}(\mathbf{x},\mathbf{x}';t)\phi_i(\mathbf{x}',t), \qquad (6.12)$$

$$-i\hbar\frac{\partial}{\partial t}\phi_i^*(\mathbf{x},t) = \left[-\frac{\hbar^2\nabla_{\mathbf{x}}^2}{2M}+U_{\mathrm{tr}}(\mathbf{x})+\frac{\Gamma^{\mathrm{Dir}}(\mathbf{x},t)}{2}\right]\phi_i^*(\mathbf{x},t)+\int \mathrm{d}^3x'\Gamma^{\mathrm{Ex}}(\mathbf{x}',\mathbf{x};t)\phi_i^*(\mathbf{x}',t). \qquad (6.13)$$

Let us consider a few properties of the equations (6.12)–(6.13) which are relevant for the following discussion. A key feature of these equations is the fact that the two-particle potential is represented by the mean-field direct (6.10) and exchange (6.11) potentials, which are one-particle in nature. If the interaction potential would have the short-range, Dirac-delta form

$$V_\delta(\mathbf{x},\mathbf{x}') = g\delta(\mathbf{x}-\mathbf{x}'), \qquad (6.14)$$

then the direct and exchange terms would cancel each other, as one could expect from the Pauli exclusion principle. For long-range interactions, on the contrary, both contributions survive and have quite different characters. While the direct term is local, the exchange term is nonlocal.

It is important to point out that it is the presence of the one-particle orbitals $\phi_i(\mathbf{x},t)$ in the direct (6.10) and exchange (6.11) potentials that shows the self-consistent nature of the equations (6.12) and (6.13). They are usually solved iteratively by providing some educated guess for the orbitals, such as their noninteraction values, and using this guess to evaluate $\Gamma^{\mathrm{Dir}}(\mathbf{x},t)$ and $\Gamma^{\mathrm{Ex}}(\mathbf{x},\mathbf{x}';t)$. Then, one solves the N coupled differential equations and obtains in this way a new set of orbitals $\{\tilde{\phi}_i(\mathbf{x},t)\}$. By proceeding along these lines, convergence is eventually achieved.

6.3 One-particle Density Matrix

The Hartree-Fock equations derived in the last section provide a reasonable starting point to deal with fermionic systems. In nuclear physics and chemistry, for example, modern numerical methods are commonly used to solve these and similar equations. This is possible because, in those cases, one deals with a few hundred particles at most. In cold atoms physics, however, the systems are usually composed of several ten thousand particles, at least. Therefore, instead of solving the Hartree-Fock equations, we find it rather convenient to write them in another form. To this end, we introduce the definition of the one-body density matrix according to

$$\begin{aligned} n^{(1)}(\mathbf{x},\mathbf{x}';t) &= \prod_{i=2}^{N}\int \mathrm{d}^3x_i \Phi^*(\mathbf{x},\mathbf{x}_2,\cdots,\mathbf{x}_N;t)\Phi(\mathbf{x}',\mathbf{x}_2,\cdots,\mathbf{x}_N;t), \\ &= \sum_{i=1}^{N}\phi_i(\mathbf{x},t)\phi_i^*(\mathbf{x}',t). \end{aligned} \tag{6.15}$$

It is worth remarking that the definition chosen in this chapter for the one-body density matrix is, of course, compatible with the one introduced in the case of bosonic quantum fields, given in Eq. (2.2).

The physical description of Fermi gases in terms of the one-particle density matrix has the obvious advantage of reducing dramatically the number of functions one has to work with. For this reason, before we proceed to the derivation of the equation of motion for the one-particle density matrix (6.15), it is illustrative to explore how the elements of the Hartree-Fock theory can be expressed in terms of the density matrix (6.15). The particle density, for example, can be obtained according to

$$n(\mathbf{x};t) = \sum_{i=1}^{N}\phi_i^*(\mathbf{x},t)\phi_i(\mathbf{x},t) = n^{(1)}(\mathbf{x},\mathbf{x};t). \tag{6.16}$$

Moreover, the expectation value of the Hamiltonian (6.2) can also be conveniently expressed in terms of this density matrix. Dividing the one-particle Hamiltonian (6.3) into two constituents, one obtains

$$\langle\Phi(t)|\hat{H}^{(1)}|\Phi(t)\rangle = E_{\mathrm{kin}}(t) + E_{\mathrm{tr}}(t), \tag{6.17}$$

where the kinetic and trapping energies are given by

$$E_{\mathrm{kin}}(t) = \frac{\hbar^2}{2M}\int \mathrm{d}^3x\, \nabla_{\mathbf{x}}\cdot\nabla_{\mathbf{x}'}\, n^{(1)}(\mathbf{x},\mathbf{x}';t)\Big|_{\mathbf{x}'=\mathbf{x}}, \tag{6.18}$$

$$E_{\mathrm{tr}}(t) = \int \mathrm{d}^3x\, n(\mathbf{x},t)U_{\mathrm{tr}}(\mathbf{x}), \tag{6.19}$$

respectively.

In terms of the density matrix (6.15), the direct Hartree term, to which only the diagonal density matrix elements contribute, reads

$$\Gamma^{\mathrm{Dir}}(\mathbf{x},t) = \int \mathrm{d}^3y V_{\mathrm{int}}(\mathbf{y},\mathbf{x})n(\mathbf{y},t). \tag{6.20}$$

In contrast, the Fock exchange term, which is given in terms of the density matrix by

$$\Gamma^{\mathrm{Ex}}(\mathbf{x},\mathbf{x}';t) \;=\; -V_{\mathrm{int}}(\mathbf{x},\mathbf{x}')n^{(1)}(\mathbf{x},\mathbf{x}';t), \tag{6.21}$$

also involves off-diagonal elements of the density matrix.

Let us now express the total interaction energy, given by the expectation value of the third term in Eq. (6.2) with respect to the Slater determinant (6.7), in terms of the one-particle density matrix $n^{(1)}(\mathbf{x},\mathbf{x}';t)$. This expected value is, as before, decomposed into two contributions: the direct and the exchange mean-field energies. Thereby, the direct contribution is found to be

$$E^{\mathrm{Dir}}(t) \;=\; \frac{1}{2}\int \mathrm{d}^3x\mathrm{d}^3x' n(\mathbf{x},t)V_{\mathrm{int}}(\mathbf{x},\mathbf{x}')n(\mathbf{x}',t), \tag{6.22}$$

while the exchange part reads

$$E^{\mathrm{Ex}}(t) \;=\; -\frac{1}{2}\int \mathrm{d}^3x\mathrm{d}^3x' n^{(1)}(\mathbf{x},\mathbf{x}';t)V_{\mathrm{int}}(\mathbf{x},\mathbf{x}')n^{(1)}(\mathbf{x}',\mathbf{x};t). \tag{6.23}$$

In order to obtain an exchange term, which is a function of the particle density $n\,(\mathbf{x})$ alone, one can apply different approaches. One of these possibilities is the local density approximation, discussed already in the case of bosonic particles in the context of the Bogoliubov-de Gennes theory (see Chapter 5). Another possibility is to introduce specific assumptions, which are tailored to match the physical properties of the system under consideration. The latter will be explored in detail in the next chapter.

We finally turn ourselves to the problem of determining the time dependence of the density matrix. To this end, we notice that performing suitable manipulations of the equations (6.12) and (6.13) leads to a Hartree-Fock equation for the one-body density matrix $n^{(1)}(\mathbf{x},\mathbf{x}';t)$ in the form

$$\begin{aligned} i\hbar\frac{\partial n^{(1)}(\mathbf{x},\mathbf{x}';t)}{\partial t} \;=\; & \left[\frac{-\hbar^2}{2M}\left(\nabla^2_{\mathbf{x}}-\nabla^2_{\mathbf{x}'}\right)+U_{\mathrm{eff}}(\mathbf{x})-U_{\mathrm{eff}}(\mathbf{x}')\right]n^{(1)}(\mathbf{x},\mathbf{x}';t) \\ & +\int \mathrm{d}^3y\left[\Gamma^{\mathrm{Ex}}(\mathbf{x},\mathbf{y};t)n^{(1)}(\mathbf{y},\mathbf{x}';t)-\Gamma^{\mathrm{Ex}}(\mathbf{y},\mathbf{x}';t)n^{(1)}(\mathbf{x},\mathbf{y};t)\right]. \end{aligned} \tag{6.24}$$

Since the direct contribution is a local one, we followed reference [158] and introduced an effective local potential given by

$$U_{\mathrm{eff}}(\mathbf{x},t) = U_{\mathrm{trap}}(\mathbf{x}) + \Gamma^{\mathrm{Dir}}(\mathbf{x},t). \tag{6.25}$$

Introducing the definition (6.25) has two advantages. On the one hand, it simplifies the notation, and, on the other hand, it puts the external harmonic trapping potential and the Hartree interaction potential on equal footing, thereby, making the idea behind the mean-field approximation explicit. Indeed, in mean-field approximation, the real two-particle interaction is substituted by an average one-particle potential which is felt by an individual particle while being generated by all others.

A simplified version of this equation, which is restricted to the first line in Eq. (6.24), has been derived before from field theoretical considerations and used in studies of the hydrodynamic properties of noninteracting, one-component Fermi gases [159]. In the following, we will show how such an investigation can be carried out, thereby generalizing the corresponding theoretical considerations to cope with the effects of long-range interactions.

6.4 Hydrodynamic Equations

In the usual formulation, hydrodynamic studies of degenerate Fermi gases are based on closed equations for the particle density $n(\mathbf{x},t)$ and the velocity field $\mathbf{v}(\mathbf{x},t)$. The dynamic properties of this system are determined by solving simultaneously the continuity equation and the Euler equation. In this section we obtain this set of coupled equations by expanding the equation of motion for the one-body density matrix around the center of mass [159].

In order to derive the conservation laws corresponding to the hydrodynamic equations, we perform an expansion around the center-of-mass coordinate $\mathbf{R} = (\mathbf{x}+\mathbf{x}')/2$ in powers of the relative coordinate $\mathbf{s} = \mathbf{x} - \mathbf{x}'$. In zeroth order in $\mathbf{s}$, we obtain from (6.24) the continuity equation

$$\frac{\partial n(\mathbf{x},t)}{\partial t} + \nabla \cdot \mathbf{j}(\mathbf{x},t) = 0, \tag{6.26}$$

with the particle density $n(\mathbf{x},t) = n^{(1)}(\mathbf{x},\mathbf{x};t)$ and the current density

$$\mathbf{j}(\mathbf{x},t) = \frac{\hbar}{2Mi}\left(\nabla_{\mathbf{x}} - \nabla_{\mathbf{x}'}\right) n^{(1)}(\mathbf{x},\mathbf{x}';t)\Big|_{\mathbf{x}'=\mathbf{x}}. \tag{6.27}$$

The first order in $\mathbf{s}$ yields from (6.24) the Euler equation

$$M\frac{\partial j_i(\mathbf{x},t)}{\partial t} = -\nabla_{\mathbf{x}_j}\Pi^0_{ij}(\mathbf{x},t) - n(\mathbf{x},t)\nabla_{\mathbf{x}_i}U_{\text{eff}}(\mathbf{x},t) + \int \mathrm{d}^3x' n^{(1)}(\mathbf{x},\mathbf{x}';t) n^{(1)}(\mathbf{x}',\mathbf{x};t)\nabla_{\mathbf{x}}V_{\text{int}}(\mathbf{x},\mathbf{x}'), \tag{6.28}$$

with the non-interacting kinetic stress tensor

$$\Pi^0_{ij}(\mathbf{x},t) = -\frac{\hbar^2}{M}\frac{\left(\nabla_{\mathbf{x}} - \nabla_{\mathbf{x}'}\right)_i}{2}\frac{\left(\nabla_{\mathbf{x}} - \nabla_{\mathbf{x}'}\right)_j}{2} n^{(1)}(\mathbf{x},\mathbf{x}';t)\Big|_{\mathbf{x}'=\mathbf{x}}. \tag{6.29}$$

Introducing the velocity field according to $\mathbf{v}(\mathbf{x},t) = \mathbf{j}(\mathbf{x},t)/n(\mathbf{x},t)$ and assuming that the effective potential $U_{\text{eff}}(\mathbf{x})$ from Eq. (6.25) is sufficiently smooth, the kinetic stress tensor takes the form [159]

$$\Pi^0_{ij}(\mathbf{x},t) = \delta_{ij}P^0(\mathbf{x},t) + Mn(\mathbf{x},t)v_i(\mathbf{x},t)v_j(\mathbf{x},t), \tag{6.30}$$

where the pressure $P^0(\mathbf{x},t)$ obeys some equation of state $P^0(\mathbf{x},t) = F\left(n(\mathbf{x},t)\right)$.

In case of an irrotational flow, where the circulation of the velocity field vanishes due to $\nabla \times \mathbf{v} = \mathbf{0}$, the Euler equation (6.28) can be rewritten in the form

$$M\frac{\mathrm{d}\mathbf{v}(\mathbf{x},\mathrm{t})}{\mathrm{dt}} = -\nabla\left[\int^{n(\mathbf{x},t)} \mathrm{d}n' \frac{F(n')}{n'} + U_{\text{eff}}(\mathbf{x},t)\right] + \int \mathrm{d}^3x' \frac{n^{(1)}(\mathbf{x},\mathbf{x}';t)n^{(1)}(\mathbf{x}',\mathbf{x};t)}{n(\mathbf{x},t)}\nabla_{\mathbf{x}}V_{\text{int}}(\mathbf{x},\mathbf{x}') \tag{6.31}$$

with the transport derivative $\mathrm{d}/\mathrm{dt} = \partial/\partial t + \mathbf{v}\cdot\nabla$. If one sets the last term in Eq. (6.31) to zero, the time derivative of the velocity field is given by a gradient. Therefore, the circulation of the velocity field over a closed loop vanishes, as a statement of Kelvin's theorem [160]. Now the effect of the Fock exchange term for non-local interaction potentials becomes clear: it breaks the conservation of the

circulation of the velocity field $\mathbf{v}(\mathbf{x},t)$ and Kelvin's theorem does not hold although we consider an irrotational flow. This obvious contradiction is a consequence of the fact that the exchange term in this approximation contains nondiagonal elements of the one-particle density matrix. Nonetheless, since the true exchange correlation is a function of the density alone, as is guaranteed by the Kohn theorem [161], circulation is conserved. Thus, due the presence of the Fock exchange term, the hydrodynamic treatment commonly used for dipolar Bose-Einstein condensates [97] and noninteracting Fermi gases [159] cannot immediately be applied to Fermi gases with long-range interactions.

In order to fix the inconsistency with the conservation of circulation, one could, for example, write the exchange term in the local density approximation, as is done in density functional theory [162]. In this thesis, however, we present another approach which we have worked out in previous publications [127,128]. Indeed, we shall like to preserve the influence of the non-diagonal part of the one-particle density matrix, yet assure the conservation of the velocity circulation. Before we come to the discussion of this method, it is useful to explore the link between the Hartree-Fock equation (6.24) to the Boltzmann-Vlasov equation. We proceed to this topic in the next section.

6.5 Wigner Representation

The theoretical description of physical systems in terms of the one-particle density matrix $n^{(1)}(\mathbf{x},\mathbf{x}';t)$ can be made more simple and adequate if one switches to the so called Wigner representation.In particular, this procedure is specially fruitful when one has the semiclassical approximation in mind. Moreover, working in the Wigner space is a natural way to bridge the gap between the Hartree-Fock theory and the Boltzmann-equation formalism.

The density matrix $n^{(1)}(\mathbf{x},\mathbf{x}';t)$ could also be considered as a function of the center-of-mass position $\mathbf{R}=(\mathbf{x}+\mathbf{x}')/2$ and the relative coordinate $\mathbf{s}=(\mathbf{x}-\mathbf{x}')$. Or, equivalently, the physical properties of the quantum system at hand can be described by the Wigner function $\nu\left(\mathbf{R},\mathbf{p};t\right)$ which is a function of the center-of-mass coordinate and the Fourier transformed of the relative coordinate according to

$$\nu\left(\mathbf{R},\mathbf{p};t\right) \;=\; \int \mathrm{d}^3 s\, n^{(1)}\left(\mathbf{R}+\frac{\mathbf{s}}{2},\mathbf{R}-\frac{\mathbf{s}}{2};t\right) e^{-i\mathbf{p}\cdot\mathbf{s}/\hbar}. \tag{6.32}$$

The corresponding inverse transformation reads

$$n^{(1)}(\mathbf{x},\mathbf{x}';t) \;=\; \int \frac{\mathrm{d}^3 p}{(2\pi\hbar)^3}\,\nu\left(\frac{\mathbf{x}+\mathbf{x}'}{2},\mathbf{p};t\right) e^{i\mathbf{p}\cdot(\mathbf{x}-\mathbf{x}')/\hbar}. \tag{6.33}$$

Before, we discuss how the Hartree-Fock equation (6.24) looks like in the Wigner representation, let us comment on a few quantities which will be useful in the following. In the Wigner representation all quantities can be expressed in terms of the function $\nu\left(\mathbf{x},\mathbf{p};t\right)$. For example, the particle density is given by

$$n(\mathbf{x};t)=n^{(1)}(\mathbf{x},\mathbf{x};t)=\int \frac{\mathrm{d}^3 p}{(2\pi\hbar)^3}\,\nu\left(\mathbf{x},\mathbf{p};t\right), \tag{6.34}$$

and the momentum distribution is obtained via

$$n(\mathbf{p};t)=\int \frac{\mathrm{d}^3 x}{(2\pi\hbar)^3}\,\nu\left(\mathbf{x},\mathbf{p};t\right). \tag{6.35}$$

With the help of these quantities, the kinetic energy (6.18) and the trapping (6.19) energy can be written as

$$E_{\mathrm{kin}}(t) = \int \frac{\mathrm{d}^3x\mathrm{d}^3p}{(2\pi\hbar)^3}\,\nu\left(\mathbf{x},\mathbf{p};t\right)\frac{\mathbf{p}^2}{2M}, \tag{6.36}$$

$$E_{\mathrm{tr}}(t) = \int \frac{\mathrm{d}^3x\mathrm{d}^3p}{(2\pi\hbar)^3}\,\nu\left(\mathbf{x},\mathbf{p};t\right)U_{\mathrm{tr}}(\mathbf{x}), \tag{6.37}$$

respectively. Accordingly, the Hartree energy contribution in (6.22) reads

$$E_{\mathrm{int}}^{\mathrm{Dir}}(t) = \frac{1}{2}\int \frac{\mathrm{d}^3x\mathrm{d}^3p\mathrm{d}^3x'\mathrm{d}^3p'}{(2\pi\hbar)^6}\nu\left(\mathbf{x},\mathbf{p};t\right)V_{\mathrm{int}}(\mathbf{x}-\mathbf{x}')\nu\left(\mathbf{x}',\mathbf{p}';t\right). \tag{6.38}$$

Performing the momentum-space integrals and recalling Eq. (6.34), one obtains that Eq. (6.38) reduces to the direct term in Eq. (6.22). This is due to the fact that the direct energy is a functional of the particle density alone. In contrast, the exchange interaction term (6.23), given by

$$E_{\mathrm{int}}^{\mathrm{Ex}}(t) = -\frac{1}{2}\int \frac{\mathrm{d}^3R\mathrm{d}^3p\mathrm{d}^3s\mathrm{d}^3p'}{(2\pi\hbar)^6}\nu\left(\mathbf{R},\mathbf{p};t\right)V_{\mathrm{int}}(\mathbf{s})\nu\left(\mathbf{R},\mathbf{p}';t\right)e^{i\mathbf{s}\cdot(\mathbf{p}-\mathbf{p}')/\hbar}, \tag{6.39}$$

turns out to be rather linked to the momentum distribution (6.35).

Working in the Wigner space, the total energy of the system can be written as

$$E_{\mathrm{total}}(t) = \int \frac{\mathrm{d}^3x\mathrm{d}^3p}{(2\pi\hbar)^3}\,\mathcal{E}\left(\mathbf{x},\mathbf{p};t\right)\nu\left(\mathbf{x},\mathbf{p};t\right). \tag{6.40}$$

In this equation, the implicitly time-dependent phase-space energy density is given by

$$\mathcal{E}\left(\mathbf{x},\mathbf{p};t\right) = \frac{\mathbf{p}^2}{2M} + U_{\mathrm{tr}}(\mathbf{x}) + \frac{1}{2}\int \mathrm{d}^3x' n\left(\mathbf{x}';t\right)V_{\mathrm{int}}(\mathbf{x}-\mathbf{x}') - \frac{1}{2}\int \frac{\mathrm{d}^3p'}{(2\pi\hbar)^3}\nu\left(\mathbf{x},\mathbf{p}';t\right)\tilde{V}_{\mathrm{int}}\left(\mathbf{p}-\mathbf{p}'\right), \tag{6.41}$$

where $\tilde{V}_{\mathrm{int}}\left(\mathbf{p}\right)$ denotes the Fourier transformed of the interaction potential. In particular, we remark that the energy density (6.41) is consistent with the representations of $\Gamma^{\mathrm{Dir}}(\mathbf{x},t)$ and $\Gamma^{\mathrm{Ex}}(\mathbf{x},\mathbf{x}';t)$ in the Wigner space, which we shall like to write down explicitly

$$\Gamma^{\mathrm{Dir}}(\mathbf{R},\mathbf{p};t) = \Gamma^{\mathrm{Dir}}(\mathbf{R},t)\delta\left(\mathbf{p}\right), \tag{6.42}$$

$$\Gamma^{\mathrm{Ex}}(\mathbf{R},\mathbf{p};t) = -\int \frac{\mathrm{d}^3p'}{(2\pi\hbar)^3}\nu\left(\mathbf{x},\mathbf{p}';t\right)\tilde{V}_{\mathrm{int}}\left(\mathbf{p}-\mathbf{p}'\right). \tag{6.43}$$

6.6 Boltzmann-Vlasov Equation

The Hartree-Fock equation for the one-particle density matrix Eq. (6.24), which was derived in Section 6.3, can be reinterpreted in terms of the Wigner function. Indeed, as shown in Ref. [163], the lowest order of a semiclassical expansion of the Wigner function corresponds to the classical phase-space distribution. In addition, such a reinterpretation leads to the Boltzmann-Vlasov equation which allows to study both the collisionless and the hydrodynamic regime as well as the transition between these two regimes. In the second part of this thesis, we are interested in the dipole-dipole interaction in

Fermi gases, for which a collisionless approach was already available in the literature [164]. Therefore, we concentrate ourselves here mainly on the hydrodynamic regime [127,128] and provide only a brief discussion for the collisionless regime. Moreover, we also comment on how to estimate the range of temperature and interaction strength in which the system is either collisionless or hydrodynamic within the relaxation time approximation.

In order to derive the Boltzmann-Vlasov equation starting from the Hartree-Fock equation of motion for the one-particle density matrix Eq. (6.24), we first write this equation in the center-of-mass coordinates and then switch to the Wigner representation. Afterwards we perform an expansion in the spatial argument of the Wigner functions. If the effective potential (6.25) is a smooth one, it is justified to assume that the spatial variation of the Wigner function is not too strong. Retaining only the first nonvanishing terms in the expansion, we obtain

$$\left[\frac{\partial}{\partial t}+\mathbf{p}\cdot\nabla_{\mathbf{R}}-\nabla_{\mathbf{R}}U_{\mathrm{eff}}(\mathbf{R},t)\cdot\nabla_{\mathbf{p}}+\nabla_{\mathbf{p}}\Gamma^{\mathrm{Ex}}(\mathbf{R},\mathbf{p};t)\cdot\nabla_{\mathbf{R}}-\nabla_{\mathbf{R}}\Gamma^{\mathrm{Ex}}(\mathbf{R},\mathbf{p};t)\cdot\nabla_{\mathbf{p}}\right]\nu\left(\mathbf{R},\mathbf{p};t\right) = 0. \tag{6.44}$$

This is the so called Boltzmann-Vlasov equation which can be classically interpreted as follows. At first, we rewrite it in the form

$$\left[\frac{\partial}{\partial t}+\nabla_{\mathbf{p}}H\left(\mathbf{x},\mathbf{p};t\right)\cdot\nabla_{\mathbf{x}}-\nabla_{\mathbf{x}}H\left(\mathbf{x},\mathbf{p};t\right)\cdot\nabla_{\mathbf{p}}\right]\nu(\mathbf{x},\mathbf{p};t)=0, \tag{6.45}$$

with the Hamilton function defined according to

$$H\left(\mathbf{x},\mathbf{p};t\right)=\frac{\mathbf{p}^2}{2M}+U_{\mathrm{tr}}(\mathbf{x})+\int \mathrm{d}^3x' n^{(1)}\left(\mathbf{x}';t\right)V_{\mathrm{int}}(\mathbf{x}-\mathbf{x}')-\int\frac{\mathrm{d}^3p'}{(2\pi\hbar)^3}\nu\left(\mathbf{x},\mathbf{p}';t\right)\tilde{V}_{\mathrm{int}}\left(\mathbf{p}-\mathbf{p}'\right), \tag{6.46}$$

By recalling the Hamilton equations of classical mechanics [165],

$$\frac{\mathrm{d}\mathbf{x}}{\mathrm{d}t} = \nabla_{\mathbf{p}}H\left(\mathbf{x},\mathbf{p},t\right), \tag{6.47}$$

$$\frac{\mathrm{d}\mathbf{p}}{\mathrm{d}t} = -\nabla_{\mathbf{x}}H\left(\mathbf{x},\mathbf{p},t\right), \tag{6.48}$$

equation (6.45) can be cast into the form

$$\frac{\mathrm{d}\nu(\mathbf{x},\mathbf{p};t)}{\mathrm{d}t}=0, \tag{6.49}$$

with the total derivative

$$\frac{\mathrm{d}}{\mathrm{d}t}=\frac{\partial}{\partial t}+\frac{\mathrm{d}\mathbf{p}}{\mathrm{d}t}\cdot\nabla_{\mathbf{p}}+\frac{\mathrm{d}\mathbf{x}}{\mathrm{d}t}\cdot\nabla_{\mathbf{x}}. \tag{6.50}$$

The physical meaning of Eq. (6.49) can be understood by considering phase-space volume $\mathrm{d}^3x\mathrm{d}^3p$ in which $\nu(\mathbf{x},\mathbf{p};t)\mathrm{d}^3x\mathrm{d}^3p$ particles enter at time t. In this case, Eq. (6.45) accounts for the variation in time of this number by including two mechanisms. The first is that the finite momentum of the particles might drive them away from the corresponding spatial part of the volume and is accounted for by the second term in that equation. The second mechanism, embodied in the third term in Eq. (6.45), is that of force fields acting on the particles, thereby changing their momenta. These effects add up to

zero. Therefore, the total derivative of the distribution function $\nu(\mathbf{x}, \mathbf{p}; t)$ vanishes. Notice that, due to the smoothness assumption for the spatial variation, the function $\nu(\mathbf{x}, \mathbf{p}; t)$ in Eq. (6.45) is not the full quantum mechanical Wigner function of Eq. (6.32).

Equation (6.45) is sometimes referred to as the *collisionless* Boltzmann-Vlasov equation. This denomination bears on the fact that collisional effects, a further mechanism which changes the number of particles in an infinitesimal volume in phase space, are completely neglected in this equation. One common way to solve the collisionless Boltzmann-Vlasov equation is that of adopting a scaling transformation for the Wigner function. Denoting by $\nu_{\mathrm{eq}}(\mathbf{x}, \mathbf{p})$ the Wigner function in equilibrium, one possible solution ansatz is

$$\nu_{\mathrm{eq}}(\mathbf{x}, \mathbf{p}; t) = \nu_{\mathrm{eq}}\left(\mathbf{X}(t), \mathbf{P}(t)\right) \tag{6.51}$$

together with

$$X_i(t) = \frac{x_i}{b_i(t)}, \qquad P_i(t) = p_i b_i(t) - M\dot{b}_i(t) x_i. \tag{6.52}$$

Inserting the ansatz (6.51), (6.52) into the Boltzmann-Vlasov equation (6.49), multiplying by $X_i^2(t)$, and integrating over the phase space leads to equations of motion for the scaling parameters $b_i(t)$. These equations, in turn, can be used to investigate the static as well as the dynamic properties of the system under consideration. Indeed, this scaling approach, which is in agreement with the ballistic law [166], has been applied before to investigate the time-of-flight expansion of Fermi gases [167] and of Bose-Fermi mixtures [168]. Moreover, the time-of-flight expansion of dipolar Fermi gases in the collisionless regime was also investigated in Ref. [164] with the help of the present scaling approach.

Let us now consider the effects of collisions. Deriving the collisional term requires going beyond the Hartree-Fock approximation and is not necessary for the objectives we have here. Therefore, we limit ourselves to writing down this term and briefly discussing the approximations involved in it.

In the presence of collisions, Eq. (6.49) must be extended to the form

$$\frac{\mathrm{d}\nu(\mathbf{x}, \mathbf{p}; t)}{\mathrm{d}t} = C\left[\nu(\mathbf{x}, \mathbf{p}; t)\right]. \tag{6.53}$$

Denoting the Fourier transformed of the two-particle interaction potential by $\tilde{V}_{\mathrm{int}}(\mathbf{p})$, the collision integral $C\left[\nu(\mathbf{x}, \mathbf{p}; t)\right]$ is given by [158]

$$\begin{aligned} C\left[\nu(\mathbf{x}, \mathbf{p}_1; t)\right] \;=\; & \frac{1}{2\hbar} \int \frac{\mathrm{d}^3 p_2}{(2\pi\hbar)^3} \int \frac{\mathrm{d}^3 p_3}{(2\pi\hbar)^3} \int \frac{\mathrm{d}^3 p_4}{(2\pi\hbar)^3} \left[\tilde{V}_{\mathrm{int}}\left(\mathbf{p}_1 - \mathbf{p}_2\right) - \tilde{V}_{\mathrm{int}}\left(\mathbf{p}_1 - \mathbf{p}_4\right)\right]^2 \\ & \times (2\pi\hbar)^3 \delta\left(\mathbf{p}_1 + \mathbf{p}_2 - \mathbf{p}_3 - \mathbf{p}_4\right) 2\pi\delta\left(\frac{p_1^2}{2M} + \frac{p_2^2}{2M} - \frac{p_3^2}{2M} - \frac{p_4^2}{2M}\right), \\ & \times \left[\left(1 - \nu_1\right)\left(1 - \nu_2\right)\nu_3\nu_4 - \nu_1\nu_2\left(1 - \nu_3\right)\left(1 - \nu_4\right)\right] \end{aligned} \tag{6.54}$$

together with the abbreviations $\nu_1 = \nu(\mathbf{x}, \mathbf{p}_1; t)$, $\nu_2 = \nu(\mathbf{x}, \mathbf{p}_2; t)$ and so on. The fermionic statistics is taken into account in the Born-approximation cross section, i.e., in the brackets in the first line of Eq. (6.54). In the case of contact interactions at low temperatures, the potential $\tilde{V}_{\mathrm{int}}(\mathbf{p})$ does not depend on the momentum and, therefore, the cross section for intra species collisions vanishes identically in accordance with the Pauli principle. In addition, the collisional term Eq. (6.54) describes changes in the phase space volume around the point $(\mathbf{x}, \mathbf{p})$ due to the scattering of particles in and out

of this volume. The first term in Eq. (6.54), for example, describes a scattering process in which the particles with momenta $\mathbf{p}_3$ and $\mathbf{p}_4$ collide and acquire momenta $\mathbf{p}_1$ and $\mathbf{p}_2$. The probability for this process to occur is proportional to the combination

$$P_{\mathrm{In}} \propto (1-\nu_1)\,(1-\nu_2)\,\nu_3\nu_4, \tag{6.55}$$

and the subscript In means that it leads to a particle entering the differential volume centered at $\mathbf{p}_1$ in phase space. Correspondingly, the second term, which contains the probability

$$P_{\mathrm{Out}} \propto \nu_1\nu_2\,(1-\nu_3)\,(1-\nu_4)\,, \tag{6.56}$$

describes the scattering from a particle outwards the volume under consideration. We remark that the scattering processes in question are assumed to be confined to a small region in space.

6.6.1 Hydrodynamics from Boltzmann-Vlasov Equation

In this section, we discuss the approach to hydrodynamics of Fermi gases by considering the Boltzmann-Vlasov kinetic equation (6.53) as a starting point. We do not aim for a full description of the problem on these grounds, since this a quite difficult task. Instead, we highlight the importance of two aspects which will be useful in the following. The first aspect is the form that the Wigner function assumes in the hydrodynamic regime and the second aspect is the role of the mean velocity field.

Indeed, hydrodynamic studies of degenerate Fermi gases have been carried out by starting from the Boltzmann-Vlasov equation (6.53), see, for instance, Refs. [169,170]. To briefly sketch how this is done, let us consider that $\nu(\mathbf{x},\mathbf{p};t)$ describes the distribution of particles at position $\mathbf{x}$ with momentum $\mathbf{p}$. In the hydrodynamic regime, the frequent collisions drive the system into local thermodynamic equilibrium with a given mean velocity $\mathbf{v}(\mathbf{x},t)$, temperature $T(\mathbf{x},t)$, and density $n(\mathbf{x},t)$. The system as a whole is, however, not in equilibrium because the velocity field, the temperature and the density depend on position and time. Notice that the introduction of temperature in the present discussion is a matter of completeness, since usual treatments of the Boltzmann-Vlasov equation are done in this way. In this thesis, we restrict ourselves to very low temperatures, where the effects of quantum degeneracy are most evident.

The regime we are interested in here is that of low-energy and long-wavelength excitations. Furthermore, we consider external potentials which are smooth functions of position. Therefore, close to equilibrium, where the Wigner function changes slowly with time, the left-hand side of that equation should have a small value. For this reason, the function $\nu_{\mathrm{le}}(\mathbf{x},\mathbf{p};t)$, which solves that equation, must be one for which the collision integral Eq. (6.54) vanishes. The existence of such a distribution function characterizes the hydrodynamic regime.

For the moment, let us consider that the role of interactions is to allow for the achievement of local equilibrium and neglect them in the Hamiltonian. In this regime this is justifiable since the collision term in the Boltzmann-Vlasov equation is the dominant one [158]. Based on this reasoning and recalling the assumption that the external potential is a slowly varying one, it is clear that the

distribution function must be one which satisfies the identity

$$(1-\nu_{\mathrm{le},1})(1-\nu_{\mathrm{le},2})\,\nu_{\mathrm{le},3}\nu_{\mathrm{le},4} = \nu_{\mathrm{le},1}\nu_{\mathrm{le},2}(1-\nu_{\mathrm{le},3})(1-\nu_{\mathrm{le},4}). \tag{6.57}$$

This implies that the collisional term vanishes identically, due to the fact that particles are scattered inwards and outwards at the same rate. In the present case where interactions are omitted, one can show that the distribution function takes the form of the Fermi-Dirac distribution [158]

$$\nu_{\mathrm{le}}(\mathbf{x},\mathbf{p};t) = \frac{1}{e^{\beta(\mathbf{x},t)[\mathbf{p}-M\mathbf{v}(\mathbf{x},t)]^2/2M-\beta(\mathbf{x},t)\mu(\mathbf{x},t)}+1}, \tag{6.58}$$

where $\beta(\mathbf{x},t) = 1/k_{\mathrm{B}}T(\mathbf{x},t)$ denotes the inverse temperature and k_{B} represents the Boltzmann constant. The form (6.58) of the Wigner function is such that the right-hand-side in Eq. (6.53) vanishes [158]. It is worth remarking that the form (6.58) is not the only one solving equation (6.57) but it was chosen so as to fulfill fermionic statistics.

In the presence of interactions, it is difficult to study hydrodynamic properties of Fermi gases within the framework of the Boltzmann-Vlasov equation (6.53), due to the nontriviality in the inclusion of mean-field potentials in the local equilibrium distribution $\nu_{\mathrm{le}}(\mathbf{x},\mathbf{p};t)$. For this reason, studies along these lines were concentrated on Fermi gases where the role of interaction was restricted to the collisional integral but their mean-field potentials were neglected [169,170]. Nonetheless, we can gain some insight into this problem by investigating the one-particle density matrix which corresponds to the distribution in the hydrodynamic regime, given in Eq. (6.58). By using the inverse transformation (6.33), one has

$$\begin{aligned} n^{(1)}_{\mathrm{le}}\left(\mathbf{R}+\frac{\mathbf{s}}{2},\mathbf{R}-\frac{\mathbf{s}}{2};t\right) &= \int \frac{\mathrm{d}^3p}{(2\pi\hbar)^3}\,\nu_{\mathrm{le}}\left(\mathbf{R},\mathbf{p}-M\mathbf{v}\left(\mathbf{R},t\right);t\right)e^{i\mathbf{p}\cdot\mathbf{s}/\hbar}, \\ &= e^{iM\mathbf{v}(\mathbf{R},t)\cdot\mathbf{s}/\hbar}\int \frac{\mathrm{d}^3p'}{(2\pi\hbar)^3}\,\nu_{\mathrm{le}}\left(\mathbf{R},\mathbf{p}';t\right)e^{i\mathbf{p}'\cdot\mathbf{s}/\hbar}, \\ &= e^{iM\mathbf{v}(\mathbf{R},t)\cdot\mathbf{s}/\hbar}\,n^{(1)}_0\left(\mathbf{R}+\frac{\mathbf{s}}{2},\mathbf{R}-\frac{\mathbf{s}}{2};t\right), \end{aligned} \tag{6.59}$$

where we have performed the substitution $\mathbf{p}\to\mathbf{p}'+M\mathbf{v}\left(\mathbf{R},t\right)$ and have denoted the one-particle density matrix with $\mathbf{v}=\mathbf{0}$ by $n^{(1)}_0\left(\mathbf{R}+\frac{\mathbf{s}}{2},\mathbf{R}-\frac{\mathbf{s}}{2};t\right)$. Equation (6.59) shows that the difference between the one-particle density matrix in the presence and in the absence of local equilibrium is given by the phase involving the velocity field of the system.

6.6.2 Relaxation-Time Approximation

The collisional Boltzmann-Vlasov equation (6.53) involves many approximations which were discussed above. Notwithstanding the great deal of simplification brought by these approximations, it remains very hard to solve. An alternative to solving the Boltzmann-Vlasov equation is displayed by the method of the averages, a physically intuitive approach in which the collision integral is treated within the so called relaxation-time approximation. In this section, we use this method to provide a crude method of estimating at which temperature and interaction strength the hydrodynamic or the collisionless regime prevails.

In equilibrium in the hydrodynamic regime, the phase-space distribution obeys the condition (6.57)

and the collisional integral vanishes. In the collisionless regime the right-hand side of the Boltzmann-Vlasov equation also vanishes due to the absence of collisions. If the system, however, is not in equilibrium but close to it, the relaxation-time approximation can be applied to investigate the transition from one regime to the other by linearizing the Boltzmann-Vlasov equation. Within this approximation, the collision integral is replaced by

$$C\left[\nu(\mathbf{x},\mathbf{p};t)\right] \approx -\frac{\delta\nu(\mathbf{x},\mathbf{p};t)}{\tau}, \tag{6.60}$$

where τ is the relaxation time and

$$\delta\nu(\mathbf{x},\mathbf{p};t) = \nu(\mathbf{x},\mathbf{p};t) - \nu_{\mathrm{le}}(\mathbf{x},\mathbf{p};t) \tag{6.61}$$

denotes the deviation of the Wigner function from its local equilibrium value $\nu_{\mathrm{le}}(\mathbf{x},\mathbf{p};t)$, given in Eq. (6.58). The relaxation time τ can physically be understood as the average amount of time elapsed between two collisions. From Eq. (6.60), one sees that phase-space averages of the collision integral vanishes in both the hydrodynamic and the collisionless regimes. In the former regime, this happens because $\nu(\mathbf{x},\mathbf{p};t) = \nu_{\mathrm{le}}(\mathbf{x},\mathbf{p};t)$ and in the latter because $\tau \to \infty$.

The relaxation time τ is often used as a phenomenological input parameter, in order to investigate low-lying excitations in quantum systems in semiclassical approximation during the interpolation between the hydrodynamic and collisionless regimes. In fact, by including assumptions on the way that the phase-space distribution $\nu(\mathbf{x},\mathbf{p};t)$ deviates from its equilibrium value, it is possible to determine the relaxation time. Consider, for example, the quadrupole mode of a trapped interacting Fermi gas. In the linear regime, the variation of the distribution function is given by

$$\delta\nu(\mathbf{x},\mathbf{p};t) = -\left(\frac{\alpha_\perp \beta p_\perp^2}{2m} + \frac{\alpha_z \beta p_z^2}{2m}\right)\nu_{\mathrm{le}}(\mathbf{x},\mathbf{p};t)\left[1-\nu_{\mathrm{le}}(\mathbf{x},\mathbf{p};t)\right], \tag{6.62}$$

where, for a quadrupole motion, one must have

$$\alpha_\perp = -\frac{\alpha_z}{2}, \tag{6.63}$$

and, thererefore, the variation $\delta\nu(\mathbf{x},\mathbf{p};t)$ is proportional to $\alpha_\perp$. By choosing a quantity $\mathcal{U}(\mathbf{x},\mathbf{p})$ which is not conserved in collisions, one can evaluated the relaxation time τ according to the equation

$$\int \frac{\mathrm{d}^3x\mathrm{d}^3p}{(2\pi\hbar)^3}\mathcal{U}(\mathbf{x},\mathbf{p})C\left[\nu(\mathbf{x},\mathbf{p};t)\right] = \frac{1}{\tau}\int \frac{\mathrm{d}^3x\mathrm{d}^3p}{(2\pi\hbar)^3}\mathcal{U}(\mathbf{x},\mathbf{p})\delta\nu(\mathbf{x},\mathbf{p};t). \tag{6.64}$$

Since both sides are proportional to $\alpha_\perp$, an explicit expression for the relaxation time τ can be derived. This technique was initially introduced to investigate the collective oscillations of classical gases [171] and has, since then, been applied in different situations including studies of dynamical properties of normal Fermi gases [170].

6.7 Variational Approach to Hydrodynamics

In this section we discuss the variational time-dependent approach for a general two-particle interaction potential, which will lead to a unified formalism for elucidating the hydrodynamic properties of normal dipolar Fermi gases.

In order to study the collective motion of the gas, we employ an approximation for the one-particle orbitals $\phi_i(\mathbf{x},t)$ which was introduced before in the context of nuclear hydrodynamics [172] and is commonly used in hydrodynamic studies (see, for instance, Ref. [162]), namely that they all have the same phase

$$\phi_i(\mathbf{x},t) = e^{iM\chi(\mathbf{x},t)/\hbar}|\phi_i(\mathbf{x},t)|. \tag{6.65}$$

Notice that the orbitals $|\phi_i(\mathbf{x},t)|$ are invariant under time reversion and, therefore, are called time-even.

From Eq. (6.65) and the definition of a time-even Slater determinant

$$\Phi_0(\mathbf{x}_1,\cdots,\mathbf{x}_N;t) = \mathrm{SD}\left[|\phi_i(\mathbf{x},t)|\right] \tag{6.66}$$

we obtain

$$\Phi(\mathbf{x}_1,\cdots,\mathbf{x}_N;t) = e^{i\frac{M}{\hbar}[\chi(\mathbf{x}_1,t)+\cdots+\chi(\mathbf{x}_N,t)]}\Phi_0(\mathbf{x}_1,\cdots,\mathbf{x}_N;t). \tag{6.67}$$

Thus, the one-body density matrix (6.15) reduces to

$$n^{(1)}(\mathbf{x},\mathbf{x}';t) = e^{i\frac{M}{\hbar}[\chi(\mathbf{x},t)-\chi(\mathbf{x}',t)]}n_0^{(1)}(\mathbf{x},\mathbf{x}';t), \tag{6.68}$$

with $n_0^{(1)}(\mathbf{x},\mathbf{x}';t)$ being a time-even one-body density matrix given by

$$n_0^{(1)}(\mathbf{x},\mathbf{x}';t) \;=\; \sum_{i=1}^{N}|\phi_i(\mathbf{x},t)||\phi_i^*(\mathbf{x}',t)|. \tag{6.69}$$

At this point it becomes more evident that the present method resembles that of the collective coordinates applied for fermions, as mentioned in chapter 14 of Ref. [3].

Now the current density, defined in Eq. (6.27), becomes $\mathbf{j}(\mathbf{x},t) = n_0(\mathbf{x},t)\nabla\chi(\mathbf{x},t)$, allowing for the identification of $\chi(\mathbf{x},t)$ as the potential of the velocity field $\mathbf{v}(\mathbf{x},t)$. In addition, if the phase $\chi(\mathbf{x},t)$ is smooth enough, the one one-body density matrix (6.68) can be written as

$$n^{(1)}\left(\mathbf{R}+\frac{\mathbf{s}}{2},\mathbf{R}-\frac{\mathbf{s}}{2};t\right) = e^{iM\nabla\chi(\mathbf{R},t)/\hbar}n_0^{(1)}\left(\mathbf{R}+\frac{\mathbf{s}}{2},\mathbf{R}-\frac{\mathbf{s}}{2};t\right). \tag{6.70}$$

Comparing with Eq. (6.59), the one-body density matrix (6.70) can be identified with its local equilibrium counterpartner obtained from the Boltzmann-Vlasov equation.

It is interesting to compare the origin of the velocity fields in degenerate Fermi gases and in Bose-Einstein condensates (see Section 2.4). In the latter case, it is due to the broken gauge symmetry and the existence of the corresponding order parameter, which leads to superfluid hydrodynamics. In the former case, on the contrary, there is no order parameter and the gas is, therefore, normal. The common phase comes in as the potential of the velocity field which is characteristic of the collisional hydrodynamic regime.

With these definitions the action (6.6) reduces to

$$\mathcal{A}\left[n_0^{(1)},\chi\right] = -M\int_{t_1}^{t_2}\mathrm{d}t\int\mathrm{d}^3x\left\{\dot{\chi}(\mathbf{x},t)n_0(\mathbf{x},t)+\frac{n_0(\mathbf{x},t)}{2}\left[\nabla\chi(\mathbf{x},t)\right]^2\right\}-\int_{t_1}^{t_2}\mathrm{d}t\langle\Phi_0|\hat{H}|\Phi_0\rangle. \quad (6.71)$$

The first two terms concern the dynamical properties of the system and will be shown to give rise to the time derivatives in the equations of motion. Notice that integrating the first term by parts shows that the common phase $\chi(\mathbf{x},t)$ can be seen as the momentum conjugate to density $n_0(\mathbf{x},t)$, which represents the particle density. The second term describes the energy associated with the movement, i.e., the flow energy [3], given by

$$E_{\mathrm{flow}}(t)=\frac{M}{2}\int\mathrm{d}^3x n_0(\mathbf{x},t)\left[\nabla\chi(\mathbf{x},t)\right]^2. \quad (6.72)$$

The last term of Eq. (6.71), i.e., $\langle\Phi_0|\hat{H}|\Phi_0\rangle$, consists in total of three contributions

$$\langle\Phi_0|\hat{H}|\Phi_0\rangle=\langle\Phi_0|\hat{H}_{\mathrm{kin}}|\Phi_0\rangle+\langle\Phi_0|\hat{H}_{\mathrm{tr}}|\Phi_0\rangle+\langle\Phi_0|\hat{H}_{\mathrm{int}}|\Phi_0\rangle. \quad (6.73)$$

The first one is the expectation value of the kinetic energy operator with respect to $|\Phi_0\rangle$ and gives rise to the Fermi pressure:

$$E_{\mathrm{kin}}(t)=\frac{-\hbar^2}{2M}\int\mathrm{d}^3x(\nabla_{\mathbf{x}}-\nabla_{\mathbf{x}'})\cdot(\nabla_{\mathbf{x}}-\nabla_{\mathbf{x}'})n_0^{(1)}(\mathbf{x},\mathbf{x}';t)\Big|_{\mathbf{x}'=\mathbf{x}}. \quad (6.74)$$

Notice that the total kinetic energy is given by $E_{\mathrm{flow}}+\langle\Phi_0|\hat{H}_{\mathrm{kin}}|\Phi_0\rangle$. For simplicity, the kinetic energy in the static case, i.e., $\langle\Phi_0|\hat{H}_{\mathrm{kin}}|\Phi_0\rangle$, will be referred to as Fermi pressure or simply kinetic energy. The second term in Eq. (6.73) represents the energy associated with the external trap potential

$$E_{\mathrm{tr}}(t)=\int\mathrm{d}^3x\, n_0(\mathbf{x},t)U_{\mathrm{tr}}(\mathbf{x}). \quad (6.75)$$

The interaction energy, given by the third term in Eq. (6.73), contains both the direct and the exchange mean-field terms $\langle\Phi_0|\hat{H}_{\mathrm{int}}|\Phi_0\rangle=E^{\mathrm{Dir}}+E^{\mathrm{Ex}}$. The direct contribution is given by

$$E^{\mathrm{Dir}}(t) = \frac{1}{2}\int\mathrm{d}^3x\mathrm{d}^3x' V_{\mathrm{int}}(\mathbf{x},\mathbf{x}';t)n_0^{(1)}(\mathbf{x},\mathbf{x};t)n_0^{(1)}(\mathbf{x}',\mathbf{x}';t), \quad (6.76)$$

while the exchange part reads

$$E^{\mathrm{Ex}}(t) = -\frac{1}{2}\int\mathrm{d}^3x\mathrm{d}^3x' V_{\mathrm{int}}(\mathbf{x},\mathbf{x}';t)n_0^{(1)}(\mathbf{x},\mathbf{x}';t)n_0^{(1)}(\mathbf{x}',\mathbf{x};t). \quad (6.77)$$

Notice that the transformation (6.68) alters neither the direct (6.76) nor the exchange energy (6.77) in comparison with (6.22) and (6.23), respectively.

An important remark is in order at this point. If the interaction energy $\langle\Phi_0|\hat{H}_{\mathrm{int}}|\Phi_0\rangle$ would be a functional of the particle density $n_0(\mathbf{x},t)$ alone, conservation laws corresponding to the continuity equation and the Euler equation could be immediately derived by functionally extremizing the action

(6.71) with respect to the phase $\chi(\mathbf{x},t)$ and the density $n_0(\mathbf{x},t)$, respectively. In the present case, however, one has to extremize with respect to the full time-even one-body density matrix $n_0^{(1)}(\mathbf{x},\mathbf{x}';t)$. It turns out that the continuity equation remains unchanged

$$\frac{\partial n_0(\mathbf{x},t)}{\partial t} = -\nabla\cdot\left[n_0(\mathbf{x},t)\mathbf{v}(\mathbf{x},t)\right]. \tag{6.78}$$

The corresponding Euler equation reads, formally,

$$M\frac{\mathrm{d}\mathbf{v}(\mathbf{x},\mathrm{t})}{\mathrm{dt}} = -\nabla\left[\int \mathrm{d}^3x'\frac{\delta\langle\Phi_0|\hat{H}|\Phi_0\rangle}{\delta n_0^{(1)}(\mathbf{x},\mathbf{x}';t)}\right], \tag{6.79}$$

so that the proposed approach is circulation conserving.

6.8 Hydrodynamic Approach in Wigner Representation

In the preceding section we have derived a set of equations which could be applied to study the hydrodynamic excitations of a dipolar Fermi gas. Nevertheless, the equations (6.78) and (6.79) are not yet closed due to the lack of knowledge of the non-diagonal terms of the density matrix. Moreover, they are very complicated due to the presence of the functional derivative with respect to the bilocal time-even density matrix $n_0^{(1)}(\mathbf{x},\mathbf{x}';t)$ in Eq. (6.79). Therefore, we resort to a simpler procedure: extremizing action (6.71) by introducing appropriate variational quantities, which bear information on both the diagonal as well as the non-diagonal part of the interaction. Of course, we do loose information in this process because our variational approach may not be as precise as the solution of the complicated equation (6.24), but, on the other hand, it gives access to both the static and dynamical properties of dipolar Fermi gases in the hydrodynamic regime in a quite simple and clear way.

As we mentioned above, we switch to make use of adequate variational quantities to extremize the action (6.71). In order to do so, we find it more appropriate to change to the Wigner representation. Let us then introduce the time-even one-body density matrix according to

$$\nu_0(\mathbf{R},\mathbf{p};t) = \int \mathrm{d}^3s\, n_0^{(1)}\left(\mathbf{R}+\frac{\mathbf{s}}{2},\mathbf{R}-\frac{\mathbf{s}}{2};t\right) e^{-i\mathbf{p}\cdot\mathbf{s}/\hbar} \tag{6.80}$$

together with the corresponding inverse transformation

$$n_0^{(1)}(\mathbf{x},\mathbf{x}';t) = \int \frac{\mathrm{d}^3p}{(2\pi\hbar)^3}\,\nu_0\left(\frac{\mathbf{x}+\mathbf{x}'}{2},\mathbf{p};t\right) e^{i\mathbf{p}\cdot(\mathbf{x}-\mathbf{x}')/\hbar}. \tag{6.81}$$

With the help of Eq. (6.80), all quantities of interest can be expressed in terms of the time-even Wigner function in a quite analogous way as exposed in the Section 6.5. Due to the transformation (6.68), for example, the time-even particle density is given by

$$n_0(\mathbf{x},t) = n(\mathbf{x},t), \tag{6.82}$$

which implies that the trapping potential energy (6.19) is not altered by this transformation. The next

important quantity is the time-even momentum distribution which is obtained via

$$n_0(\mathbf{p},t) = \int \frac{\mathrm{d}^3x}{(2\pi)^3}\,\nu_0\left(\mathbf{x},\mathbf{p};t\right). \tag{6.83}$$

Due to the absence of the velocity field in Eq. (6.83), expectation values of odd powers of $\mathbf{p}$ vanish promptly. As a matter of fact, this is a consequence of the fact that the orbitals in Eq. (6.69) are time even and, therefore, carry no momentum. Expectation values of even powers of $\mathbf{p}^2$, however, are nonzero. In particular. the kinetic energy (6.74) and the trapping (6.75) energy can be written as

$$E_{\mathrm{kin}}(t) \;=\; \int \frac{\mathrm{d}^3x\mathrm{d}^3k}{(2\pi)^3}\,\nu_0\left(\mathbf{x},\mathbf{p};t\right)\frac{\mathbf{p}^2}{2M}. \tag{6.84}$$

As we have remarked in the previous section, the direct and exchange terms are not affected by the factorization (6.68). Therefore, we merely rewrite them in terms of the time-even Wigner function (6.80) for completeness according to

$$E_{\mathrm{int}}^{\mathrm{Dir}}(t) \;=\; \frac{1}{2}\int \frac{\mathrm{d}^3x\mathrm{d}^3p\mathrm{d}^3x'\mathrm{d}^3p'}{(2\pi\hbar)^6}\nu_0\left(\mathbf{x},\mathbf{p};t\right)V_{\mathrm{int}}(\mathbf{x}-\mathbf{x}')\nu_0\left(\mathbf{x}',\mathbf{p}';t\right), \tag{6.85}$$

$$E_{\mathrm{int}}^{\mathrm{Ex}}(t) \;=\; -\frac{1}{2}\int \frac{\mathrm{d}^3R\mathrm{d}^3p\mathrm{d}^3s\mathrm{d}^3p'}{(2\pi\hbar)^6}\nu_0\left(\mathbf{R},\mathbf{p};t\right)V_{\mathrm{int}}(\mathbf{s})\nu_0\left(\mathbf{R},\mathbf{p}';t\right)e^{i\mathbf{s}\cdot(\mathbf{p}-\mathbf{p}')}, \tag{6.86}$$

which completes our description of the components of the Hamiltonian (6.73) in terms of a time-even Wigner function.

We have developed a variational theory in terms of the velocity potential $\chi(\mathbf{x},t)$ and the time-even Wigner function $\nu_0\left(\mathbf{x},\mathbf{p}';t\right)$ which can be applied for hydrodynamic studies of Fermi gases. In order to apply this formalism, one still needs the corresponding ansatz for these quantities. This ansatz depends, indeed, on the particular case under investigation. In the next chapter, we will provide an application of this method to study the lowest lying excitations of a Fermi gas with dipole-dipole interaction.

7 Normal Dipolar Fermi Gases

This chapter is dedicated to the physical properties of non-superfluid dipolar Fermi gas in the collisional hydrodynamic regime [127,128]. We start our analysis with a discussion about the necessity of the hydrodynamic approach in dipolar Fermi gases. Then, by applying the Hartree-Fock approach in the Wigner space, which was developed in the last chapter, we investigate the static as well as the dynamic properties of the system, thereby emphasizing the role of the Fock exchange interaction. In order to do so, we implement the present theoretical approach variationally by adopting a suitable ansatz for the velocity potential and the time-even Wigner function. Subsequently, we extremize the action with respect to the corresponding variational parameters and obtain coupled equations of motion for the Thomas-Fermi radii and the Fermi momenta. A numerical integration of these equations allows us, on the one hand, to study static properties such as the spatial and momentum-space aspect ratios as well as the stability diagram of the system. On the other hand, we can also explore dynamical properties such as the low-lying excitations and the time-of-flight expansion.

7.1 Necessity of Hydrodynamic Treatment

The problem in which we are interested in this chapter is that of N spin-polarized fermionic dipoles of mass M trapped in the harmonic potential of Eq. (1.4) at ultralow temperatures. Since the Pauli principle inhibits the contact interaction, these particles interact dominantly through the dipole-dipole interaction. As we assume that the fermionic dipoles are polarized along the z-axis, the dipolar potential assumes the same form as in the bosonic part of this thesis

$$V_{\mathrm{dd}}(\mathbf{x}) = \frac{C_{\mathrm{dd}}}{4\pi|\mathbf{x}|^3}\left(1 - 3\cos^2\theta\right). \tag{7.1}$$

Further details about the interaction potential were given in the introductory Section 1.5. In the following we restrict ourselves to investigate the normal, non-superfluid phase of the system in the low-temperature limit. This is legitimate because the critical temperature for superfluidity is very low, depending exponentially on the length scale

$$a_{\mathrm{dd}} = \frac{MC_{\mathrm{dd}}}{4\pi\hbar^2}, \tag{7.2}$$

according to Eq. (6.1). Furthermore, this limit is restricted by the hydrodynamic requirement that the relaxation time τ, which was introduced in the framework of the relaxation time approximation in Section 6.6.2, has to be small in comparison with the time scale $1/\overline{\omega}$ defined by the average trap frequency $\overline{\omega}$.

Using the formalism of the relaxation time approximation, and results which are available for Fermi

gases with contact interaction, the necessity of a hydrodynamic approach can be inferred as follows. The relaxation time τ is not known for dipolar interactions, but it is possible to estimate it by assuming the dipole-dipole interaction to be equivalent to a contact interaction with the effective scattering length a_{dd} of Eq. (7.2). Then we use the fact that for a two-component, degenerate, normal Fermi gas with contact interaction one has

$$\frac{1}{\overline{\omega}\tau} = \left(\frac{N^{1/3}a_{\mathrm{dd}}}{\sqrt{\hbar/M\overline{\omega}}}\right)^2 F\left(\frac{T}{T_{\mathrm{F}}}\right), \tag{7.3}$$

where $F(T/T_{\mathrm{F}})$ is of the order 0.1 in the quantum temperature regime. Equation (7.3) was derived in Ref. [170] by applying the method explained in Section 6.6.2. Due to this result, we expect for the one-component, dipolar gas to enter the hydrodynamic regime for

$$N^{1/6}\epsilon_{\mathrm{dd}}^{\mathrm{f}} \gg 1, \tag{7.4}$$

with the dimensionless parameter

$$\epsilon_{\mathrm{dd}}^{\mathrm{f}} = \frac{C_{\mathrm{dd}}}{4\pi}\left(\frac{M^3\overline{\omega}}{\hbar^5}\right)^{\frac{1}{2}} N^{\frac{1}{6}}, \tag{7.5}$$

measuring the strength of the dipole-dipole interaction, as explained in Eq. (1.15).

In order to obtain a numerical estimate for the relaxation time, let us apply the experimental values of a typical set-up, say, that of Ref. [123]. In that experiment, $N = 4 \times 10^4$ heteronuclear $^{40}\mathrm{K}^{87}\mathrm{Rb}$ molecules with a measured electric dipole moment of $d \approx 0.56$ were brought close to quantum degeneracy in a trap with radial frequency of $\omega_x = \omega_y \approx 2\pi \times 175$ Hz. Assuming an average trap frequency of that value yields at least $\epsilon_{\mathrm{dd}}^{\mathrm{f}} \approx 5.3$ and $(\overline{\omega}\tau)^{-1} \approx 0.1 \times (N^{1/6}\epsilon_{\mathrm{dd}}^{\mathrm{f}})^2 \approx 96$, which clearly demonstrates that the system is driven into the hydrodynamic regime by the dipolar interaction. In addition, it should be remarked that there are molecules with much higher electric dipole moments than KRb. Prominent examples are SrO and CaO, with $d = 10.2$ Debye and with $d = 10.9$ Debye, respectively [173]. For these molecules, a hydrodynamic approach is absolutely necessary, as $(\overline{\omega}\tau)^{-1}$ can be as large as $(\overline{\omega}\tau)^{-1} \propto 10^6$ for the same particle number and average trap frequency.

7.2 Explicit Variational Approach

In the previous chapter we have developed a method to deal with the dynamic properties of Fermi gases in the hydrodynamic regime. The main constituent of that formalism is the time-even Wigner distribution function $\nu_0(\mathbf{x}, \mathbf{k}; t)$, in terms of which all physical quantities can be expressed. In addition, the time dependence is introduced by means of the velocity potential $\chi(\mathbf{x}, t)$, which is given by the common phase of the one-particle orbitals in the Slater determinant. In this section, we will derive the equations of motion for a dipolar Fermi gas by means of a well suited variational ansatz for both the velocity potential $\chi(\mathbf{x}, t)$ and the time-even Wigner function $\nu_0(\mathbf{x}, \mathbf{k}; t)$.

According to the last chapter, the properties of a fermionic system in the hydrodynamic regime can

be studied by extremizing the action

$$\mathcal{A}\left[n_0^{(1)},\chi\right] = -M\int_{t_1}^{t_2}\mathrm{d}t\int\mathrm{d}^3x\left\{\dot{\chi}(\mathbf{x},t)n_0(\mathbf{x},t)+\frac{n_0(\mathbf{x},t)}{2}\left[\nabla\chi(\mathbf{x},t)\right]^2\right\}-\int_{t_1}^{t_2}\mathrm{d}t\langle\Phi_0|\hat{H}|\Phi_0\rangle, \quad (7.6)$$

where $\langle\Phi_0|H|\Phi_0\rangle$ is a functional of the Wigner function, according to Section 6.8. To implement the variational approach, we apply the same harmonic ansatz for the velocity potential of Fermi gases in the collisional hydrodynamic regime as we did for the hydrodynamic superfluid phase of Bose-Einstein condensates in Eq. (4.22). Namely, we adopt the harmonic velocity potential of the form

$$\chi(\mathbf{x},t) = \frac{1}{2}\left[\alpha_x(t)x^2+\alpha_y(t)y^2+\alpha_z(t)z^2\right], \quad (7.7)$$

which is able to capture the monopole, the quadrupole and the two-dimensional quadrupole excitation modes. These are individually characterized by the relation between the α-parameters in the different directions. Furthermore, we use an ansatz for the time-even Wigner function which resembles that of a non-interacting Fermi gas at zero temperature in the semiclassical approximation. With this we cope with the main effect of the dipole-dipole interaction that the gas is stretched in the direction of the polarization. This ansatz is a generalization of the one presented in Ref. [112], which has the form of the zero-temperature limit of the Fermi-Dirac distribution

$$\nu_0\left(\mathbf{x},\mathbf{k};t\right) = \Theta\left(1-\sum_i\frac{x_i^2}{R_i(t)^2}-\sum_i\frac{k_i^2}{K_i(t)^2}\right), \quad (7.8)$$

where $\Theta(x)$ denotes the Heaviside step function. According to Eq. (7.8), the time-dependent parameters R_i and K_i represent the largest extension in the i-th direction of the density and momentum distribution, respectively. They will, therefore, be called the Thomas-Fermi radius and Fermi momentum in the i-th direction, respectively. It is important to remark that Eq. (7.8) allows for a variational approach in momentum space as well. Former investigations of the hydrodynamic properties of Fermi gases did not include this important feature [107].

The ansatz for the Wigner function (7.8) is required to satisfy the condition for conserving the total particle number

$$N=\int\frac{\mathrm{d}^3k\mathrm{d}^3x}{(2\pi)^3}\,\nu_0\left(\mathbf{x},\mathbf{k};t\right). \quad (7.9)$$

Inserting (7.8) into (7.9), one obtains after an elementary integration

$$\overline{R}^3(t)\overline{K}^3(t)=48N, \quad (7.10)$$

where the bar denotes geometrical average, as in Eq. (1.6). This equation shows that the variation in phase space is constrained. Using Eq. (7.10), one finds that the particle density (6.34), which is not altered by the phase factorization according to (6.82), is given by

$$n_0(\mathbf{x},t)=\frac{8N}{\pi^2\overline{R}^3(t)}\left[1-\sum_i\frac{x_i^2}{R_i^2(t)}\right]^{3/2}, \quad (7.11)$$

when the expression in brackets is non-negative and vanishes otherwise.

With the help of the ansatz (7.7) for the velocity potential and (7.8) for the Wigner function, we can evaluate the action (7.6) term by term as a functional of the variational parameters. Let us start by considering the first term under the time integral in action (7.6), which is given by

$$-M \int \mathrm{d}^3x \dot{\chi}(\mathbf{x},t) n_0(\mathbf{x},t) = -\frac{M}{2}\frac{N}{8}\sum_i \dot{\alpha}_i R_i^2(t). \tag{7.12}$$

The flow energy (6.72) can be evaluated in an analogous manner and reads

$$E_{\mathrm{flow}} = -\frac{N}{8}\frac{M}{2}\sum_i \alpha_i^2 R_i^2. \tag{7.13}$$

Combining equations (6.84), (7.8), and (7.10), we can express the kinetic energy rather in terms of the Fermi momenta according to

$$E_{\mathrm{kin}} = \frac{N}{8}\sum_i \frac{\hbar^2 K_i^2}{2M}. \tag{7.14}$$

Following a similar procedure yields for the trapping energy (6.37) the result

$$E_{\mathrm{trap}} = \frac{N}{8}\frac{M}{2}\sum_i \omega_i^2 R_i^2. \tag{7.15}$$

We come now to a discussion of the interaction contributions to the action (7.6), which consists of a direct, or Hartree, term plus an exchange, or Fock, term. For the dipole-dipole potential (7.1) together with the Wigner function (7.8) the Hartree term (6.85) is found to be a function of the Thomas-Fermi radii alone according to

$$E_{\mathrm{dd}}^{\mathrm{Dir}} = -\frac{N^2 c_0}{8\overline{R}^3} f\left(\frac{R_x}{R_z}, \frac{R_y}{R_z}\right), \tag{7.16}$$

with the constant c_0 given by

$$c_0 = \frac{2^{10} C_{\mathrm{dd}}}{3^4 \cdot 5 \cdot 7 \cdot \pi^3} \approx 0.0116\ C_{\mathrm{dd}}. \tag{7.17}$$

Correspondingly, the anisotropic part of the Fock interaction term is expressed in terms of the Fermi momenta and the Fock energy is given by

$$E_{\mathrm{dd}}^{\mathrm{Ex}} = \frac{N^2 c_0}{8\overline{R}^3} f\left(\frac{K_z}{K_x}, \frac{K_z}{K_y}\right). \tag{7.18}$$

It is interesting to note that the dipolar interaction is reflected in the same anisotropy function $f(x,y)$, which was defined in Eq. (4.34) for dipolar Bose-Einstein condensates. Due to the importance of this function, we have summarized its properties in Appendix A.

In the following, we will use the indexes 1 and 2 to denote a derivative with respect to the first and second argument. Note that, whereas $f(x,y)$ is symmetric with respect to exchanging the first and second variables, this is not the case for the functions $f_1(x,y)$ and $f_2(x,y)$. Furthermore, in the case of $x = y$, the anisotropy function $f(x,y)$ reduces to $f_s(x) = f(x,x)$.

Though both the direct and the exchange interaction contributions are determined by the same

anisotropy function $f(x,y)$, the dependence of the functions on the corresponding real-space and momentum aspect ratios is not the same. While the former enters the expression for the direct term as $f\left(\frac{R_x}{R_z},\frac{R_y}{R_z}\right)$, the latter takes part in the exchange term through $f\left(\frac{K_z}{K_x},\frac{K_z}{K_y}\right)$. Nonetheless, the properties of the function $f(x,y)$ (see Fig. 4.2) together with the minus sign of the exchange term compensate this difference and the effect of the dipole-dipole interaction turns out to be the same in both the real and the momentum space: it stretches the corresponding distribution along the z-direction. Moreover, while the particle-density deformation is directly influenced by the aspect ratio of the trapping potential, the momentum distribution is solely distorted by the presence of the dipolar exchange interaction, due to the spherical symmetry of the kinetic energy (7.14).

Now we insert the expressions (7.12)–(7.16) and (7.18) into the action (7.6). Additionally, we introduce the chemical potential μ as the Lagrange parameter in order to guarantee the conservation of the total particle number according to (7.9). Then, the action reads

$$\begin{aligned}\mathcal{A} &= -\int_{t_1}^{t_2}\mathrm{d}t\frac{N}{8}\left\{\frac{M}{2}\sum_i\left(\dot{\alpha}_i+\alpha_i^2+\omega_i^2\right)R_i^2+\sum_i\frac{\hbar^2K_i^2}{2M}-c_0\overline{K}^3\left[f\left(\frac{R_x}{R_z},\frac{R_y}{R_z}\right)-f\left(\frac{K_z}{K_x},\frac{K_z}{K_y}\right)\right]\right\}\\ &\quad-\int_{t_1}^{t_2}\mathrm{d}t\,\mu(t)\left(\frac{\overline{R}^3\overline{K}^3}{48}-N\right).\end{aligned}\tag{7.19}$$

The equations of motion follow from extremizing the action (7.19) with respect to all variational parameters α_i, R_i, K_i as well as the Lagrange multiplier μ. Through a suitable manipulation of the resulting equations one finds that the chemical potential is explicitly given by

$$\mu=\frac{1}{3}\sum_i\frac{\hbar^2K_i^2}{2M}-\frac{21c_0N}{\overline{R}^3}\left[f\left(\frac{R_x}{R_z},\frac{R_y}{R_z}\right)-f\left(\frac{K_z}{K_x},\frac{K_z}{K_y}\right)\right].\tag{7.20}$$

Furthermore, after some simple though tedious algebra, one obtains the following equations for the Fermi momenta

$$\begin{aligned}\frac{\hbar^2K_x^2}{2M} &= \frac{1}{3}\sum_i\frac{\hbar^2K_i^2}{2M}+\frac{48Nc_0}{2R_xR_yR_z}\frac{K_z}{K_x}f_1\left(\frac{K_z}{K_x},\frac{K_z}{K_y}\right),\\ \frac{\hbar^2K_y^2}{2M} &= \frac{1}{3}\sum_i\frac{\hbar^2K_i^2}{2M}+\frac{48Nc_0}{2R_xR_yR_z}\frac{K_z}{K_y}f_2\left(\frac{K_z}{K_x},\frac{K_z}{K_y}\right),\\ \frac{\hbar^2K_z^2}{2M} &= \frac{1}{3}\sum_i\frac{\hbar^2K_i^2}{2M}-\frac{48Nc_0}{2R_xR_yR_z}\frac{K_z}{K_x}f_1\left(\frac{K_z}{K_x},\frac{K_z}{K_y}\right)-\frac{48Nc_0}{2R_xR_yR_z}\frac{K_z}{K_y}f_2\left(\frac{K_z}{K_x},\frac{K_z}{K_y}\right).\end{aligned}\tag{7.21}$$

These equations are obviously not independent from one another, so we drop the third of them. Together with the condition for particle conservation (7.10), they determine the Fermi momenta K_i as functions of the Thomas-Fermi radii R_i, so that, in principle, we have three independent equations to solve for three variables.

As a consequence of the ansatz (7.7), the equations of motion for the variational parameters α_i are the same as for bosons (4.39) and read

$$\alpha_i=\frac{\dot{R}_i}{R_i}.\tag{7.22}$$

They are, in turn, used to derive the equations of motion for the Thomas-Fermi radii:

$$\ddot{R}_i = -\omega_i^2 R_i + \sum_j \frac{\hbar^2 K_j^2}{3M^2 R_i} - \frac{48Nc_0}{Mc_\mathrm{d}} Q_i(\mathbf{R},\mathbf{K}). \tag{7.23}$$

Here the auxiliary functions are given by the anisotropy function $f(x,y)$ and its derivatives according to

$$\begin{aligned}
Q_x(\mathbf{r},\mathbf{k}) &= \frac{c_\mathrm{d}}{x^2yz}\left[f\left(\frac{x}{z},\frac{y}{z}\right) - \frac{x}{z}f_1\left(\frac{x}{z},\frac{y}{z}\right) - f\left(\frac{k_z}{k_x},\frac{k_z}{k_y}\right)\right],\\
Q_y(\mathbf{r},\mathbf{k}) &= \frac{c_\mathrm{d}}{xy^2z}\left[f\left(\frac{x}{z},\frac{y}{z}\right) - \frac{y}{z}f_2\left(\frac{x}{z},\frac{y}{z}\right) - f\left(\frac{k_z}{k_x},\frac{k_z}{k_x}\right)\right],\\
Q_z(\mathbf{r},\mathbf{k}) &= \frac{c_\mathrm{d}}{xyz^2}\left[f\left(\frac{x}{z},\frac{y}{z}\right) + \frac{x}{z}f_1\left(\frac{x}{z},\frac{y}{z}\right) + \frac{y}{z}f_2\left(\frac{x}{z},\frac{y}{z}\right) - f\left(\frac{k_z}{k_x},\frac{k_z}{k_x}\right)\right],
\end{aligned} \tag{7.24}$$

where the constant c_d reads

$$c_\mathrm{d} = \frac{2^{\frac{38}{3}}}{3^{\frac{23}{6}}\cdot 5\cdot 7\cdot \pi^2} \approx 0.2791. \tag{7.25}$$

The first term on the right-hand side of equations (7.23) accounts for the harmonic trap, the second is due to the Fermi pressure, and the third represents the dipole-dipole interaction contribution, which will be discussed in more detail in the next section.

Having collected the equations of motion for all the variables, we can attempt to interpret Eqs. (7.10), (7.21), and (7.23) physically. In the case of a spherically symmetric momentum distribution one could neglect the exchange term and set to zero all terms which involve $f(K_z/K_x, K_z/K_y)$ and its derivatives. Thus, we could solve (7.10) and (7.21) for the Fermi momenta and obtain

$$K_x = K_y = K_z = \frac{\sqrt[3]{48N}}{\overline{R}}. \tag{7.26}$$

Inserting this result into Eqs. (7.23), we, then, would have a set of equations of motion for the Thomas-Fermi radii which stem from a potential $V(R_x,R_y,R_z)$. Thus, the problem would be reduced to study the motion of a fictitious particle under the influence of this potential. Due to the presence of the Fock term, however, it is not possible to solve Eqs. (7.10) and (7.21) directly, so they have to be solved simultaneously with Eqs. (7.23). For this reason, we conclude that the presence of the exchange term modifies the constraints in an anisotropic manner such that one has to give up the notion of an underlying potential $V(R_x,R_y,R_z)$.

7.3 Cylindrical Symmetry of Momentum Distribution

Before we explore the physical consequences of the equations of motion for a trapped dipolar Fermi gas, let us briefly discuss the non-interacting case, which will provide us with adequate units for the quantities of interest throughout this work. In the absence of the dipolar interaction, the momentum distribution is isotropic and the Fermi momenta in different directions are equal to each other according to Eq. (7.26). Denoting the Fermi energy of a non-interacting trapped Fermi gas by E_F, its chemical

potential takes the form

$$\mu^{(0)} = E_F = \hbar\overline{\omega}\,(6N)^{\frac{1}{3}}\,. \tag{7.27}$$

Correspondingly, the Thomas-Fermi radii and the Fermi momentum read, respectively,

$$R_i^{(0)} = \sqrt{\frac{2E_F}{M\omega_i^2}}; \qquad K_F = \sqrt{\frac{2ME_F}{\hbar^2}}. \tag{7.28}$$

This provides the motivation to express, in the interacting case, the Thomas-Fermi radii R_i in units of $R_i^{(0)}$ and the Fermi momenta K_i in units of K_F. Defining $\tilde{R}_i \equiv R_i/R_i^{(0)}$ and $\tilde{K}_i \equiv K_i/K_F$, the condition for the particle number conservation (7.10) reduces to

$$\overline{\tilde{R}}^3\,\overline{\tilde{K}}^3 = 1. \tag{7.29}$$

Thus, the equations of motion for the Thomas-Fermi radii in the dimensionless notation will be written in terms of the ratios

$$\frac{R_i}{R_j} = \frac{\tilde{R}_i}{\tilde{R}_j}\frac{\omega_j}{\omega_i}, \tag{7.30}$$

emphasizing the role played by the trap frequency ratios λ_x and λ_y, which were introduced in Eq. (1.5).

Before solving the dimensionless equations of motion, we can already obtain important information by considering the symmetries of the total energy in the static case, i.e., with the velocity potential χ set to zero. As a function of the variational parameters, the energy then reads

$$\frac{E}{NE_F} = \frac{1}{8}\left\{\sum_i\left(\tilde{K}_i^2+\tilde{R}_i^2\right) - \frac{2\epsilon_{\rm dd}^{\rm f}c_{\rm d}}{\overline{\tilde{R}}^3}\left[f\left(\frac{\tilde{R}_x\lambda_x}{\tilde{R}_z},\frac{\tilde{R}_y\lambda_y}{\tilde{R}_z}\right) - f\left(\frac{\tilde{K}_z}{\tilde{K}_x},\frac{\tilde{K}_z}{\tilde{K}_y}\right)\right]\right\}, \tag{7.31}$$

where the dimensionless dipolar-strength $\epsilon_{\rm dd}^{\rm f}$ is given in Eq. (7.5).

As a consequence of the symmetry of the anisotropy function $f(x,y) = f(y,x)$, which is proved in Appendix A, the energy (7.31) possesses the same symmetry with respect to the plane xOy in both K- and R-space. On the one hand, this implies that, in a cylinder-symmetric trap, where we have $\lambda_x = \lambda_y$, the extrema of the energy satisfy $R_x = R_y$. On the other hand, since the trap geometry does not influence the exchange contribution to the total energy, we conclude that the momentum distribution of a dipolar Fermi gas remains cylinder-symmetric even in the case of a triaxial trap geometry, i.e., one has $K_x = K_y$. Therefore, in the expression above, $f(\tilde{K}_z/\tilde{K}_x, \tilde{K}_z/\tilde{K}_y)$ can be simplified to $f_s(\tilde{K}_z/\tilde{K}_x)$ without loss of generality. Furthermore, recalling the mathematical identities for the cylinder symmetric anisotropy function given in Eqs. (4.44), we conclude that Eqs. (7.21) reduce to the single condition

$$\tilde{K}_z^2 - \tilde{K}_x^2 = \epsilon_{\rm dd}^{\rm f} C\left(\tilde{\mathbf{R}}, \tilde{K}_x, \tilde{K}_z\right) \tag{7.32}$$

with the function

$$C\left(\tilde{\mathbf{R}}, \tilde{K}_x, \tilde{K}_z\right) = \frac{3c_{\rm d}}{\overline{\tilde{R}}^3}\left[-1 + \frac{\left(2\tilde{K}_x^2+\tilde{K}_z^2\right) f_s\left(\tilde{K}_z/\tilde{K}_x\right)}{2\left(\tilde{K}_x^2-\tilde{K}_z^2\right)}\right], \tag{7.33}$$

which was first introduced in a previous publication of ours concerning the cylinder-symmetric trap [127]. In that work, we traced Eq. (7.32) back to the Fock exchange term. Thus, the presence of the exchange term of the dipole-dipole interaction deforms the momentum distribution of the Fermi gas. We emphasize that the cylindric symmetry in momentum space also holds in the dynamic case, since neither modulating the trap frequencies nor turning off the trap affects the symmetries of the exchange term.

Thus, the equation (7.23) for the Thomas-Fermi radius in the i-th direction can be written as

$$\frac{1}{\omega_i^2}\frac{d^2\tilde{R}_i}{dt^2} = -\tilde{R}_i + \sum_j \frac{\tilde{K}_j^2}{3\tilde{R}_i} - \epsilon_{\mathrm{dd}}^{\mathrm{f}}\tilde{Q}_i\left(\tilde{\mathbf{R}}, \tilde{K}_x, \tilde{K}_z\right), \tag{7.34}$$

with the corresponding simplifications in the $\tilde{Q}_i$-functions

$$\begin{aligned}
\tilde{Q}_x(\mathbf{r},\mathbf{k}) &= \frac{c_{\mathrm{d}}}{x^2yz}\left[f\left(\frac{x}{z},\frac{y}{z}\right) - \frac{x}{z}f_1\left(\frac{x}{z},\frac{y}{z}\right) - f_s\left(\frac{k_z}{k_x}\right)\right],\\
\tilde{Q}_y(\mathbf{r},\mathbf{k}) &= \frac{c_{\mathrm{d}}}{xy^2z}\left[f\left(\frac{x}{z},\frac{y}{z}\right) - \frac{y}{z}f_2\left(\frac{x}{z},\frac{y}{z}\right) - f_s\left(\frac{k_z}{k_x}\right)\right],\\
\tilde{Q}_z(\mathbf{r},\mathbf{k}) &= \frac{c_{\mathrm{d}}}{xyz^2}\left[f\left(\frac{x}{z},\frac{y}{z}\right) + \frac{x}{z}f_1\left(\frac{x}{z},\frac{y}{z}\right) + \frac{y}{z}f_2\left(\frac{x}{z},\frac{y}{z}\right) - f_s\left(\frac{k_z}{k_x}\right)\right],
\end{aligned} \tag{7.35}$$

The equations (7.29), (7.32), and (7.34) describe both the static and dynamic properties of a triaxially trapped dipolar Fermi gas in the hydrodynamic regime and represent the main result of the second part of this thesis. In what follows we shall explore their solutions in different cases of interest such as the conditions for stable equilibrium, the low-lying oscillations around the equilibrium positions, and the expansion of the gas after release from the trap, i.e., the time-of-flight dynamics.

For the sake of completeness, we express also the chemical potential (7.20) in terms of the dimensionless quantities introduced above

$$\frac{\mu}{E_F} = \sum_i \frac{\tilde{K}_i^2}{3} - \frac{7c_{\mathrm{d}}\epsilon_{\mathrm{dd}}^{\mathrm{f}}}{8\overline{\tilde{R}}}\left[f\left(\frac{\tilde{R}_x\lambda_x}{\tilde{R}_z},\frac{\tilde{R}_y\lambda_y}{\tilde{R}_z}\right) - f_s\left(\frac{\tilde{K}_z}{\tilde{K}_x}\right)\right]. \tag{7.36}$$

Now that we have explained in detail how our equations of motion arise and how they are expressed in dimensionless units, we are allowed to drop the tilde on the Thomas-Fermi radii as well as in the Fermi momenta and obtain a cleaner notation without any danger of misunderstandings.

7.4 Static Properties

The static properties of a dipolar Fermi gas are obtained by requiring the left-hand side of Eqs. (7.34) to vanish together with the normalization condition (7.29) and the condition for the deformation of the Fermi momenta (7.32). However this only gives us the conditions for an extremal mean-field energy. Since the dipolar interaction also contains an attractive part, it is useful to have a criterion for deciding whether a given state, i.e., a point $(\mathbf{R}, K_x, K_z)$ in the five-dimensional space of variational parameters, is stable or unstable. To that end we turn to the total energy, given by Eq. (7.31), which shall be minimized under the constraint $\overline{R}^3\overline{K}^3 = 1$ due to particle number conservation. A dimensional analysis

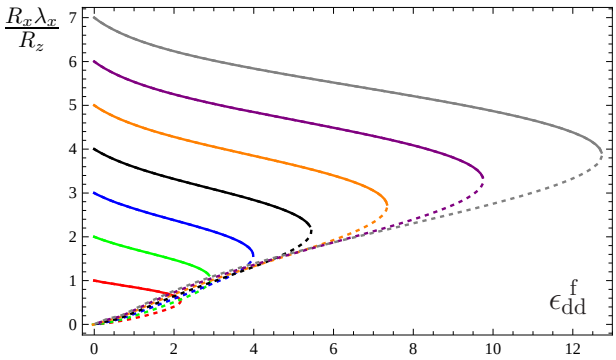

Figure 7.1: Aspect ratio in real space $R_x\lambda_x/R_z$ for a cylinder-symmetric trap with $\lambda_x = \lambda_y = 1, 2, 3, 4, 5, 6, 7$ (bottom to top). The upper branch (continuous) corresponds to a local minimum of the total energy, while the lower branch (dotted) represents an extremum but not a minimum.

of the energy (7.31) shows that the system cannot have a global minimum for any non-vanishing $\epsilon_{\rm dd}^{\rm f}$. This can be seen by noticing that the stabilization comes from the factor $K^2 \sim R^{-2}$ whereas the dipolar interaction goes with R^{-3}, rendering the energy unbounded from below. Nonetheless, for weak enough dipolar interactions a local minimum might exist, to which the system would return after a small perturbation. The regions satisfying this property will be called stable, while inflection points and local maxima will be denoted unstable equilibrium points. The mathematical criterion behind this classification scheme is given by the eigenvalues of the Hessian matrix associated with the four effectively independent variables of the problem.

One of the consequences of the unboundedness of the internal energy is that, for each value of the interaction strength $\epsilon_{\rm dd}^{\rm f}$, where the system has a stable configuration, there is also another unstable one. This can be seen by considering the aspect ratio of the cloud, which is depicted in Fig. 7.1 for different values of the trap aspect ratio $\lambda_x = \lambda_y$, as a function of $\epsilon_{\rm dd}^{\rm f}$. Here, we recognize that the stable branch (continuous) of the real space aspect ratio starts at $\epsilon_{\rm dd}^{\rm f} = 0$ with $R_x = R_z = 1$ and extends itself until the value $\epsilon_{\rm dd}^{\rm f,crit}$, where it meets the unstable branch (dotted). For $\epsilon_{\rm dd}^{\rm f} > \epsilon_{\rm dd}^{\rm f,crit}$, no stationary solution for the equations (7.34) exists. The unstable branch, on the other hand, possesses a vanishing aspect ratio for $\epsilon_{\rm dd}^{\rm f} = 0$. This is due to the fact that the dipole-dipole interaction tends to stretch the sample along the polarization direction. For a small value of $\epsilon_{\rm dd}^{\rm f}$, the unbounded energy solution is obtained with $R_x \to 0$ and, consequently, $R_x/R_z \to 0$, although the Thomas-Fermi radius in the axial direction R_z remains finite. We remark that the upper branch corresponds to a local minimum of the energy such that the Hessian matrix has only positive eigenvalues, while the lower one is an extremum but not a minimum, corresponding to a Hessian matrix with at least one negative eigenvalue. The corresponding graph for a dipolar Bose-Einstein condensate shown in Fig 4.3 in the Thomas-Fermi regime bears a crucial difference: unstable solutions only become available for $\epsilon_{\rm dd}^{\rm b} > 1$ [97]. The physical reason for this effect is that in dipolar condensates the stabilization comes from the contact interaction Eq. (4.30), which scales with R^{-3}, just like the dipole-dipole interaction.

In order to study the effect of a triaxial trap on the static properties of a dipolar Fermi gas, we explore further the symmetry $f(x, y) = f(y, x)$ of the anisotropy function as defined by Eq. (4.34). Due to this symmetry, we only need to discuss the aspect ratio $R_x\lambda_x/R_z$ since the properties of $R_y\lambda_y/R_z$ can

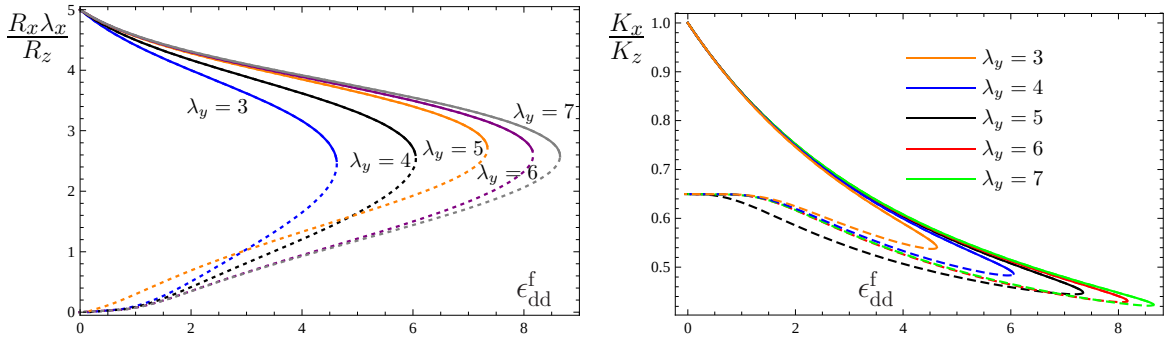

Figure 7.2: Aspect ratios in real and momentum space. The upper branch (continuous) corresponds to a local minimum of the total energy, while the lower branch (dashed) represents an extremum but not a minimum. Fig. 7.2a) Aspect ratio in real space $R_x\lambda_x/R_z$ for a triaxial trap with $\lambda_x = 5$ for various values of $\lambda_y = 3, 4, 5, 6, 7$. Notice that, for a fixed λ_x, making λ_y larger corresponds to flattening the trap in the direction perpendicular to the dipoles, allowing for stable configurations for larger interaction strengths. Fig. 7.2b) Corresponding aspect ratios in momentum space K_x/K_z.

be obtained by analogy. As indicated in Fig. 7.2a), varying λ_y for fixed λ_x clearly affects the stability of the system. For $\lambda_y > \lambda_x$, stable solutions are admitted for larger values of $\epsilon_{\rm dd}^{\rm f}$, i.e., $\epsilon_{\rm dd}^{\rm f,crit}$ is shifted to the right, whereas in the case $\lambda_y < \lambda_x$, $\epsilon_{\rm dd}^{\rm f,crit}$ decreases. This reflects the fact that more oblate traps tend to allow for larger $\epsilon_{\rm dd}^{\rm f}$ because they favor the repelling part of the interaction. Another remarkable feature in Fig. 7.2a) is that reducing λ_y for fixed λ_x reduces the value of $\epsilon_{\rm dd}^{\rm f,crit}$ much more than it is enlarged by increasing λ_y.

Concerning the aspect ratio in momentum space, we have studied its dependence on the dipolar strength $\epsilon_{\rm dd}^{\rm f}$ and found an analogous behavior to the one in real space. This goes back to the property of the function $f_s(x)$ of changing sign at $x = 1$, so that the minus sign in front of $f_s(K_z/K_x)$ in the total energy partially compensates its dependence on the reciprocal momentum aspect ratio K_z/K_x, and its behavior with respect to $\epsilon_{\rm dd}^{\rm f}$ turns out to be analogous to the one in real space. This is explicitly shown in Fig. 7.2b), where the aspect ratio in momentum space K_x/K_z is plotted as a function of $\epsilon_{\rm dd}^{\rm f}$ for $\lambda_x = 5$ and $\lambda_y = 3, 4, 5, 6,$ and 7. The main difference, which appears in momentum space, is the observation that the unstable solution converges to a finite value of the aspect ratio as the interaction strength $\epsilon_{\rm dd}^{\rm f}$ approaches zero. This reflects the fact that the collapse is a real-space phenomenon which is dominated by the shrinking of the radial Thomas-Fermi radius R_x, while the axial Thomas-Fermi radius R_z remains finite. As the momentum-space variables are accounted for only by the constraint (7.29) and the condition for momentum deformation (7.32), both K_x and K_z diverge as $\epsilon_{\rm dd}^{\rm f}$ approaches zero in the unstable branch, but their ratio always remains finite.

To conclude our investigation of the static properties of a trapped dipolar Fermi gas, we have also calculated the stability diagram for the cylinder-symmetric case $\lambda_x = \lambda_y$, where we obtain similar quantitative results as in Ref. [112], and for $\lambda_x \neq \lambda_y$, where the lack of axial symmetry has a considerable influence. The results are presented in a log-log plot in Fig. 7.3. If we consider a situation in which $\lambda_y = 5\lambda_x$ (red, upper curve), we do not obtain a large variation with respect to the cylinder-symmetric case $\lambda_y = \lambda_x$ (black, middle curve). On the contrary, if we take $\lambda_y = \lambda_x/5$, appreciable differences can be noticed as λ_x increases. This can be understood if one realizes that it is the weaker trap frequency

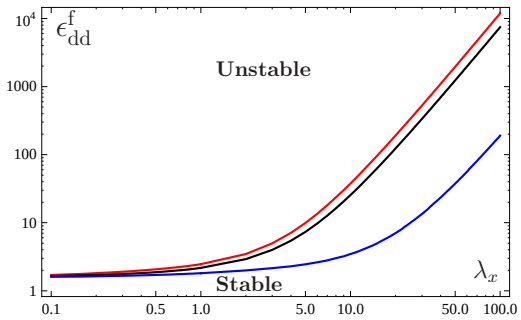

Figure 7.3: Stability diagram of a dipolar Fermi gas. The middle, black curve represents the cylinder-symmetric case $\lambda_y = \lambda_x$, while the upper, red one represents the case $\lambda_y = 5\lambda_x$ and the lower, blue curve is for $\lambda_y = \lambda_x/5$.

which determines the highest value of $\epsilon_{\rm dd}^{\rm f}$, for which the system remains stable. Therefore, by enlarging λ_y with respect to λ_x one obtains a smaller difference with respect to the case $\lambda_y = \lambda_x$ than by reducing it, explaining the effect already anticipated in Fig. 7.2a). Also remarkable is the fact that, for small trap frequency ratios, the three curves lie very close to each other.

7.5 Low-lying Excitations

The low-lying excitations of a dipolar Fermi gas are studied in this section by linearizing the equations of motion (7.34) around the equilibrium and, simultaneously, requiring conditions (7.29) and (7.32) to be fullfilled. This is done by assuming that at time t the following ansatz is valid

$$R_i(t) = R_i(0) + \eta_i \sin(\Omega t + \varphi)\,; \qquad K_i(t) = K_i(0) + \zeta_i \sin(\Omega t + \varphi)\,, \tag{7.37}$$

where η_i and ζ_i denote the small amplitudes in real and momentum space, respectively. Moreover, Ω represents the frequency of the oscillations and φ is a phase determined by the initial conditions. Due to the cylinder symmetry in momentum space, there are only two independent momentum-space amplitudes ζ_x and ζ_z, while three independent real-space amplitudes occur for a general triaxial harmonic trap.

In order to derive a matrix equation for the amplitudes in real space, we must obtain the ζ_i's as functions of the η_i's. To that end, we expand Eqs. (7.29) and (7.32) up to first order in the respective amplitudes and get

$$\zeta_i = \left(\sum_j \frac{\eta_j}{R_j} \right) K_i W_i \tag{7.38}$$

with the abbreviations

$$\begin{aligned} W_x &= -\frac{K_x^2 + K_z^2 - \epsilon_{\rm dd}^{\rm f} K_z C_{,K_z}}{4K_z^2 + 2K_x^2 - 3\epsilon_{\rm dd}^{\rm f} K_z C_{,K_z}}, \\ W_z &= -\frac{2K_z^2 - \epsilon_{\rm dd}^{\rm f} K_z C_{,K_z}}{4K_z^2 + 2K_x^2 - 3\epsilon_{\rm dd}^{\rm f} K_z C_{,K_z}}. \end{aligned} \tag{7.39}$$

To make the notation succinct, we have introduced here the shorthand $A_{,K_z} = \partial A(\mathbf{R}, K_x, K_z)/\partial K_z$ to

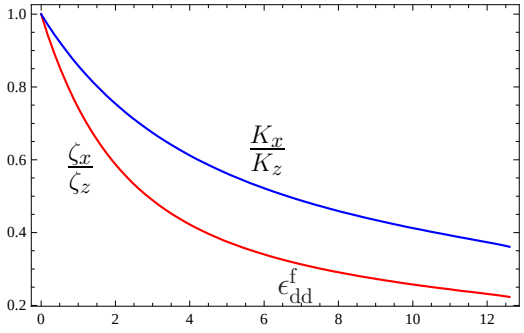

Figure 7.4: The lower (red) curve shows the ratio of the amplitudes ζ_x/ζ_z as a function of $\epsilon_{\rm dd}^{\rm f}$ for $\lambda_x = \lambda_y = 7$. For comparison, the stable branch of the equilibrium aspect ratio in momentum space against $\epsilon_{\rm dd}^{\rm f}$ for $\lambda_x = \lambda_y = 7$ is depicted by the upper (blue) curve.

denote a partial derivative of the quantity $A(\mathbf{R}, K_x, K_z)$ with respect to K_z evaluated at equilibrium. These results show explicitly that the presence of the dipolar exchange term drives the momentum oscillations *anisotropic*. In Fig. 7.4 we plot the ratio ζ_x/ζ_z as a function of $\epsilon_{\rm dd}^{\rm f}$ for $\lambda_x = \lambda_y = 7$. There, we show also the stable branch of the corresponding equilibrium aspect ratio in momentum space, which is represented by the upper (blue) curve. In order to appreciate the meaning of this curve, let us consider a typical experimental situation with $N \approx 4 \cdot 10^4$ KRb molecules and trap frequencies of $(\omega_x, \omega_y, \omega_z) = 2\pi\ (40, 40, 280)$ Hz. By using an external electric field and tuning the electric dipole moment to $d = 0.2$ Debye, one obtains the dipole-dipole-interaction strength $\epsilon_{\rm dd}^{\rm f} \approx 0.43$ which leads to an oscillation anisotropy of $\zeta_x/\zeta_z \approx 0.87$ and an equilibrium momentum deformation of $K_x/K_z \approx 0.93$. More striking effects result for a stronger dipolar interaction. Considering an electric dipole moment of $d = 0.57$ Debye yields a larger value $\epsilon_{\rm dd}^{\rm f} \approx 3.53$ and, therefore, also larger anisotropies for both the momentum oscillation $\zeta_x/\zeta_z \approx 0.45$ and the equilibrium momentum distribution $K_x/K_z \approx 0.64$. These results exhibit clearly the effects of the exchange term on the low-lying oscillations and make room for a clear detection of the dipole-dipole interaction in ultracold degenerate Fermi gases.

Linearizing the equations for the Thomas-Fermi radii (7.34) and taking the definitions (7.38) and (7.39) into account, we obtain

$$\left[\frac{\Omega^2}{\omega_i^2} - 1 - \frac{2K_x^2 + K_z^2}{3R_i^2}\right]\eta_i - \sum_j \left[\frac{P}{R_i R_j} + \epsilon_{\rm dd}^{\rm f} Q_{i,R_j}\right]\eta_j = 0, \tag{7.40}$$

where we have introduced the shorthand

$$P = \frac{2}{3}\frac{K_x^4 + K_z^4 + 4K_x^2K_z^2 - \left(2K_x^2 + K_z^2\right)\epsilon_{\rm dd} K_z C_{,K_z}}{4K_z^2 + 2K_x^2 - 3\epsilon_{\rm dd}^{\rm f} K_z C_{,K_z}}, \tag{7.41}$$

which approaches the value $2/3$ as $\epsilon_{\rm dd}^{\rm f}$ goes to zero. With this the study of the low-lying oscillations in a dipolar Fermi gas has been reduced to the eigenvalue problem (7.40): the oscillation frequencies Ω are given by the square root of the corresponding eigenvalues and the eigenmodes describe the real-space motion during the oscillations.

For a non-interacting Fermi gas, this formalism recovers the oscillation frequencies of a triaxial trap

as the solutions of the algebraic equation

$$3\Omega^6 - 8\Omega^4\left(\omega_x^2+\omega_y^2+\omega_z^2\right) + 20\Omega^2\left(\omega_x^2\omega_y^2+\omega_x^2\omega_z^2+\omega_y^2\omega_z^2\right) - 48\omega_x^2\omega_y^2\omega_z^2 = 0. \qquad (7.42)$$

This result is in agreement with Ref. [174], where a deeper analysis, initially devised for Bose-Einstein condensates [140], is carried out. It is shown there that, despite the lack of an obvious spatial symmetry, the wave equation for the hydrodynamic modes is separable in elliptical coordinates. We remark that the solutions of Eq. (7.42) reduce to the respective frequencies in the presence of cylindrical [159] or spherical symmetries [169], where this problem was first tackled.

In the following, we discuss separately the effects of the dipole-dipole interaction in cylindric and triaxial traps. The modification introduced in Eq. (7.42) due to the inclusion of the dipole-dipole interaction makes this equation too cumbersome to be displayed here. The same is true for the corresponding solutions. For this reason, we shall provide detailed expressions for the three oscillation frequencies only in the case of cylinder symmetry.

7.5.1 Oscillation Frequencies in Cylinder-symmetric Traps

In the presence of cylinder symmetry, we find three well characterized oscillation modes: one two-dimensional mode, the radial quadrupole, and two three-dimensional ones, the monopole and the quadrupole mode.

The first mode we consider is the radial quadrupole mode, which is depicted in Fig. 7.5a). It is characterized by a vanishing amplitude in the Oz-direction, while the oscillations in Ox- and Oy-directions have the same amplitude but are completely out-of-phase. We find the frequency $\Omega_{\rm rq}$ to be given by

$$\Omega_{\rm rq} \;=\; \omega_x\left\{2+\frac{3c_{\rm d}\epsilon_{\rm dd}^{\rm f}}{R_x^4R_z}\frac{R_x^2\lambda^2}{R_z^2}\frac{2\left(R_z^2-R_x^2\lambda^2\right)-\left(4R_z^2+R_x^2\lambda^2\right)f_s\left(R_x\lambda/R_z\right)}{\left(R_z^2-R_x^2\lambda^2\right)^2}\right\}^{1/2}, \qquad (7.43)$$

where the Thomas-Fermi radii R_x and R_z correspond to the static values calculated in Section 7.4.

The radial quadrupole mode can be experimentally excited by adiabatically deforming the circular trap in the xOy-plane into an ellipse and suddenly switching off the deformation. In the case of a two-component Fermi gas with contact interaction, the radial quadrupole mode was used to probe the transition from the collisionless to the hydrodynamic regime throughout the BEC-BCS-crossover [175]. For a dipolar Fermi gas, a similar experiment could be thought of, where controlling the collisions through applied electric fields would play the role of a Feshbach resonance to tune the system all the way from a ballistic to a hydrodynamic dipolar behavior in the normal phase. Fig. 7.5a) depicts $\Omega_{\rm rq}$ as a function of $\epsilon_{\rm dd}^{\rm f}$ for $\lambda = 5$ in units of ω_x. We find that, for a given λ, the frequency $\Omega_{\rm rq}$ is quite insensitive to changes in the interaction strength over the range of values in which the gas is stable. Although we have varied the trap anisotropy λ from 0.2 up to 20, no significant alteration of this behavior could be detected. Fig. 7.5b) shows the dependence of $\Omega_{\rm rq}$ on λ for $\epsilon_{\rm dd}^{\rm f} = 0.8$ and $\epsilon_{\rm dd}^{\rm f} = 1.2$ in units of its non-interacting value, i.e., $\sqrt{2}\omega_x$, which is directly given in Eq. (7.43) by setting $\epsilon_{\rm dd}^{\rm f} = 0$.

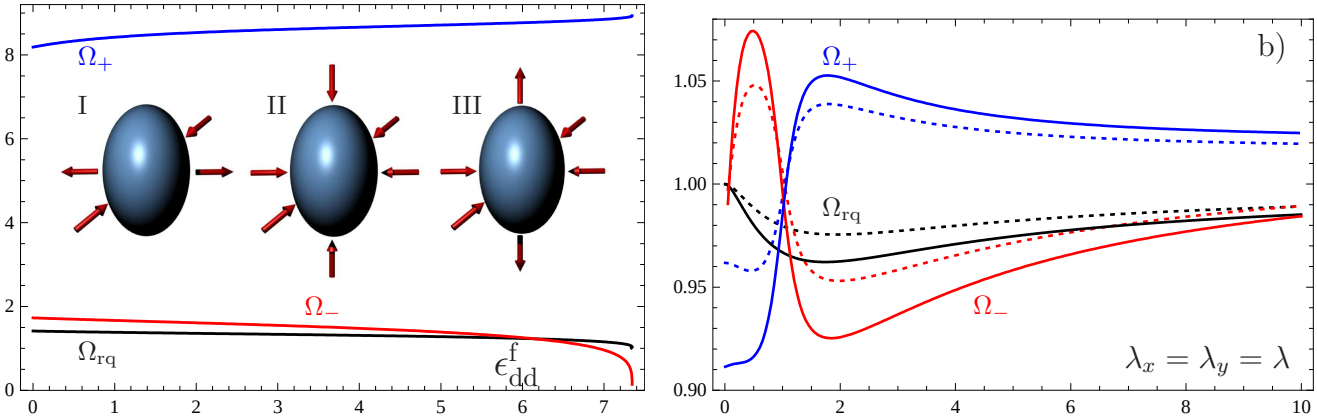

Figure 7.5: Oscillation modes in the cylinder-symmetric configuration. Fig. 7.5a) displays the oscillation frequencies for $\lambda = 5$ in units of ω_x. The frequencies of the radial quadrupole $\Omega_{\rm rq}$ (black), the monopole Ω_+ (blue), and the three-dimensional quadrupole mode Ω_- (red) are plotted as functions of the dipolar interaction strength $\epsilon_{\rm dd}^{\rm f}$. The inset shows the behavior of the corresponding eigenmodes. Inset I characterizes the radial quadrupole eigenmode, while II and III refer to the monopole and quadrupole mode, respectively. Fig. 7.5b) shows the oscillation frequencies in units of the corresponding non-interacting values as functions of λ for $\epsilon_{\rm dd}^{\rm f} = 0.8$ (dotted) and $\epsilon_{\rm dd}^{\rm f} = 1.2$ (continuous). The monopole and quadrupole modes are displayed in blue and red, respectively, while the radial quadrupole mode is shown in black.

We remark that the function

$$\frac{2\left(R_z^2 - R_x^2\lambda^2\right) - \left(4R_z^2 + R_x^2\lambda^2\right) f_s\left(R_x\lambda/R_z\right)}{\left(R_z^2 - R_x^2\lambda^2\right)^2} \tag{7.44}$$

in Eq. (7.43) is a function of the ratio $R_x\lambda/R_z$ alone which approaches the value $-16/35$ as $R_x\lambda/R_z$ tends to 1, so that no divergence arises for $R_z = R_x\lambda$. We would also like to point out that, despite the fact that the radial quadrupole mode is inherent to cylinder-symmetric systems, its calculation requires that one starts from a triaxial framework, which is then specialized to axial symmetry. This is the reason, why this important mode was explored in initial studies of dipolar Fermi gases neither in the hydrodynamic [127] nor in the collisionless regime [164].

We now concentrate on the three-dimensional monopole and quadrupole modes. The first, also known as breathing mode, is a compression mode characterized by an in-phase oscillation in all three directions and is denoted with an index +. The second, in analogy with the radial quadrupole mode, is an out-of phase oscillation in radial and axial directions and is denoted with an index −. In a spherical trap, these modes are decoupled from each other, but, here, they are coupled due to the cylinder symmetry of the trap. Their frequencies are given by

$$\Omega_\pm = \frac{\omega_x}{\sqrt{2}}\sqrt{M_{xx} + M_{zz} \pm \sqrt{2M_{xz}^2 + \left(M_{xx} - M_{zz}\right)^2}}, \tag{7.45}$$

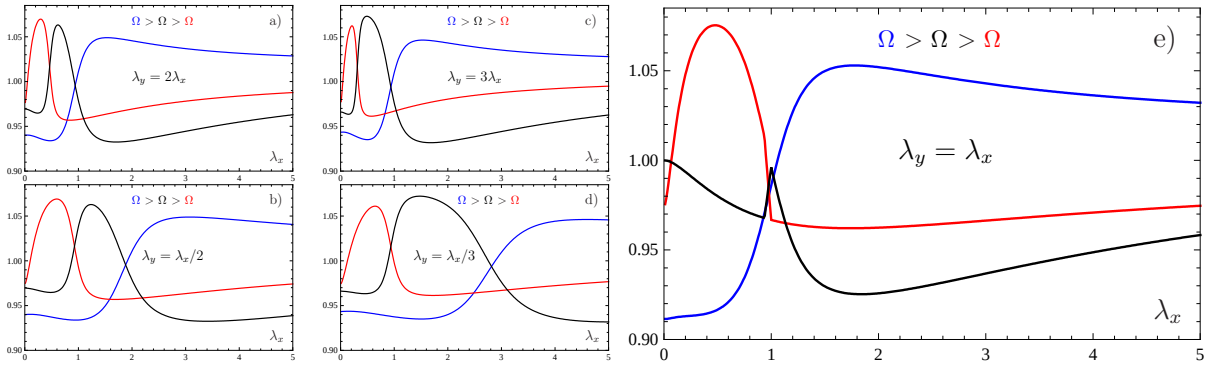

Figure 7.6: Low-lying oscillation frequencies for triaxial traps as functions of the trap aspect ratio λ_x for $\epsilon_{\rm dd}^{\rm f} = 1.2$ and different values of λ_y/λ_x. The frequencies are normalized by their respective non-interacting values. The curves are marked with the colors blue, black, and red corresponding to the highest, moderate, and lowest value, respectively. Figs. 7.6 a-d) show the mixing of the two quadrupole-like modes, which go continuously over into each other. In Fig. 7.6 e) a level-crossing in the cylinder-symmetric case becomes apparent through an abrupt permutation of the quadrupole modes (see Fig. 7.7 for more details).

together with the abbreviations

$$
\begin{aligned}
M_{xx} &= 2+\frac{2P}{R_x^2}+\frac{c_{\rm d}\epsilon_{\rm dd}^{\rm f}}{R_x^4 R_z}\left[\frac{-2R_z^4+7R_z^2R_x^2\lambda^2-5R_x^4\lambda^4}{\left(R_z^2-R_x^2\lambda^2\right)^2}-\frac{3R_x^2\lambda^2\left(2R_z^2+3R_x^2\lambda^2\right)}{2\left(R_z^2-R_x^2\lambda^2\right)^2}f_s\left(\frac{R_x\lambda}{R_z}\right)+2f_s\left(\frac{K_z}{K_x}\right)\right],\\
\frac{M_{zz}}{\lambda^2} &= 2+\frac{P}{R_z^2}+\frac{c_{\rm d}\epsilon_{\rm dd}^{\rm f}}{R_x^2 R_z^3}\left[\frac{2\left(4R_z^4-5R_z^2R_x^2\lambda^2+R_x^4\lambda^4\right)}{\left(R_z^2-R_x^2\lambda^2\right)^2}-\frac{3R_z^2\left(3R_z^2+2R_x^2\lambda^2\right)}{\left(R_z^2-R_x^2\lambda^2\right)^2}f_s\left(\frac{R_x\lambda}{R_z}\right)+f_s\left(\frac{K_z}{K_x}\right)\right],\\
\frac{M_{xz}}{2\lambda} &= \frac{P}{R_xR_z}+\frac{c_{\rm d}\epsilon_{\rm dd}^{\rm f}}{R_x^3R_z^2}\left[-\frac{R_z^4+R_z^2R_x^2\lambda^2-2R_x^4\lambda^4}{\left(R_z^2-R_x^2\lambda^2\right)^2}+\frac{15R_z^2R_x^2\lambda^2}{2\left(R_z^2-R_x^2\lambda^2\right)^2}f_s\left(\frac{R_x\lambda}{R_z}\right)+f_s\left(\frac{K_z}{K_x}\right)\right].
\end{aligned}
\tag{7.46}
$$

The dependence of the mono- and quadrupole oscillation frequencies on the dipole-dipole interaction strength $\epsilon_{\rm dd}^{\rm f}$ for a fixed trap anisotropy λ is shown in Fig. 7.5a). We find that the frequencies behave for different values of $\lambda > 1$ is qualitatively like in Fig. 7.5a), where we have chosen $\lambda = 5$: The monopole frequency increases monotonically and its derivative with respect to $\epsilon_{\rm dd}^{\rm f}$ blows up as $\epsilon_{\rm dd}^{\rm f,crit}$ is approached. On the contrary, the frequency of the two quadrupole modes decrease and their inclinations fall down abruptly in the neighborhood of $\epsilon_{\rm dd}^{\rm f,crit}$. In the case of $\lambda < 1$, the monopole frequency changes its behavior, which ceases to be monotonic in $\epsilon_{\rm dd}^{\rm f}$. It grows for small $\epsilon_{\rm dd}^{\rm f}$, but, as the critical interaction strength is approached, it starts decreasing as $\epsilon_{\rm dd}^{\rm f}$ grows. The radial quadrupole and three-dimensional quadrupole frequencies behave as functions of $\epsilon_{\rm dd}^{\rm f}$ for $\lambda < 1$ qualitatively nearly the same as for $\lambda > 1$. For specific values of λ, though, they might cease to be monotonically decreasing. The characteristic feature here is that, for both $\lambda < 1$ and $\lambda > 1$, the three-dimensional quadrupole frequency vanishes at $\epsilon_{\rm dd}^{\rm f,crit}$, as a signal of global collapse of the gas.

How the oscillation frequencies depend on λ is shown in Fig. 7.5b) for the two specific dipolar interaction strengths $\epsilon_{\rm dd}^{\rm f} = 0.8$ (dotted) and $\epsilon_{\rm dd}^{\rm f} = 1.2$ (continuous). For $\lambda < 1$, the quadrupole frequency is larger in comparison to the non-interacting case, while the contrary is true for the monopole frequency. As λ eventually becomes larger than 1, the monopole (quadrupole) becomes larger (smaller)

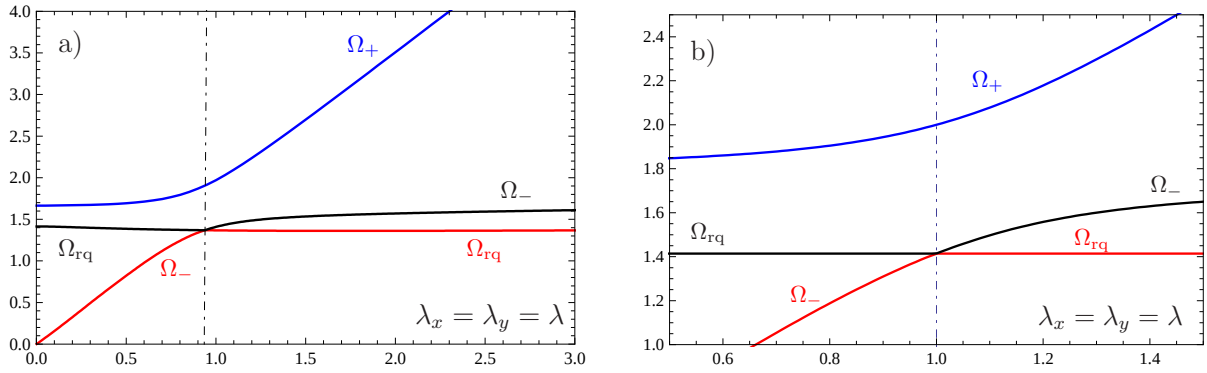

Figure 7.7: a) Frequencies of the low-lying oscillations in units of ω_x in the cylinder-symmetric configuration as functions of λ for $\epsilon_{\rm dd}^{\rm f} = 1.2$. The colors blue, black, and red label the frequencies in decreasing value. At $\lambda \approx 0.94$ a level-crossing takes place between the two quadrupole modes. b) Same frequencies for $\epsilon_{\rm dd}^{\rm f} = 0$. Notice that in the absence of the dipolar interaction, the level-crossing happens precisely at $\lambda = 1$. This difference explains the steep curves in Fig. 7.6e) for $0.94 < \lambda < 1$.

than in the absence of interactions. Concerning the radial quadrupole frequency, it turns out to be the most insensitive with respect to the dipolar interaction strength and is always smaller in the presence of the dipole-dipole interaction with a minimum around $\lambda \approx 1.74$. The behavior of the three-dimensional modes normalized by their non-interacting values agrees qualitatively with both dipolar Bose-Einstein condensates, shown in the right-hand side of Fig. 4.5, and with dipolar Fermi gases in the collisionless regime [164].

7.5.2 Oscillation Frequencies in Triaxial Traps

In the most general case, i.e., in absence of trap symmetry, the oscillation modes do not behave as indicated in the inset of the Fig. 7.5a) each of the three modes becomes a superposition of in- and out-of-phase oscillations in all three spatial directions. For this reason, the modes are better characterized by their frequencies and these are naturally mixed, even if one looks at the cylinder-symmetric limit of the triaxial solutions. We thus plot the frequencies in Fig. 7.6 and Fig. 7.7 according to their values and the colors blue, black, and red correspond to the highest, moderate, and lowest value, respectively. We exhibit in Fig. 7.6 the dependence of these frequencies on λ_x for different values of λ_y/λ_x and $\epsilon_{\rm dd}^{\rm f} = 1.2$, with the frequencies normalized by their respective non-interacting values. The situations $\lambda_y/\lambda_x = 2, 1/2, 3, 1/3$ correspond to Figs. 7.6 a), b), c) and d), respectively. These pictures show explicitly that the two quadrupole-like modes, denoted by the colors red and black, are now mixed. If the cylinder-symmetric situation is considered, a level-crossing becomes evident at $\lambda \approx 0.94$, shown in Fig. 7.6 e). In contrast to the bosonic case [152], the dipole-dipole interaction affects the value of λ at which the level-crossing takes place. For this reason, instead of a discontinuous transition, as for dipolar bosons, there is a steep continuous line in both the radial and the three-dimensional quadrupole modes for the trap anisotropy range $0.94 < \lambda < 1$.

The level-crossing in the cylinder-symmetric case can be seen more clearly in Fig. 7.7a), where the frequencies are plotted in units of ω_x for $\epsilon_{\rm dd}^{\rm f} = 1.2$. The vertical line marks the level-crossing, which takes place at $\lambda \approx 0.94$. Fig. 7.7b) contains a zoomed picture of the frequencies for $\epsilon_{\rm dd}^{\rm f} = 0$. There,

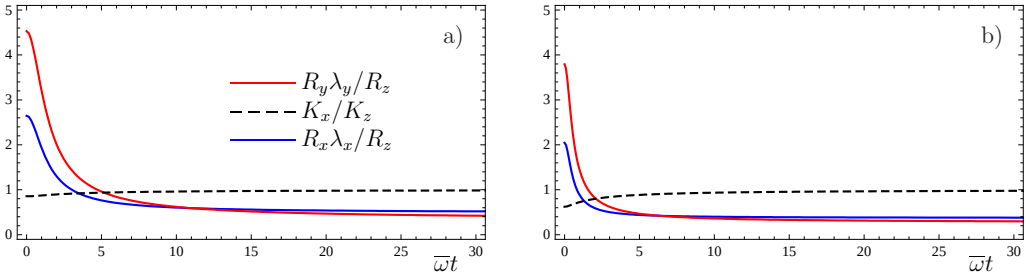

Figure 7.8: Aspect ratios in real and momentum space as functions of time. The trap is characterized by $\lambda_x = 3$ and $\lambda_y = 5$. The plots in the left-hand side correspond to $\epsilon_{\rm dd}^{\rm f} = 1$ while the ones in the right-hand side are for $\epsilon_{\rm dd}^{\rm f} = 3.5$.

the level-crossing happens at $\lambda = 1$, explaining the steep lines which show up in the spectra of the quadrupole modes in Fig. 7.6 e). This shift of the level-crossing can be traced back to the Fock exchange interaction, which is absent in dipolar Bose-Einstein condensates.

7.6 Time-of-flight Expansion

Time-of-flight expansion experiments are a key diagnostic tool in the field of ultracold quantum gases. In condensates, for example, the effects of the magnetic dipole-dipole interaction were observed for the first time in ^{52}Cr by measuring the time dependence of the aspect ratios for two different polarization directions after release from a triaxial trap [98]. In this section, we explore the corresponding problem for a strong dipolar normal Fermi gas.

Dipolar effects are expected to be observed in polar molecules due to their large electric dipole moment. Trapping and cooling these molecules requires a strong confinement in the polarization axes, to assure robustness against collapse. Therefore, the suppression of the attractive part of the dipole-dipole interaction indicates that this system is better described by normal hydrodynamics. Accordingly, we expect the dynamics of the dipolar Fermi gas to be described by the equations

$$\frac{1}{\omega_i^2}\frac{d^2R_i}{dt^2} = \sum_j \frac{K_j^2}{3R_i} - \epsilon_{\rm dd}^{\rm f} Q_i\left(\mathbf{R}, K_x, K_z\right), \tag{7.47}$$

together with the conditions for number conservation (7.29) and momentum deformation (7.32). Notice that equation (7.47) differs from (7.34) only due to the absent term $-R_i$, which is responsible for the trapping potential. In the following, we discuss the results obtained by solving these equation numerically, using the static values of Section 7.4 for the initial conditions of the parameters $R_i(0)$ and $K_i(0)$ as well as $\dot{R}_i(0) = 0$ and $\dot{K}_i(0) = 0$.

Until now, only axial symmetric traps were involved in experimental investigations of dipolar Fermi gases. Nevertheless, we have learned from studies of dipolar BECs how useful triaxial traps can be, for instance in the context of time-of-flight experiments.

Concerning the momentum space, we obtain in the triaxial case similar results as for the cylinder-symmetric one [127], where the aspect ratio K_x/K_z becomes asymptotically unity as a result of local equilibrium in the absence of the trap. The anisotropic aspect ratios $R_x\lambda_x/R_z$ and $R_y\lambda_y/R_z$ are

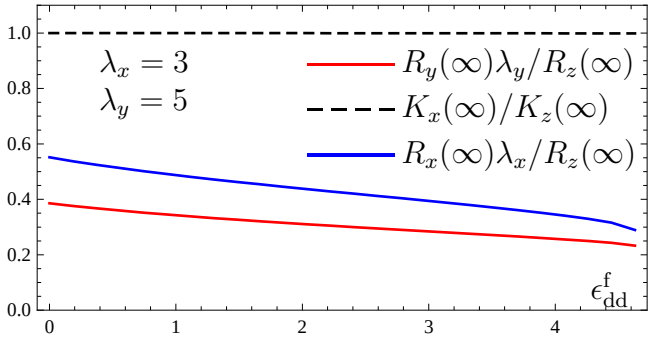

Figure 7.9: Asymptotic behavior in time of the aspect ratios as function of the dipole-dipole interaction strength $\epsilon_{\rm dd}^{\rm f}$ after release from the trap.

plotted as functions of time in Fig. 7.8 for $\lambda_x = 3$ and $\lambda_y = 5$. In Fig. 7.8a) and Fig. 7.8b) we have set $\epsilon_{\rm dd}^{\rm f} = 1$ and $\epsilon_{\rm dd}^{\rm f} = 3.5$, respectively, and we find that both aspect ratios, which are initially larger than 1, become smaller than 1 in the course of time. Also for traps with $\lambda_x < 1$ or $\lambda_y < 1$, an inversion of the corresponding aspect ratio takes place, but in the opposite direction. Such an inversion is typical for the hydrodynamic regime and was already observed for a two-component, normal Fermi gas with strong contact interaction [56,122]. The value $\epsilon_{\rm dd}^{\rm f} = 3.5$, chosen above, corresponds to $N = 4 \cdot 10^4$ ^{40}K^{87}Rb-molecules with a dipole moment of $d \approx 0.51$ Debye induced by an applied electric field and with trap frequencies characterized by $\omega_z = 2\pi \times 280$, $\lambda_x = 3$, and $\lambda_y = 5$.

A further important quantity of the time-of-flight analysis of dipolar Fermi gases is the asymptotic values of the aspect ratios. After the expansion the gas becomes more and more dilute and the interaction becomes less and less important, even in the case of long-range dipolar interactions. Nevertheless, studying the values of the aspect ratios at large times may still be useful because they are approached very fast. This is particularly relevant for strong pancake traps, where this happens just a few $\overline{\omega}^{-1}$ seconds after release of the trap, as is shown in Fig. 7.8. Although we are aware of the inaccuracy of the hydrodynamic approach for small dipole moments, we plot the long-time aspect ratios in Fig. 7.9 for the whole $\epsilon_{\rm dd}^{\rm f}$ range. There, we can identify the tendency of the dipole-dipole interaction to stretch the gas in the direction of the applied field in real space, whereas the momentum distribution remains always asymptotically spherical.

We would like to remark that the results presented here are in overall disagreement with those obtained by Sogo et al. in Ref. [164]. Translating their findings into our notation, the ballistic formalism predicts an inversion of the aspect ratio only for $\lambda > 1$. In addition, the aspect ratio in real space $R_x\lambda/R_z$ asymptotically approaches the one in momentum space K_x/K_z for every value of λ and $\epsilon_{\rm dd}^{\rm f}$. This disagreement stems from the difference in the nature of both approaches: while hydrodynamics assumes local equilibrium provided by collisions, the ballistic approach relies on the assumption of no interaction during the expansion. While the latter might be true for weak interactions, the former seems to be more adequate for strongly interacting gases like the one made out of KRb molecules.

During the time-of-flight expansion, the gas becomes more and more dilute, thereby weakening the interaction between the particles. Therefore, one could expect that the hydrodynamic assumption, which requires strong interaction, may not hold along the whole process and the expansion could acquire a collisionless character after some time. The determination of how the transition between the

two regimes occurs is a hard task which is beyond the scope of the present thesis. Nonetheless, we can estimate the validity of these results if we assume the previous hydrodynamic criterion to be valid also during the expansion. Before the expansion, the criterion for the hydrodynamic regime, given in Eq. (7.4), can be rewritten as

$$\frac{C_{\mathrm{dd}} M N^{1/2}}{4\pi\hbar^2 \overline{R}^{(0)}} \gg 1, \tag{7.48}$$

where $\overline{R}^{(0)}$ denotes the non-interacting mean Thomas-Fermi radius. As a result of a numerical analysis of the expansion dynamics, one finds that the mean Thomas-Fermi radius $\overline{R}(t)$ in units of $\overline{R}^{(0)}$ approaches for large times the asymptotic behaviour $\overline{R}(t) \sim \overline{\omega} t$. This scaling law can be understood if one considers that, at large times both the interaction and the Fermi pressure vanish. For this reason, the equations of motion imply $d^2 R_i / dt^2 = 0$ for large times. Performing the substitution $\overline{R}^{(0)} \to \overline{R}(t)$ this into equation (7.48) leads to the conclusion that the hydrodynamic condition is fullfilled for those times satisfying [127]

$$(\overline{\omega} t)^2 \ll (\overline{\omega}\tau)^{-1} \approx 0.1 \cdot (N^{1/6} \epsilon_{\mathrm{dd}})^2. \tag{7.49}$$

For SrO and CaO molecules, for example, Eq. (7.49) predicts the expansion to be hydrodynamic for $\overline{\omega} t \ll 1000$. As can be read off from Fig. 7.8, these times are long enough for the aspect ratios to reach their asymptotic values and no trace of a collisionless expansion is expected.

8 Conclusion

Motivated by major experimental breakthroughs in the area of dilute quantum gases possessing a long-range and anisotropic interaction potential, we theoretically investigated beyond-mean field properties of dipolar Bose-Einstein condensates as well as hydrodynamic properties of non-superfluid dipolar Fermi gases.

Initially, we presented a historically oriented introduction of the key experiments and concepts. The context which led to the latter and the advances which made the former possible was thereby explored as a mean to better understand the achievements as well as the difficulties preventing them from happening before. Proceeding in that way, we briefly discussed in Chapter 1 the main developments in low-temperature physics from the experimental discovery of superconductivity in solid mercury almost a century ago [1] all the way to the present day experiments of the JILA group with ^{40}K^{87}Rb-molecules [123]. During this journey we took the opportunity to describe the main ingredients of the forthcoming investigations such as the trapping (1.4) and the dipolar interaction (1.12) potentials as well as the bosonic and fermionic relative dipole strength, given in Eq. (1.14) and in Eq. (1.15), respectively.

The **first part** of this thesis was dedicated to dipolar Bose-Einstein condensates. Starting from the definition of Bose-Einstein condensation, we discussed in Chapter 2 the Bogoliubov prescription (2.11) which decomposes the bosonic field operator into a mean field, which plays the role of an order parameter, and an operator, which describes the quantum fluctuations around the mean field. Subsequently, we showed that the Heisenberg equation for the field operator in mean-field approximation Eq. (2.24), known as the Gross-Pitaevskii equation, can also be obtained from an action principle. Moreover, we derived from the Gross-Pitaevskii equation the hydrodynamic formalism for the condensate properties. In order to study dipolar condensates beyond the mean-field approximation, we extended the Bogoliubov-de Gennes theory of trapped condensates to include long-range interactions, thereby deriving general expressions for the physical quantities of interest such as the condensate depletion Eq. (2.70) and the corrected the ground-state energy Eq. (2.72).

As a starting point for the experimentally more relevant case of a harmonically trapped system, we considered in Chapter 3 a homogeneous dipolar Bose-Einstein condensate. Within the framework of the Bogoliubov theory we could reproduce the excitation spectrum (3.15), which is already available in the literature [92]. In addition, we obtained the explicit result Eq. (3.30) for the condensate depletion as a function of the s-wave scattering length and of the dipolar relative interaction strength. The next step was the calculation of the correction of the ground-state energy due to quantum fluctuations in Eq. (3.36) and, correspondingly, the Lee-Huang-Yang correction to the chemical potential given in Eq. (3.39). With the help of the corrected equation of state, the beyond-mean-field sound velocity was calculated in Eq. (3.41) and compared to the mean-field value in Fig. 3.3, which extends the Beliaev result for short-range interaction [73] to dipolar interaction [129].

Concerning trapped dipolar Bose-Einstein condensates, we considered the Gross-Pitaevskii theory

as the basis for the beyond-mean-field corrections. Since exact Gross-Pitaevskii results were already available in the literature [96,97], we revisited them in Chapter 4 by developing our own variational approach.

In Chapter 5 we studied beyond-mean-field effects in dipolar condensates by specializing the previously discussed Bogoliubov-de Gennes theory [129]. In order to treat the exchange interaction term between the condensate and the excited component analytically, we used the local density approximation which is the leading term of a systematic semiclassical gradient expansion [154]. In this way, we derived the semiclassical Bogoliubov spectrum in Eq. (5.7) and used it to calculate the condensate depletion, given in Eq. (5.12). Subsequently, we calculated the corrections to the ground-state energy due to the quantum fluctuations in Eq. (5.15) which allowed us to obtain the corresponding equations of motion (5.22) for the Thomas-Fermi radii of the condensate. The static solutions of these equations allow to determine the effect of the quantum fluctuations on the Thomas-Fermi radii, given by Eq. (5.28), and on the condensate aspect ratio (5.32). In particular, we investigated the dependence of the quantum correction to the aspect ratio on the dipolar strength $\epsilon_{\mathrm{dd}}^{\mathrm{b}}$ in Fig. 5.1a) and on the trap anisotropy in Fig. 5.1b). By linearizing the equations of motion around the equilibrium positions, we derived the beyond-mean-field excitation spectrum of the low-lying modes in Eq. (5.40), which generalizes the Pitaevskii-Stringari result for a condensate with contact interactions [15] to a dipolar condensate. Thereby, we plotted the corrections to the oscillation frequencies as functions of the trap aspect ratio for possible experimental setups in Fig. 5.3. In addition, removing the term corresponding to the harmonic confinement and solving the resulting equations with the initial conditions provided by the corrected equilibrium Thomas-Fermi radii, we investigated the time dependence of the condensate aspect ratio after release from the trap. The resulting dependence was plotted in Fig. 5.4, where, for reasonably large values of both the s-wave scattering length a_s and the relative dipolar interaction strength $\epsilon_{\mathrm{dd}}^{\mathrm{b}}$, we find beyond-mean-field corrections which are within the reach of the present day measurement precision.

The **second part** of this thesis deals with the physical properties of trapped dipolar Fermi gases in the non-superfluid phase in the hydrodynamic regime, where frequent collisions assure local equilibrium [127,128].

First, in Chapter 6, we discussed the theoretical methods for studying interacting normal Fermi gases by starting from the Hartree-Fock theory which follows from extremizing the action (6.6). In this way, we derived the Hartree-Fock equations for the one-particle orbitals, Eqs. (6.12) and (6.13), from which the corresponding equation of motion for the one-body density matrix Eq. (6.24) follows. By expanding this equation around the center of mass, we could derive the hydrodynamic equations of the problem, i.e., the continuity equation (6.26) and the Euler equation (6.28). We thereby showed that the presence of the Fock term leads to non-conservation of the velocity circulation so that Kelvin's theorem is not obeyed. We traced this effect back to the fact that the Fock term is not *a priori* a functional of the density alone. In order to circumvent this problem, we first switched to the Wigner representation, which was introduced in Section 6.5, and showed in Section 6.6 that the Hartree-Fock equation of motion for the one-body density matrix (6.24) leads to the collisionless Boltzmann-Vlasov equation for the phase-space distribution, given in Eq. (6.44). Subsequently, we briefly discussed how to introduce the effect of collisions in the Boltzmann-Vlasov equation (6.44) through the collisional

integral (6.54) and sketched how to perform hydrodynamic studies in the framework of the Boltzmann-Vlasov equation. Thereby, we highlighted the phase factor involving the velocity field in Eq. (6.59) as the main difference between the one-body density matrix in the presence and in the absence of local equilibrium. Furthermore, Subsection 6.6.2 was dedicated to the relaxation-time approximation, which allows to determine the time scale describing the collisional regime all the way from the collisionless to the hydrodynamic regime. Building on Eq. (6.59) and the role of the phase of the density matrix as a velocity potential, we constructed a variational approach to the hydrodynamics of fermionic systems in Section 6.7 which obeys Kelvin's theorem and, in Section 6.8, we formulated this approach in Wigner's space.

In order to justify the use of a hydrodynamic approach as opposed to a collisionless one to study the physics of dipolar Fermi gases, we could estimate the relaxation time of Subsection 6.6.2 by making use of an analogy with Fermi gases possessing contact interaction. In this way, we could devise an approximate criterion for the validity of the hydrodynamic approach, given in Eq. (7.4), which is clearly fullfilled for polar molecules. Then, by adopting an adequate ansatz for the velocity potential (7.7) and for the time-even Wigner function (7.8), we could derive coupled equations of motion for both the Fermi momenta (7.21) and the Thomas-Fermi radii (7.23). Following that, we showed that the momentum distribution possesses a cylinder symmetry even in the case of a triaxial trap. As a consequence, the equations for the Fermi momenta reduce to (7.32) while those for the Thomas-Fermi radii become (7.34). Studying the static solutions of these equations allowed us to investigate properties of the system such as the aspect ratios in real space, shown in Figs. 7.1 and 7.2a), and in momentum space, shown in Fig. 7.2b). Moreover, we also discussed the stability diagram of the system and plotted it in Fig. 7.3. Concerning the low-lying excitations, we first showed that the presence of the Fock term leads to anisotropic oscillations of the Fermi surface and discussed this anisotropy as a function of the fermionic dipolar strength in Fig. 7.4. Furthermore, we also discussed the real-space oscillations in the case of a cylinder symmetric trap in Subsection 7.5.1 and in that of a triaxial trap in Subsection 7.5.2. Finally, we investigated the time-of-flight dynamics of the system and plotted the aspect ratios as functions of time in both real and momentum space in Fig. 7.8. In addition, we also studied the asymptotic values of the aspect ratios as functions of the dipolar strength, which is shown in Fig. 7.9 and established criterion (7.49) for the validity of the hydrodynamic assumption during the expansion.

The experimental implications of the results achieved in this thesis, concerning both bosonic and fermionic dipolar quantum gases, have been discussed in the corresponding passages. In general, one can say that they are expected to be verified more easily in molecular systems, as these possess larger dipole moments.

A Anisotropy function

In this appendix we present a discussion of the function which governs the dipolar energy of both Bose-Einstein condensates and degenerate Fermi gases. Focusing on the practical use of this function in actual calculations, we present the definition used in this thesis and provide the most important identities together with a physical motivation, whereever this is appropriate.

When dealing with dipole-dipole interactions in ultracold quantum gases, the anisotropic character of the interaction is described by the following integral

$$f(x,y) = -\frac{1}{4\pi}\int_0^{2\pi} \mathrm{d}\phi \int_0^{\pi} \mathrm{d}\theta \sin\theta \left[\frac{x^2y^2 3\cos^2\theta}{\left(y^2\cos^2\phi + x^2\sin^2\phi\right)\sin^2\theta + x^2y^2\cos^2\theta} - 1\right], \tag{A.1}$$

where the coefficient in front of the integral sign was chosen in such a way that the function (A.1) interpolates between 1, for either $x \ll 1$ or $y \ll 1$, and -2, as both arguments assume large values (see Fig. 4.2). This is, indeed, not the only choice for the dipolar anisotropy function (see Ref. [112]), but has appeared often in the literature of both bosonic [149,151] as well as fermionic [127] dipolar quantum many-particle systems. In this appendix, we will bring the integral (A.1) into a closed expression and explore the properties of this function. It is worth remarking that this integral converges for all values of the variables x and y.

A.1 Closed expression (x,y<1)

In order to obtain a closed expression for the integral, we will restrict ourselves to the region $0 \leq x \leq y \leq 1$, for definiteness. Regions in which the variables x and y assume a value larger than 1 will be considered in the following sections. At first, let us split integral (A.1) in the form

$$f(x,y) = 1 - \frac{3x^2y^2}{4\pi}\int_0^{\pi} \mathrm{d}\theta \sin\theta\cos^2\theta\, g(x,y,\theta) \tag{A.2}$$

together with the auxiliary function

$$g(x,y,\theta) = \int_0^{2\pi} \mathrm{d}\phi \frac{1}{\left(y^2\cos^2\phi + x^2\sin^2\phi\right)\cos^2\theta + x^2y^2\cos^2\theta}. \tag{A.3}$$

The auxiliary function (A.3) can be integrated with the help of Eq. [176, (3.642.1)] without making any restriction for the variables x, y, or θ. Thereby, the anisotropy function (A.1) takes the form

$$f(x,y) = 1 - \frac{3x^2y^2}{2|x||y|} \int_0^\pi \mathrm{d}\theta \frac{\sin\theta\cos^2\theta}{\left[1-(1-x^2)\cos^2\theta\right]^{1/2}\left[1-(1-y^2)\cos^2\theta\right]^{1/2}}. \tag{A.4}$$

At this point the restrictions in the values of x and y start to become important. For $x, y < 1$, Eq. [176, (8.111.5)] can be used to bring expression (A.4) to the form

$$f(x,y) = 1 - \frac{3x^2y^2}{|x||y|\left(1-x^2\right)^{3/2}} \int_0^{\sin\varphi} \mathrm{d}u \frac{u^2}{\sqrt{1-u^2}\sqrt{1-k^2u^2}}, \tag{A.5}$$

with the modulus given by the relation

$$k^2 = \frac{1-y^2}{1-x^2} \tag{A.6}$$

and φ is defined according to

$$\varphi = \arcsin\sqrt{1-x^2}. \tag{A.7}$$

Finally, for $x < y$, which implies that the modulus obeys the inequality $k < 1$, and for $x, y > 0$, one obtains the following closed form for the anisotropy function

$$f(x,y) = 1 + 3xy \frac{E\left(\varphi,k\right) - F\left(\varphi,k\right)}{(1-y^2)\sqrt{1-x^2}}, \tag{A.8}$$

where $F\left(\varphi,k\right)$ and $E\left(\varphi,k\right)$ are the elliptic integrals of the first and second kind, respectively. They are defined according to

$$F\left(\varphi,k\right) = \int_0^{\sin\varphi} \mathrm{d}u \frac{1}{\sqrt{(1-u^2)(1-k^2u^2)}}, \tag{A.9}$$

$$E\left(\varphi,k\right) = \int_0^{\sin\varphi} \mathrm{d}u \frac{\sqrt{1-k^2u^2}}{\sqrt{1-u^2}}, \tag{A.10}$$

in Eq. [176, (8.111.2)] and in Eq. [176, (8.111.3)], respectively.

A.2 Analytic continuation (x,y>1)

The fact that expression (A.8) is only valid for $x, y < 1$ is quite restrictive when performing calculations. Therefore, we will also derive an expression for the anisotropy function which is valid in the region $x, y > 1$. To this end, we apply the transformation formulas presented in the last line of the table [176, (8.127)]. The final expression reads

$$f(x,y) = \frac{1+2x^2}{1-x^2} + \frac{3xy}{(y^2-1)^{1/2}(x^2-1)} E\left(\varphi_1,k_1\right), \tag{A.11}$$

together with the definitions

$$\sin\varphi_1 = \frac{\sqrt{y^2-1}}{y}, \tag{A.12}$$

$$k_1 = \frac{\sqrt{1-k^2}}{k}. \tag{A.13}$$

Equation (A.11) is valid for the case $x \geq y \geq 1$, because k_1 must be smaller than one.

A.3 Useful identities

A few identities involving the anisotropy function can be obtained from simple physical arguments, which are very useful in actual calculations. For example, once the dipoles are aligned in one fixed direction of space, say, along the z-axis, there exists a clear symmetry $x \leftrightarrow y$ with respect to the other two directions. The invariance under this change of variables can be directly obtained from definition (A.1). Nonetheless, let us illustrate another way to demonstrate this property. Starting from the Eq. (A.8), which is valid for $x \leq y \leq 1$, and switching the arguments one has

$$f(y,x) = 1 + 3xy\frac{E(\varphi_2,k_2) - F(\varphi_2,k_2)}{(1-x^2)\sqrt{1-y^2}}, \tag{A.14}$$

where the φ_2 and k_2 are given by

$$\sin\varphi_2 = \sqrt{1-y^2}, \tag{A.15}$$

$$k_2 = \sqrt{\frac{1-x^2}{1-y^2}}, \tag{A.16}$$

respectively. The arguments (A.15), (A.16) of the elliptic functions in Eq. (A.14) are such that this equation is valid for $1 \geq x \geq y$. By using the transformation in the third row of table [176, (8.127)] to make the corresponding analytic continuation, one obtains an expression which is valid in the same domain as Eq. (A.8) and reads

$$f(y,x) = 1 + 3xy\frac{E(\varphi,k) - F(\varphi,k)}{(1-y^2)\sqrt{1-x^2}}. \tag{A.17}$$

Therefore, in the region of the cartesian plane defined by $x \leq y \leq 1$, the identity

$$f(x,y) = f(y,x), \tag{A.18}$$

holds. Similar proofs can also be worked out for other regions of interest. Identity (A.18) allows for obtaining versions of Eqs. (A.8) and (A.11) which are valid for $y < x$.

Let us present another important identity involving the anisotropy function (A.8) which can be derived from a physical argument. Suppose a condensate with radii in the x-, y- and z-direction given by x, y and 1, in this order. Then, if the polarization is along the z-direction, either up or down, the dipolar interaction energy is expressed through the function $f(x,y)$, according to Eq. (4.33). For a

polarization either along the positive or negative y-direction, the corresponding function is $f(y/x, 1/x)$, and, for a polarization in the x-direction, the function $f(1/y, x/y)$ shows up. Summing over the three cases, the effect of the dipole-dipole interaction is canceled out. Therefore, the anisotropy function obeys the sum rule

$$f(x,y) + f\left(\frac{y}{x}, \frac{1}{x}\right) + f\left(\frac{1}{y}, \frac{x}{y}\right) = 0. \tag{A.19}$$

The mathematical proof of this identity can be obtained by starting out from Eq. (A.8) and proceeding in a analogous manner as in the derivation of the symmetry property (A.18). In this case, one needs the transformations listed in the second and the fifth line of table [176, (8.127)].

Using this identity together with the two expressions (A.8) and (A.11) one can derive an analytic continuation for the anisotropy function which is valid for $0 \leqslant x \leqslant 1 \leqslant y$, for example.

The practical importance of the identities presented here is very large. This is due to the fact that numerical calculations with software such as Mathematica® usually face difficulties in dealing with the tiny imaginary parts generated in the numerical analytic continuations.

A.4 Derivatives

The equations of motion for the Thomas-Fermi radii of both Bose-Einstein condensates and highly degenerate Fermi gases contain partial derivatives of the anisotropy function. They can be obtained with the help of the following properties of the elliptical functions

$$\frac{\partial E(\varphi,k)}{\partial k} = \frac{E(\varphi,k) - F(\varphi,k)}{k}, \tag{A.20}$$

$$\frac{\partial F(\varphi,k)}{\partial k} = \frac{1}{1-k^2}\left[\frac{E(\varphi,k) - \left(1-k^2\right)F(\varphi,k)}{k} - \frac{k\sin\varphi\cos\varphi}{\sqrt{1-k^2\sin^2\varphi}}\right], \tag{A.21}$$

$$\frac{\partial E(\varphi,k)}{\partial \varphi} = \sqrt{1-k^2\sin^2\varphi}, \tag{A.22}$$

$$\frac{\partial F(\varphi,k)}{\partial \varphi} = \frac{1}{\sqrt{1-k^2\sin^2\varphi}}. \tag{A.23}$$

Results (A.20) and (A.21) are listed in Eq. [176, (8.123.3)] and Eq. [176, (8.123.1)], respectively, while (A.22) and (A.23) follow from the definitions of the elliptic integrals (A.10) and (A.9).

Thus, denoting derivative with respect to the first or second argument through a corresponding subindex, one gets

$$f_1(x,y) = \frac{\partial f(x,y)}{\partial x} = 3y\frac{E(\varphi,k) - F(\varphi,k)}{(1-y^2)(1-x^2)^{3/2}} - \frac{3xy}{(y^2-x^2)(1-x^2)}\left[\frac{xE(\varphi,k)}{\sqrt{1-x^2}} - y\right], \tag{A.24}$$

$$f_2(x,y) = \frac{\partial f(x,y)}{\partial y} = 3x(1+y^2)\frac{E(\varphi,k) - F(\varphi,k)}{(1-y^2)^2(1-x^2)^{1/2}} + \frac{3xy}{(y^2-x^2)(1-y^2)}\left[\frac{yE(\varphi,k)}{\sqrt{1-x^2}} - x\right]. \tag{A.25}$$

A.5 Cylinder symmetry

It is particularly useful to study the anisotropy function (A.8) for the case where $x = y$, because this reflects the physical situation of a cylinder-symmetric trap. Let us start from Eq. (A.5) and obtain the equation

$$f_s(x) = f(x, x), \tag{A.26}$$

where $f_s(x)$ is the cylinder-symmetric anisotropy function which was introduced in Eq. (4.9). To that end, we just have to calculate the elementary integral

$$\lim_{y\to x} \frac{E(\varphi, k) - F(\varphi, k)}{k^2}, \tag{A.27}$$

which can be expressed through an elementary integral. Focusing first on the case $x < 1$, we obtain

$$\lim_{y\to x} \frac{E(\varphi, k) - F(\varphi, k)}{k^2} = -\int_0^{\sin\varphi} \mathrm{d}u \frac{u^2}{1-u^2} = \sqrt{1-x^2} - \tanh^{-1}\sqrt{1-x^2}. \tag{A.28}$$

In the second equality we have made use of the definition (A.7). For $x > 1$, one would have to start with the corresponding form of Eq. (A.5). Both cases can be combined through

$$f_s(x) = \frac{1 + 2x^2 - 3x^2\,\Xi(x)}{1-x^2}, \tag{A.29}$$

together with the abbreviation

$$\Xi(x) \equiv \begin{cases} \frac{1}{\sqrt{1-x^2}} \tanh^{-1}\sqrt{1-x^2}; & 0 \le x \le 1 \\ \frac{1}{\sqrt{x^2-1}} \tan^{-1}\sqrt{x^2-1}; & x \ge 1 \end{cases}. \tag{A.30}$$

Let us now consider the cylinder-symmetric limits of the derivatives (A.24) and (A.25). They contain the non-trivial limit of the anisotropy function involving the difference of the two elliptic functions, which has already been carried out in Eq. (A.27). Therefore, we consider the expansion of $E(\varphi, k)$ around $k^2 = 1$, which is given by

$$E(\varphi, k) = \sin\varphi + \left.\frac{\partial E(\varphi, k)}{\partial k^2}\right|_{k^2=1} (k^2-1) + \left.\frac{\partial^2 E(\varphi, k)}{\partial (k^2)^2}\right|_{k^2=1} \frac{(k^2-1)^2}{2!} + \cdots. \tag{A.31}$$

The coefficients in expansion (A.31) can be obtained with help of Eq. (A.20) and Eq. (A.21). In addition, these coefficients can be expressed in the convenient cylinder-symmetric form

$$\left.\frac{\partial E(\varphi, k)}{\partial k^2}\right|_{k^2=1} = \frac{[f_s(x) - 1](1-x^2)}{6x^2}, \tag{A.32}$$

$$\left.\frac{\partial^2 E(\varphi, k)}{\partial (k^2)^2}\right|_{k^2=1} = -\frac{(1-x^2)^{3/2} f_s(x)}{8x^2}. \tag{A.33}$$

With expansion (A.31) in mind, a couple of interesting mathematical results can be derived which are useful in studying the properties of dipolar quantum gases in symmetric traps. In particular, we

would like to state the following limits

$$\begin{aligned}
\lim_{y\to x} x f_1(x,y) = \lim_{y\to x} y f_2(x,y) &= -1 + \frac{(2+x^2) f_s(x)}{2(1-x^2)}, \\
\lim_{y\to x} f_{11}(x,y) = \lim_{y\to x} f_{22}(x,y) &= \frac{9\left[-2\left(1-x^2\right) + \left(4+x^2\right) f_s(x)\right]}{8\left(1-x^2\right)^2}, \\
\lim_{y\to x} f_{12}(x,y) = \lim_{y\to x} f_{21}(x,y) &= \frac{-2\left(4-5x^2+x^4\right) + \left(8+8x^2-x^4\right) f_s(x)}{8x^2\left(1-x^2\right)^2},
\end{aligned} \tag{A.34}$$

which are needed in deriving the analytical expressions for the oscillation frequencies in cylinder symmetric traps for both bosonic and fermionic systems.

Bibliography

[1] H. Kamerlingh-Onnes. The superconductivity of mercury. *Comm. Phys. Lab. Univ. Leiden* **120b**, **122b**, **124c** (1911).

[2] A. Einstein. Quantentheorie des einatomigen idealen Gases. *Sitzungsbericht der Preussichen Akademie der Wissenschaften, Physikalisch-mathematische Klasse* p. 3 (1925).

[3] C. J. Pethick and H. Smith. *Bose-Einstein condensation in dilute gases.* Cambridge University Press, 2nd ed. (2008).

[4] S. N. Bose. Plancks Gesetz und Lichtquantenhypothese. *Z. Phys.* **26**, 178 (1924).

[5] P. Kapitza. Viscosity of liquid helium below the λ-point. *Nature* **141**, 74 (1938).

[6] J. F. Allen and D. Misener. Flow of liquid helium II. *Nature* **141**, 75 (1938).

[7] F. London. On the Bose-Einstein condensation. *Phys. Rev.* **54**, 947 (1938).

[8] L. Tisza. The theory of liquid helium. *Phys. Rev.* **72**, 838 (1947).

[9] R. P. Feynman. Atomic theory of the λ-transition in helium. *Phys. Rev.* **91**, 1291 (1953).

[10] T. Matsubara. Quantum-statistical theory of liquid helium. *Progr. Theoret. Phys. Japan* **6**, 714 (1951).

[11] O. Penrose and L. Onsager. Bose-Einstein condensation and liquid helium. *Phys. Rev.* **104**, 576 (1956).

[12] N. Bogoliubov. On the theory of superfluidity. *J. Phys. USSR* **11**, 23 (1947).

[13] K. Huang and C. N. Yang. Quantum-mechanical many-body problem with hard-sphere interaction. *Phys. Rev.* **105**, 767 (1957).

[14] T. D. Lee, K. Huang, and C. N. Yang. Eigenvalues and eigenfunctions of a Bose system of hard spheres and its low-temperature properties. *Phys. Rev.* **106**, 1135 (1957).

[15] L. Pitaevskii and S. Stringari. Elementary excitations in trapped Bose-Einstein condensed gases beyond the mean-field approximation. *Phys. Rev. Lett.* **81**, 4541 (1998).

[16] L. N. Cooper. Bound electron pairs in a degenerate Fermi gas. *Phys. Rev.* **104**, 1189 (1956).

[17] J. Bardeen, L. N. Cooper, and J. R. Schrieffer. Microscopic theory of superconductivity. *Phys. Rev.* **106**, 162 (1957).

[18] D. D. Osheroff, R. C. Richardson, and D. M. Lee. Evidence for a new phase of solid ^{3}He. *Phys. Rev. Lett.* **28**, 885 (1972).

[19] D. D. Osheroff, W. J. Gully, R. C. Richardson, and D. M. Lee. New magnetic phenomena in liquid ^{3}He below 3 mk. *Phys. Rev. Lett.* **29**, 920 (1972).

[20] A. J. Leggett. Interpretation of recent results on ^{3}He below 3 mk: A new liquid phase? *Phys. Rev. Lett.* **29**, 1227 (1972).

[21] V. S. Bagnato, D. E. Pritchard, and D. Kleppner. Bose-Einstein condensation in an external potential. *Phys. Rev. A* **35**, 4354 (1987).

[22] K. B. Davis, M. O. Mewes, M. R. Andrews, N. J. van Druten, D. S. Durfee, D. M. Kurn, and W. Ketterle. Bose-Einstein condensation in a gas of sodium atoms. *Phys. Rev. Lett.* **75**, 3969 (1995).

[23] M. H. Anderson, J. R. Ensher, M. R. Matthews, C. E. Wieman, and E. A. Cornell. Observation of Bose-Einstein condensation in a dilute atomic vapor. *Science* **269**, 198 (1995).

[24] D. G. Fried, T. C. Killian, L. Willmann, D. Landhuis, S. C. Moss, D. Kleppner, and T. J. Greytak. Bose-Einstein condensation of atomic hydrogen. *Phys. Rev. Lett.* **81**, 3811 (1998).

[25] C. C. Bradley, C. A. Sackett, and R. G. Hulet. Bose-Einstein condensation of lithium: Observation of limited condensate number. *Phys. Rev. Lett.* **78**, 985 (1997).

[26] G. Modugno, G. Ferrari, G. Roati, R. J. Brecha, A. Simoni, and M. Inguscio. Bose-Einstein condensation of potassium atoms by sympathetic cooling. *Science* **294**, 1320 (2001).

[27] T. Weber, J. Herbig, M. Mark, H.-C. Nagerl, and R. Grimm. Bose-Einstein Condensation of Cesium. *Science* **299**, 232 (2003).

[28] Y. Takasu, K. Maki, K. Komori, T. Takano, K. Honda, M. Kumakura, T. Yabuzaki, and Y. Takahashi. Spin-singlet Bose-Einstein condensation of two-electron atoms. *Phys. Rev. Lett.* **91**, 040404 (2003).

[29] S. Kraft, F. Vogt, O. Appel, F. Riehle, and U. Sterr. Bose-Einstein condensation of alkaline earth atoms: ^{40}Ca. *Phys. Rev. Lett.* **103**, 130401 (2009).

[30] S. Stellmer, M. K. Tey, B. Huang, R. Grimm, and F. Schreck. Bose-Einstein condensation of strontium. *Phys. Rev. Lett.* **103**, 200401 (2009).

[31] Y. N. Martinez de Escobar, P. G. Mickelson, M. Yan, B. J. DeSalvo, S. B. Nagel, and T. C. Killian. Bose-Einstein condensation of ^{84}Sr. *Phys. Rev. Lett.* **103**, 200402 (2009).

[32] A Griesmaier, J. Werner, S. Hensler, J Stuhler, and T. Pfau. Bose-Einstein condensation of chromium. *Phys. Rev. Lett.* **94**, 160401 (2005).

[33] M. Lu, S. H. Youn, and B. L. Lev. Trapping ultracold dysprosium: A highly magnetic gas for dipolar physics. *Phys. Rev. Lett.* **104**, 063001 (2010).

[34] A. Robert, O. Sirjean, A. Browaeys, J. Poupard, S. Nowak, D. Boiron, C. I. Westbrook, and A. Aspect. A Bose-Einstein condensate of metastable atoms. *Science* **292**, 461 (2001).

[35] F. P. Dos Santos, J. Léonard, J. Wang, C. J. Barrelet, F. Perales, E. Rasel, C. S. Unnikrishnan, M. Leduc, and C. Cohen-Tannoudji. Bose-Einstein condensation of metastable helium. *Phys. Rev. Lett.* **86**, 3459 (2001).

[36] O. Dzyapko G. A. Melkov A. A. Serga B. Hillebrands S. O. Demokritov, V. E. Demidov and A. N. Slavin. Bose-Einstein condensation of quasi-equilibrium magnons at room temperature under pumping. *Nature* **443**, 430 (2006).

[37] D. Durfee and W. Ketterle. Experimental studies of Bose-Einstein condensation. *Opt. Express* **2**, 299 (1998).

[38] Y. Shin, M. Saba, T. A. Pasquini, W. Ketterle, D. E. Pritchard, and A. E. Leanhardt. Atom interferometry with Bose-Einstein condensates in a double-well potential. *Phys. Rev. Lett.* **92**, 050405 (2004).

[39] J. E. Williams and M. J. Holland. Preparing topological states of a Bose-Einstein condensate. *Nature* **401**, 568 (1999).

[40] J. R. Abo-Shaeer, C. Raman, J. M. Vogels, and W. Ketterle. Observation of vortex lattices in Bose-Einstein condensates. *Science* **292**, 476 (2001).

[41] W. H. Wing. On neutral particle trapping in quasistatic electromagnetic fields. *Prog. Quantum Electron.* **8**, 181 (1984).

[42] J. D. Jackson. *Classical Electrodynamics.* Wiley (1998).

[43] R. Grimm, M. Weidemüller, and Y. B. Ovchinnikov. Optical dipole traps for neutral atoms. *Adv. At. Mol. Opt. Phys.* **42**, 95 (2000).

[44] D. M. Stamper-Kurn, M. R. Andrews, A. P. Chikkatur, S. Inouye, H.-J. Miesner, J. Stenger, and W. Ketterle. Optical confinement of a Bose-Einstein condensate. *Phys. Rev. Lett.* **80**, 2027 (1998).

[45] T. L. Ho. Spinor Bose condensates in optical traps. *Phys. Rev. Lett.* **81**, 742 (1998).

[46] N. Bigelow. Bose-Einstein condensates: Spins mixed up. *Nat. Phys.* **1**, 89 (2005).

[47] A. Görlitz, T. L. Gustavson, A. E. Leanhardt, R. Löw, A. P. Chikkatur, S. Gupta, S. Inouye, D. E. Pritchard, and W. Ketterle. Sodium Bose-Einstein condensates in the $f = 2$ state in a large-volume optical trap. *Phys. Rev. Lett.* **90**, 090401 (2003).

[48] G.-B. Jo, Y.-R. Lee, J.-H. Choi, C. A. Christensen, T. H. Kim, J. H. Thywissen, D. E. Pritchard, and W. Ketterle. Itinerant Ferromagnetism in a Fermi Gas of Ultracold Atoms. *Science* **325**, 1521 (2009).

[49] W. Ketterle and N. J. van Druten. Evaporative cooling of atoms. *Adv. At. Mol. Opt. Phys.* **37**, 181 (1996).

[50] E. Zaremba A. Griffin, and T. Nikuni. *Bose-Condensed Gases at Finite Temperatures*. Cambrige University Press, (2009).

[51] S. Stringari. Collective excitations of a trapped Bose-condensed gas. *Phys. Rev. Lett.* **77**, 2360 (1996).

[52] W. Kohn. Cyclotron resonance and de Haas-van Alphen oscillations of an interacting electron gas. *Phys. Rev.* **123**, 1242 (1961).

[53] B. DeMarco and D. S. Jin. Onset of Fermi degeneracy in a trapped atomic gas. *Science* **285**, 1703 (1999).

[54] T. Loftus, C. A. Regal, C. Ticknor, J. L. Bohn, and D. S. Jin. Resonant control of elastic collisions in an optically trapped fermi gas of atoms. *Phys. Rev. Lett.* **88**, 173201, (2002).

[55] K. Dieckmann, C. A. Stan, S. Gupta, Z. Hadzibabic, C. H. Schunck, and W. Ketterle. Decay of an ultracold fermionic lithium gas near a Feshbach resonance. *Phys. Rev. Lett.* **89**, 203201 (2002).

[56] K. M. O'Hara, S. L. Hemmer, M. E. Gehm, S. R. Granade, and J. E. Thomas. Observation of a Strongly Interacting Degenerate Fermi Gas of Atoms. *Science* **298**, 2179 (2002).

[57] S. Gupta, Z. Hadzibabic, J. R. Anglin, and W. Ketterle. Collisions in zero temperature Fermi gases. *Phys. Rev. Lett.* **92**, 100401 (2004).

[58] M. Greiner, C. A. Regal, and D. S. Jin. Emergence of a molecular Bose-Einstein condensate from a Fermi gas. *Nature* **426**, 537 (2003).

[59] S. Jochim, M. Bartenstein, A. Altmeyer, G. Hendl, S. Riedl, C. Chin, J. Hecker Denschlag, and R. Grimm. Bose-Einstein condensation of molecules. *Science* **302**, 2101 (2003).

[60] M. W. Zwierlein, C. A. Stan, C. H. Schunck, S. M. F. Raupach, S. Gupta, Z. Hadzibabic, and W. Ketterle. Observation of Bose-Einstein condensation of molecules. *Phys. Rev. Lett.* **91**, 250401 (2003).

[61] A. J. Leggett. *Quantum liquids: Bose condensation and Cooper pairing in condensed-matter systems*. Oxford Graduate Texts (2006).

[62] D. M. Eagles. Possible pairing without superconductivity at low carrier concentrations in bulk and thin-film superconducting semiconductors. *Phys. Rev.* **186**, 456 (1969).

[63] K. Miyake. Fermi liquid theory of dilute submonolayer ^{3}He on thin ^{4}He II film. *Progr. Theoret. Phys. Japan* **69**, 1794 (1983).

[64] P. Nozières and S. Schmitt-Rink. Bose condensation in an attractive fermion gas: From weak to strong coupling superconductivity. *J. Low Temp. Phys.* **59**, 195 (1985).

[65] C. A. R. Sá de Melo, M. Randeria, and J. R. Engelbrecht. Crossover from BCS to Bose superconductivity: Transition temperature and time-dependent Ginzburg-Landau theory. *Phys. Rev. Lett.* **71**, 3202 (1993).

[66] E. Timmermans, P. Tommasini, M. Hussein, and A. Kerman. Feshbach resonances in atomic Bose-Einstein condensates. *Phys. Rep.* **315**, 199 (1999).

[67] R. A. Duine and H. T. C. Stoof. Atom-molecule coherence in Bose gases. *Phys. Rep.* **396**, 115 (2004).

[68] C. Chin, R. Grimm, P. Julienne, and E. Tiesinga. Feshbach resonances in ultracold gases. *Rev. Mod. Phys.* **82**, 1225 (2010).

[69] M. W. Zwierlein, J. R. Abo-Shaeer, A. Schirotzek, and W. Schunck, C. H.and Ketterle. Vortices and superfluidity in a strongly interacting Fermi gas. *Nature* **435**, 1047 (2005).

[70] K. Xu, Y. Liu, D. E. Miller, J. K. Chin, W. Setiawan, and W. Ketterle. Observation of strong quantum depletion in a gaseous Bose-Einstein condensate. *Phys. Rev. Lett.* **96**, 180405 (2006).

[71] D. M. Stamper-Kurn, A. P. Chikkatur, A. Görlitz, S. Inouye, S. Gupta, D. E. Pritchard, and W. Ketterle. Excitation of phonons in a Bose-Einstein condensate by light scattering. *Phys. Rev. Lett.* **83**, 2876 (1999).

[72] S. T. Beliaev. Application of the methods of quantum field theory to a system of bosons. *Soviet Physics JETP-USSR* **7**, 289 (1958).

[73] S. T. Beliaev. Energy-spectrum of a non-ideal Bose gas. *Soviet Physics JETP-USSR* **7**, 299 (1958).

[74] E. Timmermans, P. Tommasini, and K. Huang. Variational Thomas-Fermi theory of a nonuniform Bose condensate at zero temperature. *Phys. Rev. A* **55**, 3645 (1997).

[75] E. Braaten and J. Pearson. Semiclassical corrections to the oscillation frequencies of a trapped Bose-Einstein condensate. *Phys. Rev. Lett.* **82**, 255 (1999).

[76] D. M. Stamper-Kurn, H.-J. Miesner, S. Inouye, M. R. Andrews, and W. Ketterle. Collisionless and hydrodynamic excitations of a Bose-Einstein condensate. *Phys. Rev. Lett.* **81**, 500 (1998).

[77] S. L. Cornish, N. R. Claussen, J. L. Roberts, E. A. Cornell, and C. E. Wieman. Stable ^{85}Rb Bose-Einstein condensates with widely tunable interactions. *Phys. Rev. Lett.* **85**, 1795 (2000).

[78] G. E. Astrakharchik, R. Combescot, X. Leyronas, and S. Stringari. Equation of state and collective frequencies of a trapped Fermi gas along the BEC-unitarity crossover. *Phys. Rev. Lett.* **95**, 030404 (2005).

[79] A. Altmeyer, S. Riedl, C. Kohstall, M. J. Wright, R. Geursen, M. Bartenstein, C. Chin, J. Hecker Denschlag, and R. Grimm. Precision measurements of collective oscillations in the BEC-BCS crossover. *Phys. Rev. Lett.* **98**, 040401 (2007).

[80] M. A. Baranov. Theoretical progress in many-body physics with ultracold dipolar gases. *Phys. Rep.* **464**, 1 (2008).

[81] T. Lahaye, C. Menotti, L. Santos, M. Lewenstein, and T. Pfau. The physics of dipolar bosonic quantum gases. *Rep. Prog. Phys.* **72**, 126401 (2009).

[82] L. D. Carr and J. Ye. Focus on cold and ultracold molecules. *New J. Phys.* **11**, 055009 (2009).

[83] M. Marinescu and L. You. Controlling atom-atom interaction at ultralow temperatures by dc electric fields. *Phys. Rev. Lett.* **81**, 4596 (1998).

[84] B. Deb and L. You. Low-energy atomic collision with dipole interactions. *Phys. Rev. A* **64**, 022717 (2001).

[85] S. Yi and L. You. Trapped atomic condensates with anisotropic interactions. *Phys. Rev. A* **61**, 041604 (2000).

[86] S. Yi and L. You. Trapped condensates of atoms with dipole interactions. *Phys. Rev. A* **63**, 053607 (2001).

[87] T. Lahaye, T. Koch, B. Frohlich, M. Fattori, J. Metz, A. Griesmaier, S. Giovanazzi, and T. Pfau. News from the lab: A quantum ferrofluid. *http://www.pi5.uni-stuttgart.de/news/shownews.php/070727/news070727.html*

[88] K. Góral, K. Rzążewski, and T. Pfau. Bose-Einstein condensation with magnetic dipole-dipole forces. *Phys. Rev. A* **61**, 051601 (2000).

[89] T. Lahaye, T. Koch, B. Frohlich, M. Fattori, J. Metz, A. Griesmaier, S. Giovanazzi, and T. Pfau. Strong dipolar effects in a quantum ferrofluid. *Nature* **448**, 672 (2007).

[90] Q. Beaufils, R. Chicireanu, T. Zanon, B. Laburthe-Tolra, E. Maréchal, L. Vernac, J.-C. Keller, and O. Gorceix. All-optical production of chromium Bose-Einstein condensates. *Phys. Rev. A* **77**, 061601 (2008).

[91] R. Chicireanu, A. Pouderous, R. Barbé, B. Laburthe-Tolra, E. Maréchal, L. Vernac, J.-C. Keller, and O. Gorceix. Simultaneous magneto-optical trapping of bosonic and fermionic chromium atoms. *Phys. Rev. A* **73**, 053406 (2006).

[92] L. Santos, G. V. Shlyapnikov, P. Zoller, and M. Lewenstein. Bose-Einstein condensation in trapped dipolar gases. *Phys. Rev. Lett.* **85**, 1791 (2000).

[93] S. Yi and L. You. Probing dipolar effects with condensate shape oscillation. *Phys. Rev. A* **66**, 013607 (2002).

[94] L. Santos, G. V. Shlyapnikov, and M. Lewenstein. Roton-maxon spectrum and stability of trapped dipolar Bose-Einstein condensates. *Phys. Rev. Lett.* **90**, 250403 (2003).

[95] D. H. J. O'Dell, S. Giovanazzi, and G. Kurizki. Rotons in gaseous Bose-Einstein condensates irradiated by a laser. *Phys. Rev. Lett.* **90**, 110402 (2003).

[96] C. Eberlein, S. Giovanazzi, and D. H. J. O'Dell. Exact solution of the Thomas-Fermi equation for a trapped Bose-Einstein condensate with dipole-dipole interactions. *Phys. Rev. A* **71**, 033618 (2005).

[97] D. H. J. O'Dell, S. Giovanazzi, and C. Eberlein. Exact hydrodynamics of a trapped dipolar Bose-Einstein condensate. *Phys. Rev. Lett.* **92**, 250401 (2004).

[98] J. Stuhler, A. Griesmaier, T. Koch, M. Fattori, T. Pfau, S. Giovanazzi, P. Pedri, and L. Santos. Observation of dipole-dipole interaction in a degenerate quantum gas. *Phys. Rev. Lett.* **95**, 150406 (2005).

[99] J. Werner, A. Griesmaier, S. Hensler, J. Stuhler, T. Pfau, A. Simoni, and E. Tiesinga. Observation of Feshbach resonances in an ultracold gas of ^{52}Cr. *Phys. Rev. Lett.* **94**, 183201 (2005).

[100] T. Koch, T. Lahaye, J. Metz, B. Frohlich, A. Griesmaier, and T. Pfau. Stabilization of a purely dipolar quantum gas against collapse. *Nat. Phys.* **4**, 218 (2008).

[101] T. Lahaye, J. Metz, B. Fröhlich, T. Koch, M. Meister, A. Griesmaier, T. Pfau, H. Saito, Y. Kawaguchi, and M. Ueda. d-wave collapse and explosion of a dipolar Bose-Einstein condensate. *Phys. Rev. Lett.* **101**, 080401 (2008).

[102] M. Lewenstein. Dancing the Bose-nova with a twirl. *Physics* **1**, 13 (2008).

[103] C. A. Sackett, J. M. Gerton, M. Welling, and R. G. Hulet. Measurements of collective collapse in a Bose-Einstein condensate with attractive interactions. *Phys. Rev. Lett.* **82**, 876 (1999).

[104] M. Vengalattore, S. R. Leslie, J. Guzman, and D. M. Stamper-Kurn. Spontaneously modulated spin textures in a dipolar spinor Bose-Einstein condensate. *Phys. Rev. Lett.* **100**, 170403 (2008).

[105] S. E. Pollack, D. Dries, M. Junker, Y. P. Chen, T. A. Corcovilos, and R. G. Hulet. Extreme tunability of interactions in a ^{7}Li Bose-Einstein condensate. *Phys. Rev. Lett.* **102**, 090402 (2009).

[106] K. Góral, B.-G. Englert, and K. Rzążewski. Semiclassical theory of trapped fermionic dipoles. *Phys. Rev. A* **63**, 033606 (2001).

[107] K. Góral, M. Brewczyk, and K. Rzążewski. Hydrodynamic excitations of trapped dipolar fermions. *Phys. Rev. A* **67**, 025601 (2003).

[108] M. A. Baranov, M. S. Mar'enko, Val. S. Rychkov, and G. V. Shlyapnikov. Superfluid pairing in a polarized dipolar Fermi gas. *Phys. Rev. A* **66**, 013606 (2002).

[109] M. A. Baranov, Ł. Dobrek, and M. Lewenstein. Superfluidity of trapped dipolar Fermi gases. *Phys. Rev. Lett.* **92**, 250403 (2004).

[110] M. A. Baranov, Klaus Osterloh, and M. Lewenstein. Fractional quantum hall states in ultracold rapidly rotating dipolar Fermi gases. *Phys. Rev. Lett.* **94**, 070404 (2005).

[111] M. A. Baranov, H. Fehrmann, and M. Lewenstein. Wigner crystallization in rapidly rotating 2d dipolar Fermi gases. *Phys. Rev. Lett.* **100**, 200402 (2008).

[112] T. Miyakawa, T. Sogo, and H. Pu. Phase-space deformation of a trapped dipolar Fermi gas. *Phys. Rev. A* **77**, 061603 (2008).

[113] G. M. Bruun and E. Taylor. Quantum phases of a two-dimensional dipolar Fermi gas. *Phys. Rev. Lett.* **101**, 245301 (2008).

[114] B. M. Fregoso, K. Sun, E. Fradkin, and B. L. Lev. Biaxial nematic phases in ultracold dipolar Fermi gases. *New J. Phys.* **11**, 103003 (2009).

[115] B. M. Fregoso and E. Fradkin. Ferronematic ground state of the dilute dipolar Fermi gas. *Phys. Rev. Lett.* **103**, 205301 (2009).

[116] C. K. Chan, C. Wu, W.C Lee, and S. Das Sarma. Anisotropic Fermi-liquid theory of ultracold fermionic polar molecules: Landau parameters and collective modes. *Phys. Rev. A* **81**, 023602 (2010).

[117] S. Ronen and J. L. Bohn. Zero sound in dipolar Fermi gases. *Phys. Rev. A* **81**, 033601 (2010).

[118] Y. Yamaguchi, T. Sogo, T. Ito, and T. Miyakawa. Density-wave instability in a two-dimensional dipolar Fermi gas. *Phys. Rev. A* **82**, 013643 (2010).

[119] A. J. Berglund, J. L. Hanssen, and J. J. McClelland. Narrow-line magneto-optical cooling and trapping of strongly magnetic atoms. *Phys. Rev. Lett.* **100**, 113002 (2008).

[120] C. Ticknor. Collisional control of ground state polar molecules and universal dipolar scattering. *Phys. Rev. Lett.* **100**, 133202 (2008).

[121] J. L. Bohn, M. Cavagnero, and C. Ticknor. Quasi-universal dipolar scattering in cold and ultracold gases. *New J. Phys.* **11**, 055039 (2009).

[122] T. Bourdel, J. Cubizolles, L. Khaykovich, K. M. F. Magalhaes, S. J. J. M. F. Kokkelmans, G. V. Shlyapnikov, and C. Salomon. Measurement of the interaction energy near a Feshbach resonance in a ^{6}Li Fermi gas. *Phys. Rev. Lett.* **91**, 020402 (2003).

[123] S. Ospelkaus, K. K. Ni, M. H. G. de Miranda, B. Neyenhuis, D. Wang, S. Kotochigova, P. S. Julienne, D. S. Jin, and J. Ye. Ultracold polar molecules near quantum degeneracy. *Faraday Discuss.* **142**, 351 (2009).

[124] S. Ospelkaus, K.-K. Ni, G. Quéméner, B. Neyenhuis, D. Wang, M. H. G. de Miranda, J. L. Bohn, J. Ye, and D. S. Jin. Controlling the hyperfine state of rovibronic ground-state polar molecules. *Phys. Rev. Lett.* **104**, 030402 (2010).

[125] K. K. Ni, S. Ospelkaus, D. Wang, G. Quemener, B. Neyenhuis, M. H. G. de Miranda, J. L. Bohn, J. Ye, and D. S. Jin. Dipolar collisions of polar molecules in the quantum regime. *Nature* **464**, 1324 (2010).

[126] D. Wang, B. Neyenhuis, M. H. G. de Miranda, K.-K. Ni, S. Ospelkaus, D. S. Jin, and J. Ye. Direct absorption imaging of ultracold polar molecules. *Phys. Rev. A* **81**, 061404 (2010).

[127] A. R. P. Lima and A. Pelster. Collective motion of polarized dipolar Fermi gases in the hydrodynamic regime. *Phys. Rev. A* **81**, 021606(R) (2010).

[128] A. R. P. Lima and A. Pelster. Dipolar Fermi gases in anisotropic traps. *Phys. Rev. A* **81**, 063629 (2010).

[129] A. R. P. Lima and A. Pelster. Quantum fluctuations in dipolar Bose-Einstein condensates. `in preparation`.

[130] E. J. Mueller, T.-L. Ho, M. Ueda, and G. Baym. Fragmentation of Bose-Einstein condensates. *Phys. Rev. A* **74**, 033612 (2006).

[131] S. B. Papp, J. M. Pino, R. J. Wild, S. Ronen, C. E. Wieman, D. S. Jin, and E. A. Cornell. Bragg spectroscopy of a strongly interacting ^{85}Rb Bose-Einstein condensate. *Phys. Rev. Lett.* **101**, 135301 (2008).

[132] E. Gross. Structure of a quantized vortex in boson systems. *Nuovo Cimento* **20**, 454 (1961).

[133] L. P. Pitaevskii. Vortex lines in an imperfect Bose gas. *Sov. Phys. JETP* **13**, 451 (1961).

[134] K. Huang. *Statistical Mechanics*. Wiley, 2nd ed. (1987).

[135] Yu. Kagan, E. L. Surkov, and G. V. Shlyapnikov. Evolution of a Bose-condensed gas under variations of the confining potential. *Phys. Rev. A* **54**, R1753 (1996).

[136] Y. Castin and R. Dum. Bose-Einstein condensates in time dependent traps. *Phys. Rev. Lett.* **77**, 5315 (1996).

[137] F. Dalfovo, S. Giorgini, L. P. Pitaevskii, and S. Stringari. Theory of Bose-Einstein condensation in trapped gases. *Rev. Mod. Phys.* **71**, 463 (1999).

[138] M.-O. Mewes, M. R. Andrews, N. J. van Druten, D. M. Kurn, D. S. Durfee, and W. Ketterle. Bose-Einstein condensation in a tightly confining dc magnetic trap. *Phys. Rev. Lett.* **77**, 416 (1996).

[139] E. Madelung. Die mathematischen Hilfsmittel des Physikers. Springer-Verlag (1922).

[140] M. Fliesser, A. Csordás, P. Szépfalusy, and R. Graham. Hydrodynamic excitations of Bose condensates in anisotropic traps. *Phys. Rev. A* **56**, R2533 (1997).

[141] Y. Kagan, E. L. Surkov, and G. V. Shlyapnikov. Evolution of a Bose gas in anisotropic time-dependent traps. *Phys. Rev. A* **55**, R18 (1997).

[142] P. G. de Gennes. *Superconductivity of metals and alloys*. Westview Press, 2nd ed. (1999).

[143] F. Dalfovo, S. Giorgini, M. Guilleumas, L. Pitaevskii, and S. Stringari. Collective and single-particle excitations of a trapped Bose gas. *Phys. Rev. A* **56**, 3840 (1997).

[144] B. M. Fregoso and E. Fradkin. Unconventional magnetism in imbalanced Fermi systems with magnetic dipolar interactions. *Phys. Rev. B* **81**, 214443 (2010).

[145] V. Schulte-Frohlinde and H. Kleinert. *Critical properties of ϕ^4-theories*. World Scientific (2001).

[146] A. L. Fetter and J. D. Walecka. *Quantum theory of many-particle systems*. Dover (2002).

[147] S. Giovanazzi, A. Görlitz, and T. Pfau. Tuning the dipolar interaction in quantum gases. *Phys. Rev. Lett.* **89**, 130401 (2002).

[148] R. M. W. van Bijnen, N. G. Parker, S. J. J. M. F. Kokkelmans, A. M. Martin, and D. H. J. O'Dell. Collective excitation frequencies and stationary states of trapped dipolar Bose-Einstein condensates in the Thomas-Fermi regime. *Phys. Rev. A* **82**, 033612 (2010).

[149] S. Giovanazzi, P. Pedri, L. Santos, A. Griesmaier, M. Fattori, T. Koch, J. Stuhler, and T. Pfau. Expansion dynamics of a dipolar Bose-Einstein condensate. *Phys. Rev. A* **74**, 013621 (2006).

[150] K. Glaum, A. Pelster, H. Kleinert, and T. Pfau. Critical temperature of weakly interacting dipolar condensates. *Phys. Rev. Lett.* **98**, 080407 (2007).

[151] K. Glaum and A. Pelster. Bose-Einstein condensation temperature of dipolar gas in anisotropic harmonic trap. *Phys. Rev. A* **76**, 023604 (2007).

[152] S. Giovanazzi, L. Santos, and T. Pfau. Collective oscillations of dipolar Bose-Einstein condensates and accurate comparison between contact and dipolar interactions. *Phys. Rev. A* **75**, 015604 (2007).

[153] C. C. Bradley, C. A. Sackett, J. J. Tollett, and R. G. Hulet. Evidence of Bose-Einstein condensation in an atomic gas with attractive interactions. *Phys. Rev. Lett.* **75**, 1687 (1995).

[154] S. Ronen, D. C. E. Bortolotti, and J. L. Bohn. Bogoliubov modes of a dipolar condensate in a cylindrical trap. *Phys. Rev. A* **74**, 013623 (2006).

[155] S. Giorgini, L. P. Pitaevskii, and S. Stringari. Thermodynamics of a trapped Bose-condensed gas. *J. Low Temp. Phys.* **109**, 309 (1997).

[156] H. Kleinert. *Path integrals in quantum mechanics, statistics, polymer physics, and financial markets*. World Scientific, 5th ed. (2009).

[157] S. Stringari and L. P. Pitaevskii. *Bose-Einstein condensation*. Oxford University Press (2003).

[158] L. P. Kadanoff and G. Baym. *Quantum statistical mechanics*. W. A. Benjamin, (1962).

[159] M. Amoruso, I. Meccoli, A. Minguzzi, and M.P. Tosi. Collective excitations of a degenerate Fermi vapour in a magnetic trap. *Eur. Phys. J. D* **7**, 441 (1999).

[160] L. D. Landau and E.M. Lifshitz. *Fluid mechanics*. Pergamon Press (1959).

[161] P. Hohenberg and W. Kohn. Inhomogeneous electron gas. *Phys. Rev.* **136**, B864 (1964).

[162] E. Lipparini. *Modern many-particle physics, atomic gases, quantum dots and quantum fluids*. World Scientific (2003).

[163] P. Ring and P. Schuck. *The nuclear many-body problem.* Springer-Verlag (2000).

[164] T. Sogo, L. He, T. Miyakawa, S. Yi, H. Lu, and H. Pu. Dynamical properties of dipolar Fermi gases. *New J. Phys.* **11**, 055017 (2009).

[165] J. L. Safko H. Goldstein, and C. P. Poole. *Classical mechanics.* Addison-Wesley Press (1950).

[166] S. Giorgini, L. P. Pitaevskii, and S. Stringari. Theory of ultracold atomic Fermi gases. *Rev. Mod. Phys.* **80**, 1215 (2008).

[167] C. Menotti, P. Pedri, and S. Stringari. Expansion of an interacting Fermi gas. *Phys. Rev. Lett.* **89**, 250402 (2002).

[168] H. Hu, X.-J. Liu, and M. Modugno. Expansion of a quantum degenerate boson-fermion mixture. *Phys. Rev. A* **67**, 063614 (2003).

[169] G. M. Bruun and C. W. Clark. Hydrodynamic excitations of trapped Fermi gases. *Phys. Rev. Lett.* **83**, 5415 (1999).

[170] L. Vichi. Collisional damping of the collective oscillations of a trapped Fermi gas. *J. Low Temp. Phys.* **121**, 177 (2000).

[171] D. Guéry-Odelin, F. Zambelli, J. Dalibard, and S. Stringari. Collective oscillations of a classical gas confined in harmonic traps. *Phys. Rev. A* **60**, 4851 (1999).

[172] M. J. Giannoni, D. Vautherin, M. Veneroni, and D. M. Brink. Variational derivation of nuclear hydrodynamics. *Phys. Lett. B* **63**, 8 (1976).

[173] M. Yoshimine. Computed ground state properties of BeO, MgO, CaO and SrO in molecular orbital approximation. *J. Phys. Soc. Japan* **25**, 1100 (1968).

[174] A. Csordás and R. Graham. Collective excitations of degenerate Fermi gases in anisotropic parabolic traps. *Phys. Rev. A* **63**, 013606 (2000).

[175] A. Altmeyer, S. Riedl, M. J. Wright, C. Kohstall, J. Hecker Denschlag, and R. Grimm. Dynamics of a strongly interacting Fermi gas: The radial quadrupole mode. *Phys. Rev. A* **76**, 033610 (2007).

[176] I. S. Gradshteyn and I. M. Ryzhik. *Table of integrals, series, and products.* Academic Press, 7th ed. (2007).

List of Publications

1. A. R. P. Lima and A. Pelster: *Spinor Fermi Gases;*
   in W. Janke and A. Pelster (Editors): Proceedings of the 9th International Conference Path Integrals – New Trends and Perspectives; Max-Planck-Institut für Physik komplexer Systeme, Dresden, Germany, September 23–28, 2007;
   World Scientific, 429-432 (2008).

2. K. Howe, A. R. P. Lima and A. Pelster: *Rotating Fermi Gases in an Anharmonic Trap;*
   European Physical Journal D **54**, 667-682 (2009).

3. A. R. P. Lima and A. Pelster: *Collective Motion of Polarized Dipolar Fermi Gases in the Hydrodynamic Regime;*
   Physical Review A **81**, 021606(**R**)/1-4 (2010).

4. A. R. P. Lima and A. Pelster: *Dipolar Fermi Gases in Anisotropic Traps;*
   Physical Review A **81**, 063629/1-15 (2010).

5. A. R. P. Lima and A. Pelster: *Quantum fluctuations in dipolar Bose-Einstein condensates;*
   `in preparation`.

Acknowledgements

In the first place I would like to thank my wife, Raquel, for her unconditional support. Right from its birth, the idea of making my PhD studies in Germany imposed severe boundary conditions on our lives. The existence of a non-trivial solution is, to a large extent, due to huge amounts of dedication and comprehension from her side. My father Aristeu, my mother Fernanda, and my brother Hélio also had their share of this heavy burden and not only carried it without complaining but also managed to support me along the way. Muito obrigado.

It is a pleasure to thank my advisor Priv.-Doz. Dr. Axel Pelster for his guidance and help throughout the preparation of this thesis and of our common publications. His sound mathematical education, his permanent desire to explain and, not at least, his everlasting good mood are a few characteristics, which are of great value for a PhD student.

The opportunity to work in the group of Prof. Dr. Dr. h.c. mult. Hagen Kleinert has been both an honour and a privilege. His wide interest in physics is responsible for creating an intense interchange of ideas. This gives rise to a unique process of physical knowledge transfer which takes place even at lunch time. Those lessons were, therefore, given the name "The universe in a piece of napkin".

I am happy to acknowledge the help from my co-advisor, Prof. Dr. Jürgen Bosse. In particular, I would like to mention his critical reading of this manuscript, which improved its readability, as well as the support letters for extending the PhD scholarship.

I would like to thank Prof. Dr. Dr. h.c. Robert Graham for the research period which I spent in his group. In this time I met, among other people, Gianmaria Falco, whom I thank for valuable discussions on physics and many other subjects.

Special thanks are due to the whole "Brazilian mafia" for support and friendship: Victor Bezerra, Ednilson Santos, Dr. Flávio Nogueira, and Tobias Graß. The latter is included in order to fullfill the "Integrationsquote". In particular, the physical discussions with Flávio Nogueira are acknowledged. Moreover, I would like to thank Dr. Jürgen Dietel for his critical reading of this thesis and the corresponding publications.

During this period at the Free University of Berlin, I have been in contact with many people whose company brought me support, joy, or both. From older times, I would like to mention Konstantin Glaum, Moritz Schütte, Steffen Rötthel, Sonja Overesch, Walja Korolewski, Parvis Soltan-Panahi, and Sebastian Kling. From the new generation, special thanks go to Markus Düttman, Christian Nietner, Matthias Ohliger, Mahmoud Ghabour, Hamid Al-Jibbouri, and Mohammad Mobarak.

I would like to acknowledge the financial support from the Innovationsfond of the Free University of Berlin and from the German Academic Exchange Service (DAAD). I am specially indebted to Mrs. Maria Salgado for her kind help throughout the period of the DAAD-scholarship.